CHARACTERISING THE BIOMECHANICAL PROPERTIES OF THE PLANTAR SOFT TISSUE UNDER THE CONDITIONS OF SIMULATED GAIT

Daniel Parker

Ph.D. Thesis 2013

CHARACTERISING THE BIOMECHANICAL PROPERTIES OF THE PLANTAR SOFT TISSUE UNDER THE CONDITIONS OF SIMULATED GAIT

Daniel Parker

School of Health Sciences
University of Salford, Salford, UK

Submitted in Partial Fulfilment of the Requirements of the Degree of Doctor of Philosophy, February 2013

Table of Contents

List of Figures

Literature Review

Part A

Part B

List of Tables

Literature Review

Part A

Part B

Appendix

Acknowledgements

Throughout the various stages of work within this PhD I have been fortunate to receive support and guidance from many people. I am sincerely grateful to my supervisory team: Prof Christopher Nester, Prof David Howard, Dr Stephen Pearson and Dr Glen Cooper, who have provided considerate mentoring and critique as I strove to expand my knowledge in new and exciting fields of research. Without them I would not have been able to find focus whilst incorporating the multiple threads from a range of disciplines. I would like to thank my funding body, SSL International Ltd, who provided the financial support for this project. I would also like to thank Dr Todd Pataky, of the University of Shinshu, for providing the basic code used in the Ultrasound tracking algorithm and for his support in the re-development of this algorithm. I would like to thank Dr Gillian Crofts for her guidance in the use and application of Ultrasound. I am extremely grateful to Mr Paul Busby of the Commercial Enterprise Unit at the University of Salford for his work in changing my concepts and sketches into engineering drawings and eventually the physical manifestation of device components, without which the novel aspects of this work would still be theoretical. I would also like to thank the workshop technicians Mr Bernie Noakes, Mr Geoff Riley and Mr Colin Smith, for assistance in the fabrication and adjustment of the device components and for their support and guidance when using the workshop. I would like to thank the gait lab technicians Mr Stephen Horton and Ms Laura Smith, for their assistance throughout my testing and for their accommodation of my sometimes awkwardly large test rig. I would like to thank Ms Anna-Maria Guiotto, for her support and assistance whilst on placement when the initial protocol was being tested, and also to her department who provided the data to allow development of a gait simulation profile based on elderly gait. Thank you to my office colleagues for making it easy to forget about the stresses of work and for always being prepared to have that quick pint. An especially large thank you to Rachel, for putting up with all the late nights I worked, and for helping me to cope when things just didn't work, most of all for just being there when I really needed her. Lastly I wish to acknowledge all of the giants, from whose shoulders I have been granted the privilege to stand and look upon the world with curiosity.

Statement of Component Contributions

Financial Contribution

The work contained in this thesis was financially sponsored by SSL International Ltd, owners of the Scholl brand of foot care products. SSL agreed to the principals of the project, its intended outcomes, and received periodic reports on project progress. SSL were not involved in data collection, analysis nor interpretation. Beyond the payment of PhD fees and standard PhD bursary, the candidate (nor members of the supervision team) did not receive any direct financial benefits from the outcome of this work.

Contributions to Work

Device Production

The concept and specification of the developed device was completed by myself, however the production of engineering drawings and the process of tendering device component manufacture was completed by Mr Paul Busby of the Commercial Enterprise Unit at the University of Salford. The tendered components of the device were manufactured outside of the university by local engineering companies.

Ultrasound Tracking Algorithm

The kernel code containing initial template matching algorithms was developed by Dr Todd Pataky of Shinshu University. This code was considerably tailored and adapted for the purpose of the Thesis work by myself.

Declaration

I declare that this thesis has been composed by myself and embodies the results of my own course of study and research whilst studying at The University of Salford from October 2009 to January 2013. All sources and material have been acknowledged.

Abstract

The plantar soft tissue at the heel and ball of the foot provide the interface between the body and the ground. This tissue is adapted to attenuate large amounts of energy during impact (heel strike) and to become rigid under continuous loading (standing). The heel pad tissue is composed of multiple specialised layers including a rigid bone (Calcaneus), a highly compliant fatty pad and a stiff rugged skin boundary. To assess this complex tissue STRIDE (Soft Tissue Response Imaging Device) has been developed. Using bespoke displacement driven profiles STRIDE is capable of simulating the vertical component of gait to compress the tissue, whilst collecting data to describe the response of the tissue via the combination of ultrasound imaging to detect vertical displacement and a miniature load cell to detect vertical load. From this data we are able to calculate tissue stress and strain and derive the characteristic mechanical properties of the tissue. A study of 38 individuals ranging in age from 18 to 85 was conducted to develop a baseline of tissue properties over age. The results show that the tissue has a highly rate dependent nature, reinforcing the need to conduct tests at rates relevant to the functional range of the tissue. Under gait conditions the elderly group displayed non-significant trends toward increased Energy loss (+45%), elastic modulus (+4%) and compressibility (+11%) whilst decreased trends were observed for viscosity (-20%) and the measured gradient of the stress strain curve throughout tissue compression. These differences suggest that the normal structural changes, which occur within the tissue as a result of aging, can cause disruption to the mechanical response of the tissue during compression. The mechanical properties derived will be used to inform the development of mechanisms (therapy/treatment) or interventions (orthotics/shoes) which may compensate for these changes.

1. Introduction

The human heel pad is a highly specialised region of the plantar soft tissue and is located on the posterior surface of the calcaneus, directly beneath the calcaneal tubercle; it is composed of three primary layers, superficially it is surrounded by a rugged and protective outer skin layer, deep to this is a dense microtubule layer which acts as a natural heel cup and provides shape to the heel region whilst also preventing excessive bulging or deformation, the most deep layer is the macrotubule layer which contains large pockets of adipose tissue bound by a highly ordered collagen and elastin matrix and acts as a viscous damper when compressed at high rates. The arrangement of adipose enclosed in chambers forms a hydrostatic structure which becomes incompressible under load, thus preventing damage to the underlying skeleton whilst also facilitating a wide variety of gaits

Atrophy can occur within the heel pad, and results in disruption of the normal structure and a reduced function of the tissue as a whole. This has been associated with the deleterious effects of glycation which accumulate throughout life and act to disrupt tissue formation. An accelerated atrophy has been observed in conditions such as obesity and diseases such as diabetes due to the greater prevalence of glycation in these conditions. The large dependence placed on the plantar soft tissue for human locomotion, means that changes which affect the function of these tissues can have a large impact on the lifestyle and ability of disease sufferers. At present interventions such as footwear and orthotics exist, which aim to compensate for the loss of function due to the effects of disease; however the most appropriate use of these interventions and the true effect of the intervention on the pathological tissue is not known. This is due largely to the lack of understanding regarding the normal response of the tissue during functional tasks, such as walking, and therefore no clear comparisons can be made between pathological tissue and healthy tissue.

Previous in-vivo work has characterised the plantar soft tissue via three techniques. (1) Using low rates of compression at a specific site, providing good repeatability but little relevance to the functional range of the tissue. (2) Using high rates of compression to characterise the response of a whole segment such as the lower leg, providing good repeatability but failing to isolate the specific response of the plantar soft tissue. (3) Using in-gait to study the response of a general area of the plantar soft tissue to loading during gait (e.g. the forefoot region),

providing functionally relevant response but in an uncontrolled manner with difficulty isolating the response of the tissue at a specific site under the foot (e.g first metatarsal head). The previous work has utilised elements from one or two of these techniques however no study has effectively combined all three approaches. Thus, to advance the understanding of the plantar soft tissue it is necessary to have a tool capable of effectively characterising the tissue's response when exposed to a range of controlled loading conditions which encompass its full functional capacity.

The main objectives of this work are therefore;

1. To design and validate a novel device to be used to characterise mechanical response of the plantar soft tissue.
2. To develop a protocol to assess the sensitivity of the plantar soft tissue to the applied loading profile.
3. To establish a normative dataset of mechanical properties for the plantar soft tissue

The development of a normative dataset will explain the mechanical response of the tissue for healthy individuals across a range of ages and of different genders. The dataset will also explain the response of the tissue for a range of loading conditions. This will provide a strong basis for comparison when studying the effects of pathology, and in the selection of suitable materials to compensate for known pathological effects. Furthermore a broad approach to the assessment of the tissue's mechanical response to compression will permit a wider base of evidence to be used when making hypotheses relating to the mechanisms which govern the relationship between the tissue's complex structure and the response to external load. Finally the combination of a normative dataset and a comprehensive assessment of the mechanical properties will permit the identification of a number of crucial variables which can be used to explain the mechanical response of the tissue. This will allow future work to achieve effective characterisation of the tissue properties, by a relatively simple means. This may have benefits for the study of large clinical populations and community based studies.

Thesis Outline

Prior to commencement of the main body of work a review of the literature was conducted to introduce key concepts and identify the limitations and strengths within the previous methods.

The outcomes of this review were summarised in a statement of problem, and the research questions were designed to give focus to the subsequent work.

The novel work within this thesis is divided into two parts; Part A which addresses the development of STRIDE (Soft Tissue Response Imaging Device) and Part B which addresses the implementation of STRIDE. This was done to permit a focused consideration of the specific challenges faced in each part and to allow clear outcomes for each part to be discussed independently.

Part A is concerned with the development and evaluation of a device to characterise the plantar soft tissue, and is divided into seven Sections. Section One introduces the specific challenges faced in developing a device to simulate the tissue compression experienced in gait, and evaluates the potential device components which could be used for actuation and measurement. Section Two describes the device specification and assesses the demand placed on a device when simulating the motion of gait, providing a framework for the selection of device components. Section Three presents a detailed breakdown of the device components which were selected, and highlights the implications of novel device developments on the ability to characterise the plantar soft tissue. Section Four describes the selection and development of a range of loading profiles to be used to control the device motion in tissue testing, providing the capacity to evaluate the tissue response for a wide range of conditions. Section Five explains the methods used to collect and process the raw data, including the development of an algorithm to track anatomical features in ultrasound images. The measured response of the tissue during compression is normalised and presenting in terms of stress and strain. Section Six presents the design of experiments to evaluate the performance of the developed device. The results of each experiment are also presented and discussed within this Section. Finally Section Seven discusses the main outcomes of Part A, and explains the limitations present within the current device design.

Part B is concerned with the implementation of the device to characterise the plantar soft tissue in the case of the heel pad and is divided into five Sections. Section One introduces the range of previous methods used to characterise the measured plantar soft tissue response, discusses the limitations of these methods, and outlines the challenges and aims for the characterisation of the plantar soft tissue in this study. Section Two presents the design of a study to assess the repeatability of the tissue properties derived for individuals tested within and between days. The results of this study are also presented and discussed within this

Section. Section Three presents the design of a study to characterise the response of the plantar soft tissue in compression. The Section describes how the loading profiles designed in Part A were tested on a cohort of healthy individuals of mixed gender from a wide range of ages (18 – 85), and provides a detailed description of the characterisation methods used. Section Four details the results of the study outlined in Section three, with an assessment of the effects observed due to variance in the applied loading rate, and due to variance within the cohort due to age or gender. Section Five discusses these results in the context of previous studies, evaluates the characterisation methods used, and proposes the existence of two fundamental mechanisms which underpin the tissue's response to compression.

Overall conclusions were drawn to highlight the key outputs of each part of the thesis and to identify the original contributions of the work within the thesis. Finally the potential for future work was assessed based on both the advancement of the developments made in Part A, and the identification of future studies which would benefit from the developed device.

2. Literature Review

The soft tissue pads on the sole of the feet have evolved as aids to locomotion throughout the animal kingdom (R. M. Alexander, M. B. Bennett, and R. F. Ker 1986a). Human gait generates high forces at push off and impact, due to the large accelerations and decelerations required to propel the body along its trajectory (Ciacci *et al.* 2010). As the force experienced by the tissue is the resultant of the body mass and the acceleration at impact, when the speed of walking increases the force can also increase greatly (Giddings *et al.* 2000). The plantar soft tissue functions to protect the skeleton from these high loads by dampening the shock of impact (Noe 1993). Although it is a highly effective shock absorbing structure when compared to other regions of the foot it is still possible to damage the plantar soft tissue by high repetitive loading (Jorgensen 1985). This suggests that, like most biological structures, the plantar soft tissue has a functional level at which it is most effective.

2.1. Functional Anatomy of the Calcaneal Fat Pad

At ground contact the rear foot acts as a viscous damper, dissipating the large impact energy and protecting the skeleton from the high ground reaction forces experienced at impact (Salathe Jr. 1990). During stance the rear foot acts as a semi rigid support for body weight, provides compensation for uneven terrain and facilitates the maintenance of balance (Trew and Everett 2001). Thus the tissue layers which lie between the skeleton and the ground must be capable of constant adaptation, a feature highlighted by their complex structure.

2.1.1. Structure of the calcaneal fat pad

The soft tissue, which forms the calcaneal padding, has a multi-layered structure (Figures 2.1 & 2.2). Superficially the sole has a thick skin layer that acts as an impermeable barrier to protect the underlying soft tissues (Snell 2004). Deep to the skin is a densely packed fibro-adipose structure of microchambers. This layer is primarily a collagen matrix with small

regularly spaced globules of adipose (Blechschmidt 1982, Jahss 1992). The microchamber layer acts as a natural heel cup, providing shape to the plantar surface of the heel and resisting excessive tissue bulging during compression (Hsu 2007). Deep to the microchamber layer is a second, sparser, fibro-adipose structure of macrochambers. This layer consists of large fatty chambers bound by thick fibrous septae (Blechschmidt 1982, Jahss 1992). The chambers are arranged in an overlapping spiral formation around the process of the calcaneus, and the septae align with the curvature and torsion of the calcaneus such that under compression the chambers rotate and bulge out from the midline (Blechschmidt 1982). Each chamber is further divided into globules by fibro-elastic bundles of collagen and elastin, forming a closed cell honey-comb structure (Jahss 1992). The globules are filled with adipose tissue which is a combination of unsaturated and saturated fatty acids. Compared to storage fats, such as those in the abdomen, an increased percentage of unsaturated fatty acids are found in the macrochambers of the heel pad (Buschmann *et al.* 1993). Due to the lower melting point of unsaturated fatty acids, the tissue specialisation seen at the heel is suggested to result in a softer less viscous tissue; which acts to enhance efficacy of the heel pad as a viscous damper (Buschmann *et al.* 1993). Deep to the macrochamber layer is a thick fibrous tie that binds the macrochamber layer to the calcaneus (Blechschmidt 1982). The plantar aponeurosis originates at the medial and lateral processes of the calcaneus from within the fibres of the fibrous tie (Snell 2004). The most deep structure is the calcaneus which has medial and lateral processes; these provide attachment to the plantar aponeurosis and give a broad base to allow distribution of force to the soft tissue.

The heel region receives a blood supply from the anterior and posterior branches of the peroneal artery (Snell 2004), which produce a large venous plexus within the subcutaneous tissue (Weijers 2005). This plexus fills during the swing phase of gait due to internal pressure and has been shown to provide a small reduction (3%) in maximum impact force, this may act to facilitate shock absorption within the tissue (Weijers 2005). The heel is innervated by the posterior and distal plantar nerves (Snell 2004). Their main function in this region is to provide sensation via slow adapting mechanoreceptors for touch and fast adapting mechanoreceptors for vibration. Fast adapting receptors are likely to provide positional control during heel strike, while slow adapting fibres provide protective feedback to prevent damage (Vincent 1992, Hennig and Sterzing 2009).

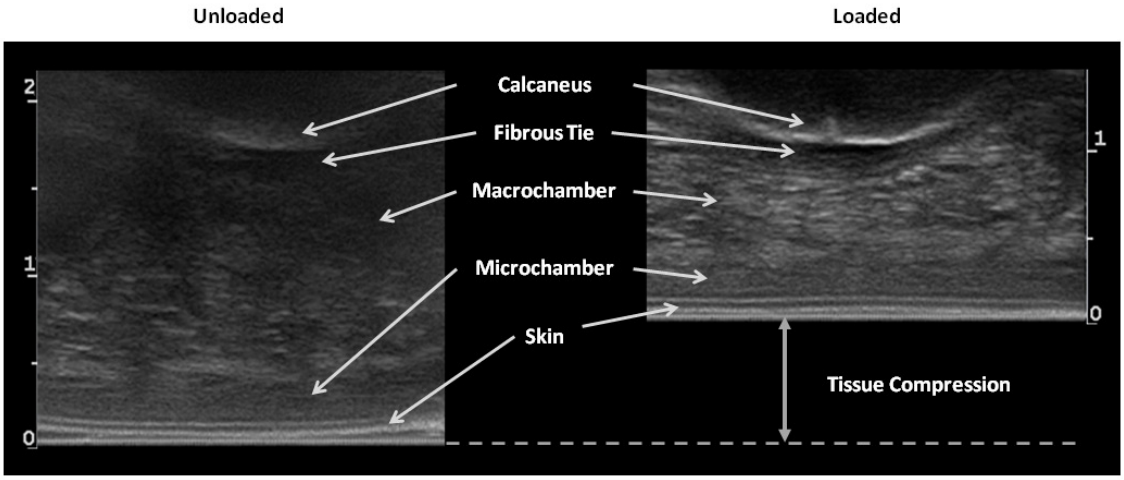

Figure 2.1: Ultrasound image of calcaneal fat pad in the unloaded and loaded states

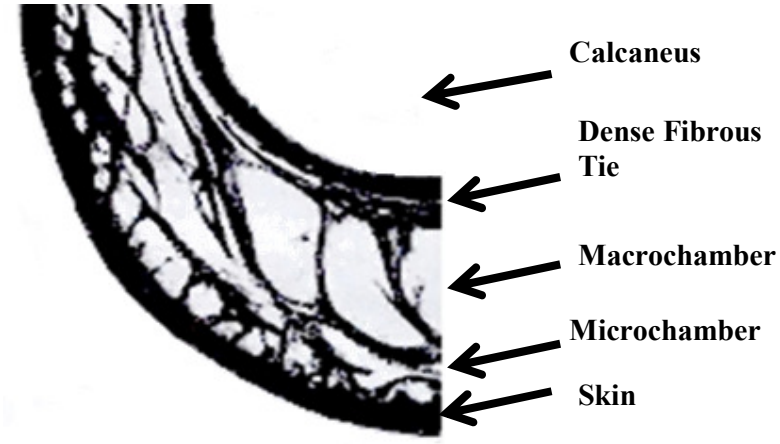

Figure 2.2: Frontal section through the calcaneal fat pad displaying the multi-layered structure. Taken from Blechschmidt (1982)

2.2 The Properties of Viscoelastic Materials

Biological structures are composites of strong ties and fluid filled chambers which give structural integrity without the use of fixed or rigid supports, this permits flexibility under load and allows them to withstand a wide range of environmental conditions.

2.2.1. Stress, Strain and Shear

2.2.1.1. Stress

Stress is the intensity of a force when distributed across a material. Stress can be defined as the force required to extend or compress a material in the axial direction, normalised for the material's cross sectional area and is expressed as N/m^2.

$$\sigma = F/A \qquad (EQ.2.1)$$

Where σ is stress, F is applied force and A is cross sectional area

In the context of this study stress refers to the normalised force used to compress an area on the surface of the plantar soft tissue. Previous studies have used plantar pressure measurements to determine an effective range for the applied stress; reporting the use of values between 74kPa to represent standing (Hsu 2002) and 156kPa to represent walking (Erdemir *et al.* 2006).

2.2.1.2. Strain

Strain is the change in length of a material in the axial direction when a force is imposed upon it. Strain can be defined as the ratio of displacement under load to original length and has no units.

$$\varepsilon = dL/L \qquad (EQ.2.2)$$

Where ε is strain, dL is the displacement and L is the original length

In the context of this study strain refers to the ratio between the unloaded tissue thickness and the tissue thickness when compressed. The peak strain can be used to define the compressive potential of the tissue and can give an indication of the potential for shock absorption within the tissue (Jorgensen 1985).

2.2.1.3. Shear

Shear is the response of a material to stress or strain in the parallel direction to its surface which causes the shape of the structure to deform. The shear stress can be defined as:

$\tau = F/A_{(parallel\ surface)}$ *(EQ 2.3)*

Where τ is shear stress, F is applied shearing force and A is area parallel to the applied force.

The effects of shear are not being directly studied in this thesis and have had little investigation in the previous literature; however an understanding of the potential mechanisms for deformation within the plantar soft tissue is crucial when exploring concepts such as viscous flow.

2.2.1.4. Stiffness and Modulus.

In the context of material characterisation stiffness describes the gradient of the load-displacement curve and is generally expressed in N/m^2. Modulus is used to describe the gradient of the stress-strain curve and is expressed in kPa as strain is a unit-less variable.

$Stiffness = dL/dK$ *(EQ.2.4)*

$Modulus = d\sigma / d\varepsilon$ *(EQ.2.5)*

Where dL is displacement, dK is change in Load, $d\sigma$ is change in stress, $d\varepsilon$ is change in strain.

For the purpose of this study the response of the tissue will be assessed by using measures of modulus. However comparisons to previous studies will use a combination of stiffness and modulus due to the wide range of previous methodologies used to characterise the tissue's response.

2.2.2. Principles of Elastic Solids

All solids are made up of atoms held together by strong inter-atomic bonds; thus the behaviour of the solid under load is determined by the arrangement of the atoms within it (Vincent 1992). A Hookean solid has a highly ordered arrangement of atoms with rows and columns joined by stiff atomic bonds (Ennos 2011): these include metals and ceramics such as bone (Vincent 1992). When stressed, the response of the solid is determined by Hooke's law which states that strain and stress are directly proportional (Figure 2.3), and thus is the result of the summed responses at each atomic bond (Vincent 1992). A Non-Hookean solid has an initially random configuration of atoms with loose atomic bonds; an example of a Non-Hookean material is rubber (Vincent 1992). Under stress the atoms are brought into order due

to strain of the inter-atomic bonds/space resulting in a region of initial compliance (Figure 2.3) where the tissue is strained with little application of force (Vincent 1992).

2.2.3. Principles of Viscous Fluids

Fluids are either liquids or gases and can be defined as substances which permit shear deformation (Vogel 1994). Liquids are fluids composed of atoms and molecules held together by inter-atomic bonds and weak inter-molecular bonds. Shear deformation acts to break intermolecular bonds allowing movement or viscous flow (Frost 1971). A Newtonian fluid permits flow with force proportional to the rate of shear strain; Newtonian fluids can be found as the components of many mechanical lubricants (Frost 1971). A Non-Newtonian fluid does not show a proportional relationship between shear strain and force, and is the predominant fluid found in biological systems (Frost 1971). Non-Newtonian fluids can occur in two forms: shear thinning and shear thickening. With shear thinning, increasing the applied force will result in a greater than proportional increase in shear rate, thus making it relatively easier to deform at high shear rates (Vincent 1992). Shear thickening shows the inverse, in which increasing the applied force will result in a lower than proportional increase in the shear rate, thus making it relatively easy to deform at low shear rates (Vincent 1992).

2.2.4. Viscoelastic Principles

A viscoelastic material is the combination of elastic components (either Hookean or Non-Hookean) and viscous components (Newtonian or Non-Newtonian) (Lockett 1972). viscoelastic materials take various forms and under load have complex behaviours which are dependent on the interplay between their constituent parts. This leads to a spectrum of viscoelasticity which spans the space between purely elastic and purely viscous behaviour (Lockett 1972). As with a viscous fluid, the rate of strain affects the amount of work which must be done to deform a viscoelastic material. However, unlike the fluid, when stress or strain is removed the material will return to its original shape (Ennos 2011). A discrepancy is present between the path of loading and unloading response due to energy lost within a viscoelastic material as a result of the increased work required to deform the tissue against the viscous resistance to loading (Figure 2.3) (Vincent 1992).

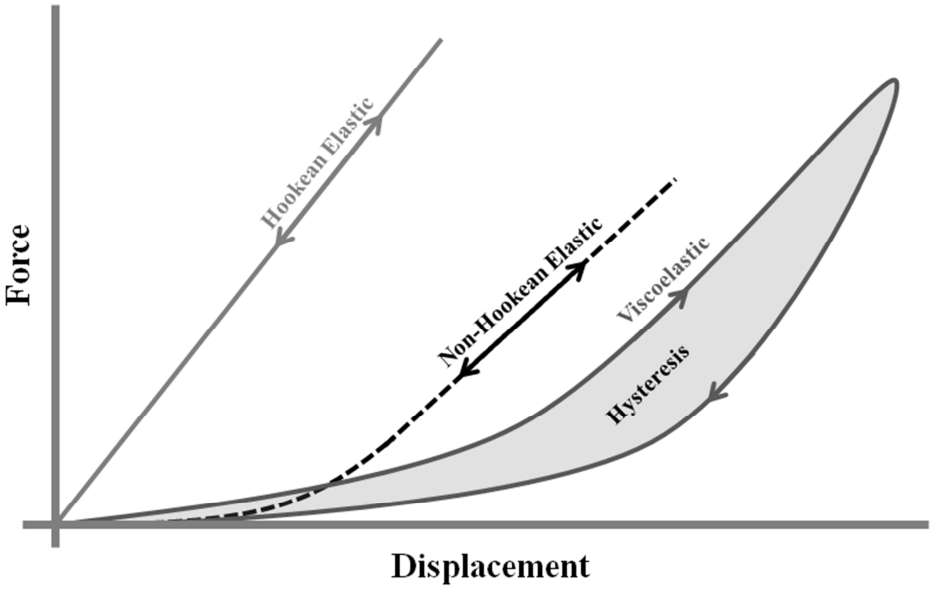

Figure 2.3: Mechanical Response of Elastic and Viscoelastic Materials in Compression

2.2.5 Characterisation of Viscoelastic Materials

To characterise the response of a viscoelastic material in compression it is necessary measure the applied stress and strain during a compressive test under axial load. The resulting stress-strain curve (Figure 2.3) can be characterised directly by isolating features such as the peak stress and peak strain which occurred within the material. In tests where the applied load is controlled the peak strain can be used to give an indication of the compressibility of a material, with incompressible materials displaying a sharp increase in the stress required to impose deformation. In tests where the applied displacement is controlled the peak stress can be used to give an indication of the stiffness of a material, with stiff materials producing large stresses in response to compression. The linear relationship between peak stress and peak strain permit the characterisation of the secant modulus, this value is highly dependent on the imposed compression conditions, however when conditions are controlled permits comparison of various materials to be conducted using a single value. The nonlinear relationship between stress and strain can also be characterised throughout compression via curve fitting, the curve's shape is determined by the interaction of the elastic and viscous components in response to compression. Although the elastic and viscous elements cannot be isolated from curve analysis alone it is possible to derive variables which give an indication of

these components. The hysteresis of the curve can be quantified by calculating the area bound by the loading and unloading curves and provides an indication as to the degree to which the viscous response has resulted in energy loss within the tissue. Modelling techniques can be used to isolate the elastic and viscosity of the stress-strain response by assigning components of the response to simplified elements represented as springs or dampeners. Due to the simplified assumptions upon which these models are dependent, the application to a complex biological tissue is often extremely difficult and can pose challenges when proving the efficacy.

2.3. Previous Experimental Methods

The range of experimental methods used to characterise the viscoelastic properties of the plantar soft tissue are vast, allowing for a good assessment of variables. Methodologies can be divided as material or mechanical, with mechanical being further divisible into: controlled compression, pendulum and in-gait experiments.

2.3.1. Material Studies

Material studies are conducted on tissue sections in-vitro using highly accurate material testing machines (Ledoux 2007). Tissue sections are geometrically symmetrical permitting the imposed stress to be calculated exactly (Miller-Young 2002) with previous studies using a range of square (20mmx20mm Ledoux, 2007) and circular (19mm diameter Pai 2010) sections, these samples are taken from the tissue at the location of the calcaneal tuberosity and thus represent the tissue which is exposed to the highest stress during normal function (Spears 2007). The tissue samples are compressed between two platen (one fixed, one dynamic), and displacement of the dynamic platen relates directly to tissue compression. The use of platen position for the measurement of displacement does not require the tissue to be imaged throughout loading and thus displacement transducers can be used to provide high resolution and accuracy (Miller-Young, 2002). The absolute displacement of the loading platen can be adjusted for each tissue based on an assessment of the tissue's thickness or to permit loading which produces a target stress within the tissue (Ledoux, 2007). The nature of in-vitro testing

restricts the assessment to a single state and does not allow for the analysis of intra-individual variance such as time, conditioning or treatment. The use of sectioning to isolate the tissue of interest also removes the natural boundaries such as the microchamber layer which function to prevent lateral bulging of the tissue (Hsu, 2007). This change to the structural arrangement of the tissues may also result in differences in the observed loading response.

2.3.2. Mechanical Studies

Mechanical studies can be conducted in-vivo or in-vitro and aim to characterise the response of a tissue as a functional unit (i.e. heel pad). The methods of mechanical testing can be grouped as controlled compression, pendulum impact and in gait experiments.

2.3.2.1. Controlled Compression Studies

Controlled compression studies use a dynamic platen to compress a complete region (rearfoot or forefoot) of the plantar soft tissue whilst the foot or foot region is fixed. This method retains the structural integrity of the plantar soft tissue, as opposed to the sectioning techniques used in material studies, thus the functional response of the foot region can be assessed. Fixing of the foot region can be done in-vitro by rigidly attaching the calcaneus to a static or dynamic platen (R. M. Alexander, M. B. Bennett, and R. F. Ker 1986b, Bennett and Ker 1990, Ker 1996, Erdemir *et al.* 2006) or in-vivo by bracing the subject's lower leg (Hsu, Wang, *et al.* 1998, Klaesner *et al.* 2001). Studies can be conducted by compressing the specific region of interest with a small diameter probe or by compressing the whole tissue area uniformly.

Indentation studies are conducted using probes with small compression areas. Typically these areas range from 1cm to 5cm diameter (Zheng *et al.* 2000, Klaesner *et al.* 2001). The use of miniature load cells in series with the indenter surface permits the calculation of stress for the area of the compressive surface, thus providing a measures of the tissue's response for a specific site (Klaesner *et al.* 2001). Finite element studies have shown the stress within plantar soft tissue's to become concentrated beneath the bony landmarks such as the apex of the calcaneal tubercle (Spears 2007) and at the Metatarsal Heads (MTHs) (Chen 2001). The use of an indentation probe, with a compression area equivalent to that of the surface area of the

bony landmark, may provide a greater understanding of the functional response of the tissue's which are exposed to the most demanding conditions during gait. However the use of small indentation probes are limited due to the edge effects caused during compression; skin surrounding the probe is brought into tension adding to the tissues resistance to loading and skewing the measurements of tissue stress (Erdemir *et al.* 2006). These edge effects can be accounted for by the use of modelling methods which normalise the measured stress; however assumptions as to the tissue's nature (Poisson's ratio) must be made with these techniques (Han *et al.* 2003). Misalignment of the indentation probe can influence the direction in which load is applied and the thickness of the tissue being compressed; as a result the measured tissue response is affected by misalignment errors (Y. P. Zheng, A. F. . Mak, and B. Lue 1999). For the heel, target indentation would expect to compress the tissue at the point of the apex of the calcaneus and in the normal direction to the tissue; however the small surface area of this feature and the natural curvature present in both anterior-posterior and medio-lateral directions mean that misalignments can easily occur. Correctly aligning the probe can be improved by using imaging methods such as ultrasound to detect the true apex of the calcaneus and to ensure this apex remains in the line of compression throughout testing.

Bulk compression studies can be conducted in-vivo and in-vitro using a platen to compress the tissue either manually or mechanically (Aerts *et al.* 1995, Ker 1996, Hsu 2007). The use of bulk compression retains the functional tissue structure whilst also applying a uniform load to the whole tissue region without the edge effects seen in indentation studies. During compression data, is collected for the applied load and displacement of the tissue as a whole. The contact area can be established by using pressure systems and calculating the sum of the area of the active sensors for the region of interest (Wearing *et al.* 2009). When the region's area is known an effective stress can be calculated for the foot region as the total measured load divided by the contact area. The calculation of an effective stress for the whole region is limited by the assumption that stress is uniform throughout the tissue region. Previous studies have shown that the internal distribution of stress is not uniform, but in fact concentrated at the apex of the bony landmarks (Chen 2001, Spears 2007), thus an effective stress measure for the whole foot region may not fully explain the response of the tissue under load.

The drive mechanism used to compress the tissue has a large effect on the level of displacement and velocity control possible. Manual drive mechanisms use an operator to push or pull the platen to compress the soft tissue with effective rates of between 0.0006m/s and 0.006m/s (Tong 2003, Hsu *et al.* 2009). Testing at this level has been shown to be highly

accurate and reliable for both inter and intra-rater assessments (Klasesner 2002). However the complexity of the applied loading routine is limited, as routines are often regulated by operator pace or metronome alone (Zheng *et al.* 2000, Hsu 2005). The use of motorised drive mechanisms such as Instron devices for in-vitro studies (Bennett and Ker 1990, Aerts *et al.* 1995) or bespoke indentation systems for in-vivo testing (Erdemir *et al.* 2006, Zheng *et al.* 2012a), permit a much greater control of the loading profile. These methods also allow a greater range of displacement rates to be implemented, with previous motorised drive systems ranging from 0.006m/s to 0.37m/s, allowing for assessment of rate dependent tissue properties up to the level experienced in gait (Aerts *et al.* 1995, Erdemir *et al.* 2006). In an effort to make test mechanisms more portable, and thus clinically applicable, small mechanisms have been introduced. However these devices are predominantly manually controlled and are not capable of producing compression at high rates, tending to use rates which represent only 1% of the average rate experienced in normal walking gait (Chao *et al.* 2010, Chen *et al.* 2011). Due to the rate dependent nature of the plantar soft tissue (Hsu 2005), the relevance of the derived mechanical properties is restricted to the rate at which the tissue was tested, unless a full understanding of the relationship between rate and tissue response is first established.

2.3.2.2. Pendulum Impact Studies

Pendulum impact studies are conducted in-vivo and use a mass, accelerated to impact the foot, simulating the ground contact phase of gait (Alcántara 2002, Weijers 2005). This method of assessment requires minimal control and can achieve loading conditions equivalent to gait, giving both repeatable and highly accurate measures of device motion during tissue compression (Alcántara 2002, Weijers 2005). This technique is capable of producing a wide range of impact velocities, with previous studies using impacts in the range 0.2 to 1m/s to assess the tissue's response (Frederick 1984, Weijers 2005). The test velocity can be tailored to each subject easily by simply adjusting the arc of the pendulum (Weijers 2005). The test force imposed on the tissue during compression can be calculated by measuring the acceleration of the mass during impact (Alcántara 2002). However difficulty is found when attempting to generate tissue specific compression, as opposed to whole leg movement in response to impact. To counteract this, bracing is used and leg segments are secured against solid supports (Alcántara 2002), however, soft tissue compression within the joints and auxiliary soft tissues in the leg, and compliance within the bracing remain a limiting factor of

impact studies (Pain 2001). The lack of tissue imaging used in impact studies also means that the mechanical properties must be derived based on motion of the ballistic mass, as the compression cannot be restricted to a single tissue in-vivo, the values reported by these studies represent the combined response of all tissue components in series with the point of load application, which has led to the overestimation of some factors (Percentage Energy Loss) and has been termed the 'Lower leg effect' (Aerts *et al.* 1995, Pain 2001).

2.3.2.3. In-Gait Studies

In-Gait studies are conducted in-vivo, using walk ways or raised platforms with a combination of force plates, pressure plates and a method of imaging tissue thickness. The subject is asked to walk at normal pace through the imaging window and to target a force plate during a normal walk (De Clercq 1994, Cavanagh 1999). Target windows vary in volume depending on the method of imaging used for tissue thickness measurement. Ultrasound uses a 2 Dimensional (2D) imaging plane, which makes it difficult for a subject to consistently target the same point during normal gait (Cavanagh 1999). This results in the measured location differing with each trial. Due to the complex structure of the heel pad (Blechschmidt 1982) and the concentration of stress beneath the apex of the calcaneus (Spears 2007), even small deviations or misalignments from the target location are expected to observe a varied mechanical response (Y. P. Zheng, A. F. . Mak, and B. Lue 1999). X-ray fluoroscopy allows for a larger imaging window, which makes targeting easier (Wearing *et al.* 2009). However, fluoroscopy also gives a 2D flattened representation of the tissue, which can result in the loss of some position detail (Rome *et al.* 1998). Xray techniques also require the use of heavy protective clothing which can result in an unnatural gait and reduced walking speed (De Clercq 1994). Although research to investigate tissue function during gait aims to record the true physiological function, this approach is limited by the difficulty found in targeting and isolating a specific tissue region over multiple compressive steps.

2.3.3. Summary of Previous Methods

The range in previous methodologies reflects the difficulties found in defining the plantar soft tissue mechanical properties. Standardised, highly repeatable definitions of mechanical properties can be found by testing the tissue at low rates of compression with accurate and

reliable mechanisms. However, these definitions are not relevant to the functional range of the tissue. Physiologically relevant definitions of the mechanical properties can be found by testing the tissue in-gait, however these methods are difficult to replicate and standardise. Pendulum impact methods allow physiologically relevant conditions to be imposed in repeatable and standardised ways but do not permit the isolation of the specific tissue compression and thus represent the lower leg response as a whole. Combining the beneficial elements from the previous methodologies will permit more effective characterisation of the mechanical response of the plantar soft tissue.

2.4. The Plantar Soft Tissue as a Viscoelastic Material

2.4.1. Structure

The calcaneal fat pad exhibits a honeycomb structure, composed of collagen and elastin septae which completely enclose globules of adipose in a closed cell type structure (Figure 2.4) (Jahss 1992, Brash *et al.* 1999). Taking this tissue as a single viscoelastic layer, the components can be separated into the septae which provides the elastic component, and the adipose which provides the viscous component. The closed cell structure of the globules results in a fixed volume of adipose tissue, which may be pressurised via osmosis (Jahss 1992, Ennos 2011). The internal pressure acts to bring the elastic septae into tension thus creating a hydrostatic skeleton (Ennos 2011). Although it is not stated in the literature, it is expected that the fibres in the septal walls will exhibit a helical arrangement (Figure 2.5). This arrangement permits compression whilst resisting torsion and kinking of the structure (Ennos 2011), allowing the chambers to act in line with the greatest force during gait (Jahss 1992). When compression is imposed on this structure a change of shape will occur, causing the tension in the septal walls to increase in an elastic fashion, whilst the compressive load is borne by the enclosed adipose (Figure 2.5) (Ennos 2011). This arrangement means that the viscosity of the enclosed adipose tissue will directly control the capacity of the tissue to dampen the high impact forces imposed upon it during ground contact. When the tissue is offloaded the tension in the elastic component is removed and thus it will recoil to recover the tissue's original shape.

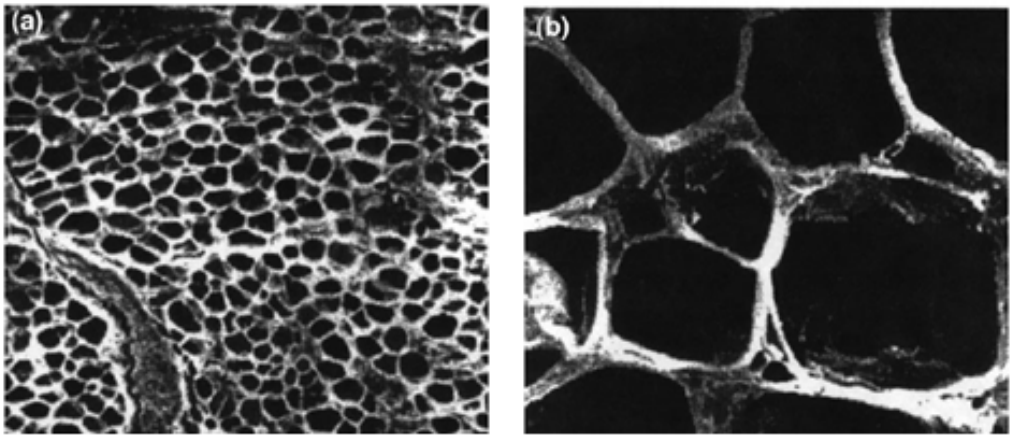

Figure 2.4: Histological images of the fat pad septal structure for the 1st metatarsal head. Images were taken from Brash (1999) (a) low power x100 (b) high power x650

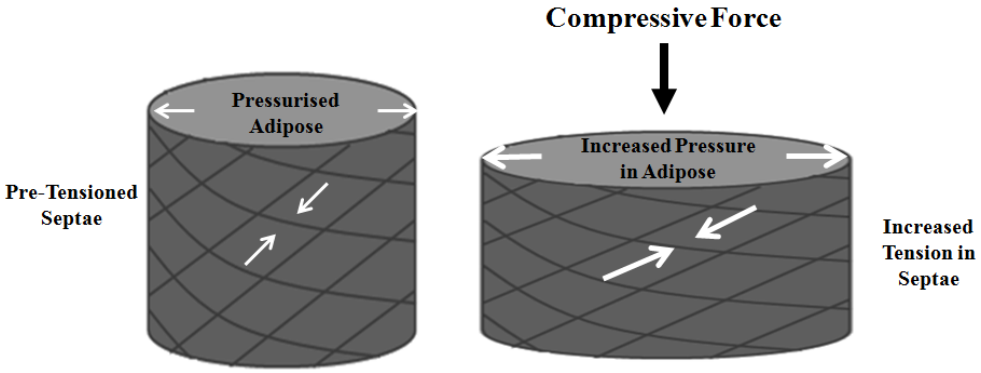

Figure 2.5: Arrangement of fibres in the closed cell hydrostatic structure of the fibroadipose globules.

2.4.2. Biomechanical Properties

Due to the wide range of previous methodologies used to test the plantar soft tissue and the range of methods which can be used to determine key features of the tissue's response, comparisons between studies were difficult.

Assessment of the unloaded tissue thickness and the peak strain permit knowledge of the compressive capacity which can be achieved during axial compression. The unloaded tissue

thickness from in-vivo studies tends to be between 12 and 19mm at the heel (Table 2.1). However an in-vitro study has reported lower tissue thickness (9.81mm) (Pai and Ledoux 2010, p. 20) and calculations based on other in-vitro papers which give an indication of the tissue thickness (radiographic images) also display a slightly decreased unloaded tissue thickness (Bennett and Ker 1990, Aerts *et al.* 1995). This suggests the heel in-vivo is sustained at a greater thickness, and this may be due to the perfusion of blood into the venous plexus of this area (Weijers 2005). The range of compressive capacity is reported as between 35 and 60% of the unloaded thickness (Table 2.1), suggesting a large variance is observed between studies. For studies conducted in normal walking gait and for those based on the loading conditions of normal walking gait the compressibility is slightly more consistent with a range of 35 – 50%, with a weighted average of 40.6%. The trend observed in the loading curve was consistent throughout the majority of the literature. An initially low stiffnes region which permits large tissue strain with little increase in stress, followed by an exponentially increasing stiffness such that the tissue becomes incompressible and the stress increases greatly (Figure 2.6). One key exception to this was the results of a study conducted for normal walking by Wearing (2009), in this study an initially high stiffness is found, followed by a levelling off of the curve and finally an increased stiffness as the tissue becomes incompressible (Figure 2.6). This suggests that the initial response during normal gait may differ from that observed using standard loading devices. However this trend was not observed in Gefen's study of walking gait, in which a similar device setup was used.

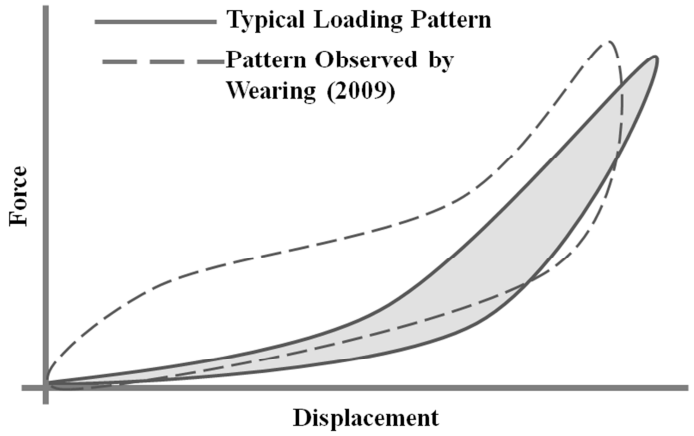

Figure 2.6:Typical Loading Patterns Reported for the Heel Pad.

Measurements of the secant modulus display a large range between studies, with no consistent pattern (Table 2.1). Due to the high dependence of this technique on the applied peak stress and strain at peak stress it is likely that any between study variance is a result of varying these loading conditions. This limits the use of this characteristic to within study comparisons, such as the variation between populations. Percentage differences observed between the secant modulus of different populations may provide a more valid cross study variable.

The derivation of the elastic modulus has not been widely used in the literature and the values reported differ by a considerable degree. The two studies assessed here are a material-based study conducted in-vitro (Ledoux 2007) and an in-gait study measured during normal walking (Gefen *et al.* 2001). These represent opposite ends of the spectrum for tissue property derivation and thus the observed difference is expected to be the result of the vastly different conditions under which the tissues were tested, and the varied modelling approaches used to evaluate the response of the tissue.

The percentage energy dissipated ranged from 17.8% to 90% in the assessed studies (Table 2.1). This wide variation has been explored previously within the literature (Aerts *et al.* 1995, 1996, Pain 2001) and the large percentage energy loss observed in some studies has been widely attributed to the inclusion of a 'lower leg' effect, in which energy loss within the tissues of the lower leg are incorporated into the measurements and thus the results of these studies do not represent the tissue specific response. When the studies which do not measure the specific changes to the tissue thickness throughout loading are removed the observed values ranged from 17.8% to 69% with a weighted average of 37%.

2.5. Factors known to affect Tissue Structure and Biomechanics

2.5.1. Effects of age

The process of ageing causes a decline in both metabolic and cellular functions of the body, leading to tissue atrophy and less capable organs and structures, which in turn become more susceptible to injury (Masoro and Austad 2006). In elderly western populations body fat composition is increased and muscle mass is reduced. This is due to a largely sedentary

Table 2.1.: Compiled Table of Biomechanical Characteristics of the Heel Pad for a range of Methodologies

Paper	Method type	Control type	Rate type	Frequency/Disp rate	n	UTT (mm)	Comp	Peak Load/Stress	Ktrend	S (kPa)	E	% EL
Ledoux 2007	Material - invitro	Disp Controlled T-Wave	Constant	0.01 - 10Hz	11	-	-	89.5kPa	Low - Exponential Inc	200	800 kPa	36.00%
Aerts 1995	Mechanical - invitro	Disp Controlled S-Wave	Variable	Impact vel 0.37m/s	4	-	-	-	Low - Exponential Inc	-	-	50.40%
Pai 2010	Mechanical - invitro	Disp Controlled T-Wave	Constant	0.02-0.2m/s !	4	9.81	50%	73.3kPa	Low - Exponential Inc	124	-	63.30%
Bennet 1990	Mechanical - invitro	Load Controlled S-Wave	Variable	0.1 - 70Hz	11	12.5 !	-	2kN	Low - Exponential Inc	-	-	28.60%
Ker 1996	Mechanical - invitro	Load Controlled S-Wave	Variable	5.5Hz	3	13.5 !	-	1.4kN	Low - Exponential Inc	-	-	32.80%
Tong 2003	Bulk Compression	Manual Stepped load	Static	-	21	15.5	35%	30N	Low - Exponential Inc	-	-	-
Zheng 2011	Bulk Compression	Manual T-Wave	Constant	0.006m/s	10	13.83	12%	80% BW	Low - Exponential Inc	-	-	-
Uzel2006	Bulk Compression	Manual Stepped load	Static	-	42	20	38%	BW	Low - Exponential Inc	-	-	-
Klaesner 2002	Manual Indentation	Manual T-Wave	Constant	20-30N/s	20	-	-	9N	Low - Exponential Inc	-	0.81 N/mm	-
Hsu 2000	Manual Indentation	Manual T-Wave	Constant	0.0006m/s	20	16.5	46%	74kPa	Low - Exponential Inc	168	-	27.00%
Hsu 2009	Manual Indentation	Manual T-Wave	Constant	0.006m/s	16	18.4	36%	78kPa	Low - Exponential Inc	221	-	-
Wang 1999	Manual Indentation	Manual T-Wave	Constant	0.0006m/s	5	18.42	40%	74kPa	Low - Exponential Inc	118	-	20.70%
Erdemir 2006	Mechanical Indent	Load Controlled T-Wave	Constant	0.0057m/s	20	18.6	50%	156kPa	Low - Exponential Inc	-	-	-
Alcantara 2002	Pendulum Impact	Accelerated Mass	Variable	Impact vel 0.64m/s	36	-	-	557.8kPa	Low - Exponential Inc	-	-	>80.00%
Weijers 2005	Pendulum Impact	Accelerated Mass	Variable	Impact vel 0.2-0.6m/s	11	-	-	-	Low - Exponential Inc	-	-	51 - 77%
Aerts 1995	Pendulum Impact	Accelerated Mass	Variable	Impact vel 0.2-0.8m/s	4	-	-	-	Low - Exponential Inc	-	-	65.40%
Cavanagh 1984	Pendulum Impact	Accelerated Mass	Variable	Impact vel 1m/s	10	-	-	338N	Low - Exponential Inc	-	-	85-90%
Declerq 1994	In-Gait (Run)	Subject Controlled	Variable	Impact vel 1.1m/s	2	14.9	60%	1835N	Low - Exponential Inc	-	-	-
Wearing 2009	In-Gait (Walk)	Subject Controlled	Variable	-	9	19.1	43%	246kPa	High - Med - Highest	580	-	69.00%
Gefen 2001	In-Gait (Walk)	Subject Controlled	Variable	Impact vel 0.06m/s !	2	12.15	35%	-	Low - Exponential Inc	214	175 kPa	17.80%
! Denotes figures calculated based on information within paper				Minimum	2	9.81	0.12			118		0.178
				Maximum	42	20	0.6			580		0.69

Abbreviations: n is the Number of subjects in the study; UTT is the Unloaded Tissue Thickness; Comp is the Compressibility; S is the Secant Modulus; Ktrend is the Trend in modulus throughout compression; E is the Elastic Modulus; %EL is the Percentage Energy Loss; BW is Body weight.

lifestyle coupled with natural hormonal and body composition changes which occur in the elderly (Masoro and Austad 2006).

2.5.1.1. The Effect of Aging on the Structure of the Plantar Soft Tissue

Breakdown of the organised honeycomb structure of the fat pads has been identified in the heel (Jahss 1992, Buschmann *et al.* 1995) and in the MTH (Brash *et al.* 1999). A central factor in the disruption caused within these tissues is the altered properties of collagen and elastin due to glycation (Jahss 1992, Paul and Bailey 1996). Collagen and elastin are affected by glycation in three main ways; (1) their ability to form aggregates or multi molecular fibres, (2) their charge profile and thus its interaction with cells and (3) their oxidation state.

The most important factor in terms of fat pad structure is the disruption to the ability to form aggregates (Figure 2.6). When glucose binds to the protein structure of collagen or elastin it blocks the normal binding site which prevents the formation of long multi-protein fibres (Figure 2.7). It also causes cross links to form at the middle of the proteins which can lead to clumps of collagen or elastin in nodular masses (Brash *et al.* 1999). These act to disrupt the regular structure of the tissue.

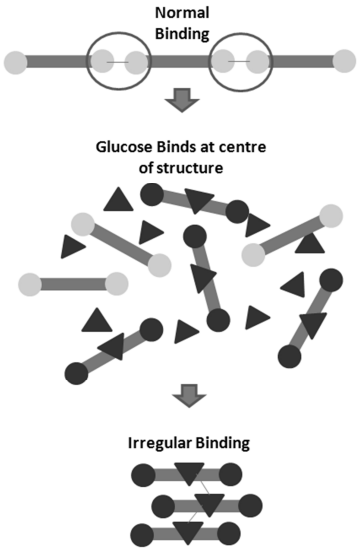

Figure 2.7: Mechanism for Disruption of Protein Binding.

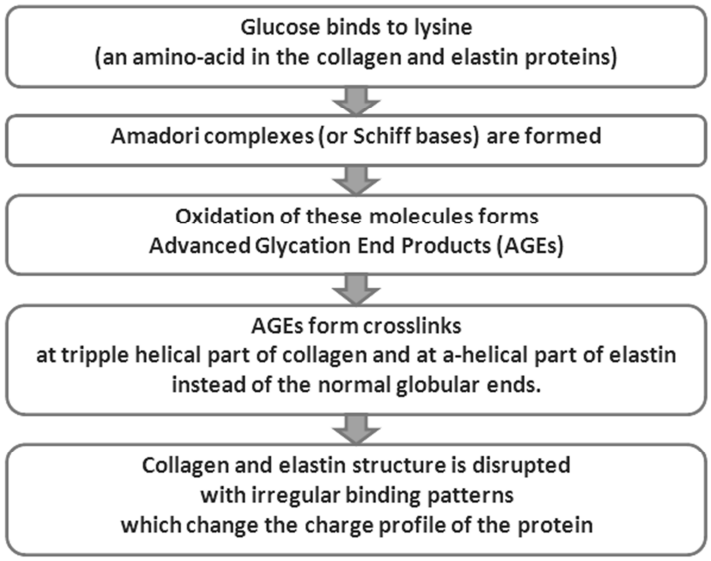

Figure 2.8: Glycation Pathway for collagen and elastin

2.5.1.2. The Effect of Aging on the Biomechanics of the Plantar Soft Tissue

Compressibility

For the heel region the absolute peak strain has been shown to be reduced in the elderly population when tested at low velocities suggesting a less compressible heel pad (Hsu, Wang, *et al.* 1998) (Table 2.2). When tested at high velocities it has been suggested that this peak strain is increased (Alcántara 2002), however the pendulum system used in this study does not permit tissue specific measurement of displacement, and thus increased displacement of the leg as a whole may account for the differences observed. For the MTH region the peak strain has been shown to be lower in the elderly population at both low and high velocities (Hsu 2005).

Stiffness

For the heel region the linear stiffness of the plantar soft tissue, assessed at low velocities, has been shown to be greater in healthy elderly populations when compared to healthy young populations (Hsu, Wang, *et al.* 1998, Chao *et al.* 2010) (Table 2.2). At other regions of the foot (MTH region) the linear stress-strain behaviour has also been shown to be greater in the elderly population (Kwan *et al.* 2010). However, when assessed at high velocities using a pendulum system the inverse has been shown (Alcántara 2002) highlighting the rate dependent nature of the tissue. The elastic modulus has been shown to be greater in the elderly population when assessed at low velocities (Zheng *et al.* 2000), and has also been shown to be greater in this population when calculated across a range of loading rates (Gefen *et al.* 2001, Hsu 2005) suggesting isolation of elastic and viscous components may give a clearer image of the change which has occurred.

Percentage Energy Loss

For the heel region the Percentage Energy Dissipated has been shown to be greater in the elderly population when tested at low velocities (Hsu, Wang, *et al.* 1998) suggesting a greater capacity for shock absorption exists in the elderly tissue. However, when tested at high velocities using a pendulum system no significant difference is found (Alcántara 2002) this may be the result of the inclusion of whole lower leg response to the pendulum and not specific response within the heel region. At other regions of the foot (MTH region) the Percentage Energy Dissipated has been shown to be greater in the elderly population when tested at both low and high velocities (Hsu 2005).

2.5.2 Effect of Pathology

As with the processes of natural aging, pathology can have a large effect on the mechanical capacity of a tissue due to atrophy within a tissue's structure. In the case of the plantar soft tissue even small negative changes to the structure of the tissue can result in a large loss of function. The effect of Diabetes has been studied due to the prevalence of ulceration within the plantar soft tissue (R. Sopher, J. Nixon, E. McGinnis, and A. Gefen 2011a). To effectively treat or manage a condition such as Diabetes it is necessary to gain a full understanding of the mechanisms which lead to loss of function and in the case of ulceration, eventual tissue breakdown.

2.5.2.1. The Effect of Diabetes on the Structure of the Plantar Soft Tissue

Diabetes has been associated with increased activation of glycaton pathways in many tissues (Paul and Bailey 1996), and thus the effect of this disease on the plantar soft tissue is similar to the changes seen naturally with age, however at a much greater level. This can have a severe impact on the structure of the plantar soft tissue. Histomophological studies of the heel and forefoot regions of individuals who had suffered from diabetes displayed significant increases in amount of fibrous septae present (Brash *et al.* 1999, Wang *et al.* 2011). Observations of the tissue sections also showed fragmentation and disruption of the regular fibrous structure (Brash *et al.* 1999), (Figures 2.4 and 2.9). The size of the fatty globules also tended to be larger (Wang *et al.* 2011) in the diabetic tissue, however their number was generally reduced (Brash 1999).

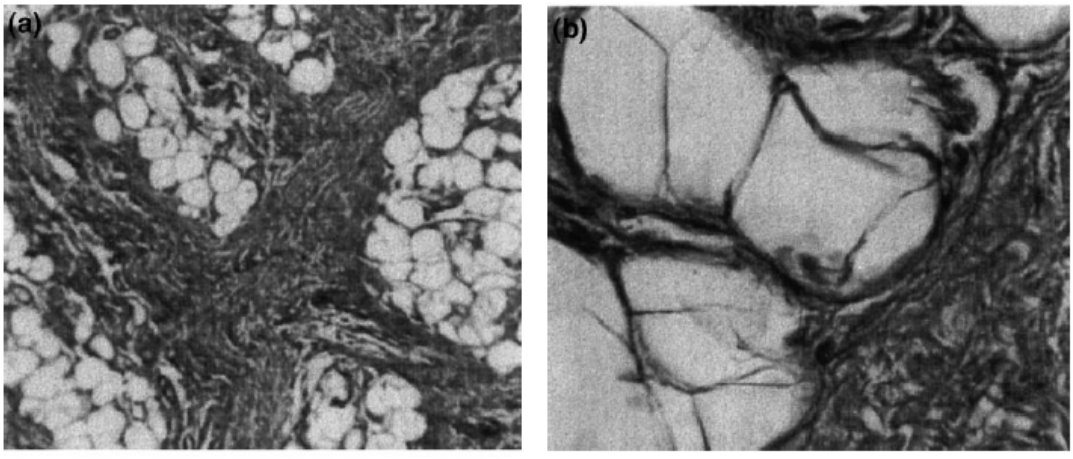

Figure 2.9: Histological images of the fat pad septal structure for the 1st metatarsal head of Diabetic neuropathic subjects. Images were taken from Brash (1999) (a) low power x100 (b) high power x650

2.5.2.2. The Effect of Diabetes on the Biomechanics of the Plantar Soft Tissue

Compressibility

Previous studies have shown the tissue in individuals with diabetes to be generally thicker than that of healthy control individuals (Table 2.2); however the effect of this on the measured compressibility of the tissue has been varied. Reductions of up to 40% have been observed in bulk compression experiments, while slight increases of up to 6% have been observed for mechanical studies conducted in-vitro. The variance observed for compressibility may be related to the large range of methods used to characterise the plantar soft tissue.

Stiffness

A general increase is reported in the secant modulus of the plantar soft tissue across a wide range of assessment techniques, and for a range of loading rates (Table 2.2). Due to the structurally similar changes which occur in the plantar soft tissue with age and as a result of diabetes, it is expected that these increases in tissue stiffness represent a similar mechanism as that observed in ageing. However the presence of an increased stiffness at both low and high displacement rates suggests that changes have occurred which effect both the elastic and viscous responses of the fat pads. This is confirmed by the observations made in the structural studies, which displayed significant disruption to these components.

Percentage Energy Loss

The percentage energy dissipated at the heel was shown to be greater in subjects with diabetes across the range of studies identified and for a range of loading conditions, with increases ranging from 10 to 35% (Table 2.2). Due to the energy loss within a tissue being linked to the viscous component of the tissue's response, the observed increases in this variable give further evidence to the hypothesis that structural change has affected both the elastic and viscous element of the plantar soft tissue's response to load.

2.5.3. Effect of Gender

The function of the foot and plantar soft tissue in both genders is identical and as a result it is expected that little variation will occur within the mechanical properties of the tissues. However previous studies have reported differences in the mechanical properties between the

Table 2.2: Factors That Affect Plantar Soft Tissue Properties.

Factor	Paper	n	Unloaded Tissue Thickness (mm)			Compresibility			Tissue Stiffness (kPa)			% Energy Loss		
Gender		(M:F)	Male	Female	% Diff	Male	Female	% Diff	Male	Female	% Diff	Male	Female	% Diff
	Alcantara 2002	(27:27)	-	-	-	-	-	-	82.23	78.03	-5.38%	84.33	82.33	-2.43%
Age		(Y:E)	Young	Elderly	% Diff	Young	Elderly	% Diff	Young	Elderly	% Diff	Young	Elderly	% Diff
	Hsu 1998	(20:13)	17.6	20.1	12.44%	0.46	0.38	-21.05%	3.76	3.97	5.29%	23.7	35.3	32.86%
	Kwan 2010	(7:17)	20.88	22.49	7.16%	-	-	-	32.4	76.7	57.76%	-	-	-
	Alcantara 2002	(36:18)	-	-	-	-	-	-	85.15	70.1	-21.47%	83.4	83.2	-0.24%
Diabetes		(C:D)	Control	Diabetic	% Diff	Control	Diabetic	% Diff	Control	Diabetic	% Diff	Control	Diabetic	% Diff
	Zheng 1999	(4:4)	12	15	20.00%	-	-	-	40	45	11.11%	-	-	-
	Hsu 2000	(20:21)	16.5	17.8	7.30%	0.45	0.45	0.00%	168	170	1.18%	27.9	43.2	35.42%
	Pai 2010	(4:4)	-	-	-	0.51	0.54	5.56%	502	846	40.66%	60	67	10.45%
	Hsu 2009	(28:29)	18.4	19.3	4.66%	0.37	0.34	-8.82%	221	241	8.30%	-	-	-
	Hsu 2002	(20:21)	-	-	-	-	-	-	-	-	-	27.9	36.1	22.71%
	Tong 2003	(21:17)	15.5	16.1	3.73%	0.35	0.25	-40.00%	-	-	-	-	-	-

genders; differences have been largely attributed to the size (tissue thickness) and structural differences due to the influence of chemical/hormonal factors.

2.5.3.1. The Effect of Gender on the Structure of the Plantar Soft Tissue

The unloaded tissue thickness has been shown to be greater in male subjects when compared to female subjects (Prichasuk *et al.* 1994). It has been suggested that this is the result of increased concentrations of growth hormone in men (Rome 1998). Studies on tendon and ligaments have shown changes to the levels of collagen within tissue as a result of the hormone oestrogen (Nordin and Frankel 2001). Because the level oestrogen is greater in females it has been suggested that the concentration of collagen within the septal walls of the fatty pads may also vary between genders (Rome 1998); however no structural studies exist to confirm this.

2.5.3.2. The Effect of Gender on the Biomechanics of the Plantar Soft Tissue

Only one study could be identified which assessed the difference between genders for the biomechanical properties of the plantar soft tissue. Alćantara (2002) reported a significant increase in the stiffness (average across loading) and the Percentage Energy Dissipated for the heel region in males when tested at high compression rates using a pendulum system (Table 2.2). This relationship was present between genders in both young and elderly populations (Alcántara 2002).

2.6. Conclusion

The plantar soft tissue is a highly adapted viscoelastic tissue with a hydrostatic structure. This complex structure makes it capable of dampening impact forces and resisting compression, whilst also permitting recovery of shape when offloaded, allowing for multiple consecutive cycles to occur without the loss of functionality. To characterise the tissue effectively it is necessary to measure both the stress and strain which occur within the tissue during

compression. To fully understand the tissue's rate dependent nature it is necessary to evaluate the measured stress-strain relationship throughout the functional range of compressive rates. Thus for the plantar soft tissue testing must be conducted at rates analogous to those experienced in gait. The achievement of these criteria requires a novel device composed of three elements: (1) A drive system with accurate and repeatable movement even at high rates of displacement. (2) A load cell which is in series with the specific region of interest. (3) An imaging method which permits measurement of the tissue thickness throughout loading in a repeatable manner.

Statement of Problem

The key limitations which arose from the literature review were:

Loading rates and peak loads used to derive tissue properties are below the levels experienced in normal walking.

Many of the controlled in-vivo studies have applied low loads at slow rates using simple or manually driven devices (Zheng *et al.* 2000, Klaesner *et al.* 2001, Hsu 2005, Erdemir *et al.* 2006). Devices such as this are very applicable to clinical assessments with fast test methods and simple mechanical property derivation permitting easy inter-subject comparisons. However, due to the rate-dependent nature of the plantar soft tissue, the properties derived are limited to the range in which they are tested. Therefore previous controlled compression studies do not allow us to fully understand the tissue's ability to respond to a more complex mechanism such as walking.

No standard methodology for locating anatomical sites

The large range of methodologies used and the variance in the size of the indentation/compression platen have resulted in a lack of standard methodology for location of a loading site at which to collect data for tissue displacement and load. The use of load measured for a whole region has resulted in the derivation of less specific tissue properties.

Research Questions

Following the assessment of the literature and statement of problem the research questions were identified to provide focus to the PhD work.

1. Which properties of the plantar soft tissue are most sensitive to variation in the applied loading routine?
2. Are differences between populations (Gender, Age) present within the mechanical properties of the plantar soft tissues?

The work within this PhD will provide a greater resolution and understanding of the rate dependent nature of the plantar soft tissue and the specific effects of this on the derived mechanical properties. The combined assessment of properties across a wide range of loading conditions will allow an understanding of the relationship between the tissue's response at low rate and at high rates of compression. This will act to inform the selection of appropriate methodologies for assessment of tissue properties, and provide a relevant context for mechanical properties derived for either low or high rate conditions alone.

Part A

Device Development

&

Evaluation

A.1. Introduction to Part A: Development

A.1.1. Objectives of Part A

The work within part A of the thesis has a focus on the design, development and evaluation of both (a) a device capable of applying compression to the plantar soft tissue whilst recording data which will be used to characterise the response of the tissue, and (b) a novel loading protocol which aims to assess the full functional range of the plantar soft tissue, providing a broad basis for comparison to previous studies and for the development and rigorous testing of analytical models.

The main objectives of the work within this part of the thesis were to:

- Design a device capable of compressing the plantar soft tissue in a controlled and repeatable manner.
- Develop profiles to be used to drive the device which permit the response of the tissue to be characterised for the full functional range.
- Evaluate the performance of the device and developed profiles and validate this against a known standard.

A.1.2. Assessment of Device Requirements

Prior to the development of a device to test the plantar soft tissue, and the selection of device components for measurement of the tissue's response during compression, it was necessary to evaluate the requirements of such a device. To address the research aim of testing the plantar soft tissue for a range of loading conditions, an assessment of the normal range of loading experienced within the tissue during gait was conducted. This provided a basis for the selection of an appropriate mechanism to drive the developed device and for the evaluation of the controlled system which would be used for operation of the selected drive mechanism. Finally the requirements of the measurement apparatus used to record the response of the plantar soft tissue were assessed in reference to the loading conditions and operational ranges to which they will be applied.

A.1.2.1. Properties of Gait

The foot is a dynamic structure with a complex arrangement of internal joints and muscles. Throughout the gait cycle the foot constantly adapts to adopt a position that may progress motion from foot contact to push off.

A.1.2.1.1. Temporal Parameters of the Walking Gait Cycle

The gait cycle can be divided into phases based on temporal parameters such as contact times (J. Richards 2008a). The stance phase accounts for 0.58s (~60%) of each walking gait cycle, while the swing phase accounts for 0.43s (~40%) (Titianova *et al.* 2004, J. Richards 2008a).

The stance phase can be further divided based on the temporal characteristics of plantar pressure measurements as: initial contact (IC), forefoot contact (FFC), foot flat (FF) and forefoot push-off (FFPO) (De Cock *et al.* 2005) (Figure A.1.1).

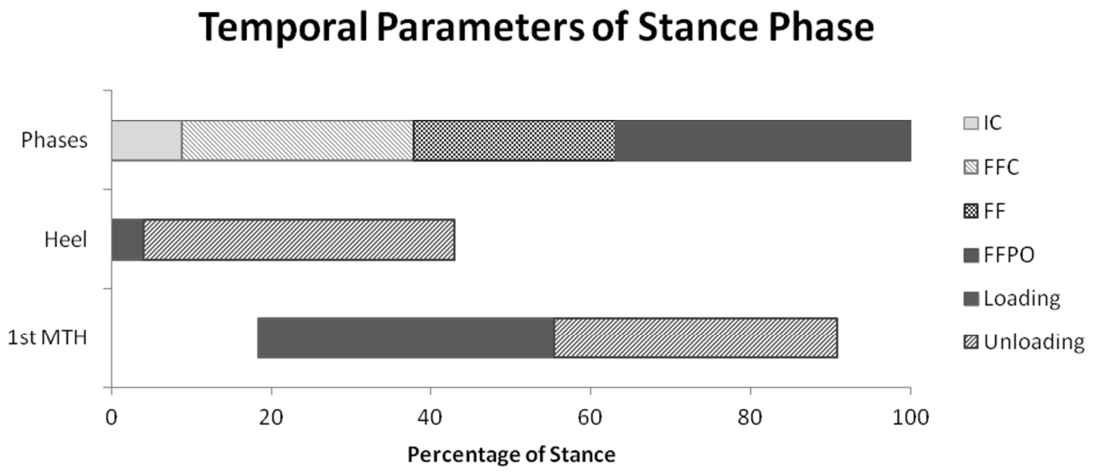

Figure A.1.1: Temporal Parameters of the Stance Phase for the Heel and 1st MTH. Legend Abbreviations: IC-Initial Contact; FFC-Forefoot Contact; FF-Footflat; FFPO- Forefoot push off

For the study of foot region it is important to further define the temporal characteristics of the stance phase. The heel region makes contact with the ground first in normal walking; a rapid period of loading occurs to peak load in only 4% of total stance time, followed by a prolonged period of unloading to heel off which occurs at 42% stance (De Cock *et al.* 2005). The 1st

MTH region makes contact with the ground at 18% of total stance and undergoes gradual loading to a peak load at 55% stance. Following peak load a gradual unloading occurs to final contact at 91% stance (De Cock *et al.* 2005).

A.1.2.1.2. Motion of the foot and Joints

When the foot is taken as a whole, the ankle joint motion can be taken as the movement of the foot about the tibia. At initial contact, the ankle joint is in the neutral position and a short period of plantar flexion occurs (3-5^{o}) until the foot is brought back to the neutral position at approximately 20% of the gait cycle in preparation for the foot flat phase (Trew and Everett 2001, J. Richards 2008a). From the foot flat position dorsiflexion occurs (10^{o}) as the tibia moves over the foot leading to heel lift at approximately 50% of the gait cycle (Trew and Everett 2001, J. Richards 2008a). The raised heel brings the foot into plantar flexion (20^{o}) at 60% of the gait cycle when toe-off occurs (Trew and Everett 2001, J. Richards 2008a). Throughout the swing phase the foot is brought back to the neutral position in preparation for heel strike.

A.1.2.1.3. Temporal parameters of the Ground Reaction Force

During stance the body's weight is transferred to the ground and ground reaction forces (GRF) are imposed on the body. If the whole foot vertical GRF profile is inspected, four phases of foot loading can be distinguished (Figure A.1.2): heel strike to first peak (GRF1), first peak to trough (GRF2), trough to second peak (GRF 3) and second peak to toe-off (GRF 4) (J. Richards 2008a).

For greater resolution of the GRF response Harris etal (1996) used dosimeter load cells (2.5cm diameter) specific to the heel and 1st MTH regions. The heel sensor was shown to bear the highest load (30% Body Weight), while the 1st MTH sensor detecting 11% body weight at its peak (Harris *et al.* 1996). A preliminary gait study in which subjects were asked to target the force plate with either the fore or rear foot showed the rear-foot to play a role in the initial contact and then gradually offload, with the forefoot becoming initially loaded early into stance; however not reaching peak load until approx. 80% stance and then rapidly offloading (Figure A.1.2).

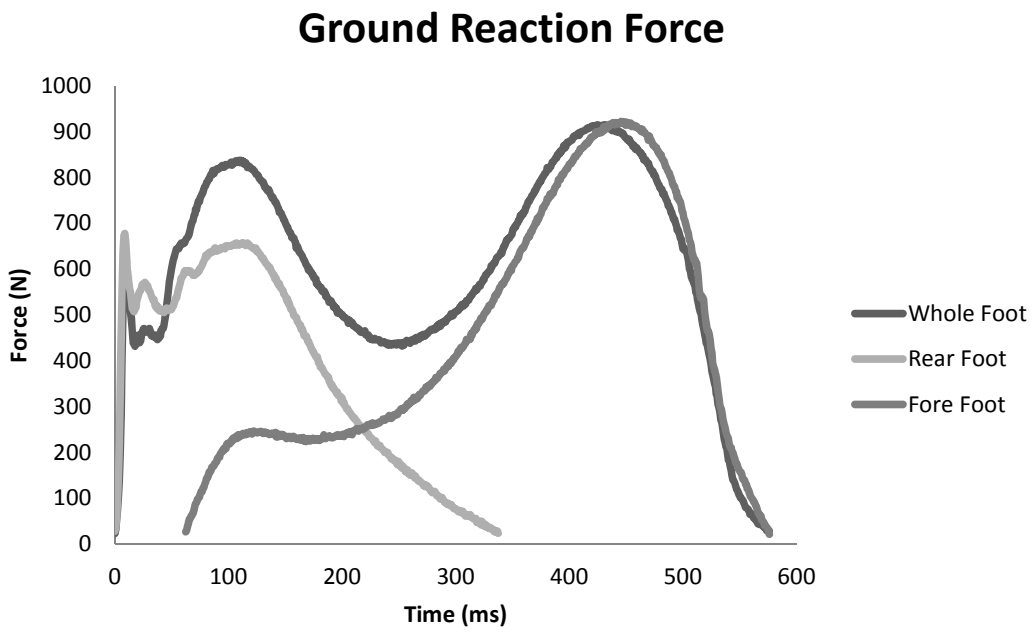

Figure A.1.2: Ground Reaction Force profiles for the whole foot, rear foot and forefoot during normal walking.

A.1.2.1.4 Implications on the Selection of a Drive Mechanism

The distinctions found between the rear-foot and the forefoot highlight the need to apply a loading profile specific to each region to fully capture the functional range of the tissue. To fully explore the functional response of the tissue a profile with a variable rate of compression based on gait motion is required. The time to peak load, rate of compression and peak force for the rear foot represents a rapid, high force loading response which should be taken into account when assessing the appropriate drive mechanism. The short duration of loading and unloading time require measurement apparatus with a high temporal resolution to permit effective characterisation of the tissues response to dynamic compression. To ensure the device has scope beyond the work within this study, the specification of the device will act to consider both the rear foot and the forefoot motion.

A.1.2.2. Application and Control of Tissue Compression

The review of the literature (Chapter 2), and assessment of normal gait (A.1.2.1) have highlighted the need for a device which can apply controlled and uniform tissue compression at rates within the functional range of the tissue. These requirements point to a method which

combines bulk compression of the tissue and the use of a mechanical drive system which can be controlled accurately.

A.1.2.2.1. Non-actuated systems

Tissue compression can be achieved without the use of a complex mechanical drive system by utilising a pulley or pendulum setup (Frederick 1984, Alcántara 2002, Weijers 2005). The benefits of this method of tissue compression are the highly adaptable nature of a system which depends solely on Newton's second law of motion (Force = mass*acceleration). Thus under the constant acceleration of gravity adjustment of the mass will result in an increased force (Weijers 2005). Adjustment for the distance from tissue impact at release of the mass will also permit the velocity at impact to be varied according to velocity = acceleration*time (Weijers 2005). However this system is limited by the simplicity of its control, following release of the mass from the chosen distance all further control is removed and following impact the pendulum will slow down and eventually come to a stop preventing the application of multiple compressive cycles.

A.1.2.2.2. Actuated systems

Actuated drive systems include the use of a wide range of rotary or linear motors to provide controlled displacement throughout tissue compression. The main systems of interest for application to testing of the plantar soft tissue are stepping motors and servo motors.

Stepping motors can be used in combination with Ball screw systems to convert rotary motion of a motor used to drive a screw into the linear motion of a nut which travels along the length of the screw. The motion of the nut is smoothed by the use of ball bearings which increase efficiency and reduce wear within the system. These systems can provide displacement control based on the number of steps or parts of a rotation which are conducted. For example a single step of ¼ rotation may result in 0.1mm linear displacement thus for a 10mm displacement 100 steps are required. Both constant rate and variable rate profiles can be created to permit controlled compression of a tissue to be conducted (Hsu *et al.* 2009). The main limitation of these actuators is their lack of feedback control. When high resistance to displacement occurs, steps may be missed which results in position error which cannot be corrected.

Servo motors can also be used in combination with ball screw systems and are commonly found in material testing machines. These systems have previously been used extensively to derive the mechanical properties of the plantar soft tissue (Bennett and Ker 1990, Ker 1996, Erdemir *et al.* 2006, Ledoux 2007, Pai and Ledoux 2010). The benefit of a servo-motor over a stepper motor is the capacity for feedback control; this reduces the positioning errors which occur during motion against high resistance, which is a large factor of compression testing. The use of feedback control also permits the variability of the input loading routine to be increased, allowing complex profiles similar to the dynamics of gait to be developed.

A.1.2.2.3. Implications for Device Design

The capacity of Servo-motors to permit a wide range of loading profiles to be used to drive the device, and the increased performance associated with an adaptive feedback control suggest they are ideally suited for testing the plantar soft tissue across a large range of conditions.

A.1.2.3. Measurement of tissue compression

To understand the response of the tissue when subjected to the range of loads and displacement velocities discussed (A.1.2) an accurate and reliable technique must be used to measure both the tissue compression and the load applied for the specific region compressed. An effective compression measurement method must be capable of both high temporal resolution, due to the short phases of gait present in each foot region, and high accuracy, due to the small incremental displacement as the tissue nears incompressibility. The load measurement must also be capable of providing high temporal resolution and accuracy, but must also be made specific for the region of interest.

A.1.2.3.1. Tissue Compression Measurement

The range of imaging modalities which have previously been employed to measure the compression within the plantar soft tissue during loading has been large (Petre *et al.* 2008).

Each method of measurement has its own benefits and limitations when utilised for the assessment of the plantar soft tissue.

Whole Segment Displacement

The tissues response to compression can be measured by external means alone. This technique has been used extensively for pendulum impact studies in which the acceleration of a ballistic pendulum is used to derive the displacement pattern using integration (Frederick 1984, Alcántara 2002, Weijers 2005). This method has also been used for indentation studies where the motion of the indenter alone was measured (Rome and Webb 2000, Klaesner *et al.* 2001). The main limitation of this form of tissue compression measurement in the context of the plantar soft tissue is the inability to isolate compression occurring within the tissue from the compression/motion for the leg as a whole. It is also impossible to locate internal structures such as the apex of the calcaneus using external features alone, making the variance of application between subjects greater. The main benefits of this method are the reduced equipment required to conduct the tissue testing, and the ease at which these techniques can be adapted to portable devices making study design and application of the device much easier (Rome and Webb 2000).

Dynamic X-ray Imaging

X-ray fluoroscopy and Cineradiography both utilise X-ray radiation to produce images of a tissue in real time and can be recorded dynamically to allow imaging of a tissue throughout compression. X-rays can be projected and can travel in air permitting a tissue to be measured without contact from an imaging probe; this makes positioning and isolation of features easy even during in-gait testing (De Clercq 1994, Gefen *et al.* 2001, Wearing *et al.* 2009). Because X-ray images are a result of absorption of the transmitted rays within high calcium regions of the body (Suetens 2002), isolation of the soft tissue from the underlying bone is achieved easily. However this also acts to limit the resolution of X-ray techniques when assessing the response within the soft tissues, with images representing a single layer and not displaying the boundaries between tissue layers. The radiation used in X-ray imaging can be harmful to tissues in high doses; this restricts the time over which tests can be conducted and requires the use of heavy protective clothing (De Clercq 1994). A large restriction in the use of X-ray

systems is the relative expense of the equipment required for testing and the lack of portability afforded within a fluoroscopy or cineradiography systems, which make adaptation of these systems to research involving large subject numbers difficult.

Magnetic Resonance Imaging

Magnetic Resonance Imaging (MRI) utilises the response of atoms within a tissue, when subjected to a magnetic field, to visualise the tissue structure (Suetens 2002). This technique is non-harmful and is generally used to produce static 3-Dimensional (3D) images of a tissue with a high spatial resolution. The ability to image in 3D provides a greater level of detail when assessing a tissues response to load permitting shear and bulging to be observed as well as compression in the vertical direction (Petre *et al.* 2008). However testing using MRI is restricted to a small imaging volume and the use of high power magnetic fields means no metallic parts can be used to induce tissue compression. This restricts the test methods to static loading conditions and does not permit the dynamic loading response of the tissue to be assessed. The advances in real-time MRI have proven applicable to the measurement of soft tissue motion (Asakawa *et al.* 2003), however this technology is not easily accessible as a measurement method.

Ultrasound Imaging

The most widely used technique for measuring tissue thickness is Ultrasound imaging (Cavanagh 1999, Wang *et al.* 1999, Tong 2003, Hsu 2007, Hsu *et al.* 2009). Ultrasound provides a non-ionising, non-harmful, method of imaging internal structures by utilising sound waves with frequencies greater than 20 kHz (Suetens 2002). Images can be observed in real time and can be recorded dynamically allowing the full response of a tissue to compression to be imaged. The spatial resolution of clinical ultrasound devices is lower than that seen for MRI, however it is able to provide effective identification of structures and layers within the tissue being imaged, permitting compression of a specific tissue to be measured. The greatest restriction with clinical ultrasound is the requirement for constant contact during imaging; when the ultrasound probe is removed from the surface of the tissue the image is lost. Due to the thin, 2-Dimensional image which is acquired using ultrasound, it

can be difficult to find and maintain the position of a feature of interest between multiple compressions, which may affect the consistency of measurement (Cavanagh 1999).

A.1.2.3.2. Tissue Load Measurement

The previous literature has reported three methods of measuring the load across the plantar soft tissue during compression; for the tissue as a whole using force plate systems (De Clercq 1994), for a region of the tissue using bulk compression, at the heel or forefoot (Zheng *et al.* 2012b) and for a specific point on the surface of the soft tissue using indentation (Zheng *et al.* 2000, Klaesner *et al.* 2001). The methods suggested have increasing specificity with decreasing contact area, with the smallest indenter systems able to detect loads specific to the area below the apex of the calcaneus. The advantage of this level of specificity over a whole region assessment is due to the concentration of stress beneath the bony prominences in the foot which occur during compression (Chen 2001, Spears 2005). The tubercle which forms the apex of the calcaneus acts as a base through which load is transferred from the skeleton to the ground during walking, thus the region of tissue which lies in the normal direction to the transferred load will receive the greatest compressive force, while the regions surrounding this will receive a lesser distributed force (Spears 2005). Effort should be made to measure the force at the focal point of the load; i.e. in the normal direction to compression, in line with the apex of the calcaneus and specific to an area no bigger than that of the calcaneal tuberosity.

A.1.2.3.3. Implications on Device Design

The most appropriate method of imaging for this study is Ultrasound, due to its ability to record dynamic tissue compression specific to a tissue region of interest and the portability and adaptability of ultrasound systems for use in clinical and lab based environments. Due to the thin 2D section and ability to measure compression for a single point such as the calcaneus apex using ultrasound, the most appropriate load measurement method would be to provide the greatest degree of region specificity.

A.1.3. Conclusions

Following an assessment of the parameters of gait and an evaluation of the available device drive mechanism and measurement components, a combination of a servo-motor drive, ultrasound imaging and specific region load have been identified as the ideal elements of a bespoke device to characterise the plantar soft tissue. The use of a highly adaptive feedback controlled system such as the servo motor will permit the plantar soft tissue to be dynamically tested for a range of compression profiles with a high level of accuracy. Furthermore, the combination of compression load and tissue displacement measurement for a single location will permit effective characterisation of the soft tissue response at the site within the plantar soft tissue which has the greatest internal stress.

A.2. Specification

A.2.1 Initial Requirements

Based on the literature and statement of problem there are four key features required of a device to assess the plantar soft tissue under conditions akin to normal walking. (1) The ability to compress a whole tissue region uniformly, via bulk compression; requiring the interface between the device and the tissue to have a large surface area. (2) The capacity to measure and record the load which is applied during compression; this must be specific to the region of interest. (3) The capacity to measure and record the displacement which occurs within the tissue region during compression; this must be specific for the tissue of interest and not include compression which occurs in auxiliary tissues. (4) The device must be capable of applying a loading profile based on displacement and velocity parameters; this must permit a large range of loading rates and produce repeatable tissue compression. The profiles used to drive the device must also be capable of generating realistic tissue loading and must be comparable to ground reaction force data.

A.2.2. Initial Device Concept

Prior to The full device development initial device concepts were proposed. These concepts provided the basis for the specification of the device proper and allowed for the assessment of the requirements of a drive system.

A.2.2.1. Tissue Compression

The device platen will be composed of two sections which will move as one permitting bulk compression of the foot segment (Figure A.2.1). A large section 15x15cm will permit the whole foot region to be compressed while a small central section (15mm diameter) which is isolated from the large indenter will permit a separate path for load.

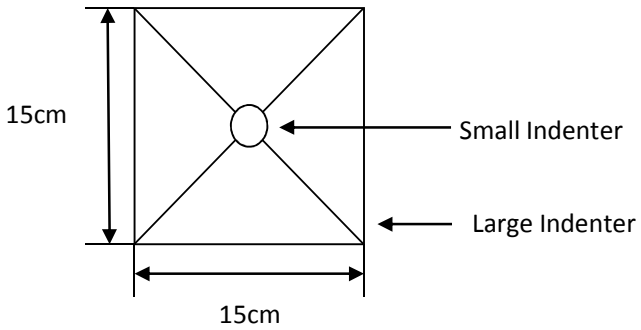

Figure A.2.1: Loading Platen Schematic

A.2.2.2. Measurement Apparatus

To allow effective characterisation of the mechanical properties of the plantar tissue, the device requires an imaging method and a method of load measurement.

The imaging method must be capable of:

- Producing high resolution images of the plantar soft tissue with an accuracy of at least 0.1mm.
- Must be capable of penetrating plastic and tissue to depth of at ~30mm; permitting hard interfaces to be used on the top plate of the platen.

The load measurement device must be:

- Capable of dynamic output which can be split to allow data logging and feedback to provide safety functions within the drive mechanism.
- Able to provide single axis loading to an accuracy of 0.5N.
- Be small in size to reduce the overall vertical height of the system; controlling the height to which the subject must be elevated for testing.

A.2.2.3. Drive Mechanism

The mechanism selected to drive the platen must be able to replicate the loading patterns and peak loads seen in gait and thus must be able to operate in the following ranges:

- Platen motion will be in the vertical direction and permit a minimum of 2cm of displacement (based on a heel pad thickness of 17mm (Ledoux et al, 2007).

- The mechanism must be capable of supporting the body weight of an individual, thus based on testing of healthy individuals a static minimum load of 100kg is required.

A.2.3 Assessment of Gait Parameters

A.2.3.1. Meta-Analysis

To assess the requirements of a drive mechanism, a small meta-analysis of standing and walking studies was conducted (Table A.2.1). In terms of device selection the key factors are the short loading time (<0.1s) and the large potential loads (+450N). To match these short loading times it is expected that a device would need to be capable of producing large velocity and accelerations. The device design should be robust enough to bear both the static weight of the subject and the high dynamic loads generated by tissue compression at rates equivalent to gait.

Table A.2.1: Gait Characteristics for Heel

Standing Studies	References	Units	Values
Contact Area	1	cm^2	39.1
Tissue Depth	2	mm	17.1
Peak Pressure	3	kPa	78
Walking Studies	**References**	**Units**	**Values**
Contact Time	1,4,5	s	0.410
Non Contact Time	#-5	s	0.585
Loading Time	#-6	s	0.096
Unloading Time	#-6	s	0.319
Peak Load	1,6	N	478.7
Peak Pressure	1,6	kPa	259.7

Table A.2.1: Meta analysis: Data compiled from 1. Putti (2009);2. Ledoux(2004);3. Rozema (1996);4. Bosch(2009);5. Titanova (2004);6. Harris (1996); # denotes data which have been calculated based on a reference.

A.2.3.2. Maximum Velocity and Acceleration

To gain a greater understanding of the kinematics specific to tissue compression and provide realistic limits for device selection, typical curves from two in-gait studies were explored. The deformation profiles from a rear foot study conducted using X-ray cinematography (Gefen *et al.* 2001) and the deformation profiles from a forefoot study using ultrasound (Cavanagh 1999) were used. The typical curves presented by these studies were fit with Sine waves to estimate the peak loading and unloading velocities and accelerations experienced in tissue compression.

The Sine wave equation utilised was:

$$y_{(t)} = A*\mathrm{Sin}(wt + \varphi)$$

For which:

$$w = 2\pi f$$

$$f = 1/p$$

The derivatives of the sine equation give:

$$\text{Maximum Velocity} = A*w$$

$$\text{Maximum Acceleration} = A*w^2$$

Where:

Parameter	Symbol	Units
Amplitude	A	mm
Frequency	f	Hz
Angular Frequency	w	rad/s
Time	t	s
Period	p	s

Study A: Deformation at Heel, taken from Gefen 2001

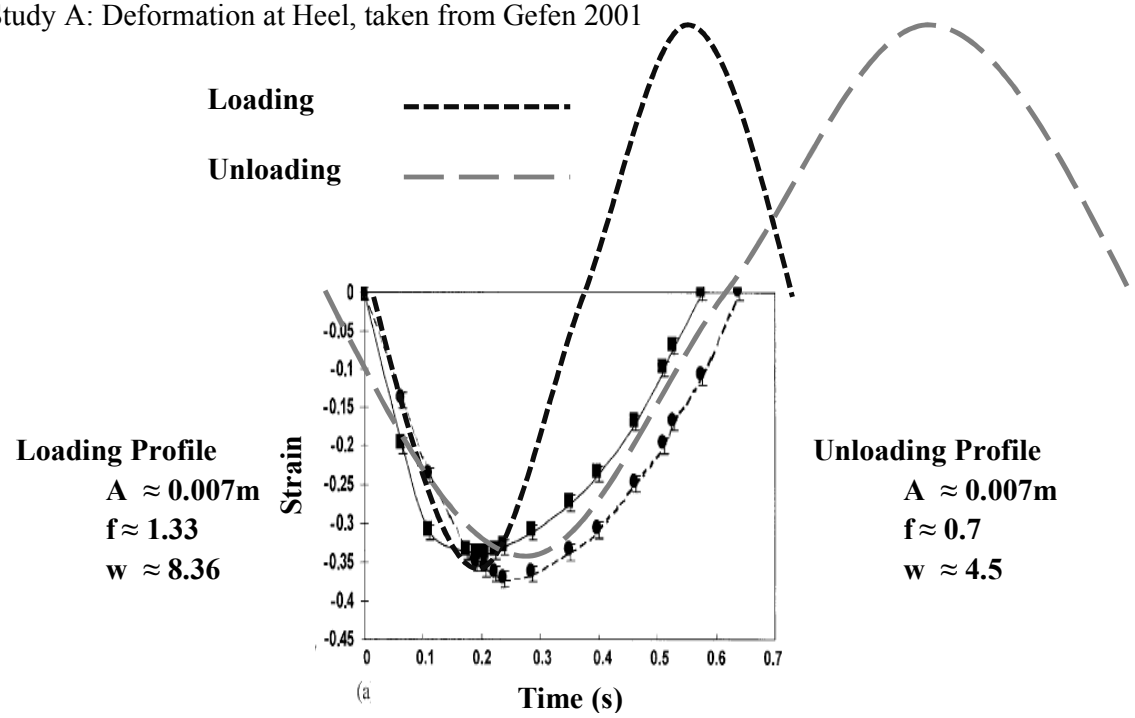

Figure A.2.2: Walking deformation of Heel measured using X-ray images

The maximum velocity for the sine curve fit to the typical data for the heel was 0.059m/s and the maximum acceleration was 0.49m/s^2 (Figure A.2.2). The derived values for the unloading profile were lower with a maximum velocity of 0.032m/s and maximum acceleration of 0.14m/s^2 (Figure A.2.2).

Study B: Deformation at 1st MTH, taken from Cavanagh (1999)

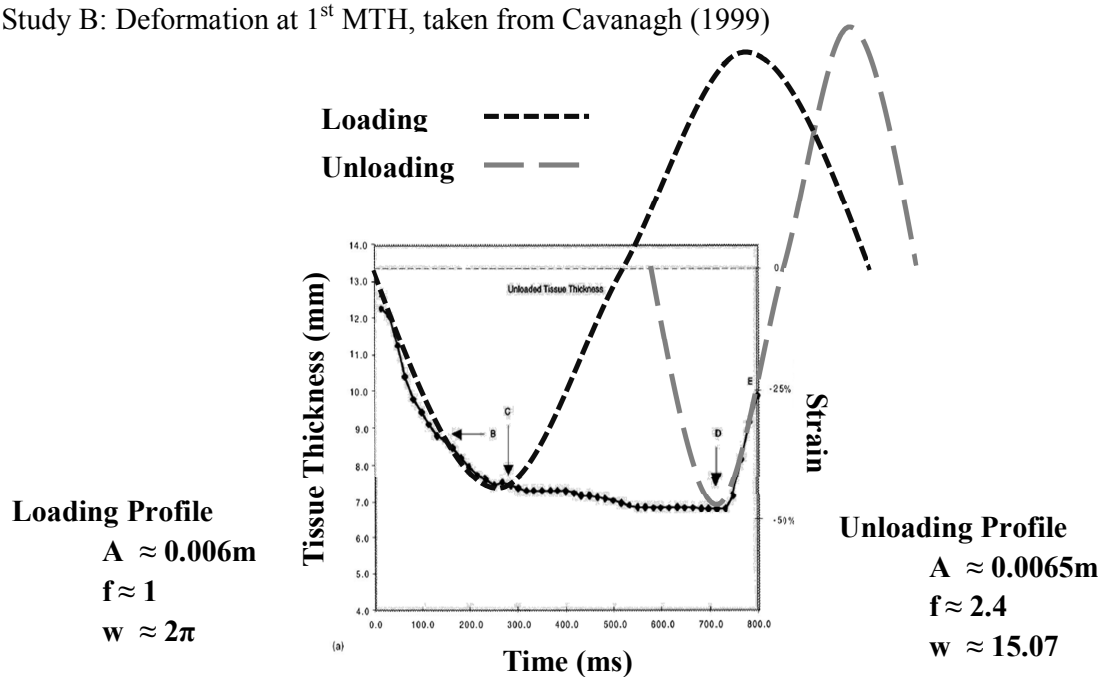

Figure A.2.3: Walking deformation of 1st MTH

The maximum velocity for the sine curve fit to the loading profile was 0.037m/s and the maximum acceleration was 0.24m/s^2 (Figure A.2.3). The derived values for the unloading profile were higher with a maximum velocity of 0.098m/s and maximum acceleration of 1.48m/s^2 suggesting a more rapid tissue offloading occurs compared to loading at the forefoot.

The highest values for velocity and acceleration were reported for the unloading (push-off) phase of the forefoot motion. A drive mechanism must therefore be capable of achieving velocities of at least 0.1m/s and accelerations of at least 1.5m/s^2. This data provided a crude basis for specifying the drive mechanism and was used to isolate potential methods to produce the gait simulation profiles. However peak values only account for some of the demand on the drive mechanism. To allow the motor demand over a full gait cycle to be modelled, realistic walking data were required.

A.2.3.3. Tissue specific kinematics throughout stance

A preliminary 2 person study was conducted to collect data for foot segment motion and ground reaction forces. A Vicon motion capture system (V612, Vicon Motion Systems Ltd., Oxford, UK) was used in combination with a force plate (9286a, Kistler Instruments Ltd., Alton, UK). Retro reflective markers were placed on the foot as in fig A.2.4. This allowed the vertical displacement at the heel to be tracked during stance by a posterior calcaneus marker Fig A.2.4 (a) and the vertical displacement at the forefoot to be tracked during stance via a metatarsal head marker, Fig A.2.4 (b). Each subject walked at normal pace throughout testing performing at least 2 steps before entering the capture window for the Vicon system. To acquire ground reaction force profiles each subject was asked to walk over the force plate striking the plate with the right foot. Each subject was allowed to practice walking with the markers and to pace their walking to hit the force plate without need for conscious targeting of the force plate. After the initial practice period 10 walks were collected for each subject. The data were logged to a PC using the Vicon BodyBuilder software and saved in C3D format. The marker displacement trajectories of the calcaneus and metatarsal head were then imported into Visual 3D. The raw displacement and ground reaction force trajectories and were filtered at 15Hz using a lowpass butterworth filter and exported to ascii files allowing further processing and plotting of the vertical displacement profiles (Figure A.2.5).

Figure A.2.4: Motion Capture Marker Placement on foot
(a) posterior calcaneus marker (b) metatarsal head marker
Image courtesy of prosenjit 2009

Visual assessment of the marker displacement curves showed similarities to the in-gait tissue deformation curves, suggesting a good approximation of tissue can be achieved from surface marker motion alone (Figure A.2.5). However for the Metatarsal head region the gait data

showed discrepancies between the peak tissue compression detected by marker motion (18mm) and the previous studies (~7mm). The discrepancy between these values may be due to errors in the definitions of gait events and thus the offset of zero for the metatarsal head profile.

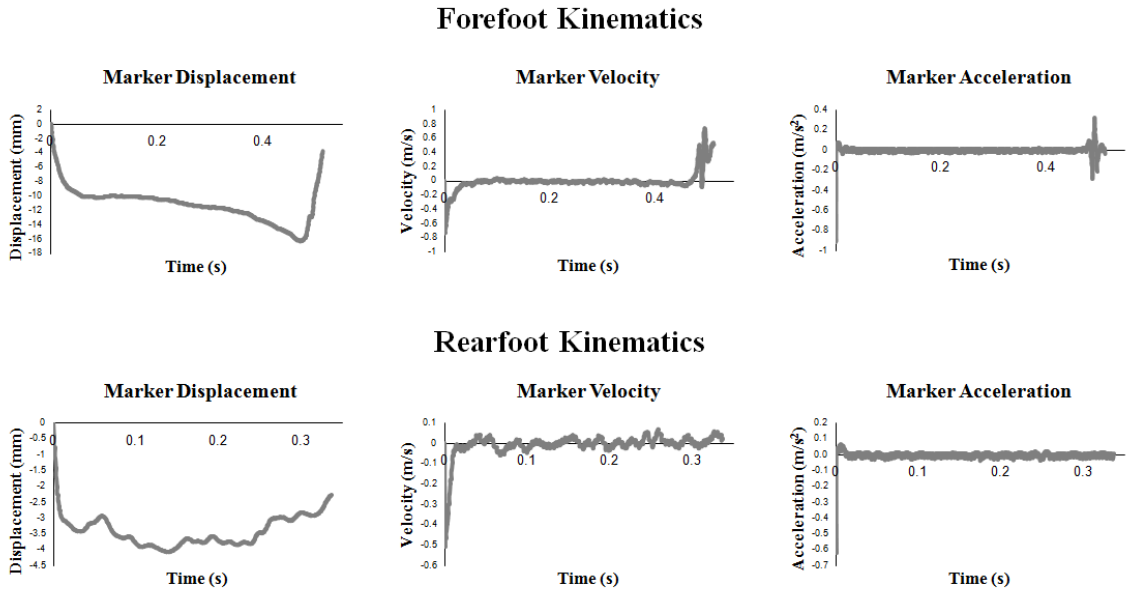

Figure A.2.5: Kinematics Data for Foot Segment Motion

A.2.3.4. Region specific Ground Reaction Force Profiles

Using the whole foot Ground Reaction Force (GRF) plate data coupled with data from a pressure plate (Emed-x/r high speed system, Novell inc, Munich, Germany) it was possible to isolate region specific loading profiles. Bespoke Pedobarographic statistical mapping software (Pataky 2008 Software under restricted licence) was used to determine the pressure within a specific region, across the full stance phase. A 2cm diameter circular mask was applied at the region of interest in the heel, and 1st MTH (Figure A.2.6). The sum of the pressure within each mask was calculated for each plantar pressure frame across the duration of stance. This generated a profile for pressure/time for the specific region mask. The sum of the pressure for the whole foot was also calculated across the duration of stance to create a total pressure profile over stance. The ratio of region specific profile and total pressure profile could then be used to calculate the region specific GRF (Figure A.2.7).

$$Region\ Specific\ GRF = Vertical\ GRF\ \times \frac{Region\ Specific\ Pressue\ Profile}{Whole\ Foot\ Pressure\ Profile}$$

Figure A.2.6: Plantar pressure with Region of Interest

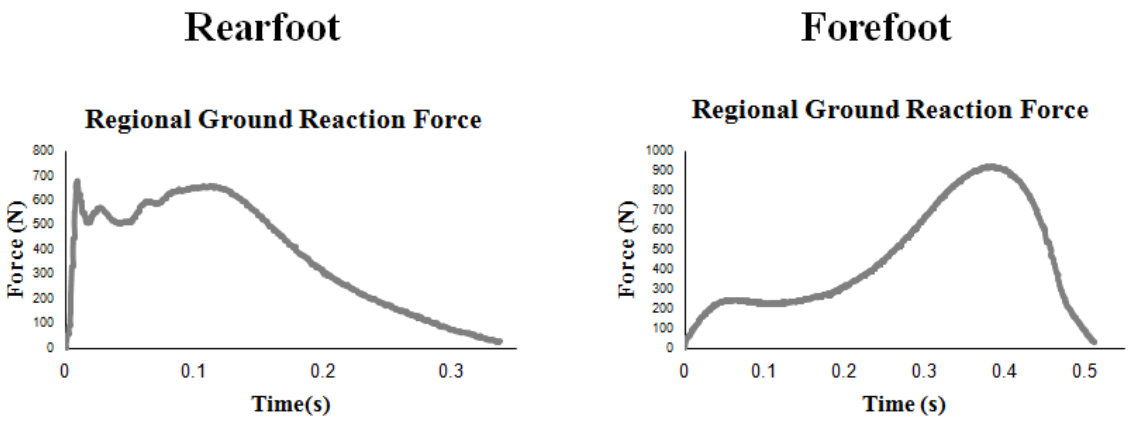

Figure A.2.7: Region Specific Ground Reaction force during stance.

A.2.3.5. Smoothed estimation of rear foot tissue compression

For the purpose of this study the rear foot profile was selected as it provided a good match between the rear foot marker data and Gefen's compression data permitting it to be used as the basis for a gait simulation profile. To allow smoothing, the raw displacement data were divided into three sections; Compression, Holding and Decompression. Curves were fit to each section using 3rd order polynomial functions. This removed noise due to marker motion but retained the shape of the raw displacement curves (Figure A.2.8).

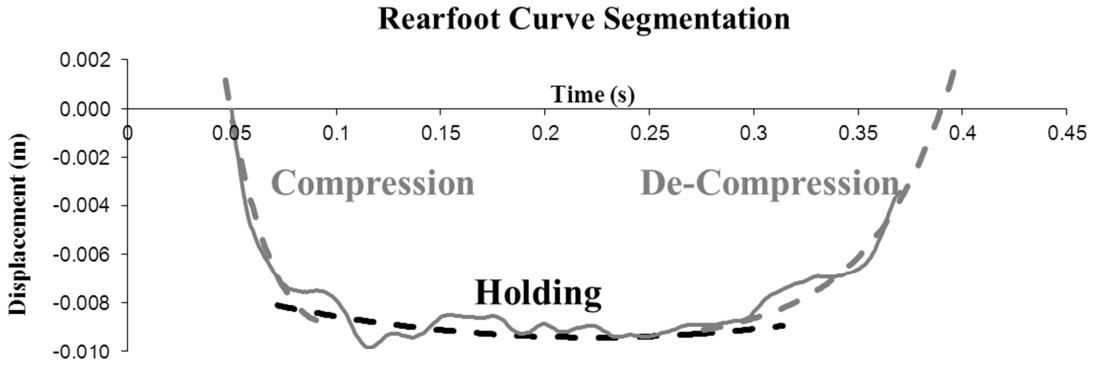

Figure A.2.8: Curve Fitting to Raw Displacement Profile for Rear Foot

A Combined Smoothed curve was created by knitting together the polynomial curves for each of the three sections. The points at which the polynomial curves intersect with the axis or with each other were used to define boundaries for each segment. A composite curve was then generated based on the three polynomial curve equations which represented the smoothed marker motion (Figure A.2.9). Constant acceleration regions were added to the start and end of the curves to allow initial and end velocities to be brought to zero (Figure A.2.9). With this composite curve method the transitions between region boundaries were not smooth; to remove the high accelerations present due to these noisy transitions a univariate cubic spline function was used in python (scipy.interpolate.univariatespline, k=3, s=0.005). The cubic spline function was used because it forced the curve through the original data points for the composite curve and produced smoothed transitions between curve segments (Figure A.2.9).

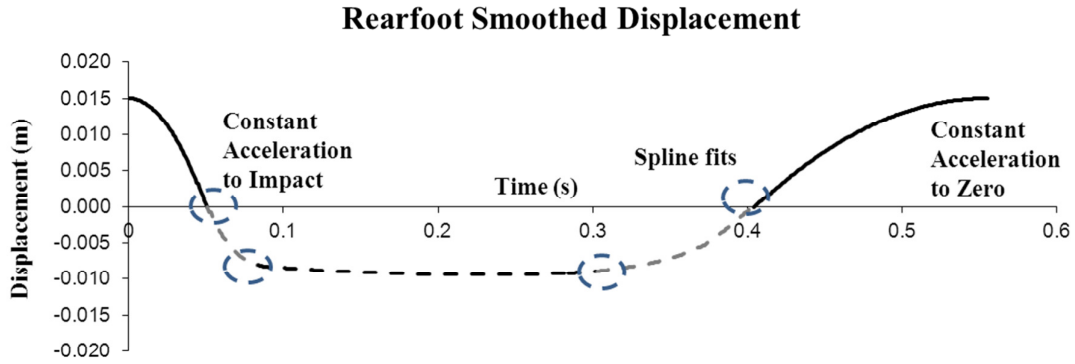

Figure A.2.9: Smoothing of Curve Fit Profile for Rear Foot

Velocity and acceleration profiles were calculated as the first and second derivatives for the smoothed Rear foot displacement profile (Fig A.2.10). These profiles resulted in a peak velocity of 0.6m/s and a peak acceleration of 15m/s^2 which occurred at the transition from negative to positive displacement. These values are much greater than those derived by single Sine-wave fits to the literature data, and it is likely that this is due to the reduced time to peak displacement in the motion capture data (0.05s) compared to the literature data (0.2s). It is also possible that the single sine wave fits did not represent the true loading or unloading curvature.

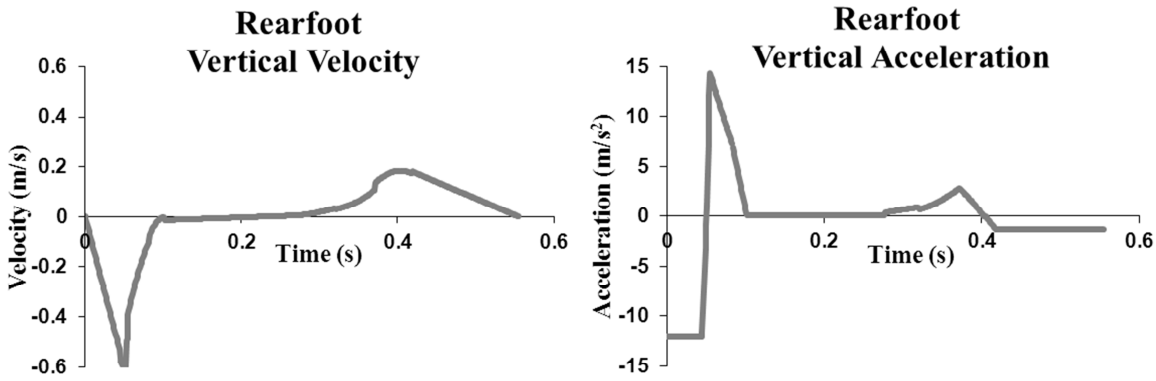

Figure A.2.10: Smoothed Velocity and Acceleration for Rear Foot

A.2.4 Models of Device Motion

A.2.4.1. Direct Vertical Loading

To approximate the reaction forces and mechanism loading which is likely to be generated during compression of the plantar soft tissue using the rear foot gait simulation profile, simple models were developed. The models took into account the foot loading, the mass of the moving parts of the device and the acceleration of the device to generate realistic profiles for device loading. An initial model of the device used direct loading in line with the reaction force (Figure A.2.11).

Where:

F_f = Reaction Force (Subject Loading)

F_d = Device Force (Mechanical Loading)

a = Acceleration of Device

m_v = Mass of Moving Parts

g = gravity (9.81)

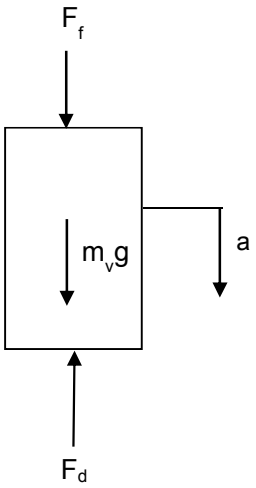

Figure A.2.11: Model of Device

Direct Vertical Loading

From F=ma the Sum of forces Vertical: $\mathbf{F_f - F_d + m_v*g = m_v*a}$

Thus the Device Loading (F_d): $\mathbf{F_d = F_f + m_v*g - m_v*a}$

Assuming the following to represent the most work for the device:

Peak load = 120kg (based on subject of 100kg * 1.2BW)

Vertical moving mass = 7kg (based on initial models of device components)

Using the acceleration profile and specific regional ground reaction force profile for the rear foot, the predicted device loading was calculated across the full displacement profile (Figure A.2.12). Using a direct vertical loading mechanism requires the following features:

- Motor mounting in the vertical direction
- Peak Loads of 1500N
- Peak velocity of 0.6m/s
- Peak accelerations of $15m/s^2$
- Minimum travel of 30mm

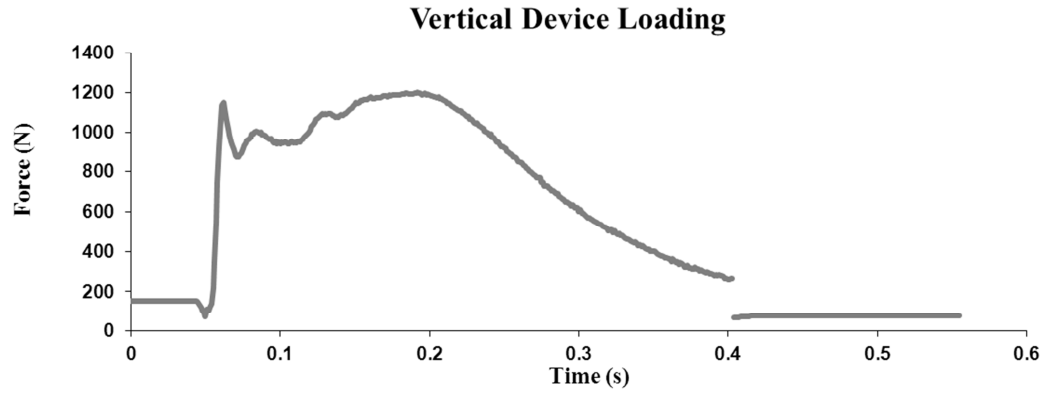

Figure A.2.12: Vertical Device Loading

A.2.4.2. Models Including a Mechanical Advantage

Due to the high mechanical loading required in a vertical device setup, another model including a mechanical advantage was constructed. The mechanical advantage is modelled as a simple ramp which acts to convert horizontal motion of the motor into vertical motion of the platen (Figure A.2.13). This reduces the direct loading borne by the motor, however it increases the requirement for total travel.

Where:

F_f = Reaction Force (Subject Loading)

F_d = Vertical Force (Coupling Vertical Loading)

F_m = Motor Force (Mechanical Loading)

r = Mechanical Advantage

a = Acceleration of Device

m_v = Mass of Moving Parts (vertical)

m_h = Mass of Moving Parts (Horizontal)

g = gravity (9.81)

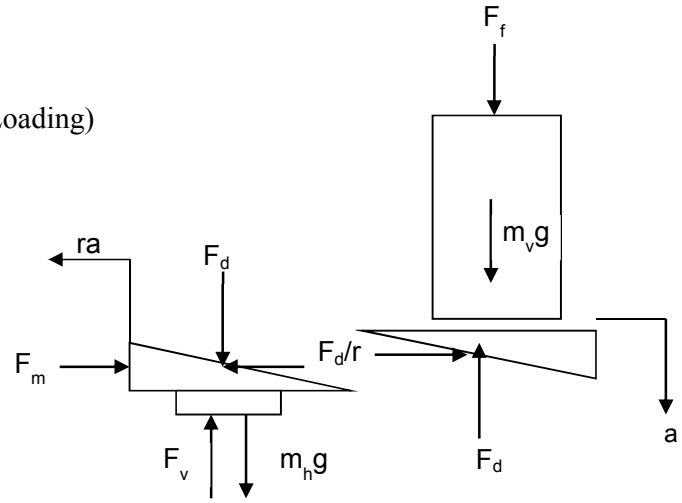

Figure A.2.13: Model of Device Loading with Mechanical Advantage via Ramp.

Sum of forces Vertical: $\mathbf{F_f - F_d + m_v*g = m_v*a}$

Sum of forces Horizontal: $\mathbf{F_d/r - F_m = m_h*a*r}$

Assuming the following to represent the most work for the device:

Peak load = 120kg (based on subject of 100kg * 1.2BW)
Vertical moving mass = 7kg (based on initial models of device components)
Horizontal moving mass = 8.2kg (based on initial models of device components)

From horizontal forces, motor force (F_m) can be derived as: $\mathbf{\underline{Fm = (Fd - m_h*a*r^2)/r}}$

Horizontal device profiles were calculated using the rear foot profile for vertical displacement, velocity and acceleration from section 2.3.5, in combination with the regional ground reaction force profile for the rear foot from section 2.3.4.

A.2.4.2.1. Utilising a 2:1 Mechanical Advantage

Device profiles with a mechanical advantage of 2:1 were calculated for the full smoothed rear foot vertical displacement profile (Figure A.2.14). Using a coupling with a mechanical advantage of 2:1 requires the following features.

- Motor mounting in the horizontal direction
- Peak Loads of 600N
- Peak velocity of 1.2m/s
- Peak accelerations of $30m/s^2$
- Travel of 60mm

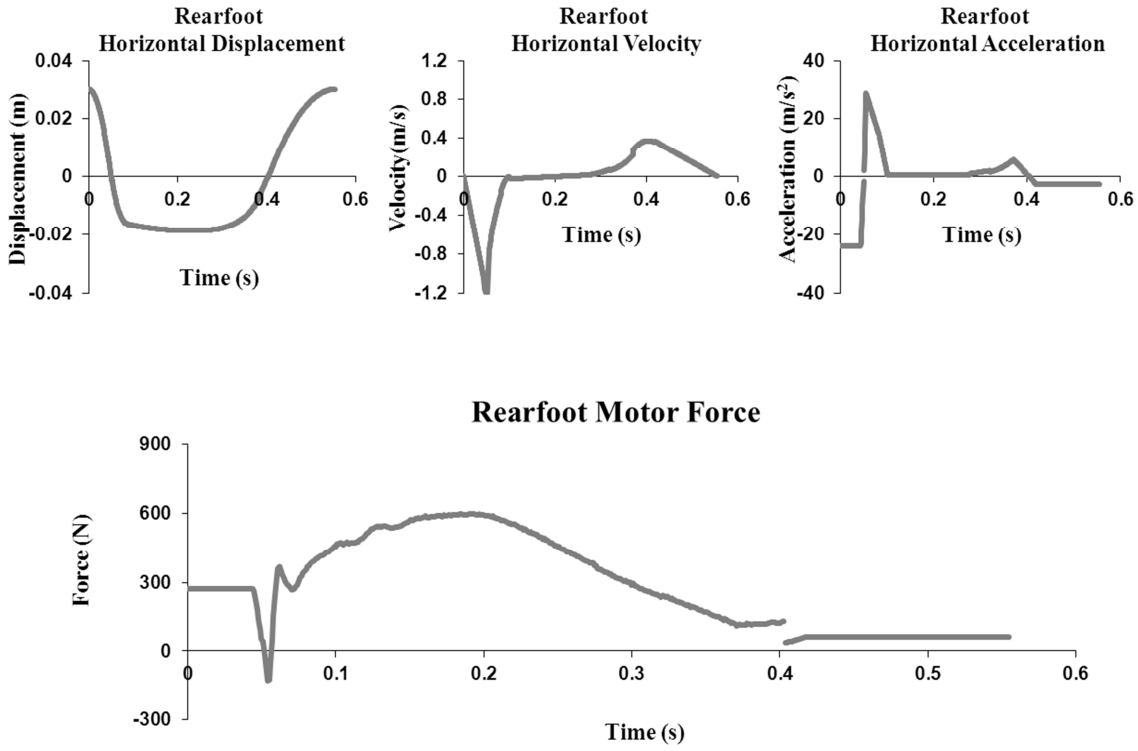

Figure A.2.14: Horizontal motion and Motor force with 2:1 Mechanical advantage

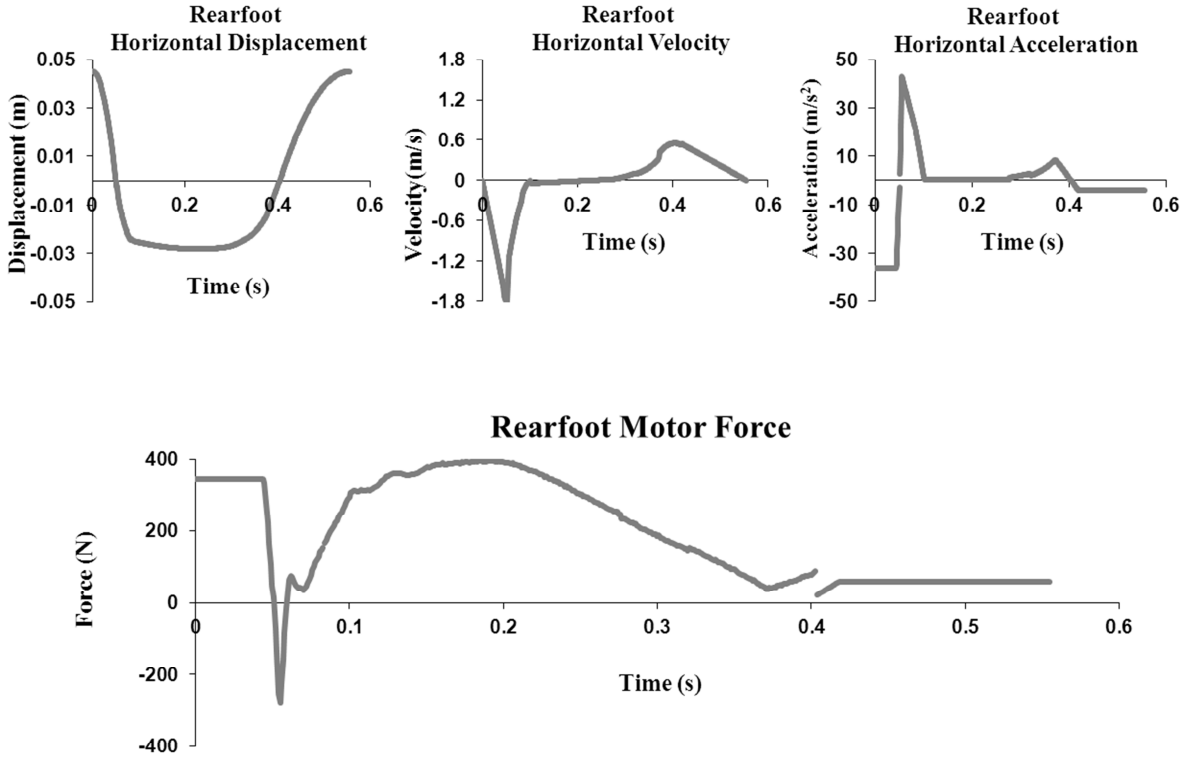

Figure A.2.15: Horizontal motion and Motor force with 3:1 Mechanical advantage

A.2.4.2.2: Utilising a 3:1 Mechanical advantage

Device profiles with a mechanical advantage of 3:1 were calculated for the full smoothed rear foot vertical displacement profile (Figure A.2.15). Using a coupling with a mechanical advantage of 3:1 requires the following features.

- Motor mounting in the horizontal direction
- Peak Loads of 500N
- Peak velocity of 1.8m/s
- Peak accelerations of 45m/s^2
- Travel of 90mm

A.2.5 Final Specification

From these data, a comprehensive specification was drafted to identify the key requirements of individual device components and of a system intended to replicate tissue compression with dynamics akin to normal walking. A detailed breakdown of component requirements can be found in Appendix A.

In summary the key specification of the complete system was:

- A device platen with minimum dimensions of 15cmx15cm capable of producing bulk compression of the plantar soft tissue.
- A tissue imaging device capable of accuracy to at least 0.1mm, and minimum depth of 30mm.
- A load measurement device with an operational range of 0 – 1000N capable of dynamic output to data logger and for feedback / control of the drive mechanism.

A drive mechanism with a minimum operational range of 500N continuous force, 2m/s peak velocity and 50m/s^2 peak acceleration. Higher capacity for load would permit a reduced peak velocity.

A.3. Concept & Design

A.3.1. Device Concept Designs

Based on the Specification, an initial concept schematic was drawn to combine the key components (Figure A.3.1). Items A & B represent the drive mechanism and control system for the device. The measurement apparatus are components D (Load Cell) and E (Imaging method). The measurement components and the drive mechanism are connected via an actuation stage which permits vertical motion of the measurement apparatus. The device platen is composed of parts G (small section) and F (large section). The position of G, E and D will permit a single path through which the applied load and tissue compression may be measured in series to enhance region specificity.

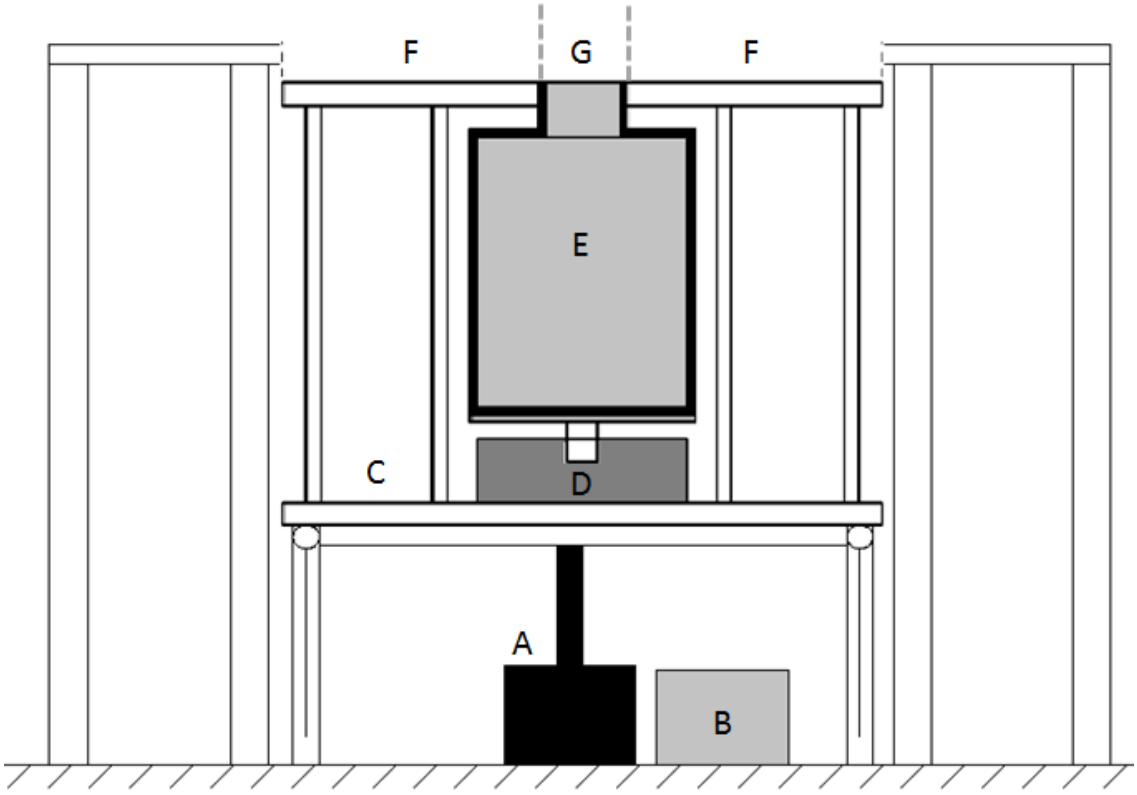

Figure A.3.1: Schematic Drawing of Device Concept. A: Actuator; B: Controller; C; Moving Stage; D: Load Cell; E: Imaging Device; G: Small Section of Loading Platen (Imaging Window); F; Large Section of Loading Platen

A.3.2. Selection of Device Components

A.3.2.1. Ultrasound Imaging

An ultrasound system (Mylab 70, Esaote, Italy) was chosen to provide images for the tissue thickness during compression. The 4-13MHz Ultrasound Probe available with this system permitted the tissue to be assessed to a maximum thickness of 40mm at an accuracy of 1.75% (±0.7mm). The ultrasound signal was capable of transmission through a thin plastic interface allowing a 3cm diameter circular imaging window to be used in place of the rectangular probe surface (5cmx1cm); this provided a more specific imaging region which could be focused below an anatomical feature of interest. The Esaote system had a maximum capture rate of 200Hz and could record dynamic video for a total of 17s permitting a maximum of 3400 frames to be captured per test. Image data were stored in an uncompressed video format to an internal hard drive and could be transferred to a portable storage device via USB. The features of the Esaote system complied with all previous specifications for an imaging method.

A.3.2.2. Load Measurement

A Precision Miniature Load Cell (TC34, Amber Instruments, UK) was chosen to provide load measurements for the tissue response during compression. The load cell provided single axis (tension and compression) measurement of load to an accuracy of 0.2%. The load cell had a maximum capacity of 2225N (500lb) with a tolerance of 2mV/V. The maximum capture frequency for the load cell was limited by the Data Acquisition system to 3000Hz. Data were logged to PC via LabView (National Instuments, Uk) and recorded in ascii format. The device provided adequate accuracy and resolution for the purposes of this study and complied with all previous specifications.

A.3.2.3. Platen Displacement Measurement

A Linear Variable Differential Transformer (LVDT) (S-Series, Solartron, UK) was also selected to provide an accurate measurement of the device platen's vertical displacement. The LVDT had an effective range of 50mm with an accuracy of 0.2%. The maximum capture

frequency for the LVDT was limited by the Data Acquisition system to 3000Hz. Data were logged to PC via LabView (National Instuments, Uk) and recorded in ascii format. Inclusion of this measurement method permitted the true platen motion to be evaluated for each loading profile to ensure fidelity of the input to the output motion.

A.3.2.4. Drive Mechanism

To drive the platen a brushless linear servo-motor (BLMH142, Aerotech Ltd, UK) was chosen, which uses a magnetic piston to drive a platform horizontally. This system had multiple advantages over other possible systems. Due to its non-contact piston it does not require lubrication or pressurised vessels as in the case of hydraulic systems, thus allowing a much cleaner device suited to a human performance lab. The electromagnetic drive requires little maintenance and has a reduced risk of clogging or sticking associated with ball screw and belt driven systems, allowing more precise control of motion and rapid acceleration. However, the system could not be mounted vertically and was not capable of generating or maintaining the high load requirements without the use of a mechanical advantage.

Initial Device Capacity (Pre-Mechanical Advantage):

Peak Load:	1080N
Continuous Load:	270N
Peak Velocity:	5m/s
Peak Acceleration:	$50m/s^2$

The motion of the actuator was controlled via commercial software provided by the suppliers of the actuator (Ensemble, Aerotech Ltd, UK). This software permits control of the device via displacement, velocity or acceleration, with feedback controls for displacement error, velocity error and limits for maximum current; which is associated with motor force; giving a large potential for profile development.

A.3.3 Detailed Device Design

A.3.3.1 Device Platen

To allow bulk compression of the tissue and region specific load measurement a bespoke platen was designed (Figure A.3.2). The platen uses a large circular top plate (15cm diameter) to achieve uniform compression of a whole foot region (Rear foot). An imaging window (3cm diameter) intersects the larger plate at the central point, with a clearance of 1mm around its circumference. The central window is made of plastic and has a metal rim attached to an internal frame to provide a well-defined measurement site. The platen is mounted on vertical bearings to restrict motion to the vertical direction, making it easy to repeat compression of a specific tissue site over multiple loading cycles.

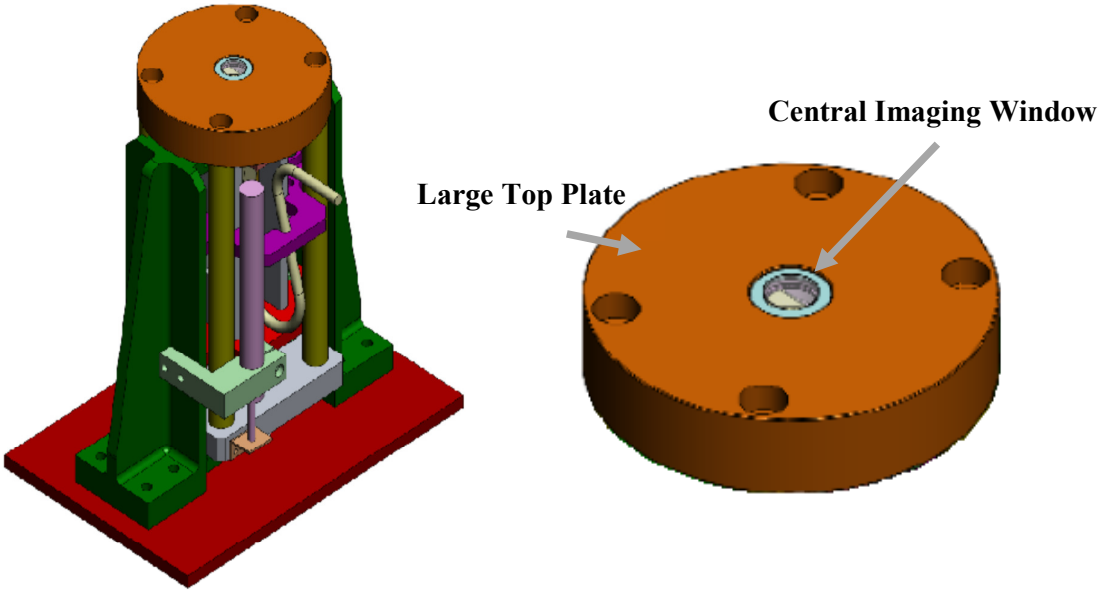

Figure A.3.2: Isometric View of Platen and Measurement Apparatus Housing

A.3.3.2. Measurement Apparatus

The device platen houses the measurement apparati, which are arranged in series (Figure A.3.3). The vertical axis of the device, through which the device can move to contact/compress the tissue, is the direction of measurement for both load and displacement allowing compression and tissue response to be aligned. The inclusion of the ultrasound probe

permits tissue thickness and compression to be measured for a specific anatomical location of interest within the foot region, while the use of an isolated plastic loading surface permits specific load measurement for a 3cm diameter area beneath the anatomical feature of interest.

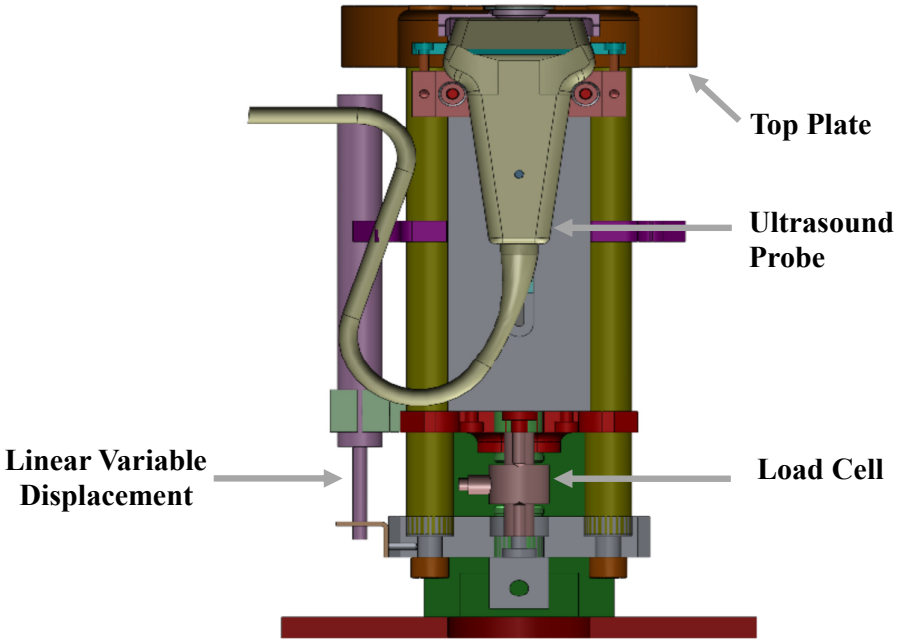

Figure A.3.3: Cross sectional view of Platen

A.3.3.3. Mechanical Advantage

To allow the horizontal motion of the actuator to be transferred to vertical motion of the platen and to introduce a mechanical advantage to reduce the demand on the motor, a ramped coupling was used (Figure A.3.4). This coupling was also capable of carrying high vertical loads when the device was static which prevented the actuator from being overloaded.

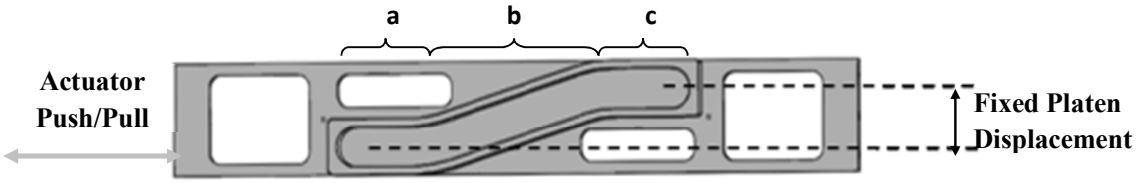

Figure A.3.4: Side view of coupling ramp. (a) Initial flat section, (b) Impact and tissue loading (mechanical advantage 3:1), (c) Final flat section

The coupling ramp acted to create a fixed range of vertical motion, preventing the device from overshooting its vertical target. A region of runoff either side of the loading ramp was

introduced in case of device failure or activation of an emergency stop. The ramp's gradient provided a mechanical advantage of 3:1, which increased the load bearing capacity of the device. This increased capacity places the device safely within the specified requirements. The mechanical advantage also results in an increase in horizontal travel compared to vertical displacement, which increases the demand on the vertical velocity and acceleration which must be implemented by the device. This increased velocity demand was within the specified requirements so was an acceptable compromise.

Post Coupling Device Capacity (Mechanical Advantage of 3:1):

Peak Load:	3240N
Continuous Load:	720N (can be borne by the coupling)
Peak Velocity:	1.66m/s
Peak Acceleration:	1.66g

A.3.3.4 Housing, Brace & Subject Positioning

A stage was constructed to enclose the actuator, coupling, platen, control systems and safety systems. This stage prevented the subject from gaining access to the moving mechanism and electrical elements and acted to raise the subject's position, allowing them to stand directly above the loading platen (Figure A.3.5).

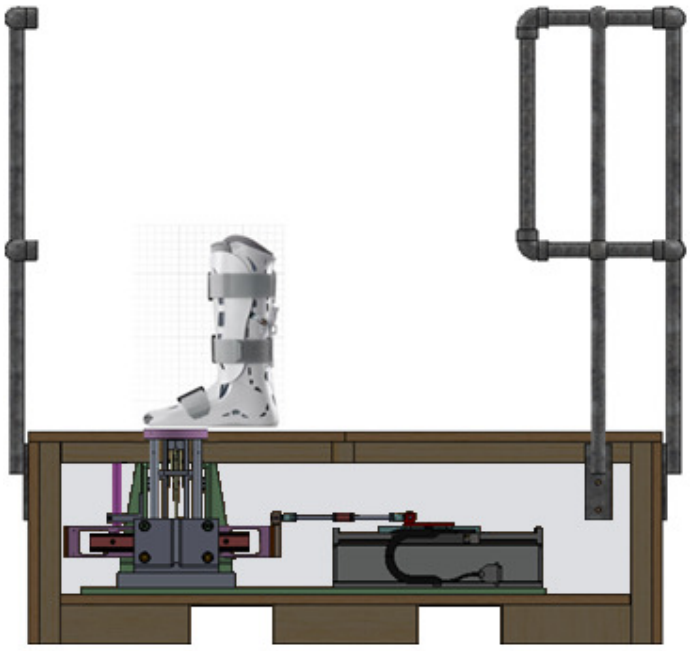

Figure A.3.5: Cut away view of Device Housing

An Aircast Boot (XP Walker Extra Pneumatic, DJO, LCC, USA) was adapted for use as a foot brace. The boot used inflatable bladders along the shank and above the dorsal aspect of the foot to create a firm grip on the leg and fix the foot. The rubber sole of the boot was removed and two apertures were cut in its plantar surface to allow hind and forefoot regions to be accessed (Fig A.3.6 (b)). The brace was then fixed to a wooden frame which allowed it to be suspended on threaded rod above the loading platen. The brace arrangement allows for adjustment in 3 planes (Fig A.3.6); medio-lateral, anterior-posterior and vertical. This permits the anatomical site of interest to be located easily for each subject. The brace could then be locked in position to ensure repeated compression of the identified feature.

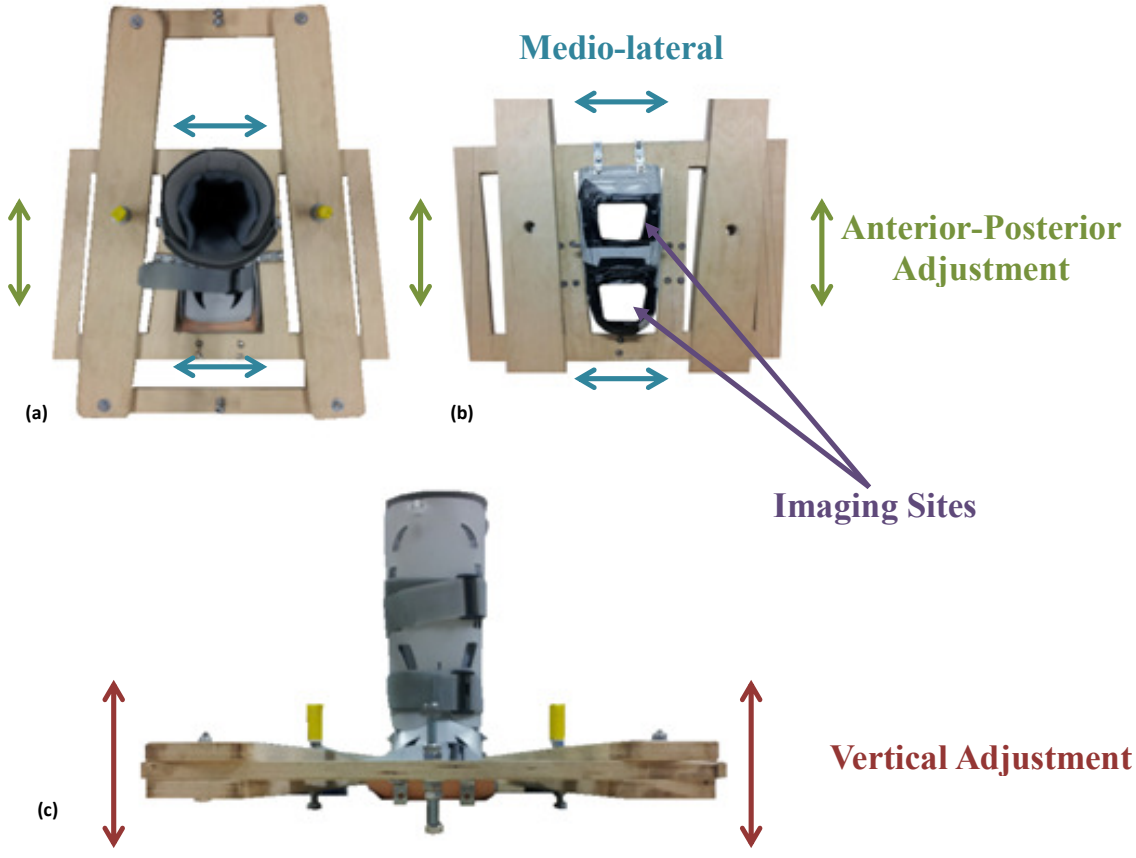

Figure A.3.6: Brace Setup. (a) Top View of Brace, (b) Bottom View of Brace, (c) Front View of Brace

A.3.4. Health & Safety

A full health and safety review was conducted by a University of Salford health and safety operative and H&S procedures were written (see Appendix B)

The housing was fitted with hand railing and steps to aid the subject when accessing the raised platform and when over the device. The housing also had ventilation holes cut to prevent overheating of the actuator.

The device control was setup to generate a fault condition if position error exceeded 1.5mm or velocity error exceeded 0.4m/s. In the event of a fault condition, the device was programmed to disable the axis, which would remove all power from the motor and cancel all outstanding commands. Due to the coupling ramp the platen would then fall away from the subject's foot under gravity. In the case of an error or fault, the flat sections of the coupling ramp would prevent over compression of the subject's foot.

For electrical safety (Fig A.3.7), the mains supply to the device was routed through a Residual Current Device (RCD), and then the live supply is taken through a Miniature Circuit Breaker (MCB). The Live supply was then, along with the neutral supply, routed through a contactor. The coil of the contactor was driven by a safety relay circuit. This in turn is driven by an e-stop circuit in line with safety switches. The e-stop circuit includes two cut-off switches. (1) The operator switch was a push-to-break switch with twist release button preventing power from being restored to the system before the fault had been corrected. (2) The subject switch was a hold to make switch, and as such required the subject to hold a push button throughout testing, as soon as the subject released the button power was removed from the system. When the E-Stop circuit was activated, all power was removed from the components in contact with the subject and power could not be restored until physical blocks (switches) and software blocks (axis enable) had been reset. To protect the subject from risks associated with the electrical components of the device, all equipment was earthed; this acted to isolate the subject in the event of an electrical fault.

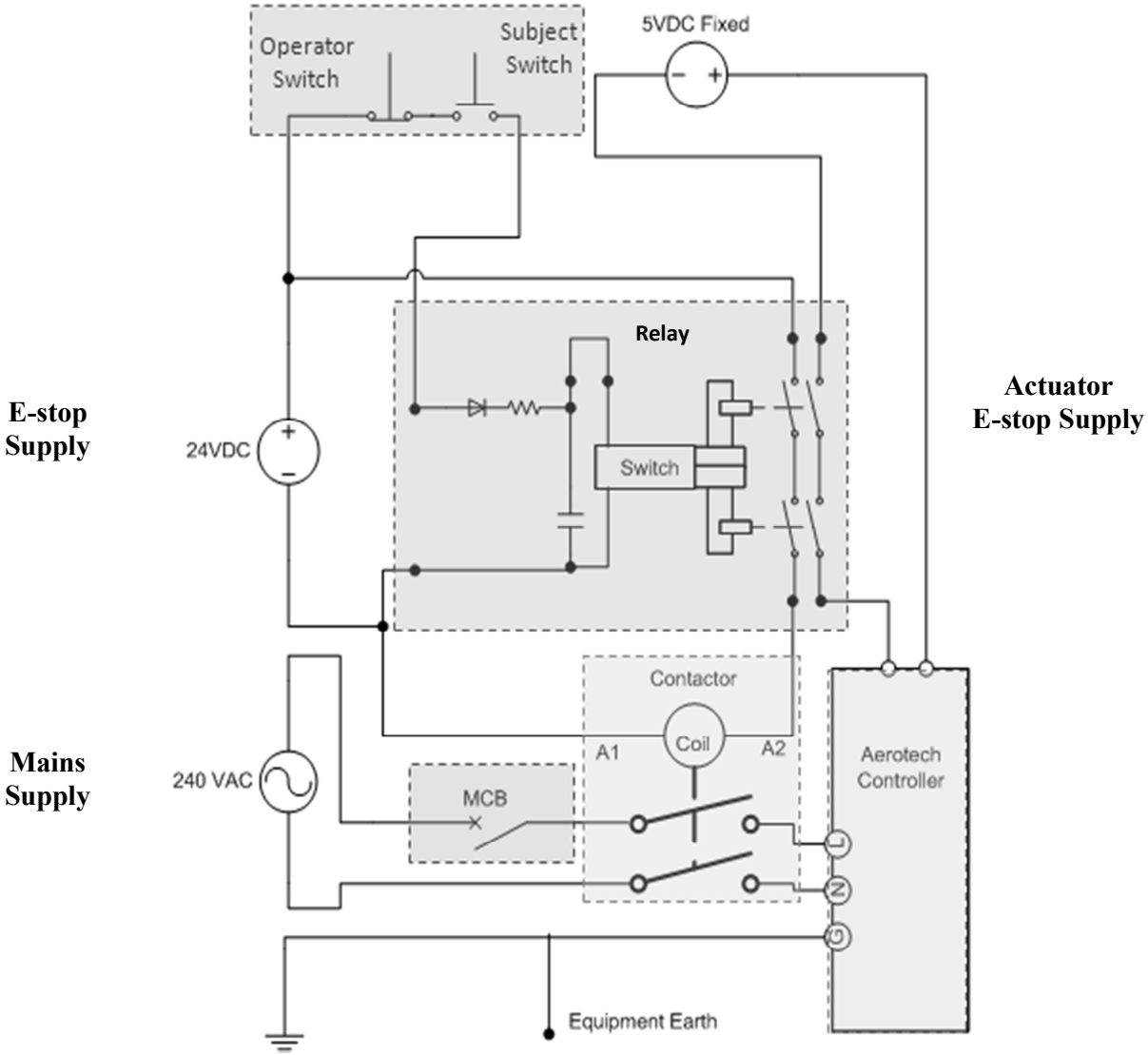

Figure A.3.7: Electrical Safety Setup

A.4. Dynamic Tissue Testing Routines

A.4.1 Introduction

Previous techniques to characterise the mechanical properties of the plantar soft tissue have focused on the use of standard profiles, such as triangle (Erdemir *et al.* 2006, Hsu *et al.* 2009) or sinusoidal (Aerts *et al.* 1995, Zheng 1999) wave forms, to compress the tissue. Standard profiles allow for the use of simple device control systems (Aerts *et al.* 1995, Erdemir *et al.* 2006) or in many cases manual application (Zheng 1999, Hsu *et al.* 2009). As a result, low velocities are used in the standard profiles, which gives long compression and decompression stages, allowing for many data points to be collected at relatively low capture frequencies (Zheng 1999), and providing a good basis for curve fitting and modelling. The reasonable level of accuracy and repeatability which can be achieved by hand make these methods very suitable for clinical application (Rome and Webb 2000, Klaesner *et al.* 2001). However standard profiles do not produce rates or loads which are representative of gait, thus properties derived are only relevant for the tissue within certain bounds of its functional range (Gefen *et al.* 2001). To characterise the functional response of the tissue, studies have previously been conducted in-gait. Techniques such as Ultrasound (Cavanagh 1999), X-ray Fluroscopy (De Clercq 1994, Wearing *et al.* 2009) and X-ray Cinemaradiography (Gefen *et al.* 2001) can all be configured to allow capture of tissue compression during a single step. This allows for the isolation of true tissue compression and true tissue loading in unison. The main challenge with these techniques is the small imaging window available for each imaging modality. The imaging methods themselves are also very position sensitive which makes repetitively aligning an internal feature (Calcaneus) with a positioning target impossible for multiple independent steps (Cavanagh 1999, Gefen *et al.* 2001). To reduce error due to misalignment, targeting of step placement during walking is unavoidable with these methods, thus requiring the subject to adopt an un-natural gait, which may also affect some factors of the tissue compression (Cavanagh 1999, Gefen *et al.* 2001).

The control system for STRIDE is capable of producing both standard (Triangle wave, Sinusoidal wave) and complex (variable position, velocity and acceleration) profiles. This allows for the replication of the previous standard methods, which gave large datasets for the compression and decompression responses. The ability to input profiles in the form of

position, velocity and acceleration allows for profiles which replicate the dynamics of gait to be created. These Gait simulation profiles may then be used to compress a tissue which is held in a fixed position, allowing for a repeatable method of characterising the functional response of the tissue without the introduction of alignment and targeting errors.

A.4.2 Feature Identification and Foot Positioning

A.4.2.1. Anatomical feature Identification

An ultrasound assessment was conducted to identify the apex of the calcaneus in the heel. The heel region was cleaned with an alcohol wipe to remove dirt and provide optimal ultrasound transmission. The ultrasound probe was then applied to the plantar surface to acquire a frontal plane image of the heel region (Figure A.4.1.a). The probe centre was located above the apex of the calcaneus and a mark was made onto the foot at this point using a permanent marker. This process was repeated for the sagittal plane (Figure A.4.1.b). The foot was placed into a reference frame and the marks were used to acquire the location of the internal calcaneus in reference to the posterior and lateral borders of the foot (Figure A.4.2).

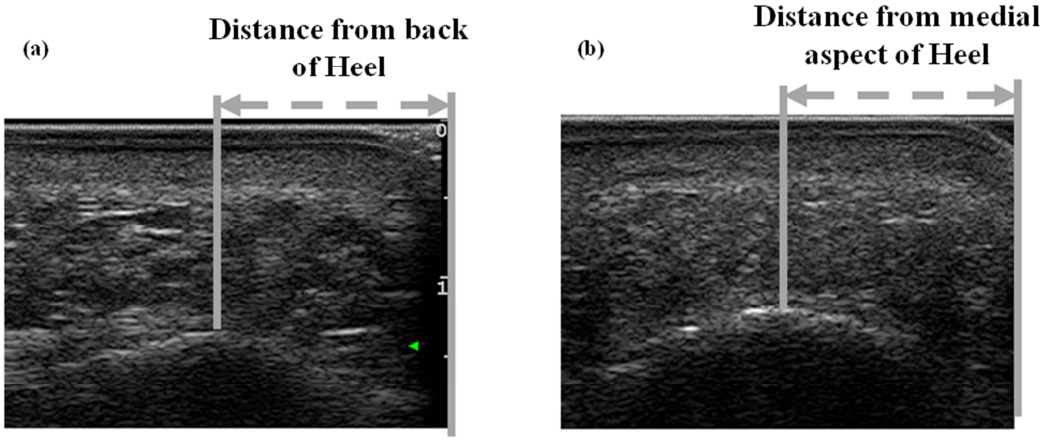

Figure A.4.1: Sagittal plane (a) and Frontal plane (b) images of heel showing the position of the apex of the calcaneus

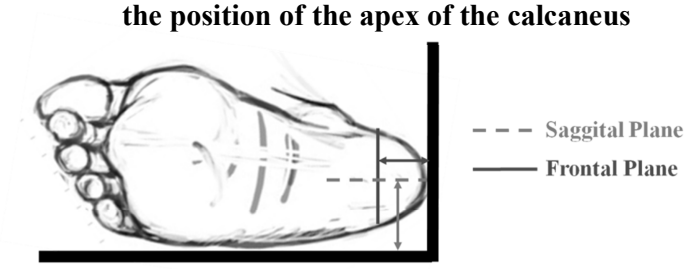

Figure A.4.2: Reference marks made for the heel region to identify internal feature of interest. (Image courtesy of prosenjit 2009)

A.4.2.2 Unloaded Tissue Thickness Measurement

The methodology for unloaded thickness was based on the protocol of Cavanagh (1999) due to the use of ultrasound and effective measurement reported in this study. The ultrasound probe was placed over the location of the anatomical feature of interest to acquire a frontal plane image. The plantar tissue was then loaded until the tissue became incompressible using the ultrasound probe and then gradually unloaded until contact with the tissue was lost. The unloaded tissue thickness was measured for the final image in which the anatomical feature was visible. This was repeated three times and an average unloaded thickness was calculated.

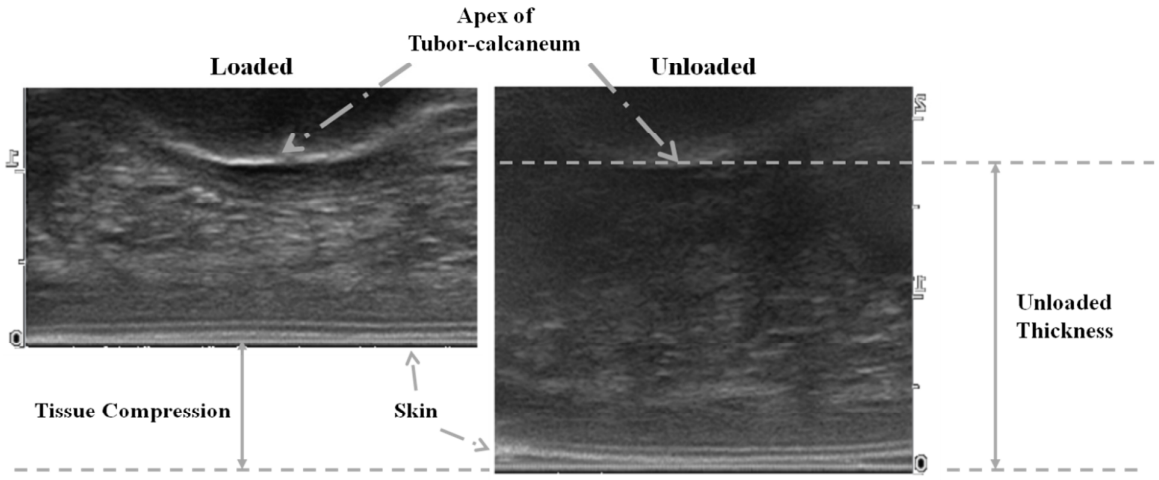

Figure A.4.3: Frontal plane image of heel region showing loaded and unloaded states

A.4.2.3 Subject Positioning

The subject was then asked to stand above the STRIDE loading platen and the right foot was braced using an Aircast boot (see section A.3.3). For testing of the heel region, padding was added under the forefoot region to create dorsiflexion at the ankle, thus acting to shift weight to the rear foot during compression. The bracing allows the anatomical feature to be located above the imaging section of the STRIDE platen by horizontal (medio-lateral, anterior-posterior) adjustment (Figure A.4.4). When located, the level of tissue compression was set by adjusting the bracing in the vertical direction. In all cases the profiles were set to produce a peak vertical displacement of 15mm by the STRIDE platen from the home position. This was a safety feature which prevented over compression of the subject's tissue. To allow the same

level of compression to be applied to each subject, a target compressive strain of 0.4 was selected as this could be easily achieved during the initial assessment and sat within the range of previously recorded values for peak strain (De Clercq 1994, Tong 2003). Due to the large range in unloaded tissue thickness between subjects for the heel pad, adjustment of the subject's position was required prior to testing. The STRIDE platen was raised to the level of peak displacement (15mm) and locked. The bracing was then lowered incrementally whilst observing the tissue thickness using the ultrasound. When compressed thickness reached 60% of the unloaded thickness, the bracing was locked. This secured compression in the region of interest to a peak of 40% (Figure A.4.5). Throughout testing, the subject was asked to stand with weight distributed evenly between both legs.

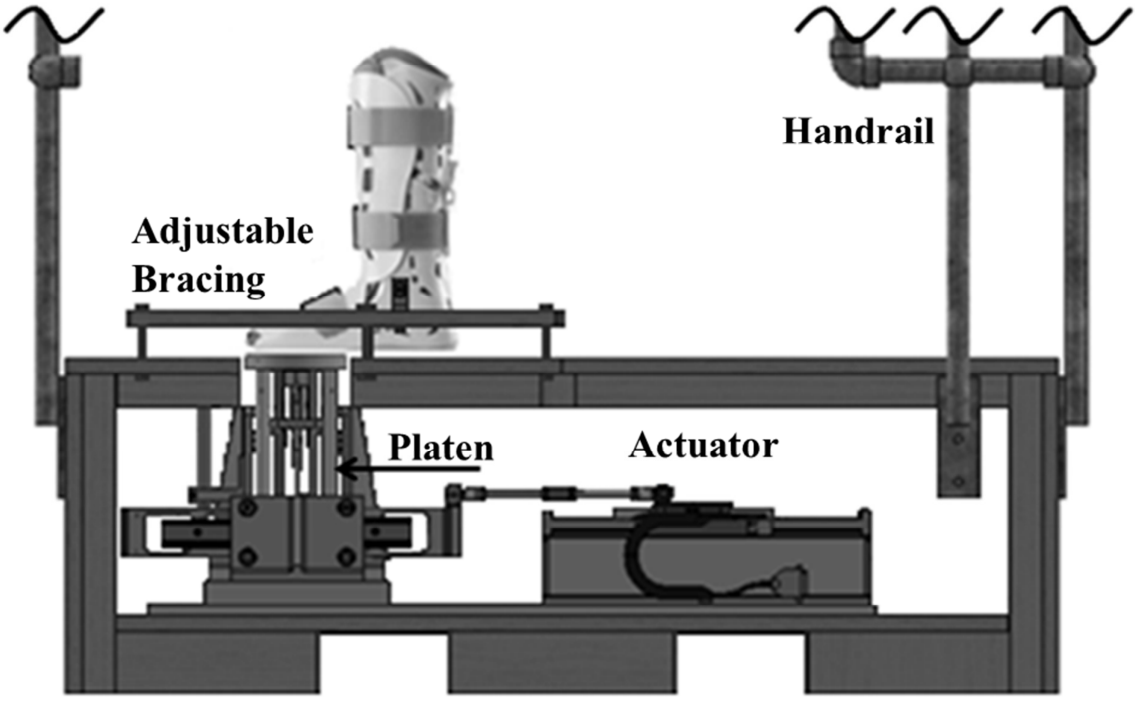

Figure A.4.4: Test setup and brace positioning

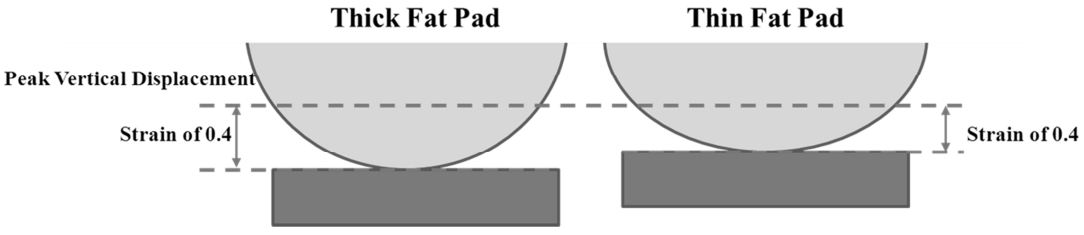

Figure A.4.5: Positioning of Subject to achieve compressive strain of 0.4 for a range of tissue thickness

A.4.3 Standard Mechanical Profiles

Two standard profiles were designed to test the mechanical response of the plantar soft tissue under compression. The design of these profiles was based on the methods used in previous literature and provides a basis for comparison to the existing soft tissue mechanical properties derived from such studies. These profiles permit very controllable compression with the capacity to capture a large number of images due to the slow loading and unloading phases. The standard profiles were generated using the ensemble motion designer software (Ensemble, Aerotech Ltd, UK) which allows the creation of displacement trajectories from predefined sine and triangle waves.

A.4.3.1. Triangle wave profile with constant velocity of 5mm/s

This profile is based on previous mechanical testing methods that used low constant velocity compression (0.0057m/s; 0.006m/s) to a defined peak load (Erdemir *et al.* 2006, Hsu *et al.* 2009). Each compressive cycle of the Impact-Compression triangle wave profile starts with the platen at rest in the home position (zero displacement). An initial positive acceleration of $5m/s^2$ permits a constant positive velocity of 0.005m/s to be achieved prior to contact with the plantar soft tissue (Figure A.4.6). Impact and tissue compression occur at the positive 0.005m/s velocity and continues as such to the peak platen displacement of 15mm. An instantaneous negative acceleration of $10m/s^2$ is then applied to create a negative velocity of 0.005m/s. The tissue is offloaded and the device returns to the home/start position at the velocity of 0.005m/s. 2 cycles are used for this profile, providing a short tissue rest time between each compression.

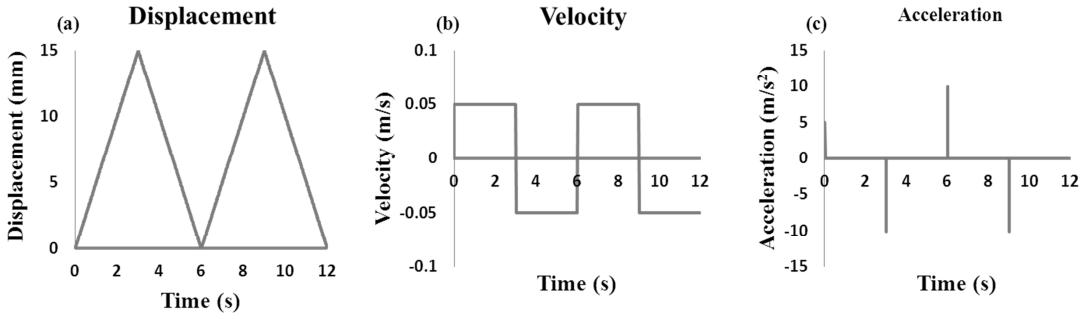

Figure A.4.6: Triangle wave profile with constant velocity of 5mm/s.
(a) Vertical Displacement, (b) Vertical Velocity, (c) Vertical Acceleration

A.4.3.2. Sine Wave profile at 0.5Hz

This profile is based on previous mechanical and material testing methods which used a 'half-cycle' sinusoidal compression to imitate impact dynamics (Aerts *et al.* 1995, Zheng 1999). The peak velocity occurs at tissue impact and then decreases to zero at peak compression. Each compressive cycle of the Sine wave profile starts with the platen at rest in the home position (mid-point of coupling ramp). The amplitude of the sine wave is matched to the target strain (0.4) and as such, vertical displacement is variable between individuals (Figure A.4.7). This is intended to match the peak velocity of the sine wave with tissue impact. For safety, the profile is aligned such that the peak positive amplitude of the sine wave coincides with the 15mm vertical displacement of the platen. A positive acceleration is then applied to initiate the sinusoidal wave. The velocities and accelerations throughout the tissue compression vary dependent on the absolute amplitude of the sine wave. 5 sinusoidal cycles are used for this profile, providing a short tissue rest time between each compression (Figure A.4.7).

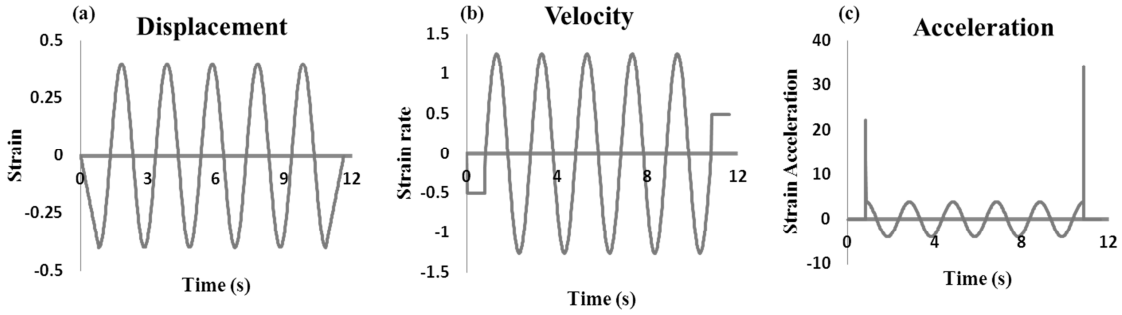

Figure A.4.7: Sine Wave profile at 0.5Hz
(a) Vertical Displacement, (b) Vertical Velocity, (c) Vertical Acceleration

A.4.3.3. Limitations

Two main limitations exist within the current standard mechanical testing profiles.

The ultrasound device used in this study permits only 17s of dynamic imaging to be captured at the maximal 200Hz capture rate. This restricts the number of repetitive cycles which can be recorded for each test. A T-Wave conducted at 5mm/s over the full dynamic range (±15mm) takes 6s per cycle, permitting only 2 cycles to be recorded per test.

Load control has been used widely in the literature and loading rate has been shown to affect tissue properties (Spears 2005). The actuator and control system used in this study permits only displacement control, which prevents the development of profiles based on achieving a consistent tissue loading rate. The peak load achieved is dependent only on the body weight of the subject and the efficacy of the bracing, and thus can vary greatly between subjects. However the absolute peak loads achieved in normal gait have also been shown to vary with body weight (J. Richards 2008a). The setup in this study reflects this normal variation.

A.4.4 Gait Studies

To permit the development of a loading profile based normal walking gait motion capture data was converted to position and velocity data for input to the device controller. Elderly gait was chosen for the purpose of this study, as this represented the less extreme condition, and thus permitted testing on both young and elderly individuals using a single profile, without the risk of damage to the tissue due to compression outside of the normal range.

A.4.4.1. Motion Capture Data

The data used to derive the gait simulation profile was provided from a study conducted at the University of Padova. The data included mean vertical marker velocity profiles from 10 healthy older people (3 female/7 male, mean age 61.2 (SD 5.27) mean height 1.71m (SD 0.81), mean weight 73.8kg (SD 11.73), mean BMI 24.98 (SD 2.3)). The study used a 6 camera stereophotogrammetric system (BTS S.r.l, Padova - 60 Hz). Subjects were asked to walk at a self-selected speed over a Bertec force platform (FP4060–10, Bertec Corporation, USA – 960 Hz) while an Imago system (410x410 x 0.5 mm, 0.64 cm^2 resolution, 150 Hz, Imagortesi, Piacenza) was used to collect plantar pressure data. Vertical co-ordinate data for the calcaneus were taken from -10% stance to stance +10% to encompass total heel contact. The first derivative of the vertical co-ordinate data was calculated for each trial. Trials which had a correlation coefficient of >0.75 to the average profile were used to calculate a mean and standard deviation of the vertical marker velocity.

A.4.4.2. Data Processing and Device Drive Profile Generation

The vertical velocity marker data were loaded into python for further processing. Data were re-sampled and converted from percentage stance to milliseconds based on the average total stance of 0.779s (Figure A.4.8.a); this was orientated such that positive velocity is movement away from the ground and negative velocity is movement toward the ground. The velocity profile was then integrated via the trapezoid rule using Python (scipy.integrate.cumtrapz) to give the vertical displacement of the region marker (Figure A.4.8.b) with the same marker orientation. To allow the actuator to drive the device platen, the orientation of the displacement profile was inverted giving positive displacement as displacement of the device platen toward the fixed foot (Figure A.4.8.c). The vertical displacement was then converted to horizontal displacement using the equation for the gradient of the coupling ramp and displacement offset:

$$Horizontal\ Displacement = (3 \times Vertical\ Displacement) + 12.576 \quad \textit{(EQ 4.1)}$$

The start and end of the horizontal profile was then padded with zeros and a spline fit was applied using the univariate spline function in Python (scipy.interpolate.univariatespline, k=3, s=0.005). The spline function was used because it forced the curve through all of the data points of the original profile and produced a smoothed transition to the zero padded regions (Figure A.4.8.d). This allowed zero values to be achieved for displacement, velocity and acceleration at both the start and end of the profile, permitting profiles to be run consecutively as compression cycles.

A.4.4.3. Gait Simulation Profile Generation

As with the standard profiles, a peak vertical displacement of 15mm was set to prevent over compression of the subject's tissue. The subject's foot was braced such that a tissue strain of 0.4 was achieved when the platen of the device was at its peak vertical position. The gait simulation profile takes the form of an impact and rapid offloading trajectory (Figure A.4.9). Each compressive cycle starts with the platen at rest in the home position (mid-point of coupling ramp). The platen is then displaced vertically with velocity increasing to a peak of ~0.3m/s. Tissue compression occurs rapidly, with the platen reaching a peak vertical displacement of 15mm in ~0.1s.

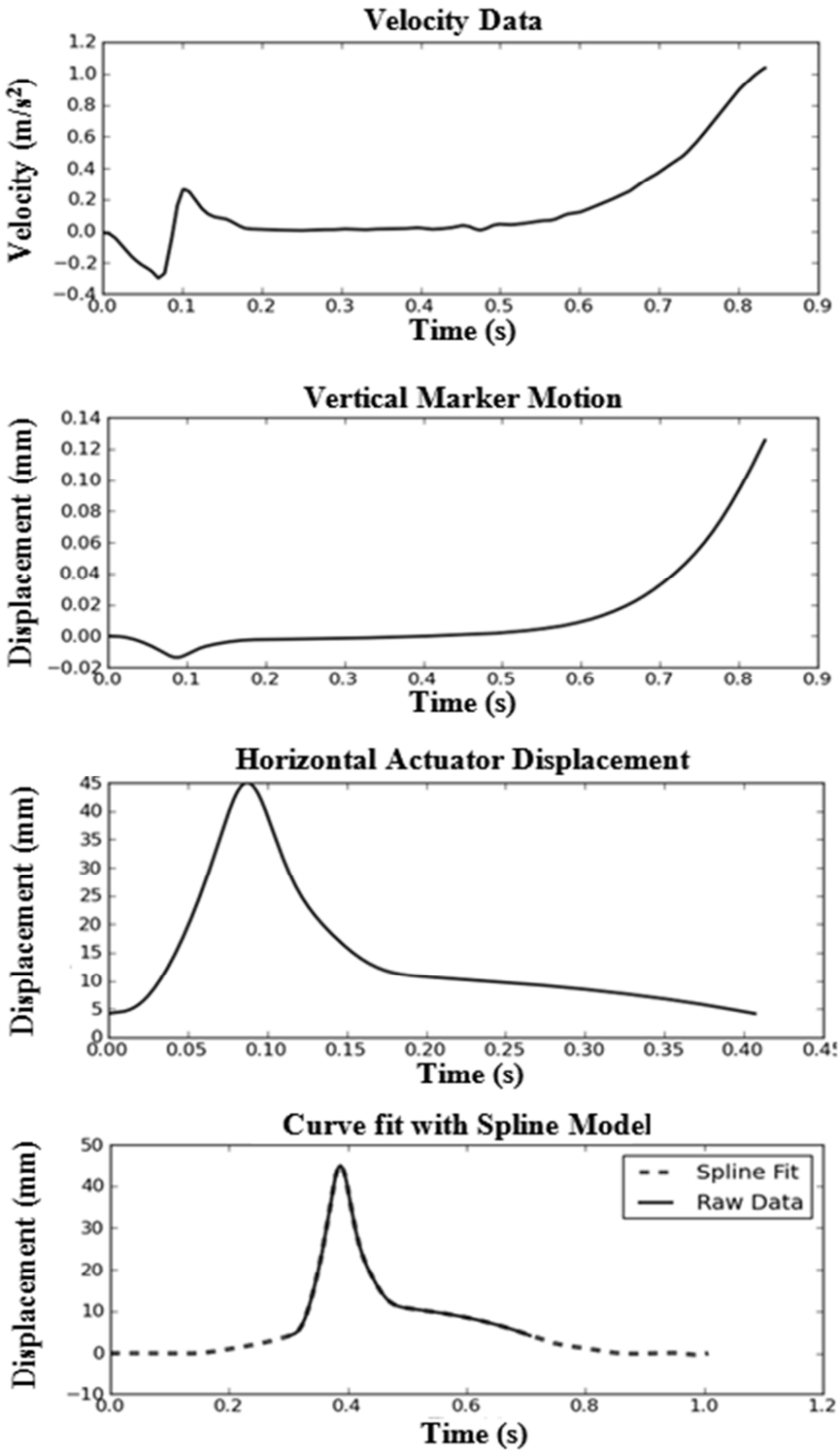

Figure A.4.8: Device Drive Profile Development
(a) Vertical Velocity of Marker, (b) Vertical Displacement of Marker, (c) Vertical Displacement of Device Platen, (d) Smoothed Vertical Displacement of Device Platen.

A large negative acceleration (-75m/s^2) is then applied which brings the platen to a stop and initiates decompression of the tissue. The initial decompression is also rapid simulating the transfer of load from the rear foot to the forefoot in gait. The remaining decompression occurs over ~0.3s at a steadily decreasing negative velocity. This returns the platen to zero displacement allowing 10 compressive cycles to be run consecutively.

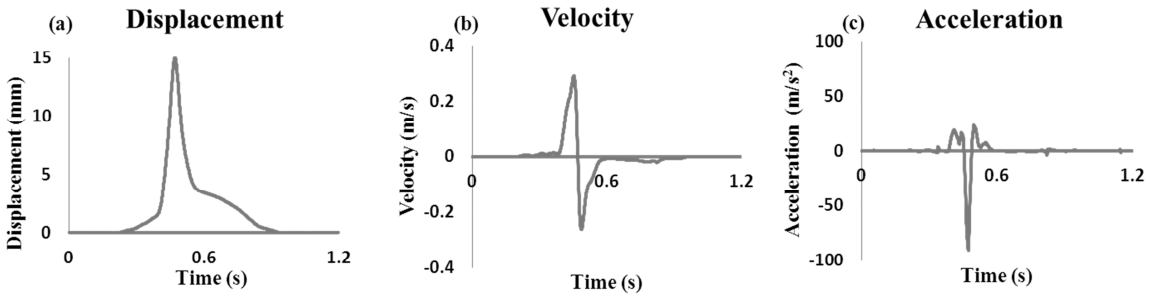

Figure A.4.9: Gait Simulation Profile for the Rear Foot
(a) Vertical Displacement, (b) Vertical Velocity, (c) Vertical Acceleration

A.4.4.4 Limitations of Gait simulation Profiles

Limitations exist within both the data used to derive the profiles and the methods of application.

The derived gait simulation profiles for each region are based on individual surface markers. Although markers which provided both stability and proximity to the region of interest were selected, an individual marker cannot truly represent the motion of an internal structure such as the Calcaneus. The small range over which the tissue compression occurs (10 – 20mm) makes the influence of errors generated by marker movement a potential problem. Surface markers are susceptible to vibration and skin movement, which introduces error within the motion capture data. Detection errors are also present due to the accuracy of the camera system used, although this can be minimised by using a close arrangement of motion capture cameras it cannot be completely removed without smoothing. The short duration of the compression and decompression phases (~0.1s) may result in smoothing and sampling techniques having an influence on the derived trajectories due to the attenuation of some high frequency components which are not pure noise (Winter, 1987). The device and profiles

developed allow for the application of load and compression of tissue at rates which aim to replicate gait; however the profiles are limited to only the vertical plane of motion and therefore represent a greatly simplified version of the overall gait dynamics. The restriction of the loading profiles to displacement only control also limits the gait-like nature of compression. Due to compliance within the subject bracing the foot is not rigidly fixed during testing, thus without feedback or control based on the load applied to the tissue the displacement driven compression may not be capable of maximally compressing the tissue in a repeatable manner. Controlled compression capable of encompassing both low and high rate trials in-vivo has not previously been attempted and thus the use of displacement only control provides a new benchmark for future studies, which should aim to control both the displacement and load conditions during dynamic testing in-vivo.

A.4.6 Conclusion

Standard profiles were developed in two forms, a triangle wave with low constant velocity and a sinusoidal wave with low variable velocity. These profiles aim to provide data to assess the effect of loading rate on tissue mechanics, whilst also providing a means to compare the derived properties to the data reported within the literature. Gait simulation profiles were developed based on the measured vertical velocity of a marker at the heel during normal gait of healthy elderly subjects. These profiles aim to provide data to characterise the functional response of the tissue during gait, whilst also providing a means to compare to the derived properties to those of the previous in-gait studies. The capacity to assess the response of the tissue at a single anatomical location under both standard and complex conditions provides a unique opportunity to compare the two approaches. This method also allows for models derived based on one condition to be tested under dynamically different conditions, thus permitting the development of robust modelling methods.

A.5. Measurement & Processing

A.5.1 Data Collection

A.5.1.1 Analogue Data Collection

Analogue outputs from the Linear Variable Differential Transformer (LVDT) (S-Series, Solatron, UK) and load cell (TC34, Amber Instruments, UK) were converted into digital signals via a 12bit conversion at 3000Hz and input to a PC via USB using a National Instruments Data Acquisition (NIDAQ) module (NI USB-6008, National Instruments, UK). Data was then logged via LabView (Signal Express LE, National Instruments, UK) and saved to an external hard drive in ascii format for further processing.

A.5.1.2 Ultrasound Data Collection

A 13-4MHz linear array ultrasound probe (LA523, Mylab 70, Esaote, Italy) with 5cm^2 imaging surface was used, the device was set to an effective detectable depth of 40mm with operating frequency of 4MHz to permit increased penetration through the multiple device and tissue interfaces. The capture frequency of the ultrasound video was 201Hz and data were saved to an external hard drive as low compression avi video files.

A.5.1.3 Data Synchronisation

During testing a 5V square wave was simultaneously input to the ultrasound system and to the NIDAQ module to allow synchronisation of the two data sets.

A.5.2 Digital Data Pre-Processing & Signal Conditioning

A.5.2.1 Digital Data Pre-Processing

The raw data from the LVDT and load cell contained high frequency noise due to an electromagnetic field created by the actuator and vibrational oscillation within the device. Using Python (Enthought Python Distribution, Version 6.6.1), an analysis of the frequency spectrum for the raw data was conducted via the Fast Fourier Transform (fft) function in Python (numpy.fft). To identify the useful data range, residuals were calculated for the fit between raw data and the data filtered using low pass Butterworth filters with cut-off frequencies from 0 to 30 Hz. For the displacement data, the frequency spectrum showed a reduction to nominal power at approx. 20Hz while the residual data showed a linear low residual error when filtered above 5Hz (Figure A.5.2). This suggested that the noise within the signal was predominantly within the high frequency range. To preserve the raw data, a cut-off of 20Hz was selected as this resulted in low attenuation of the true displacement signal but removed the high frequency noise (Winter 1987). For the load data, a more complex signal was found. The frequency spectrum displayed 2 regions of interest (Figure A.5.3), an initial region for the true load response (0-10Hz) and a subsequent region attributed to vibration based noise (10-28Hz). Assessment of the residual plot showed a large transition region between a filter cut-off which resulted in high signal distortion and a filter which resulted in high amounts of noise passed through (Winter 1987). To provide a balance, a cut-off frequency was selected at 10Hz allowing retention of the true signal with minor attenuation whilst signal noise was reduced greatly. To match the sampling frequency of the ultrasound data, the analogue data was down sampled to 201Hz via piecewise linear interpolation (Figure A.5.1).

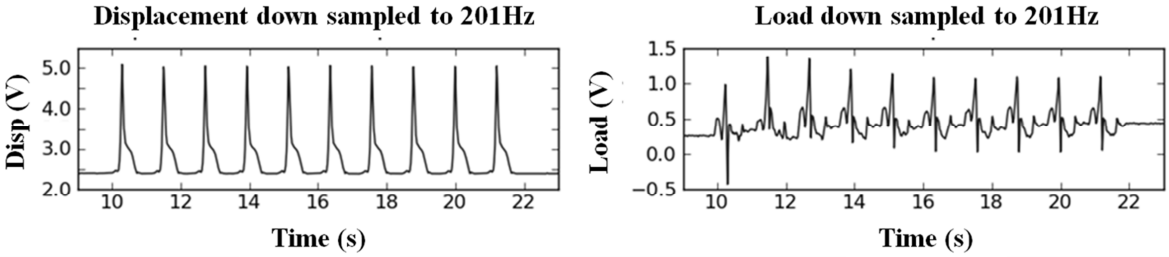

Figure A.5.1: Digital Signal Re-Sampling

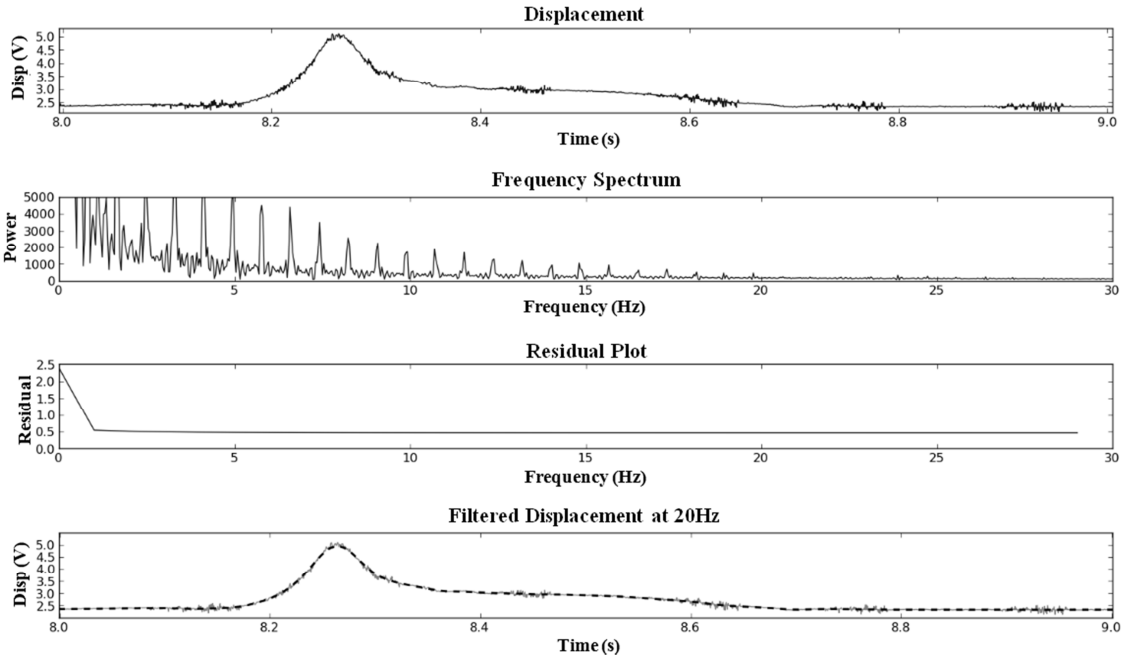

Figure A.5.2: Digital Signal Filtering of Displacement Data

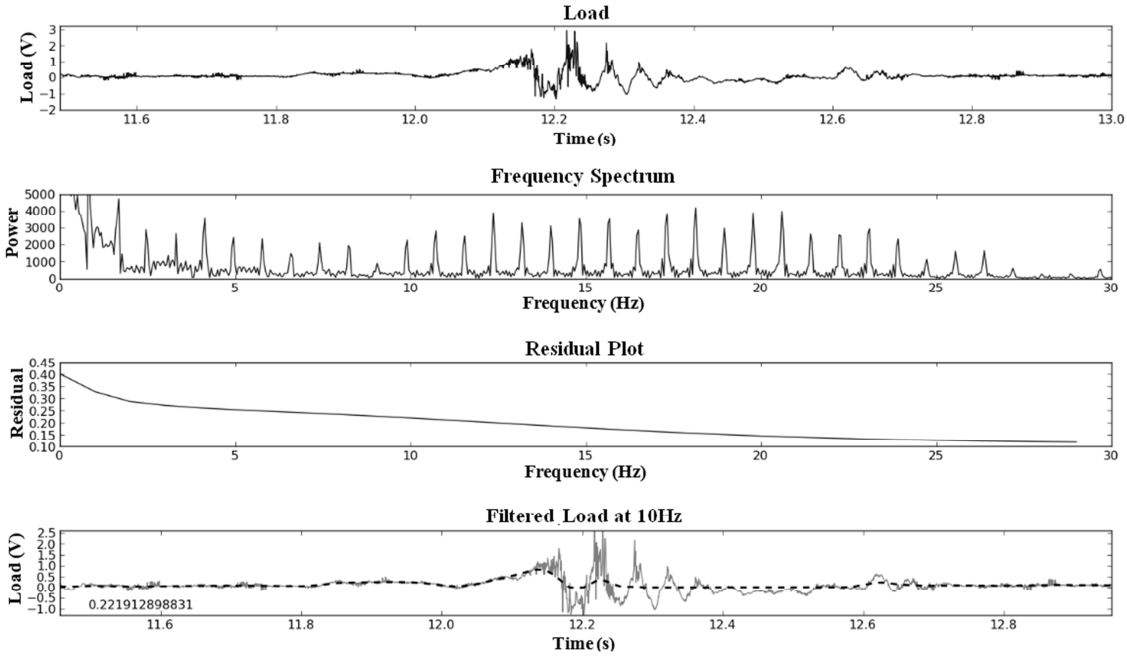

Figure A.5.3: Digital Signal Filtering of Load Data

A 5.2.2 LVDT Calibration

A static calibration of the LVDT was conducted to find the conversion factor from Volts to mm. The platen set to the home position (taken as a displacement of zero), the platen was then raised by the following increments using metric gauge blocks; 3mm, 6mm, 9mm, 15mm, 30mm and 45mm. At each position, the voltage was recorded for 10s and the average voltage for the 10s period was calculated (Table A.5.1). This was plotted with standard deviation (Figure A.5.4), and a line was fit to the voltage against displacement data to derive the conversion equation.

Table A.5.1: LVDT Calibration Values with Standard Deviation

Vertical	Voltage	SD
0	2.3969	0.0231
1	2.5668	0.0235
2	2.7365	0.0275
3	2.9076	0.0241
5	3.2443	0.0226
10	4.0954	0.0280
15	4.9609	0.0298

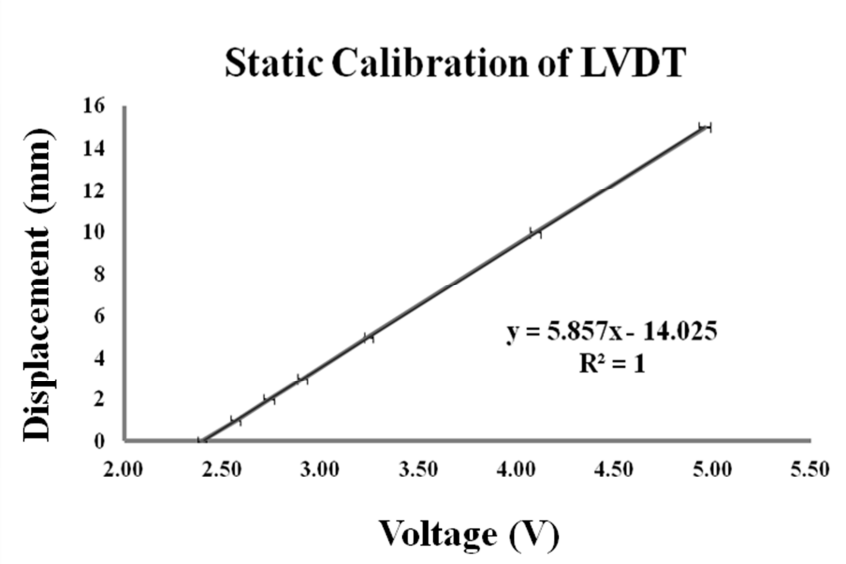

Figure A.5.4: Calibration of LVDT. Curve equation and Pearson's Correlation Coefficient are given.

A linear curve fit ($R^2 = 1$) provided the conversion equation:

Displacement *(mm) = (Volts *5.857) -14.025* (EQ A.5.1)

A.5.2.3 Load Cell Calibration

A.5.2.3.1. Static Calibration

The load cell was calibrated statically to find a conversion factor from Volts to Newtons. The device was loaded with known weights in the range 1 – 30kg in the following increments: 1kg, 3kg, 5kg, 10kg, 15kg 20kg, 25kg and 30kg (Table A.5.2). For each load, the voltage was recorded for 10s and the average voltage for the 10s period was plotted along with the standard deviation (Figure A.5.5). A line was fit to the voltage against displacement data to derive the conversion equation.

Table A.5.2: Load Cell Calibration in kg & N Values with Standard Deviation

kg	Newtons	Voltage	SD
0	0	0.0582	0.0087
1	9.81	0.5312	0.0087
3	29.43	1.1517	0.0085
5	49.05	1.9068	0.0090
10	98.1	3.5708	0.0087
15	147.15	5.1906	0.0088
20	196.2	7.0295	0.0083
25	245.25	8.5120	0.0084
30	294.3	9.9669	0.0000

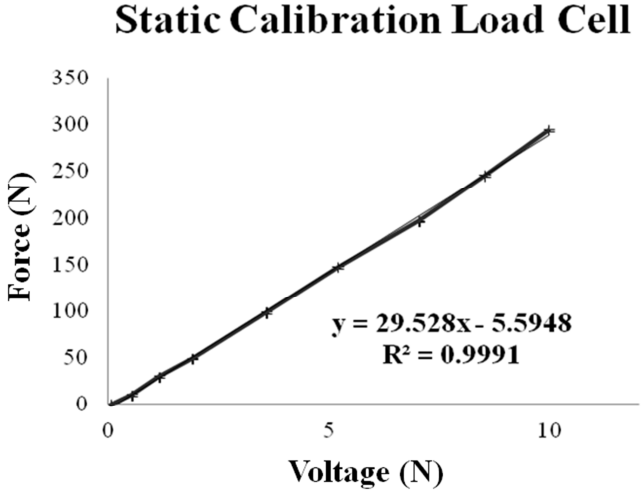

Figure A.5.5: Calibration of Load Cell. Curve equation and Pearson's Correlation Coefficient are given.

A linear curve fit ($R^2 = 0.9991$) provided the conversion equation:

*Force (N) = (Volts * 29.528) - 5.5948* (EQ A.5.2)

A.5.2.3.2. Dynamic Calibration

To remove dynamic error generated by the mechanism (inertia and frictional loading), calibration load profiles were created for each test condition. The device was run in free-air for a total of 60 cycles whilst data for load were recorded using the load cell. An average load cycle for the dynamic error was calculated as the mean load across the time series for all 60 cycles to create a calibration profile (Figure A.5.6). This calibration profile was used to correct the load data measured for each cycle during the dynamic tests. The efficacy of the dynamic calibration was dependent on the repeatability of the device displacement, which was shown to perform well for all conditions in separate free air tests (Section A.6.2)

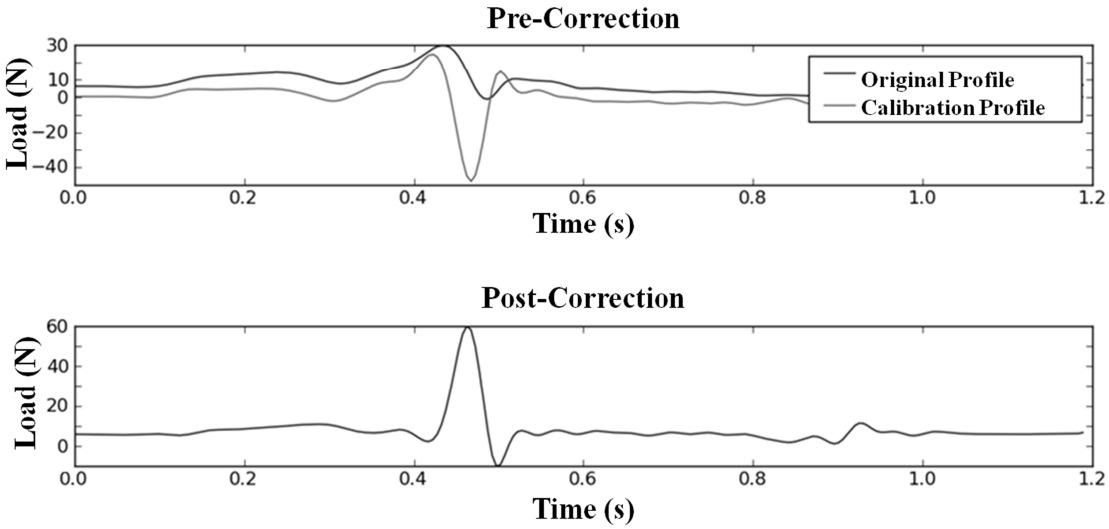

Figure A.5.6: Dynamic Calibration of Load Cell.

A.5.3 Ultrasound Tracking Algorithm

The use of ultrasound tracking permits the large data sets collected using dynamic ultrasound to be processed quickly. The removal of operator-based manual feature identification also removes errors and assumption made when measuring the ultrasound images by eye.

A.5.3.1 Image format and Features of interest

The ultrasound images were cropped to a width of 248 and a height of 480 pixels. The features within the image can be divided into two categories, common features and anatomical features. Common features are structural elements and inputs, labelled to the left of figure A.5.7. Anatomical features for the heel region are the calcaneus and the mircochamber / macrochamber boundary (figure A.5.7).

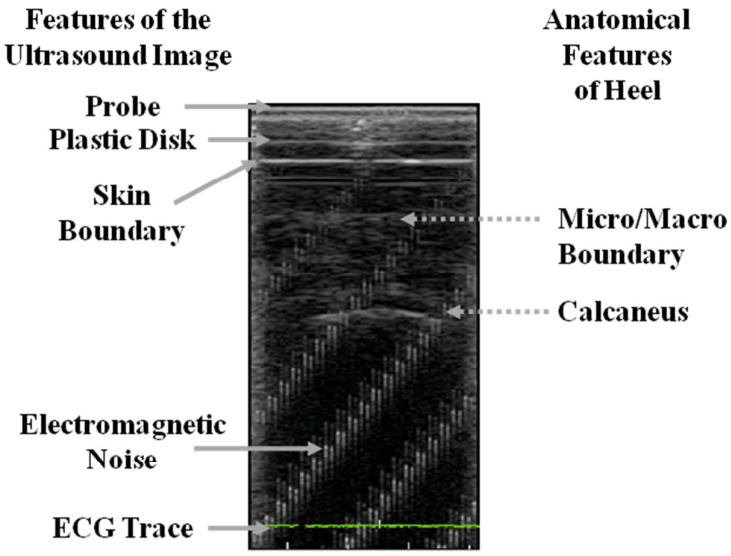

Figure A.5.7: Ultrasound Features of Interest

A.5.3.2 Feature Template Generation

To enable the calcaneus to be identified and tracked automatically throughout compression using the ultrasound tracking algorithm, an adjustable curve template was created.

The curve template takes the form:

$$y = \sqrt{w^2 - \Big(c \times \big((x - 0.5) \times (w - x0)\big)\Big)^2} - (0.5 \times h) + y0 \quad \text{(EQ A.5.3)}$$

Where:

c is the curvature of the template; this is matched to the curvature of the calcaneus

w is image width which is fixed to 608 pixels

h is image height which is fixed to 800 pixels

x0 is horizontal apex of the curve with respect to the image centre

y0 is vertical curve offset from the bottom of the image

Using a Python script the template was generated and adjusted manually for each subject. A template image which displays the calcaneus is selected for each subject and plotted using Python (Figure 5.8). For identification of the inputs x0 and y0, the operator is prompted to click on the apex of the calcaneus in the Python figure and the click co-ordinate was recorded as (x0,y0). To define the template width (w) the operator is prompted to click on the medial and lateral borders of the calcaneus, the co-ordinates of each click were recorded as (xa,ya) and (xb,yb), the width is calculated as xb-xa. For selection of curvature, the template image is loaded with example curvatures overlaid (Figure 5.9), the optimum fit was then selected and input to the Python command line. For selection of line-width, the optimum curvature is overlaid onto the template with a range of example line widths (Figure 5.10), the optimum fit is then selected and input to the python command line.

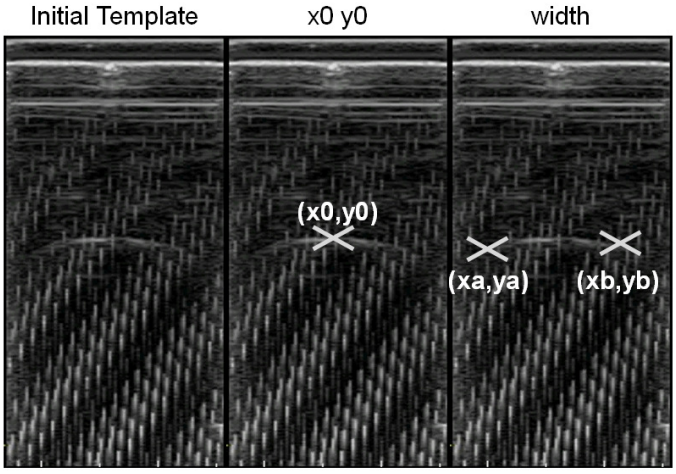

Figure A.5.8: Template Generation and Identification of calcaneus apex and medial and lateral boundaries

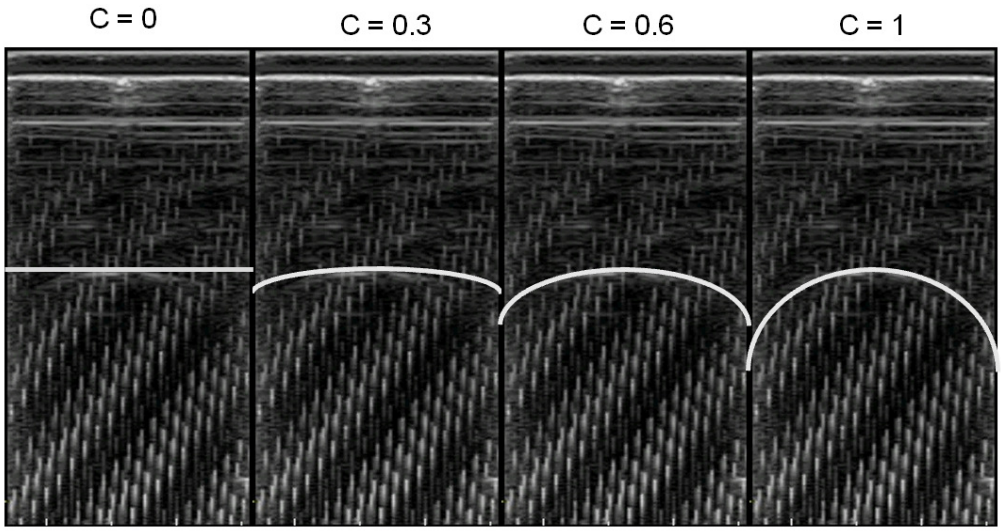

Figure A.5.9: Template Generation and Adjustment for Curvature

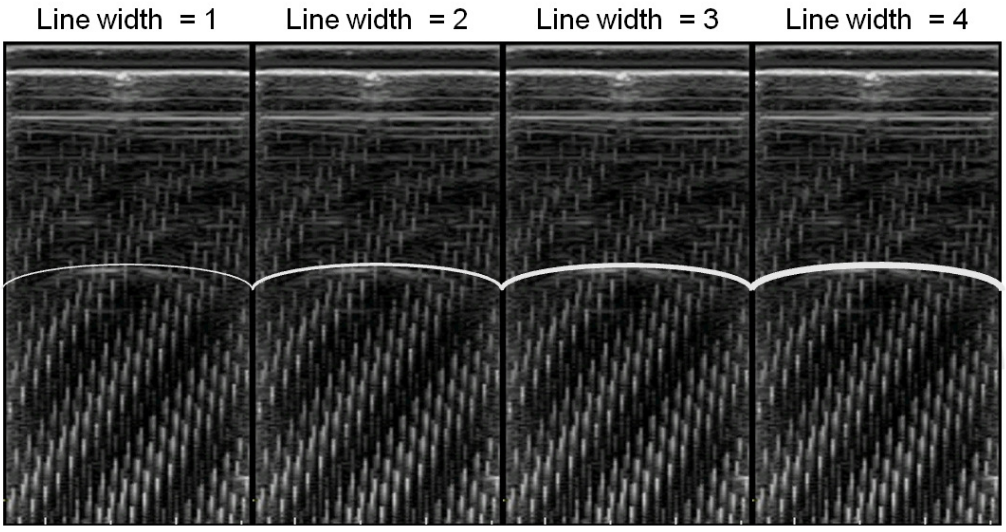

Figure A.5.10: Template Generation and Adjustment for Line Width

The result of this process was a subject specific template which could be applied to all ultrasound images recorded for that individual (Figure A.5.11).

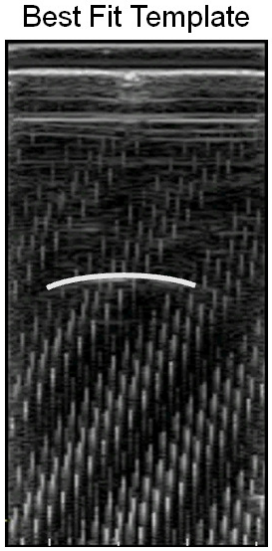

Figure A.5.11: Best fit template for calcaneus

A.5.3.3 Search Range for Template

For each subject, two images were manually selected to represent initial contact and peak compression (Figure A.5.12). The pixel values for the apex of the lowest position of the anatomical feature ($Y_{(min)}$) and the highest position of the anatomical feature ($Y_{(max)}$) were selected. The total search range for each anatomical feature represented the $Y_{(min)}$ and $Y_{(max)}$ values ±50pixels to account for variation between trials. The value for $Y_{(min)}$ was taken as an initial guess when tracking.

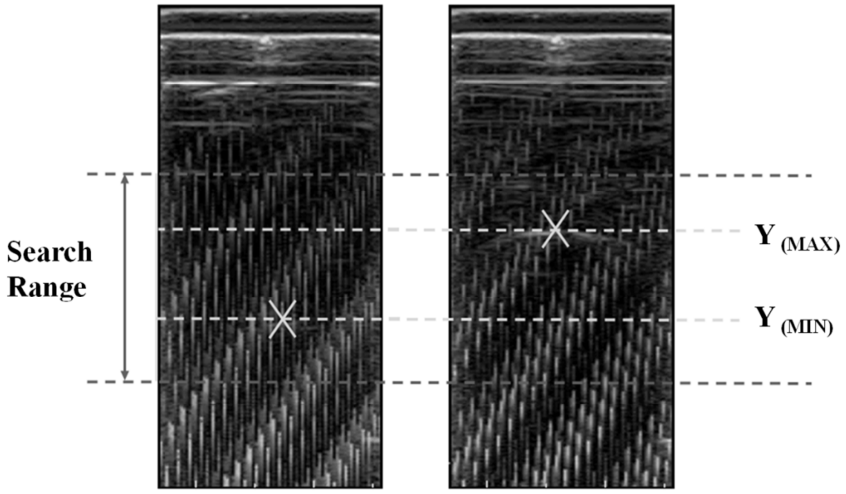

Figure A.5.12: Search Range for Template

A.5.3.4 Ultrasound Feature Tracking

FFmpeg software (FFmpeg 1.1, Fabrice Bellard. France) was used to split the avi ultrasound files into individual frames. A Python code then applied the best fit template for the calcaneus to the image at each point throughout the search range (Figure A.5.13), for each frame and a masked image sum was calculated as:

Masked Image Sum = Template + Value of pixels for image beneath template

The highest value for masked image sum represents the maximal correspondence between template and ultrasound image. The coordinates of the maximal correspondence value are recorded for each frame to form a co-ordinate against time profile for the calcaneus.

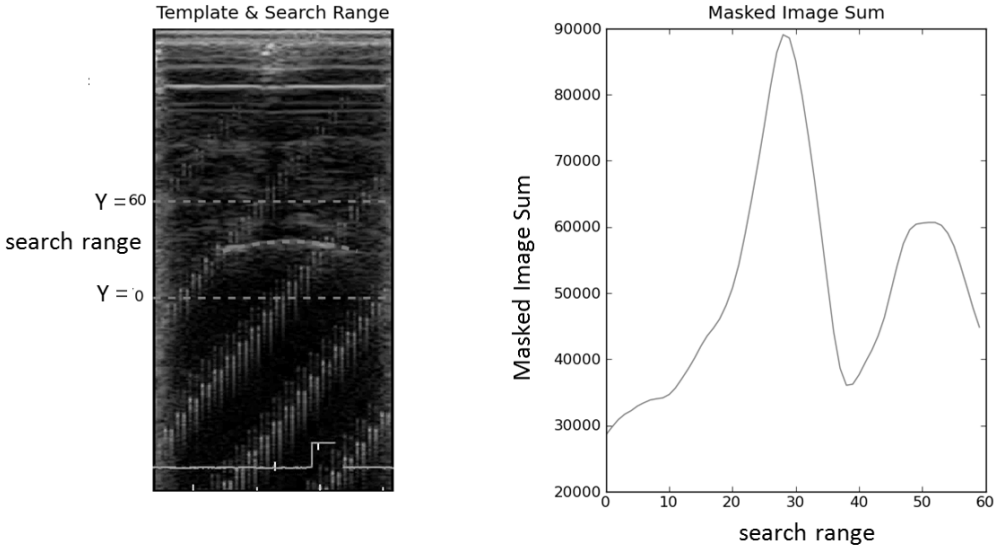

Figure A.5.13: Template Matching Throughout Search Range

A.5.3.5 Ultrasound Tracking Data Pre-Processing

The tracked co-ordinate data include noise where contact with the tissue was lost between compressive cycles and where the electromagnetic noise within the image shows a higher maximal correspondence to the template than the calcaneus (Figure A.5.14). The tracking noise was removed by applying a minimum threshold to the 2nd derivative of the tracked displacement. The second derivative was used as this value is consistently low during regions of effective tracking and consistently high during regions of erroneous tracking. The use of the

second derivative in place of simply applying a minimum threshold to the raw tracking data prevents removal of actual calcaneus tracking data at the lower bounds of the search range.

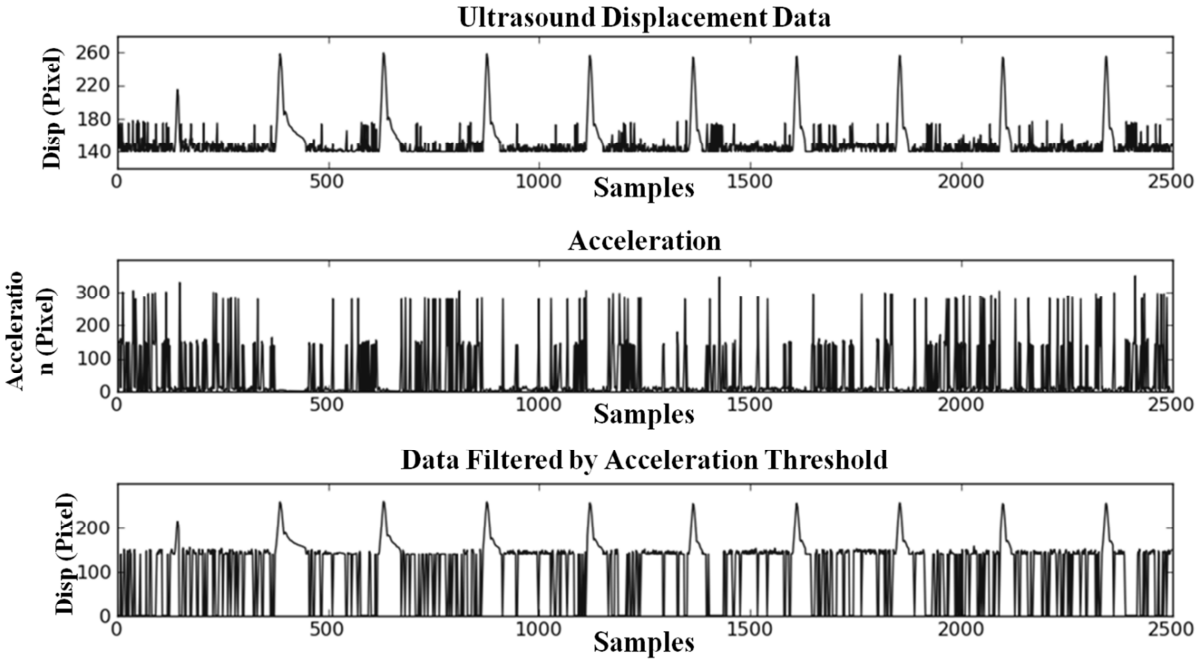

Figure A.5.14: Filtering of Ultrasound Tracking Data

Following thresholding, the data were cut to individual compression cycles based on the trigger position and the known sample length of the input profile (input profile time/capture frequency). The remaining displacement noise was then removed by sweeping back and forward from the displacement peak and cutting when displacement drops to zero. This resulted in a clean ultrasound tracking co-ordinate profile for each cycle of compression (Figure A.5.15).

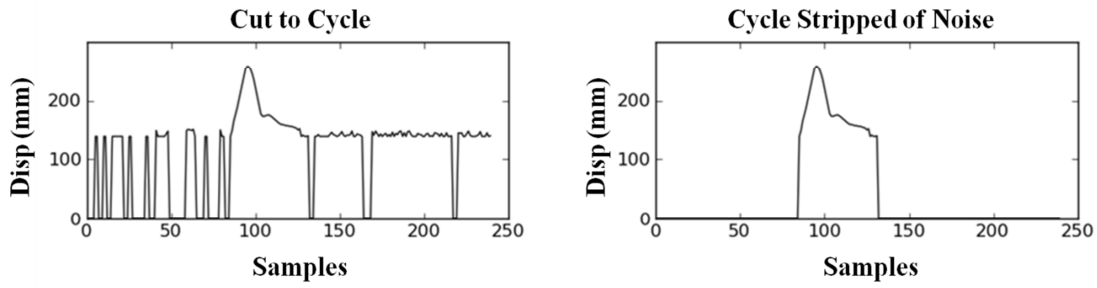

Figure A.5.15: Filtered Ultrasound Tracking Data per cycle

A.5.3.6 Tissue Thickness Calibration

Using the millimetre scale on the ultrasound images, a conversion factor was established for the conversion of pixel co-ordinate values to mm (Figure A.5.16).

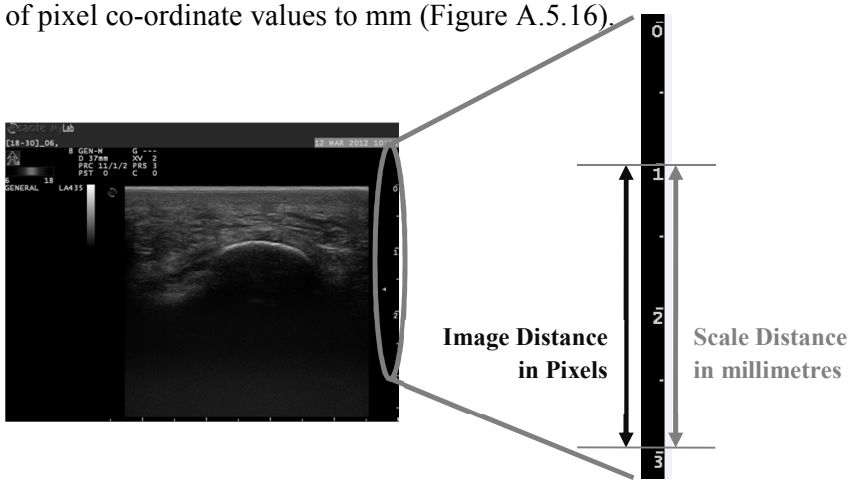

Figure A.5.16: Ultrasound Calibration Frame

Conversion Factor = Depth of Image (mm) / Depth of Image (Pixels) (EQ A.5.4)

The pixel co-ordinate values measured by the tracking algorithm were converted to tissue thickness measurements (Figure A.5.17) by calculating the number of pixels between the plastic disk boundary and the tracked calcaneus apex co-ordinate.

Thickness (pixels) = Disk (Pixel Value) – Apex co-ordinate (Pixel Value) (EQ A.5.5)

This was converted to mm thickness (Figure A.5.17) using the conversion factor.

*Thickness (mm) =Thickness (pixels) * Conversion Factor* (EQ A.5.6)

To calculate the tissue displacement (Figure A.5.17) for the calcaneus, the measured tissue thickness was subtracted from the unloaded tissue thickness for each point to give:

Tissue Displacement $_{(t)}$ *=Unloaded Thickness – Loaded Thickness* $_{(t)}$ (EQ A.5.7)

This produced a profile for tissue displacement at the calcaneus for each cycle of compression.

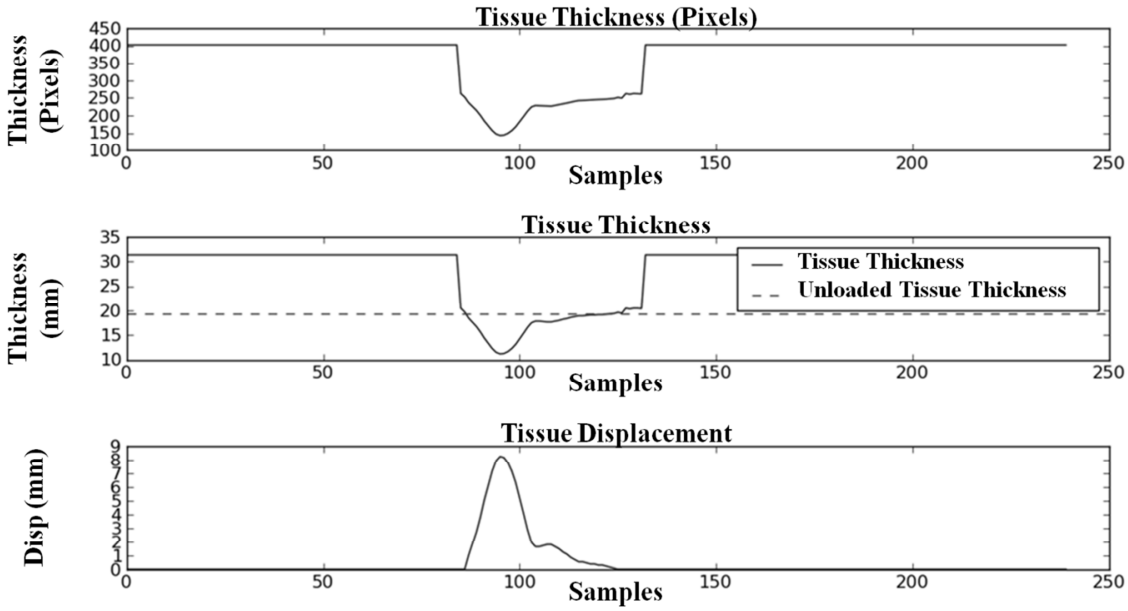

Figure A.5.17: Conversion of Pixel Data to Displacement Measurements

A.5.4 Mechanical Property Derivation

A.5.4.1 Tissue Stress Derivation

To produce a stress profile (Figure A.5.18) from the pre-processed load data, the following equation was used:

Stress = Load/Area (EQ A.5.8)

Where: Load was force measured via the miniature load cell (N) and the Area was the top surface area of the plastic disc which made contact with the bottom surface of the tissue (m^2).

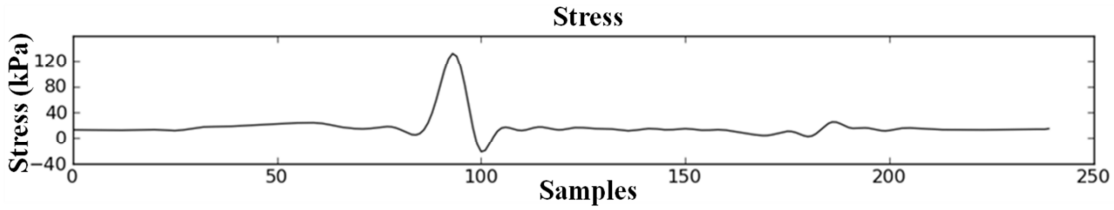

Figure A.5.18: Conversion of Measured Load to Tissue Stress

A.5.4.2 Tissue Strain Derivation

To produce a strain profile (Figure A.5.19) from the pre-processed displacement data, the following equation was used:

Strain (ε) = Displacement / Unloaded Thickness (EQ A.5.9)

Where: Unloaded Thickness is the measured thickness of the tissue pre-compression and Displacement is the change from the unloaded state (EQ A.5.7 Section 5.3.6).

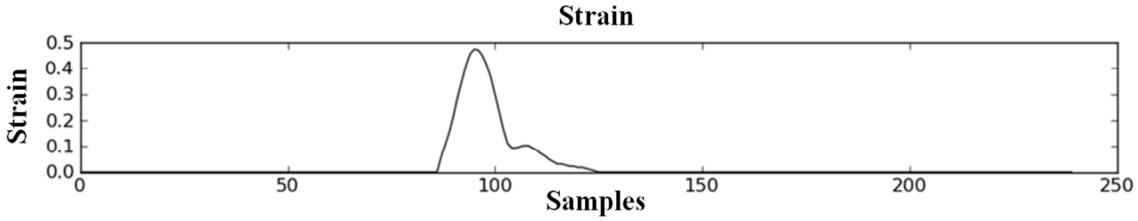

Figure A.5.19: Conversion of Measured Displacement to Tissue Strain

A.6. Device Validity / Evaluation

A.6.1. Introduction

To evaluate the device's performance a range of tests were conducted. The drive mechanism and coupling system was evaluated on its ability to produce the expected vertical platen displacement. The subject positioning and brace system was evaluated based on its ability to restrict motion of the foot during soft tissue compression. The measurement apparatus was evaluated on its capacity to capture the stress and strain response of the tissue throughout compression. And finally the validity of the recorded response was tested by comparison to a standard materials testing machine.

A.6.2. Input / Output conformance

A.6.2.1. Protocol

To assess the ability of the drive mechanism and coupling systems to conform to the input displacement profile, the data for vertical displacement of the device platen were collected via the LVDT for displacement of the device in free air and for displacement of the device during tissue compression.

A.6.2.1.1. Assessment in Free-Air

For the assessment of conformance without tissue compression, data were collected for each of the loading profiles (T-Wave, S-Wave and Gait Sim). Due to the variability of the S-Wave profile both a low amplitude and high amplitude input profile were tested. For each profile, a total of 60 cycles were conducted to produce a total of 60 displacement profiles describing the vertical motion of the STRIDE platen in free air.

A.6.2.1.2. Assessment in Compression

For the tissue compression assessment, data were collected for only the T-Wave and Gait Simulation Condition. The S-Wave condition was excluded from this assessment due to the inherent variation caused by matching the sine wave amplitude to a percentage of the

subject's tissue thickness. 10 Compression cycles for each profile were conducted on 10 subjects to produce a total of 100 displacement profiles describing the vertical motion of the STRIDE platen during tissue compression.

A.6.2.2. Analysis

To assess the level of fit, each cycle was compared to the input profile using Pearson's Correlation coefficient (R^2) and RMS Error in Python. The R^2 value was calculated for each measured displacement profile as compared to the input profile using the pearsonr function in the scipy.stats package of Python. The RMS error was calculated for each test cycle by the following equation:

$$RMS = \sqrt{\frac{1}{n}\sum_{i=1}^{n} (Input\ Profile - Measured\ Platen\ Displacement)^2} \quad \text{(EQ A.6.1)}$$

The average RMS error and average R^2 values were calculated as the mean across all measured displacement cycles. To assess how stable the peak displacement was for each condition, the absolute target error was calculated by subtracting the target peak (15mm) from the actual measured peak displacement.

A.6.2.3. Results and Discussion

The without tissue results display good conformance of input and measured output values (Table 6.1), with all conditions displaying correlations above 0.99 and RMS error below 0.4mm. Both the high amplitude S-Wave and the Gait simulation profiles displayed higher values for RMS and target displacement error. It is expected that this is due to the high accelerations required at the transitions from positive to negative displacement rates in these profiles. Visual assessment of the profile curves (Figure 6.1) show deviations at the transition from positive to negative displacement for the Gait-Sim condition suggesting over-shooting of the target peak compression. The high values for target error in the Gait-Sim profile may put the tissue at risk of over-compression during testing. The tissue compression results display a very good conformance of input and measured output values (Table 6.2), with all conditions displaying correlations above 0.99 and RMS errors below 0.15. Visual assessment

of the profile curves (Figure 6.2) show a reduction in the deviations at the transition from positive to negative displacement rates for the Gait-Sim condition. The reduction in error for the tissue compression profile may be due to the contact with the tissue acting to aid the deceleration of the STRIDE platen, thus reducing the demand on the actuator. The target displacement error of 0.36mm for the Gait-Sim condition is within a more acceptable level compared to the results from the free air trials, and due to compliance within the device bracing is not likely to impose serious over-compression of the subject's tissue.

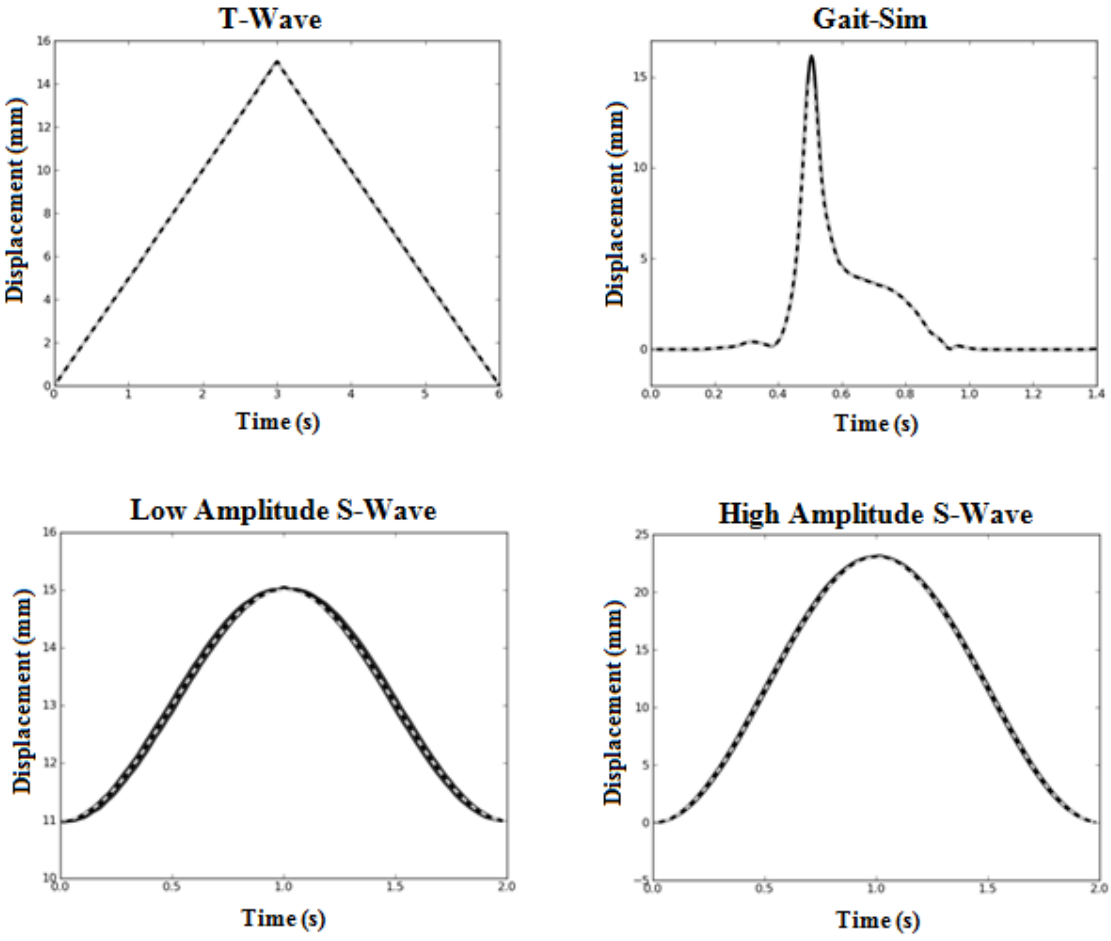

Figure A.6.1: Input/Output conformance for all test conditions, when tested without tissue (in free-air). Dashed grey line (- - - -) is input profile, Solid black line (—) is measured path with a width of 1 standard deviation.

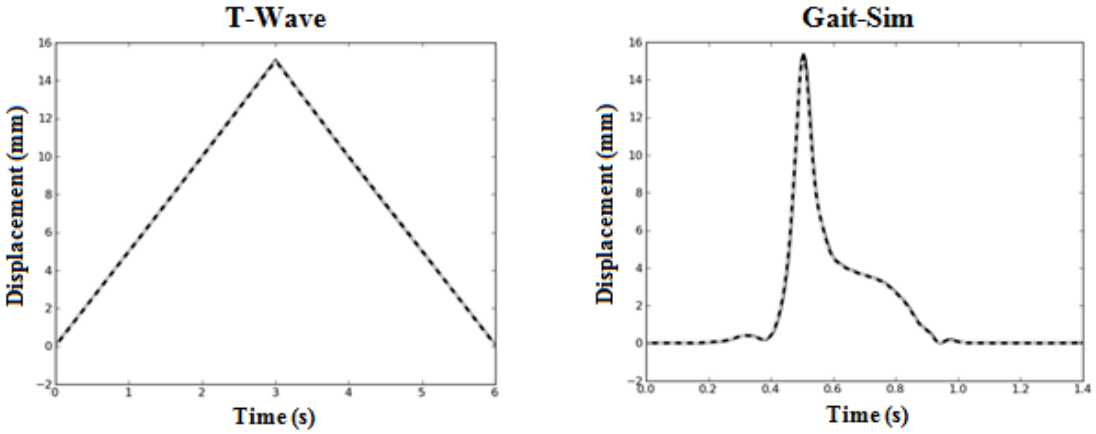

Figure A.6.2: Input/Output conformance for all test conditions, when tested with tissue (in compression). Dashed grey line (- - - -) is input profile, Solid black line (—) is measured path with a width of 1 standard deviation.

Table A.6.1: Input/Output conformance for tests conducted in without tissue compression (in free-air)

No Tissue I/O Conformance	Target Error (mm) Mean SD	RMS Error (mm) Mean SD	Pearsons R^2 Mean SD
T-Wave	0.035 ± 0.023	0.047 ± 0.017	1.000 ± 0.000
S-Wave low amplitude	0.047 ± 0.014	0.083 ± 0.059	0.998 ± 0.004
S-Wave high amplitude	0.111 ± 0.034	0.354 ± 0.195	0.999 ± 0.001
Gait-Sim	1.178 ± 0.073	0.209 ± 0.026	0.999 ± 0.000

Table A.6.2: Input/Output conformance for tests conducted with tissue compression

Tissue Compression I/O Conformance	Target Error (mm) Mean SD	RMS Error (mm) Mean SD	Pearsons R^2 Mean SD
T-Wave	0.065 ± 0.055	0.067 ± 0.040	1.000 ± 0.000
Gait-Sim	0.359 ± 0.093	0.139 ± 0.056	0.999 ± 0.001

A.6.3 Target Strain Conformance

A.6.3.1. Protocol

To assess the brace system's capacity to constrain the foot during tissue compression, measurements of the peak tissue strain were recorded during tissue compression via ultrasound for a total of 35 subjects. A target tissue strain of 0.4 was used as this sat within the range (35% - 60%) of previously recorded values for peak strain (De Clercq 1994, Tong 2003).

A.6.3.1.1. Unloaded Tissue Thickness and Subject Positioning

The region of interest identification, unloaded tissue thickness and subject positioning was conducted as per sections A.4.2.1, A.4.2.2 and A.4.2.3 to ensure a firm bracing of the subject's foot.

A.6.3.1.2. Dynamic Tissue Compression

Following effective bracing, the dynamic profiles were conducted. The applied loading conditions were the T-Wave, the S-Wave and the Gait-Sim conditions (Sections A.4.3 & A.4.5). For the T-Wave condition, three tests of two cycles were conducted for each subject yielding six cycles per subject and >200 total cycles. For the S-Wave condition, three tests of five cycles were conducted for each subject yielding 15 cycles per subject and >500 total cycles. For the Gait-Sim, condition three tests of ten cycles were conducted for each subject yielding 30 cycles per subject and >1000 total cycles. Throughout testing, the subjects were asked to stand with weight distributed evenly between both legs.

A.6.3.2. Analysis

For each cycle, the peak strain value was subtracted from the target strain (0.4) to produce the target strain error. Due to the capacity of the device to either over or under-compress the tissue, absolute values for error were used. Mean values were calculated for the peak strain and absolute error across all subjects. The average error for each condition was expressed in terms of absolute strain error and as a percentage of the target (Table 6.3).

A.6.3.3. Results and Discussion

The average true strain for all conditions was consistently below the target strain of 0.4. This suggests that the tissue did not achieve its full compressive potential during the dynamic testing (Table 6.3.). For all conditions the error was > 5% but not more than 10% of the total tissue thickness. For an average heel pad tissue thickness of 17.1mm (Ledoux 2007), this equates to a displacement error between 0.86mm and 1.71mm, which was much greater than the observed device conformance (Section 6.2). Due to the fixed vertical displacement of the device platen, the error must be accounted for by lifting of the foot within the brace or compliance within the brace structure. This is likely to be enhanced at high velocities due to the viscous response of the tissue, which acts to increase resistance within the tissue to imposed strain.

Table A.6.3: Mean Target Strain Error

	True Strain	95% Confidence Intervals		Strain Error	Percentage of Tissue
	Mean SD	low	high	Mean SD	(%)
T-Wave	0.355 ± 0.049	0.306	0.404	0.057 ± 0.036	5.74%
S-Wave	0.330 ± 0.058	0.272	0.388	0.077 ± 0.049	7.70%
Gait-Sim	0.361 ± 0.055	0.305	0.416	0.053 ± 0.044	5.25%

A.6.4. Cycle to Cycle Variability

A.6.4.1. Protocol

To assess the variability of the measured soft tissue strain and stress between test cycles, the measured strain and stress values were compared to the average strain and stress values for a total of 5 subjects.

A.6.4.1.1. Unloaded Tissue Thickness and Subject Positioning

The region of interest identification, unloaded tissue thickness and subject positioning was conducted as per sections A.4.2.1, A.4.2.2 and A.4.2.3 to ensure a firm bracing of the subject's foot.

A.6.4.1.2. Dynamic Tissue Compression

Following effective bracing, the dynamic profiles were conducted using the T-Wave and the Gait-Sim conditions (Section A.4.3 & A.4.5). For the T-Wave condition, three tests of two cycles were conducted for each subject yielding six cycles per subject for comparison. For the Gait-Sim condition, three tests of ten cycles were conducted for each subject yielding 30 cycles per subject for comparison. Throughout testing, the subject was asked to stand with weight distributed evenly between both legs.

A.6.4.2. Analysis

For each subject, average profiles were created for each condition. The average profiles were calculated as the mean for all cycles across the full time series (Figure 6.4.2.). To assess the cycle to cycle variability, the measured stress and strain for each cycle was compared to the average profiles for stress and strain using Pearson's Correlation coefficient (R^2) and RMS Error in Python. The R^2 value was calculated for each cycle compared to the average profile using the pearsonr function in the scipy.stats package of Python. The average RMS error and average R^2 values were calculated as the mean across all measured cycles for stress and strain. The RMS error for cycle to cycle variance was calculated as:

$$RMS = \sqrt{\frac{1}{n}\sum_{i=1}^{n} (Average\ Profile - Measured\ Cycle\ Profile)^2} \quad \text{(EQ A.6.2)}$$

A.6.4.3. Results and Discussion

Visual inspection of the stress and strain curves shows low standard deviation bands for the measured strain in both T-Wave and Gait-Sim conditions, and relatively greater standard

deviation bands for the measured stress (Figure 6.3). The stress-strain curves for the T-Wave condition show a consistently low standard deviation throughout (Figure 6.3). For the Gait-Sim condition, an initially large standard deviation is present, immediately after impact; however the standard deviation throughout the remainder of loading and unloading is consistently low (Figure 6.3). The average profile to measured cycle R^2 values for both stress and strain data were high (>0.95) in both the T-Wave and the Gait-Sim conditions (Table 6.3). This suggests that the pattern of loading was consistent between cycles. The average profile to measured cycle RMS error values for the measured strain were consistently low (Table 6.3) suggesting a good cycle to cycle reliability of the measured strain. The RMS error values for the measured stress were consistently higher than those observed for tissue strain (Table 6.3). This increased RMS error suggests lower cycle to cycle reliability of the measured tissue stress. The initial high standard deviations observed in the stress profiles for the Gait-Sim condition may be the result of incomplete relaxation in tissue as a result of reduced rest time between compressions. It is also possible that the greater number of compressive cycles used in the Gait-Sim condition may have induced an adaptive response within the tissue, by which the tissue becomes preconditioned to a particular loading profile (Ker 1996).

Table A.6.4: Cycle to Cycle Variance for the measured Stress and Strain.

	Tissue Strain		Tissue Stress	
Loading Condition	Pearsons R2	RMS	Pearsons R2	RMS
T-Wave	0.994 ± 0.006	0.013 ± 0.008	0.995 ± 0.005	4.242 ± 2.105
Gait-Sim	0.981 ± 0.018	0.003 ± 0.001	0.973 ± 0.021	1.624 ± 0.568

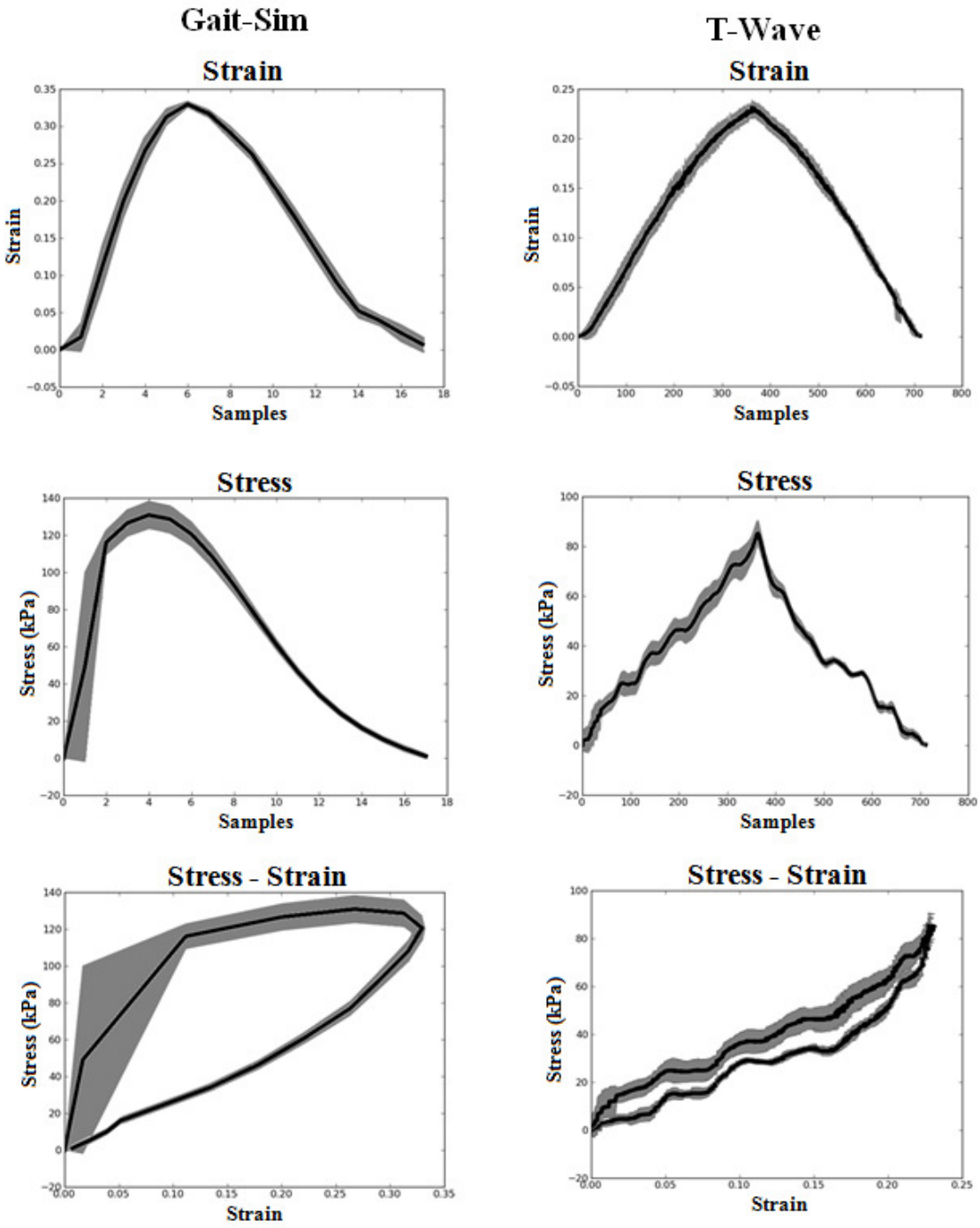

Figure 6.3. Typical Cycle to Cycle Variance curves for the T-Wave and Gait Simulation test conditions. The solid black line (—) represents the mean of the measured response for all cycles in a single trial and the grey region represents 1 standard deviation from the mean.

A.6.5. Validity Compared to Instron Tests

A.6.5.1. Protocol

To assess the validity of properties derived using STRIDE, a comparative study was designed. This study measured the stress-strain response of two tissue samples under compression at low velocities. The samples were first measured using a materials testing machine and then tested using STRIDE.

A.6.5.1.1 Specimen Preparation

A fresh sample of pork belly fat was dissected free from the underlying muscle and cut into 2 square specimens with length and width of 50mm and depth of 10mm. Specimens were stored in a water bath of saline solution until testing and between testing sessions.

A.6.5.1.2 Instron Testing

Each specimen was placed between the two platens of an Instron materials testing machine (4200 Series, Instron., Uk), which used a 100N load cell. The top platen was positioned in contact with the specimen such that a small preload was present (<0.01N). The top platen was displaced toward the specimen at a rate of 5mm/s for a total distance of 5mm before stopping. Data for force and platen displacement were acquired at 20Hz. Each specimen was tested 5 times, and between trials the specimen was allowed to return to its unloaded state in the saline solution for a period of 2 minutes.

A.6.5.1.3 STRIDE Testing

Each specimen was then tested between the STRIDE platen and a fixed upper platen. The STRIDE platen was raised such that the specimen made contact with the upper platen so that an ultrasound image of the specimen could be achieved. Although the preload could not be directly measured in this setup, it is expected that a small load was present. The STRIDE platen was displaced toward the top platen at a rate of 5mm/s for a total distance of 5mm

before stopping. Data for platen displacement and force were collected at 3000Hz and ultrasound images were recorded at 201Hz. As previously, the specimens were tested 5 times and were allowed to return to their unloaded state between trials.

A.6.5.2. Tissue Characterisation

To characterise the loading response of the tissue during compression, a curve-based analysis was conducted. Values for peak strain were based on the difference between the thickness at initial contact (first measurement) and peak compression. Values for peak stress were recorded as the absolute maximum stress measured. A secant modulus was taken as the gradient of the line between zero and peak stress-strain at peak stress. For assessment of the response throughout loading, the raw loading response data were first fit using a 3rd order polynomial curve. The fit curve was divided into three sections; initial, intermediate and final. For each section 100 data points were extrapolated from the polynomial equation for strain and stress. The Average gradient of the curve was calculated as the average of the 1st derivative, of the polynomial fit, calculated for each of the 100 data points defined for each region.

A.6.5.3. Results and Discussion

The peak strain achieved in each sample did not differ significantly between the Instron and STRIDE tests, suggesting an equivalent tissue compression was achieved in each case (Table 6.5.1 & 6.5.2). Large significant percentage differences were observed for Peak Stress (p<0.05), suggesting a potential over estimation of the tissue stress with STRIDE. It is possible that testing on the Instron device prior to testing on with STRIDE may have influenced these results. Although the tissue was allowed time to recover between compressions, a considerable amount of bulging in all directions was noted in both the Instron and STRIDE tests, which may have induced permanent deformation within the tissue and impacted on the tissue's response to subsequent loads. The assessment of zero strain as the point at which both top and bottom platens are in contact with the specimen may have also impacted on the results. Even a slight reduction in the thickness of the sample (due to deformation during Instron testing) would result in an initially pre-strained position and thus an increased stress response. Due to the dependence of the secant modulus and the final curve

gradient on the measured Peak Stress, large differences are also observed in these variables (Tables 6.5.1 & 6.5.2). The increasing trend observed in the gradient of the loading curve throughout compression was present for both the Instron and STRIDE tests (Tables 6.5.1 & 6.5.2). This suggested a good agreement for the non-linear nature of the loading response. For the purposes of this study, these results add weight to methods which act to characterise the response of the tissue throughout loading using curve-fitting techniques or modelling approaches, however suggest caution should be taken when characterising the tissue using direct measurements of Peak Stress and Strain. Further, more comprehensive testing is required to confirm the absolute accuracy for STRIDE.

Table A.6.5: Curve characteristics and Mechanical Properties for Sample A

Sample A		Instron	STRIDE	% Diff	Sig
Parameters	Units	Mean SD	Mean SD		
Peak Strain	(-)	0.17 ± 0.02	0.17 ± 0.01	0.30%	0.966
Peak Stress	kPa	60.57 ± 12.96	108.37 ± 18.73	78.93% **	0.004
Secant	kPa	364.42 ± 63.66	654.62 ± 135.34	79.63% **	0.008
Initial	kPa	49.78 ± 53.80	190.82 ± 195.57	283.35%	0.238
Intermediate	kPa	313.71 ± 75.08	359.66 ± 122.46	14.65%	0.609
Final	kPa	605.84 ± 208.63	1448.49 ± 284.64	139.09% **	0.001

* Denotes significance at $p<0.05$; ** Denotes significance at $p<0.01$

Table A.6.6: Curve characteristics and Mechanical Properties for Sample B

Sample B		Instron	STRIDE	% Diff	Sig
Parameters	Units	Mean SD	Mean SD		
Peak Strain	(-)	0.17 ± 0.05	0.19 ± 0.01	10.43%	0.436
Peak Stress	kPa	52.81 ± 16.07	82.93 ± 4.42	57.01% *	0.015
Secant	kPa	305.30 ± 38.33	439.69 ± 34.01	44.02% **	0.007
Initial	kPa	80.99 ± 49.27	62.76 ± 36.03	-22.51%	0.765
Intermediate	kPa	218.93 ± 74.32	239.76 ± 45.43	9.51%	0.613
Final	kPa	501.82 ± 119.48	975.55 ± 96.61	94.40% **	0.007

* Denotes significance at $p<0.05$; ** Denotes significance at $p<0.01$

A.6.6. Conclusions

The Drive mechanism is capable of replicating the input profile to within an RMS error of <0.4mm, this is improved during tissue compression resulting in a maximum average RMS error of <0.15mm. The brace system displayed compliance during dynamic testing which may have prevented tissue compression from reaching the target strain, this factor is likely to be enhanced at high displacement rates due to a reduction in the compressive potential of the plantar soft tissue when tested dynamically. The cycle to cycle reliability was good for measured strain suggesting a consistent compression occurred within the tissue for all cycles. A greater variance was observed between cycles for the measured stress suggesting that the tissue's response varied between cycles despite the application of a consistent compression. When comparing equivalent measurements made using an Instron device STRIDE displayed a good agreement for the non-linear pattern of loading (increasing gradient), however an increased stress was observed in all tests using STRIDE. Over-all the platen displacement applied using STRIDE was consistent for all conditions across multiple cycles, however the compression induced within the tissue showed a reduction when the rate of compression was increased.

A.7. Discussion and Conclusions

A.7.1. The Soft Tissue Response Imaging Device

A bespoke Soft Tissue Response Imaging Device (STRIDE) was developed and evaluated; good reliability was observed for the application of compression to the plantar soft tissue across the full range of developed loading routines.

A.7.1.1. Device Design

Following a comprehensive assessment of the literature, and the identification of key requirements of a system to test the plantar soft tissue in compression, a tailored specification was conducted and device components were selected for their ability to permit the effective characterisation of the plantar soft tissue under the conditions of simulated gait.

The selection of a servo-motor with incorporated device feedback and control permitted the development of a wide range of loading profiles to be used to assess the plantar soft tissue across the full functional range. A novel gait simulation profile based on the vertical component of the foot motion during gait was created which replicated both the temporal parameters of gait, providing an equivalent contact and rest time between successive steps and the load dynamics of gait for the heel region. This profile also featured an initial high impact compression, followed by a rapid decompression simulating the transfer of weight to the forefoot and finally a gradual offloading as the heel is lifted in late stance. This complex gait simulation profile enables the plantar soft tissue to be characterised at a specific location by the application of multiple repetitive cycles to mimic the regular compression in normal walking.

The adaptability of STRIDE also permits a broad range of loading conditions to be assessed for a single subject, providing a large basis for comparison to the results of previous studies. The low constant rate profile (T-Wave at 0.005m/s) developed for this study utilises a displacement rate, which is equivalent to the previous in-vitro (REFS) and in-vivo manual compression methods (Hsu 2000; Erdemir 2006). The medium variable rate profile (S-Wave with impact rate of 0.02m/s) applies a compression profile which mimics the dynamics of

pendulum impact studies, with displacement rate at its maximum for the point of contact with the plantar soft tissue (Aerts *et al.* 1995). The high variable rate profile (Gait-Sim with impact rate of 0.3m/s) utilises displacement rates comparable to previous in-gait studies (REFS) and to the previous ballistic pendulum studies (Alcántara 2002, Weijers 2005). The level of control and range of profiles which can be implemented using STRIDE represents a clear advance from the previous methods of controlled compression, which have primarily utilised single compression rates or impact style conditions, providing a unique opportunity to assess the varied response of the plantar soft tissue across the tissues full functional range.

A.7.1.2. Measurement and Processing

The novel adaptation of ultrasound imaging and load measurement in series, from a previously indentation based platform (Zheng 1999, Klaesner 2002, Hsu 2005), to application in bulk compression tests, permitted a more robust measurement of the tissues response during loading. This technique removes the potential for lateral tissue displacement by compressing the whole tissue region uniformly, however still permits effective load measurement for the focal point of stress concentration beneath the bony prominence of the calcaneal tubercle.

The high temporal resolution of the ultrasound system used within the device (201Hz) permitted data to be recorded throughout the full compression cycle, and allowed effective measurement of the soft tissue response during the rapid loading experienced for the in-gait condition. The 0.1s loading time for this condition gives a theoretical minimum of 20 images to characterise the loading response, which was equivalent to that seen in previous in-gait X-ray methods (De Clercq 1994, Wearing *et al.* 2009). However due to the necessity for a good contact, between ultrasound probe and soft tissue, to produce a stable ultrasound image some of the initial frames for the tissue compression were missed resulting in a high standard between cycle variance for the initial response.

Advances were also made in the development of objective methods to process the measured ultrasound images. Previous techniques have relied upon painstaking measurement by hand of each frame (Cavanagh 1999, Hsu *et al.* 2009). The introduction of an adaptable technique to match an anatomical feature of interest throughout a whole imaging sequence greatly reduced the time requirements for processing a dataset of this size. On average tracking for the

calcaneal tubercle of a single subject's data took under 1 hour using a standard specification PC and measured approximately 31,000 images, a considerable improvement on the time taken to process these images by hand. The use of an algorithm based on maximum conformance between template and image also removed the subjective and potentially erroneous component of human measurement. With advances in imaging methods and a demand for greater temporal resolution for the assessment of the rapid in-gait tissue responses effective tracking techniques such as this will become a necessity.

A.7.1.3 Evaluation

The developed device has been shown to perform to a highly repeatable standard when implementing the developed loading profiles. Tests conducted in both free air and during tissue compression displayed a good conformance to the input profiles, with RMS errors below 0.15mm and peak errors below 0.36mm during tests conducted on the plantar soft tissue. However during testing the tissue was found to become incompressible at a value lower than the target strain, suggesting that although the STRIDE platen motion imposed was highly repeatable the imposed compression was variable between individuals. The variability of the tissue's compressive potential is a characteristic of the measured tissue and is not as such a limitation of the device; however this is likely to impact on the peak stress produced during testing and thus derivation of mechanical properties which rely on the direct characterisation of the stress-strain relationship (Pai and Ledoux 2010), therefore care should be taken when comparing these properties if the true tissue compression varies greatly. An assessment of the measurement apparatus showed a good repeatability of the measured tissue strain and stress for all conditions with between cycle RMS error of <0.013 for strain and <5N for stress; however a greater variability was observed in the initial response of the tissue for the high displacement rate condition this is likely to be related to limitations in the measurement of the initial contact mentioned in section A.7.1.2. As a result of this low reliability for the initial tissue contact, care should be taken when assessing the mechanical response of the tissue for this region of the loading curve and trials in which the data for this region is not present should be excluded from further analysis. The validity of the device was assessed by performing a simple test, re-test protocol with both STRIDE and the gold standard Instron materials testing machine, although the applied strain was found to be the same between conditions the measured tissue response displayed large percentage differences

in properties derived directly from the loading curves. However a good agreement was observed between the measured non-linear nature of the loading response for both devices. Due to the variability observed in the application of tissue strain and the sensitivity of the observed in the use of characterisation techniques which rely upon the loading curve directly it is suggested that methods capable of accounting for the variation in applied loading conditions should be employed for effective tissue characterisation.

A.7.2 Limitations of the Soft Tissue Response Imaging Device

A.7.2.1. Limitations within the device design

In the current arrangement the ultrasound probe permits only a single 2D plane to be imaged during testing which does not allow for a full assessment of the plantar soft tissue motion (bulging, shear) to be studied. The use of ultrasound was selected for this study due to its highly adaptable nature, and even within a single plane the use speckle tracking based algorithms can permit identification of lateral tissue motion, however these techniques were beyond the scope of this study. Although within the work of this thesis characterisation of tissue response is focused on a single location and for a single plane, further work could expand on this with the need for only minor adjustments to the brace system to provide the capacity to image the tissue at various points for a single session.

The short duration of video capture time with the current ultrasound system restricts the number of compressive cycles which can be recorded for conditions conducted at low rates of compression. Based on the displacement of 15mm from the home position to the top position a minimum displacement velocity of 1.75mm/s exists, which would permit the capture of a single T-Wave loading cycle. This restricts the ability of the device to conduct quasi-static trials, such as creep or stress relaxation experiments which require the prolonged measurement of a tissues response when an imposed stress or strain is held constant. This does not however limit the capacity of the device to test the plantar soft tissue within its functional range, permitting more than 10 repetitive cycles of the Gait-Sim condition to be conducted in a single trial.

The Restriction of the device to a single axis (vertical compression) does not permit complete simulation of gait to be achieved. This results in a greatly simplified application of compression and does not account for the true dynamic nature of the plantar soft tissue. However the vertical component of foot motion is the predominant factor in the plantar soft tissue compression with both the greatest forces and the displacements in the vertical direction. Anatomical studies have also shown clear adaptations within the tissue which provide the greatest function in the vertical direction (Blechschmidt 1982). Thus an effective characterisation which represents the functional response of the tissue can be achieved using the vertical component alone. Future work should aim to retain a predominant vertical component of loading whilst also exploring the interaction of loading induced in the horizontal direction.

A.7.2.2. Limitations within loading profiles

The use of single markers to derive the displacement trajectories for the gait simulation condition may not represent the true motion of the calcaneus during tissue compression. Single markers are susceptible to error due to surface motion and errors due to accuracy of the motion capture system. The use of a multiple marker set to define a region can provide a more accurate representation of motion, removing some of the error associated with a single marker and future profile development should attempt to utilise a marker set which has been proven effective for the region of interest. However the use of a controllable, repeatable profile which is similar to the dynamics of gait has not previously been attempted and thus the efficacy of tissue characterisation under these conditions should be established before exhaustive development of a profile which replicates gait exactly is developed.

The use of displacement driven profiles to compress the plantar soft tissue does not permit control for the applied stress during compression and thus can result in large variations in the peak stress achieved when testing different individuals. This is likely to have an impact when attempting to compare between individuals for mechanical properties which are derived directly from the loading curves. However normal in-gait the stress experienced by the tissue is also not directly controlled, and is a function of the motion of the body and the body mass, such that the stress may be larger at the same rate of compression if the subjects body mass is also larger. For the purpose of characterising the full range of the tissues response future

testing should attempt to include profiles which permit control by either displacement or load allowing the tissue to be assessed to standard stress or strain limits.

A.7.2.3. Limitations within the device performance

Due to compliance within the brace system the target strain could not be achieved for all conditions, with the foot being lifted in place of the intended tissue compression. Although a degree of compliance is required, to ensure a subject is not at risk of over compression within the plantar soft tissue during testing, a more rigid brace system may enhance the device performance and the ability to achieve a target strain. Due to the large range of compressibility values reported in the previous literature (0.35 – 0.6) it may also be likely that leg lift has occurred due to the heel pad becoming incompressible at a value below that of the target strain (0.4). This suggests that selection of a lower target strain may also increase the ability of the device to achieve a consistent tissue compression.

A.7.3 Conclusions

The Development phase of this study has produced three main outcomes. (1) The development and validation of a bespoke soft tissue compression device, capable of measuring both the displacement and load response of the plantar soft tissue during compressive testing. (2) The development of a novel protocol including standard and complex loading conditions to permit a broad assessment of the plantar soft tissue function during compressive loading. (3) The development of a novel ultrasound tracking algorithm with application to the motion tracking of bony landmarks within ultrasound imaging. There is a large potential for application of these novel developments to the characterisation of the plantar soft tissue. The second part of this thesis will address the practical aspects of implementing the developed device and act to further validate the capacity of STRIDE to detect variation within and between populations for the measured mechanical properties.

Part B

Device Implementation

&

Tissue Characterisation

B.1. Introduction to Part B: Implementation

B.1.1. Objectives of Part B

The work within part B of the thesis has a focus on the implementation of STRIDE, to allow effective characterisation of the mechanical properties of the plantar soft tissue at the heel. The work has identified the most appropriate mechanical properties, for use in the characterisation of the response of the plantar soft tissue during compression. The work has assessed the reliability of these mechanical properties, within sessions, and the repeatability of the measured plantar soft tissue, between sessions. Using STRIDE, a comprehensive study of the heel pad was then conducted for a healthy cohort, of mixed age and gender. The designed loading profiles permitted the full functional range of the tissue to be assessed. The normative dataset produced in this study contained subject metrics and tissue characterisation parameters, which formed a basis for comparison to previous studies and acts to enhance the knowledge of the plantar soft tissue.

The measured mechanical properties reported by previous studies have displayed large differences when testing conditions, between the studies, have been varied (Gefen *et al.* 2001, Ledoux 2007, Zheng *et al.* 2012b). This has been suggested to be the result of the range of compression rates and the loading conditions used (indentation, bulk compression) between studies (Aerts *et al.* 1995, 1996, Pain 2001). Previous in-vitro studies have shown a clear effect of compression rate on the measured tissue response (Bennett and Ker 1990, Ker 1996). However differences between in-vitro and in-vivo studies, which may affect the measured tissue response, prompt a need for a more thorough investigation of the tissue in-vivo. The tissue's response over the full functional range of loading was tested based on the following hypothesis:

> The rate of compression will affect the response of the plantar soft tissue when tested in-vivo using controlled bulk compression.

Previous studies have reported differences in the measured mechanical response of the tissue between groups of individuals as a result of age (Hsu, Wang, *et al.* 1998, Alcántara 2002, Hsu 2005) and gender (Prichasuk *et al.* 1994, Alcántara 2002). For age, the observed differences have been largely attributed to known structural changes, such as collagen cross-linking, which occurs within the plantar soft tissue (Jahss 1992, Paul and Bailey 1996). While gender differences, are proposed to be the result of variance in the level of growth hormones present in men and women (Rome 1998). However, these between group effects have previously only been studied at isolated rates, low or high, but not throughout the full functional range of compression rates. Because the cause of variance with both age and gender are proposed to be the result of physical difference (structural or hormonal), it is expected that the compression rate used to assess the tissue will not affect the measured response of the tissue. Thus the following hypotheses were used to assess the effect of between group differences and their interactions with rate of compression.

Subject age will have an effect on the mechanical properties of the plantar soft tissue.

Subject gender will have an effect on the mechanical properties of the plantar soft tissue.

Age and gender effects will be independent of rate effects

B.1.2. Tissue Characterisation

Due to the rate dependent nature of the plantar soft tissue effective characterisation requires an understanding of the tissues response to different rates of compression. Where many previous in-vivo studies have focused on deriving the tissue properties at a single rate of compression, this study aims to assess these properties across the full functional range of the tissue, permitting a more comprehensive assessment of the plantar soft tissue.

The derivation of tissue stress and strain throughout the full compressive cycle permits the full characterisation of the stress-strain relationship. The stress-strain relationship can be characterised based on the features of the curve (Peak Stress, Peak Strain, and Gradient) or by modelling methods which attempt to fit constitutive equations to the stress-strain curves to

isolate the elastic and viscous parameters of the stress-strain curves. Due to the large range of characterisation methods employed previously within the literature both empirical and modelling approaches were undertaken in this study to permit a wide basis for comparison.

B.1.2.1. Biomechanical Empirical Studies

The biomechanical response of the tissue can be determined directly from the observed stress strain relationship via curve fitting. The flexibility of curve fitting techniques permits the effective characterisation of a curvature for a wide range of linear and non-linear stress strain relationships. For a viscoelastic tissue the properties which are derived by these methods represent the overall tissue response and cannot be easily separated into the individual elastic and viscous components.

B.1.2.1.1. Curve Features and Segmentation

The Peak Strain ($\varepsilon_{(max)}$) is derived from the stress-strain curve directly, and is defined as the point of maximum compressive strain (Tong 2003) (Figure B.1.1). This measure explains the compressive potential of the tissue when tested dynamically and has been related to the potential for energy dissipation within the tissue (Jorgensen 1985, Tong 2003).

The Peak stress (σmax) was taken as the absolute maximum recorded compressive stress. This measure gives an indication as to the level of compressive strength of the tissue, and thus its abuility to withstand loads (Ennos, 2012). The strain at peak stress ($\varepsilon_{(\sigma max)}$) may vary from the Peak strain in some conditions (Figure B.1.1).

The stress-strain response may be divided into 2 sections: Loading, which represents the response to σmax and Unloading, which represents the response of the tissue after σmax. The area bound by the loading and unloading curve represents the energy loss within the tissue.

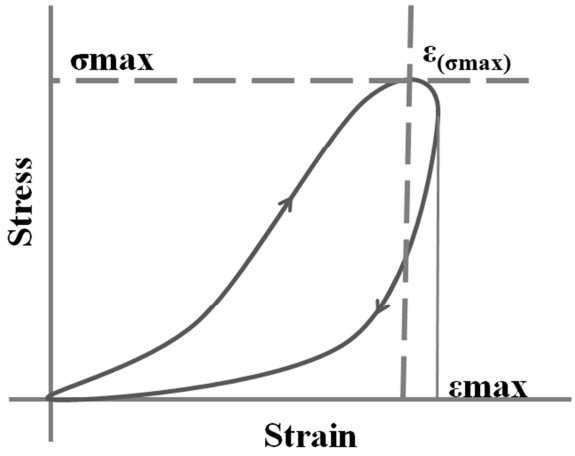

Figure B.1.1: Segmentation of the Stress-Strain Curve

B.1.2.1.2. Linear Stress-Strain Characteristics

The secant modulus (S) is derived from the measured stress-strain response of the tissue and describes the linear relationship between peak stress and strain at the point of peak stress (Wearing *et al.* 2009) (Figure B.1.2). This is a variant of Young's modulus (E) which describes the initial linear elastic relationship between stress and strain (Ennos 2011) (Figure B.1.2).

$$E = \sigma / \varepsilon \qquad \textit{(EQ B.1.1)}$$

$$S = \sigma_{(max)} / \varepsilon_{(\sigma max)} \qquad \textit{(EQ B.1.2)}$$

Where; σ = *Stress,* ε = *Strain, E = Elastic Modulus, S=Secant Modulus*

Due to the linear assumptions within these methods, application to non-linear materials is limited and can give an oversimplified representation of the tissue's stress-strain behaviour (Figure B.1.2). Despite these limitations the secant modulus is the most widely reported value for tissue characterisation within the literature (Wang *et al.* 1999, T.-C. Hsu, C.-L. Wang, Y.-W. Shau, F.-T. Tang, K.-L. Li, *et al.* 2000a, Rome 2001, Wearing *et al.* 2009).

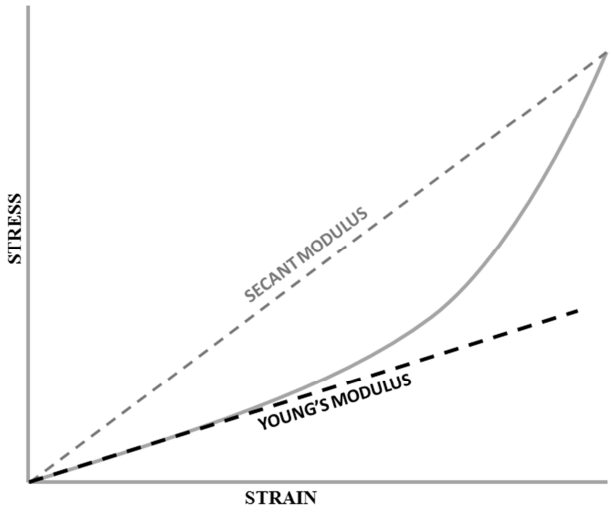

Figure B.1.2.: Linear Curve fitting with Secant and Young's modulus

B.1.2.1.3. Non-Linear Stress-Strain Characteristics

The response of a viscous material to loading is dependent on the rate at which the material is strained, and thus a viscoelastic material will exhibit a non-linear response when the applied velocity of compression varies. This is relevant for methods which do not control for the applied velocity (In-gait) or which actively vary the velocity (Sinusoidal compression, Pendulum impact, and Gait simulation). To characterise this nonlinear response of the tissue, curve fitting techniques such as polynomial fits (Klaesner 2002), spline fits (Wearing *et al.* 2009), exponential fits (Rome 2001) and parabolic fits (Hsu 2002) may be used. These techniques are able to provide a good match to the stress-strain relationship throughout the loading or unloading phases (Figure B.1.3).

Polynomial fit: $\sigma = a\varepsilon^3 + b\varepsilon^2 + c\varepsilon + d$ *(EQ B.1.3)*

Parabolic fit: $\sigma = \sigma_{Max}(\varepsilon/\varepsilon_{Max})^{\alpha}$ *(EQ B.1.4)*

Exponential fit: $\sigma = be^{(a\varepsilon)}$ *(EQ B.1.5)*

Where; a,b,c are Curve Coefficients, σ = *Stress,* ε = *Strain*

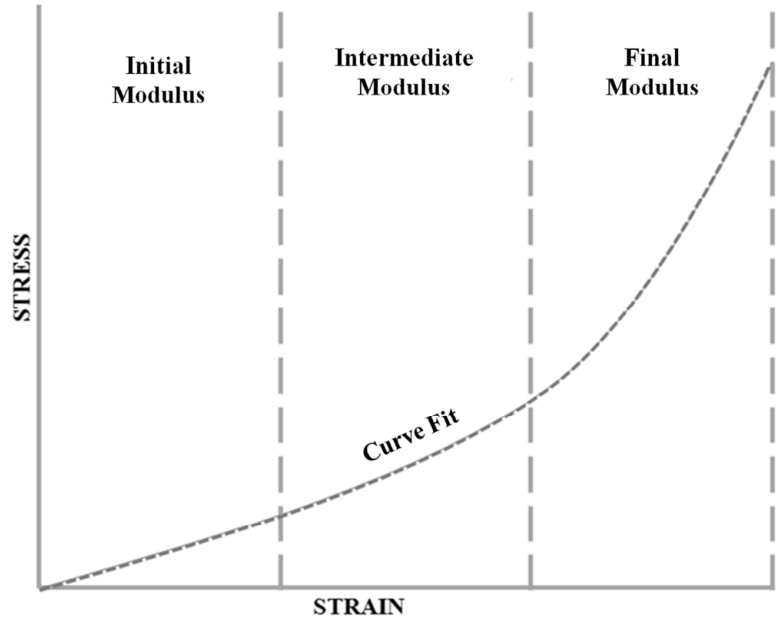

Figure B.1.3: Non-Linear Curve fitting and Curve Segmentation

An effective viscoelastic modulus (K) can then be calculated from the polynomial curve fits for three regions: Initial, intermediate and final (Figure B.1.3). For each region 100 data points for strain can be calculated between the region minimum and region maximum, using the range function in Python. The effective viscoelastic modulus is the average of the 1st derivative of the polynomial fit calculated for each of the 100 data points defined for each region. For a 3rd order polynomial this can be derived as:

$$K = \frac{1}{n}\sum_{i=m}^{n}(3a\varepsilon^2 + 2a\varepsilon + c)_i \qquad \textit{(EQ B.2.4)}$$

Where m is increment between range minimum and range maximum, n is the number of increments (n=100), a, b & c are polynomial curve coefficients for a 3rd order polynomial and ε is the strain at each increment.

B.1.2.1.4. Energy Loss and Percentage Energy Dissipated

Strain energy density (W_e) is the energy stored per unit volume while the tissue is under stress, and represents the area bound by the curve and the x axis (Ennos 2011). This can be calculated from raw data using the trapezoid rule (Wearing *et al.* 2009), or as the definite

integral of the curve fits to the compression and decompression curves (Gefen *et al.* 2001). To calculate the full W_e, the curves must first be divided into compression and decompression phases by absolute Peak Strain (εmax) (Figure B.1.4). The difference between the compression and decompression values is the energy dissipated due to viscous damping via friction and heat production within the tissue (Figure B.1.4 Bound area).

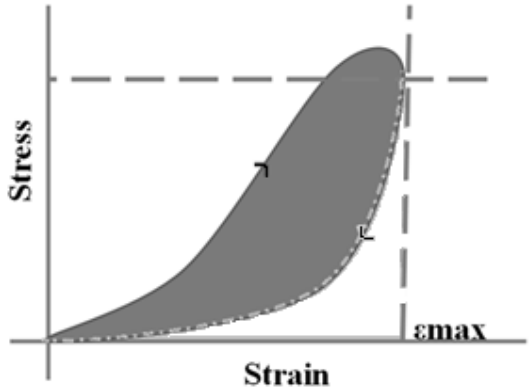

Figure B.1.4: Segmentation of stress-strain curve to Compression and Decompression phases. Bound area represents Energy Loss.

The strain energy density for the loading curve can be derived as:

$$W_{e(Compression)} = \int_{\varepsilon min}^{\varepsilon max} a\varepsilon^3 + b\varepsilon^2 + c\varepsilon + d \qquad \textit{(EQ B.1.6)}$$

Where εmin is the minimum strain, and εmax is the absolute maximum strain.

The stran energy density for the unloading curve can be calculated as:

$$W_{e(Decompression)} = \int_{\varepsilon min}^{\varepsilon max} a\varepsilon^3 + b\varepsilon^2 + c\varepsilon + d \qquad \textit{(EQ B.1.7)}$$

Where εmin is the minimum strain, and εmax is the absolute maximum strain.

The dissipated energy can be derived as:

$$W_{e(Dissipated)} = W_{e(Compression)} - W_{e(Decompression)} \qquad \textit{(EQ B.1.8)}$$

The Energy Dissipated can be normalised to give the Percentage Energy Dissipation, which permits comparison across conditions where peak stress and strain are not consistent (Bennet 1990). Percentage energy dissipation can be derived as:

$$Percentage\ Energy\ Dissipation = (We_{(Dissipated)}/We_{(Compression)}) \times 100 \quad \textit{(X)}$$

B.1.2.2. Biomechanical Modelling Studies

Modelling of the tissue permits properties to be derived which could not be obtained from curve characterisation alone. The use of analytical mechanical models permits the modelling of individual structures such as the plantar fat pads (R. M. Alexander, M. B. Bennett, and R. F. Ker 1986b, Klaesner 2002) or more complex structures like the foot and ankle (Pain 2001) by the combination of simple defined elements. Hookean springs (Figure B.1.5.a) are linearly elastic in behaviour (Lockett 1972); their stress-strain relationship is linear and can be explained by a constant known as the elastic modulus (E) (Bland 1960). Newtonian dashpots (Figure B.1.5.b) are linearly viscous in behaviour (Lockett 1972); their stress-strain rate relationship is linear and can be explained by a constant known as the viscosity (η) (Bland 1960).

Elastic Modulus: $E = \sigma/\varepsilon$ *(EQ B.1.9)*

Viscosity: $\eta = \sigma/\dot{\varepsilon}$ *(EQ B.1.10)*

Where E = *Elastic Modulus,* η = *Viscosity,* σ = *Stress,* ε= *Strain,* $\dot{\varepsilon}$ = *Strain rate*

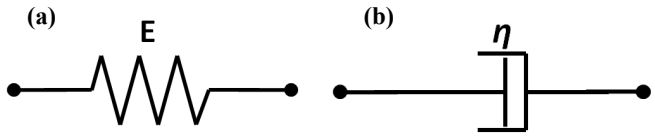

Figure B.1.5: Single Element Models (a) Hookean Spring, (b) Newtonian Dashpot

B.1.2.2.1. Two Element Models

The Maxwell Element

The Maxwell element is defined as the combination of an elastic element and a viscous element in series (Figure B.1.6.a). Thus an applied force is the same in the elastic and viscous components but the displacement within each component varies dependent on the strain rate and the stress rate (Lockett, 1972).

Model Equation: $\dot{\varepsilon} = \frac{\sigma}{\eta} + \frac{\dot{\sigma}}{E}$ *(EQ B.1.11)*

Where E =*Elastic Modulus,* η =*Viscosity,* σ =*Stress,* ε=*Strain,* $\dot{\varepsilon}$ =*Strain rate,* $\dot{\sigma}$=*Stress rate*

The Kelvin-Voigt Element

The Kelvin-Voigt element is defined as the combination of an elastic element and a viscous element in parallel (Figure B.1.6.b). Thus an applied strain will be shared equally between the elastic and viscous components, but the force within each component will vary dependent on the strain rate (Bland 1960).

Model Equation: $\sigma = E\varepsilon + \eta\dot{\varepsilon}$ *(EQ B.1.12)*

Where E =*Elastic Modulus,* η =*Viscosity,* σ =*Stress,* ε=*Strain,* $\dot{\varepsilon}$ =*Strain rate*

These models are limited under certain conditions. Under constant load, the Maxwell model will permit viscous flow and eventually degenerate to a viscous fluid (Vincent 1990). Under constant strain, the strain rate is zero. Thus a Kelvin-Voigt model will permit no viscous flow, and will eventually degenerate to an elastic solid (Vincent 1990).

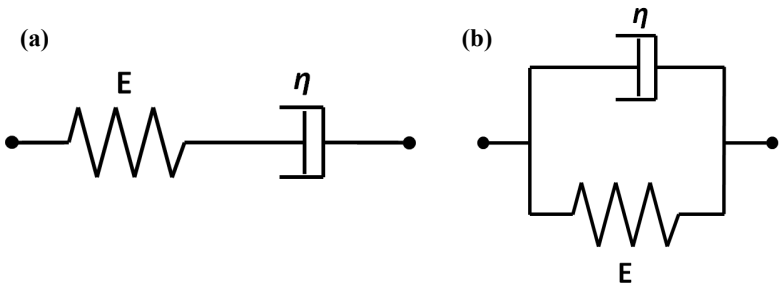

Figure B.1.6: Two Element Viscoelastic Models (a) Maxwell Model, (b) Kelvin-Voigt Model

B.1.2.2.2. The Standard Three Element Viscoelastic Solid

To prevent degeneration, an elastic element may be added; this is defined as a three element constitutive model and has two forms.

Form A consists of an elastic element and Maxwell element in parallel (Fig B.1.7.a). Thus an applied strain is shared equally between the Maxwell element and the elastic element (Bland 1960). This model prevents viscous flow leading to degeneration in the Maxwell element by resisting any excessive extension via the parallel elastic element.

Model Equation: $\dot{\boldsymbol{\sigma}} + \frac{\mathbf{E_2}}{\boldsymbol{\eta}}\boldsymbol{\sigma} = (\mathbf{E_1} + \mathbf{E_2})\dot{\boldsymbol{\varepsilon}} + \frac{\mathbf{E_1 E_2}}{\boldsymbol{\eta}}\boldsymbol{\varepsilon}$ *(EQ B.1.13)*

Where E =*Elastic Modulus,* η =*Viscosity,* σ =*Stress,* ε=*Strain,* $\dot{\varepsilon}$ =*Strain rate,* $\dot{\sigma}$=*Stress rate*

Form B consists of an elastic element and a Kelvin-Voigt element in series (Fig B.1.7.b). Thus the applied force is shared equally between the Kelvin-Voigt element and the elastic element (Bland 1960). This model permits some viscous flow when strain is constant, by compensatory extension/compression of the in series elastic element.

Model Equation: $\dot{\boldsymbol{\sigma}} + \frac{\mathbf{E_1+E_2}}{\boldsymbol{\eta}}\boldsymbol{\sigma} = \mathbf{E_2}\dot{\boldsymbol{\varepsilon}} + \frac{\mathbf{E_1E_2}}{\boldsymbol{\eta}}\boldsymbol{\varepsilon}$ *(EQ B.1.14)*

Where E =*Elastic Modulus,* η =*Viscosity,* σ =*Stress,* ε=*Strain,* $\dot{\varepsilon}$ =*Strain rate,* $\dot{\sigma}$=*Stress rate*

These models are limited to Hookean linearly elastic and Newtonian linearly viscous behaviour, and thus may only in part explain the response seen in biological tissue where Non-Hookean (Vincent 1990) and Non-Newtonian (Frost 1971) constituents are common.

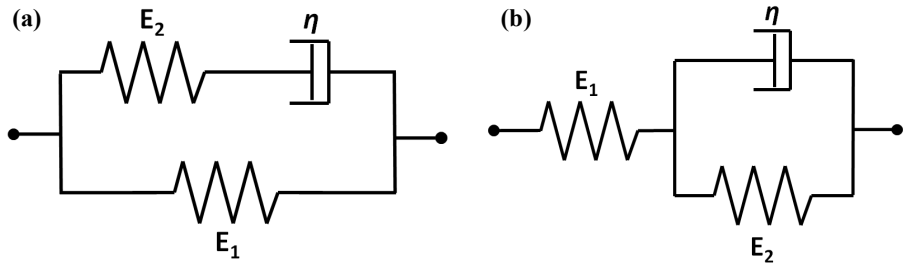

Figure B.1.7: Standard Three Element Viscoelastic Solid (a) Form A, (b) Form B

B.1.2.2.3. Non-Linear Viscoelastic Models

To include non-linear tissue responses, models can be modified by introducing Non-Hookean and Non-Newtonian components.

Non-Newtonian Kelvin-Voigt Model

This is a modified Kelvin-Voigt model, containing a Hookean, linearly elastic spring in parallel with a Non-Newtonian, non-linear damper (Figure B.1.8). Thus an applied strain will be shared equally between the elastic and viscous components, but the force within each component will vary dependent on the strain rate multiplied by the applied strain (Gefen *et al.* 2001).

Model Equation: $\sigma = \mathrm{E}\varepsilon + \eta\varepsilon\dot{\varepsilon}$ *(EQ B.1.15)*

Where E =*Elastic Modulus,* η =*Viscosity,* σ =*Stress,* ε=*Strain,* $\dot{\varepsilon}$ =*Strain rate*

This model exhibits the same limitations as the standard Kelvin-Voigt model. As such, it will permit no viscous flow and eventually degenerate to an elastic solid (Vincent 1990).

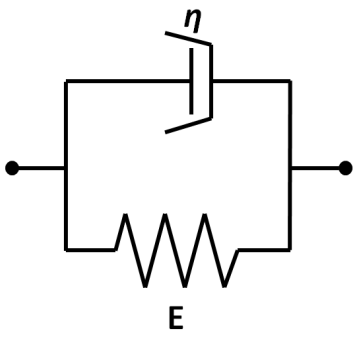

Figure B.1.8: Modified Kelvin-Voigt Model

Parallel Three Element Model

This is a modified three element, viscoelastic solid consisting of an elastic element and a Kelvin-Voigt element in parallel with a staggered arrangement (Figure B.1.9) (Klaesner 2002). The initial response is governed solely by the elastic element, and thus the model behaves in a linearly elastic fashion. The response is then changed by the introduction of the Kelvin-Voigt element at strain X_S and thus behaves in a linearly viscoelastic fashion. The step from linearly elastic to linearly viscoelastic creates an effectively non-linear response over total strain.

Model Equations:

Initial (If 0 < Strain < X_S): $\sigma = \mathrm{E}_2\varepsilon$ *(EQ B.1.16)*

Final (X_S < Strain < Strain(max)): $\sigma = \mathrm{E}_2\varepsilon + \mathrm{E}_1(\varepsilon - X_S) + \eta\dot{\varepsilon}$ *(EQ B.1.17)*

Where E =*Elastic Modulus,* η =*Viscosity,* σ =*Stress,* ε=*Strain,* $\dot{\varepsilon}$ =*Strain rate*

This model exhibits the same limitations as the standard Kelvin-Voigt model, and as such will permit no viscous flow and will eventually degenerate to an elastic solid (Vincent 1990).

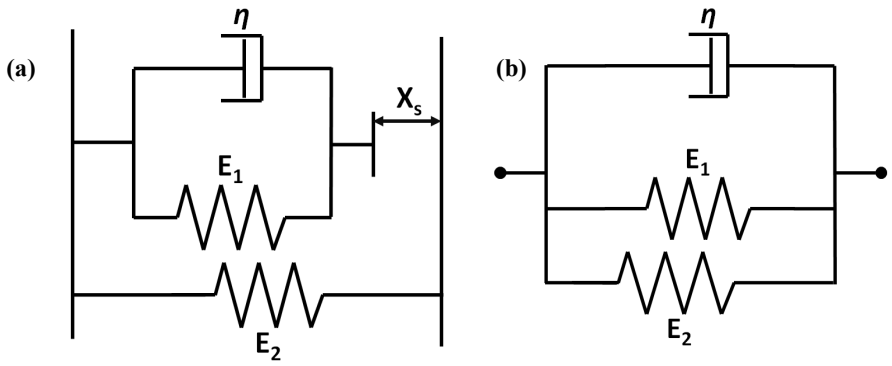

Figure B.1.9: Parallel Three Element Model (a) Initial, (b) Final

B.1.3. Conclusion

The large range of methodologies used, in the previous literature to derive the mechanical properties for the plantar soft tissues have made it difficult to draw between-study comparisons. The use of both an empirical and a modelling approach in this study allows a full exploration of the tissue response to load to be conducted, whilst also providing a large basis for comparison to the previous literature. The combined approach permits a greater understanding of the differences present between populations.

There are three main aims of this study: (1) to effectively characterise the mechanical response of the plantar soft tissue using STRIDE, (2) to investigate the effect of compression rate on the mechanical response of the plantar soft tissue and (3) to investigate the effect of age and gender on the mechanical properties of the plantar soft tissue.

B.2. Subject Repeatability & Variability

B.2.1 Introduction

The mechanical properties of the plantar soft tissue may allow for the identification of structural tissue changes that result in reduced performance. Thus the reliability and repeatability of these properties must be assessed before a clear understanding of the tissue specific variation can be determined. Previous studies have shown good inter-operator reliability for tissue thickness measurements (Rome *et al.* 1998) and for mechanical properties (Klaesner *et al.* 2001) at low rates of compression using manual devices. Good reliability has also been shown for mechanical properties derived at low rates with manual compression (Rome and Webb 2000). An assessment of reliability and repeatability at high rates of compression has not previously been conducted. It is assumed that the mechanical properties can be determined in-vivo from a single session of testing, which is the common practice in previous methods (Gefen *et al.* 2001, Klaesner 2002). This assumption was tested by conducting a within-day and between-day repeatability assessment. Reliability was also assessed within each session to assess variability of the measured mechanical properties.

B.2.2 Protocol

B.2.2.1. Subject's Characteristics

The right feet of 5 healthy individuals were tested in this study. Subjects were recruited from the student and staff population at the University of Salford. Ethical consent was approved by the University of Salford ethics committee (Appendix C) and a full Health and Safety Review (Appendix B) was conducted prior to commencement of testing. The subject characteristics are displayed in Table B.2.1. Prior to dynamic testing, each subject was informed of the testing procedure and briefed on the operation of the emergency stop system. An initial assessment of the plantar surface of the subject's right foot was then conducted to check for external damage such as cuts or scars that may affect tissue property derivation.

Table B.2.1: Subject Characteristics

Subject	Age (years)	Gender	Height (m)	Weight (kg)	BMI	UTT (mm)
A	26	F	1.61	68.60	26.47	16.70
B	35	F	1.63	62.20	23.41	15.60
C	42	F	1.68	72.00	25.50	16.50
D	25	M	1.82	83.90	25.33	19.40
E	27	F	1.65	53.00	19.47	14.70
Average	31.00	4F:1M	1.68	67.94	24.03	16.58
SD	7.31		0.08	11.49	2.78	1.77

Abreviations; BMI: Body Mass Index; UTT: Unloaded Tissue Thickness

B.2.2.2. Study Design

To study the changes which occur within the tissue over the course of a day, the subjects were tested on the morning of day 1 (Session 1) and returned for testing in the afternoon of day 1 (Session 2). To confirm that the observed changes were related to the time of day, the subjects were asked to return at the same time on the morning of day 2 (Session 3). This setup allows the assessment of within-day variance (diurnal effects), and between-day variance (test, re-test assessment). Two subjects were unable to make the entirety of the test times; details of each subject's participation are shown in Table B.2.2. This allowed for 4 within-day comparisons and 4 between-day comparisons to be made.

Table B.2.2: Subject Participation in Repeatability Study

Subject	Session 1	Session 2	Session 3
A	✓	✓	✓
B	✓	✓	×
C	✓	×	✓
D	✓	✓	✓
E	✓	✓	✓

B.2.2.3. Experimental Protocol

B.2.2.3.1. Unloaded Tissue Thickness and Subject Positioning

The region of interest identification, unloaded tissue thickness and subject positioning was conducted as per sections A.4.2.1, A.4.2.2 and A.4.2.3 to ensure a firm bracing of the subject's foot.

B.2.2.3.2. Dynamic Tissue Compression

To allow assessment of repeatability at both high and low displacement rates, two test profiles were selected, the T-Wave profile and the Gait-Sim profile.

Repeatability of tissue compression at low displacement rates was assessed using the 5mm/s triangle wave (T-Wave) profile (For full details see Section A.4.3). Each trial of the low displacement rate profile contained 2 compressive cycles, and three trials were conducted per session, yielding 6 total compressive cycles.

Repeatability of tissue compression at high displacement rates was assessed using the gait simulation (Gait-Sim) profile (For full details see Section A.4.5). This profile was derived from motion capture data for normal walking of healthy elderly individuals, based on marker velocity for the heel region. Each trial of the high displacement rate profile contained 10 compressive cycles, and three trials were conducted per session, yielding 30 total compressive cycles.

B.2.2.4. Mechanical Property Derivation

The mechanical properties chosen to describe the loading response were: seccant modulus, viscoelastic modulus, energy loss and percentage energy dissipated. These variables were derived directly from the stress-strain curves as per the tissue characterisation methods outlined in section B.1.2.

B.2.2.4.1. Loading Curve Characteristics

Peak stress and strain at peak stress were recorded to quantify the peak compressive response of the tissue under load. The linear stress-strain behaviour was then characterised using the secant modulus (see B.1.2.1.2). To characterise the non-linear stress-strain behaviour a 3rd order polynomial fit was selected as it was the lowest order polynomial, which consistently provided good fit to all conditions (figure B.2.1). The curve equation to describe the non-linear stress strain relationship was:

$$\sigma = a\varepsilon^3 + b\varepsilon^2 + c\varepsilon + d \qquad \textit{(EQ B.2.1)}$$

Where σ is stress, ε is strain and a, b, c & d are polynomial curve coefficients for a 3rd order polynomial

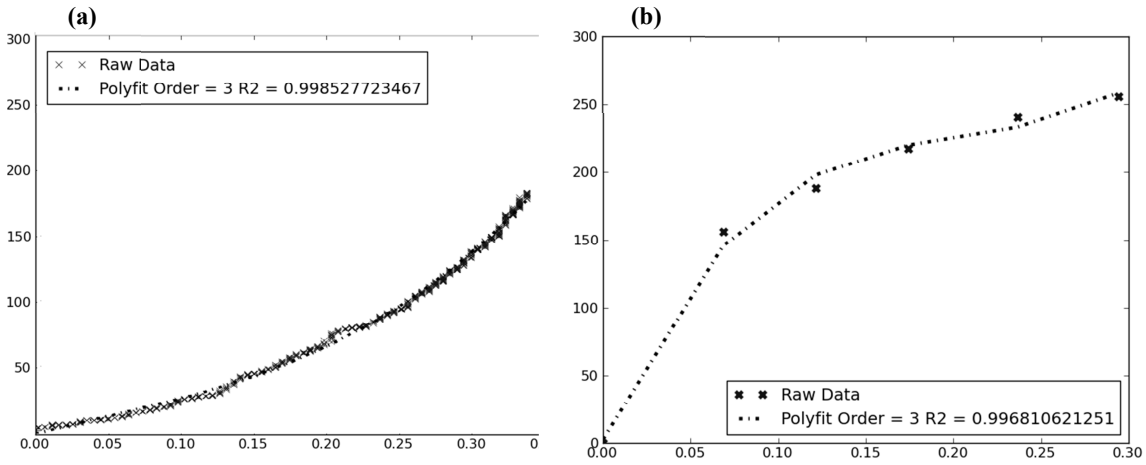

Figure B.2.1: 3rd order polynomial fit to raw Stress v Strain data.
(a) Twave, (b) Gait

The modulus can be calculated as the 1st derivative of the polynomial curve fit and is expressed as:

$$Modulus_{(\varepsilon)} = 3a\varepsilon^2 + 2b\varepsilon + c \qquad \textit{(EQ B.2.2)}$$

Where σ is stress, ε is strain and a, b, & c are polynomial curve coefficients for a 3rd order polynomial.

The non-linear response can then be described by calculating a viscoelastic modulus at three regions of the loading curve; Initial, Intermediate and Final (Figure B.2.2) as per the methods in section B.1.2.1.3.

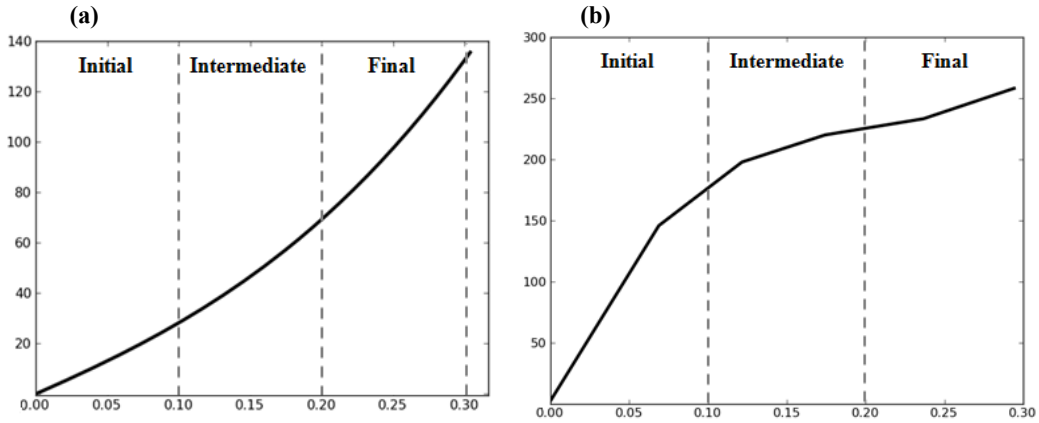

Figure B.2.2: Curve segmentation for estimation of viscoelastic modulus.

(a) Twave, (b) Gait

B.2.2.4.2. Energy Loss and Percentage Energy Dissipation

Absolute Energy Loss and Percentage Energy Dissipation were calculated via the methods stated in in section B.1.2.1.4 using 3rd order polynomial fits to the compression and decompression segments of the stress-strain curves.

B.2.2.5. Statistical Analysis

B.2.2.5.1. Within-Session Variance

Intra-individual Variance

Intra-individual within-session variability was assessed for all subjects by Standard Deviation (SD) and the Coefficient of Variation (V). The data were presented as an inter-individual average of the intra-individual Standard Deviation (S_w) and an inter-individual average of the intra-individual Coefficient of Variation (V_w), expressed as percentage for each session (Tables B.2.3 & B.2.4)

Inter-individual Variance

Inter-individual within-session variability was assessed by SD and the V. The data were presented as within session inter-individual average, inter-individual standard deviation and inter-individual coefficient of variation.

B.2.2.5.3. Between-Session Variance

Between-Session Variance was assessed by percentage difference and Intraclass Correlation Coefficients.

Percentage Difference

To assess the difference between sessions, the mean intra-individual values for difference between sessions were calculated for within-day and between-day sessions. Between session difference was tested for significance with Paired t-Tests (two-tailed, $P<0.05$) and the results were presented as percentage difference between sessions and significance (p).

Intraclass Correlation Coefficient

To assess the reliability between sessions, the intraclass correlation coefficients (ICC) were calculated for the intra-individual averages of within-day and between-day sessions. $ICC_{(3,k)}$ was used to assess reliability as subjects were tested by a single judge only (Shrout and Fleiss 1979). A good reliability was indicated in parameters which gave ICC>0.75.

B.2.3. Results

B.2.3.1. Intra-individual Variability

The loading curve parameters showed small intra-individual deviations within sessions with $V<20\%$ in all sessions and all conditions. The strain at peak stress was more variable within sessions for the Gait-Sim condition (16.50%) than the T-Wave condition (6.40%). Energy dissipation parameters showed large intra-individual deviations within sessions for all conditions; this was particularly present in the energy loss parameter with V~30%. Normalisation of Energy Loss to Percentage Energy Dissipated reduces the intra-individual variance by ~10% within sessions for all conditions. The secant modulus shows the lowest intra-individual deviations of the stress-strain characteristics in all conditions however is more variable in the Gait-Sim condition (20.83%) than in the T-Wave condition (5.17%). The effective viscoelastic modulus parameters for the T-Wave condition show moderate initial variation (20.98%) but low variation in the intermediate and final stages of tissue compression ($V<15\%$). The effective viscoelastic modulus parameters for the Gait-Sim condition show large intra-individual deviations and coefficients of variation (V>35%) within all sessions for all sections of the curve.

Table B.2.3: Intra-Individual Variability for the T-Wave Profile

Twave		Session 1		Session 2		Session 3	
	Units	S_w SD	V_w	S_w SD	V_w	S_w SD	V_w
Loading Curve Parameters							
Peak Stress	kPa	11.98 ± 8.04	11.21%	9.06 ± 2.43	10.60%	6.96 ± 1.40	8.01%
Peak Strain (at Peak Stress)	(-)	0.02 ± 0.02	6.53%	0.02 ± 0.01	8.40%	0.01 ± 0.00	4.28%
Energy Dissipation							
Energy Loss	J/m^3	1.18 ± 0.99	28.99%	1.21 ± 1.09	32.94%	1.30 ± 1.30	33.06%
Percentage Energy Loss	%	4.99 ± 2.53	17.88%	6.74 ± 3.69	23.50%	6.62 ± 5.13	23.55%
Stiffness							
Secant Modulus	kPa	18.01 ± 15.40	4.65%	17.41 ± 7.43	4.75%	21.03 ± 7.78	6.10%
Viscoelastic Modulus (K1)	kPa	31.36 ± 12.66	16.69%	77.44 ± 60.35	32.82%	47.75 ± 27.35	15.44%
Viscoelastic Modulus (K2)	kPa	29.68 ± 23.18	12.53%	26.95 ± 7.55	10.45%	33.29 ± 9.52	14.96%
Viscoelastic Modulus (K3)	kPa	51.64 ± 45.85	10.16%	43.11 ± 14.68	10.42%	52.59 ± 33.50	12.41%

Abreviations; K1: Initial Modulus, K2 Intermediate Modulus, K3 Final Modulus, S_w:Intraindividual average Standard Deviation, SD: Standard Deviation, Vw: Intraindividual average Coefficient of Variation

Table B.2.4: Intra-Individual Variability for the Gait Sim Profile

Gait		Session 1		Session 2		Session 3	
	Units	S_w SD	V_w	S_w SD	V_w	S_w SD	V_w
Loading Curve Parameters							
Peak Stress	kPa	17.22 ± 8.16	15.34%	14.05 ± 7.00	14.91%	7.25 ± 3.85	7.82%
Peak Strain (at Peak Stress)	(-)	0.04 ± 0.02	16.01%	0.03 ± 0.01	15.30%	0.03 ± 0.01	18.18%
Energy Dissipation							
Energy Loss	J/m^3	4.45 ± 1.75	35.57%	3.97 ± 2.07	34.97%	2.52 ± 0.41	32.80%
Percentage Energy Loss	%	7.63 ± 3.08	19.10%	8.60 ± 4.92	20.35%	8.32 ± 1.41	21.42%
Stiffness							
Secant Modulus	kPa	106.51 ± 82.31	21.69%	89.72 ± 20.63	17.32%	156.55 ± 131.58	23.48%
Viscoelastic Modulus (K1)	kPa	374.96 ± 122.81	35.42%	4605.62 ± 8198.19	95.95%	852.32 ± 347.46	51.31%
Viscoelastic Modulus (K2)	kPa	178.21 ± 88.63	59.52%	169.39 ± 38.45	40.80%	308.38 ± 125.48	58.81%
Viscoelastic Modulus (K3)	kPa	165.80 ± 130.34	78.64%	232.20 ± 161.81	117.83%	530.60 ± 340.68	128.35%

Abreviations; K1: Initial Modulus, K2 Intermediate Modulus, K3 Final Modulus, S_w:Intraindividual average Standard Deviation, SD: Standard Deviation, Vw: Intraindividual average Coefficient of Variation

B.2.3.2. Within-day Variance

The loading curve parameters were lower in session 2 than in session 1 for all conditions; however these differences were not found to be significant, with peak stress displaying large inter-individual within-session variance (35-55%). The energy dissipation parameters were lower in session 2 compared to session 1 for all conditions; however these differences were not significant, displaying low ICC ratings and high within session inter-individual variation. The secant modulus showed minimal difference between sessions 1 and 2 and showed a good ICC rating for the T-Wave condition (0.72). The highest percentage increase observed in both conditions was for the initial viscoelastic modulus; however this was not significantly different and high inter-individual within session variance was also present. For the T-Wave condition, intermediate and final viscoelastic modulus displayed lower values in session 2, with high inter-individual variance. For the Gait-Sim condition, intermediate viscoelastic modulus was increased in session 2 while the final viscoelastic modulus was reduced; neither difference was significant and high inter-individual variance was present.

B.2.3.3. Between-day Variance

The peak stress values for both conditions displayed little difference between sessions (<3%) with a good ICC rating (0.93) for the T-Wave condition, despite high inter-individual variance. Greater difference was observed in the strain at peak stress parameter, but this was not found to be significant. A good ICC rating (0.82) was found for the T-Wave condition. Energy dissipation parameters displayed a reduction in session 3 however differences were not significant for any parameter. The energy loss parameter displayed good ICC rating (0.93) in the T-Wave condition despite high inter-individual variance. The secant modulus displayed good ICC ratings in both T-Wave and Gait-Sim conditions (0.77, 0.84) despite between session variance (15%, 35%), but inter-individual variance was moderate for this parameter (<30%). The initial average viscoelastic modulus displayed a large increase in session 3; this was found to be significant ($p<0.05$) in the Gait-Sim condition. For the T-Wave condition, the intermediate and final viscoelastic modulus displayed no significant difference between sessions with a good ICC rating for each parameter (0.92, 0.91). For the Gait-Sim condition, large increases were displayed in the intermediate and final viscoelastic modulus in session 3, and significant difference was found for the final viscoelastic modulus ($p<0.05$). A good ICC rating was also observed for the final viscoelastic modulus in the Gait-Sim condition, despite the large session variance and large inter-individual variance.

Table B.2.5: Within-Day Variability for the T-Wave Profile

Within Day - Twave		Session 1	Session 2	Variance		
Parameters	Units	Mean ± SD	Mean ± SD	Difference	p	ICC
Loading Curve Parameters						
Peak Stress	kPa	111.92 ± 49.03	96.83 ± 38.18	-13.48%	0.88	0.44
Peak Strain (at Peak Stress)	(-)	0.29 ± 0.05	0.26 ± 0.05	-11.80%	0.51	0.00
Energy Dissipation						
Energy Loss	J/m^3	4.11 ± 1.62	3.54 ± 2.08	-13.84%	0.61	0.41
Percentage Energy Loss	%	29.75 ± 4.72	27.90 ± 5.17	-6.24%	0.40	0.00
Stiffness						
Secant Modulus	kPa	360.88 ± 120.19	354.91 ± 86.78	-1.66%	0.60	0.72
Viscoelastic Modulus (K1)	kPa	185.12 ± 62.31	232.12 ± 109.24	25.39%	0.57	0.01
Viscoelastic Modulus (K2)	kPa	302.56 ± 124.55	292.33 ± 106.11	-3.38%	0.91	0.58
Viscoelastic Modulus (K3)	kPa	511.63 ± 217.40	453.66 ± 185.42	-11.33%	0.64	0.69

Abreviations; K1: Initial Modulus, K2 Intermediate Modulus, K3 Final Modulus, SD: Standard Deviation, p: Paired t-Test Significance values, ICC: Intraclass Correlation Coeffiecient

Table B.2.6: Within-Day Variability for the Gait Sim Profile

Within Day - Gait		Session 1	Session 2	Variance		
Parameters	Units	Mean ± SD	Mean ± SD	Difference	p	ICC
Loading Curve Parameters						
Peak Stress	kPa	134.58 ± 75.09	113.47 ± 41.80	-15.69%	0.55	0.63
Peak Strain (at Peak Stress)	(-)	0.24 ± 0.03	0.21 ± 0.03	-13.24%	0.16	0.47
Energy Dissipation						
Energy Loss	J/m^3	21.52 ± 19.51	15.69 ± 8.74	-27.09%	0.57	0.40
Percentage Energy Loss	%	51.87 ± 17.04	50.50 ± 13.11	-2.64%	0.91	0.00
Stiffness						
Secant Modulus	kPa	549.50 ± 251.30	537.30 ± 150.74	-2.22%	0.93	0.39
Viscoelastic Modulus (K1)	kPa	1204.64 ± 533.12	2605.88 ± 2621.25	116.32%	0.29	0.49
Viscoelastic Modulus (K2)	kPa	349.45 ± 181.33	452.48 ± 207.40	29.48%	0.54	0.00
Viscoelastic Modulus (K3)	kPa	236.98 ± 128.73	205.64 ± 57.24	-13.22%	0.62	0.52

Abreviations; K1: Initial Modulus, K2 Intermediate Modulus, K3 Final Modulus, SD: Standard Deviation, p: Paired t-Test Significance values, ICC: Intraclass Correlation Coeffiecient

Table B.2.7: Between-Day Variability for the Twave Profile

Between Day - Twave		Session 1	Session 2	Variance		
Parameters	Units	Mean ± SD	Mean ± SD	Difference	p	ICC
Loading Curve Parameters						
Peak Stress	kPa	93.59 ± 31.64	92.06 ± 23.93	-1.63%	0.64	0.93
Peak Strain	(-)	0.28 ± 0.04	0.25 ± 0.03	-12.16%	0.17	0.82
Energy Dissipation						
Energy Loss	J/m^3	3.50 ± 1.14	3.38 ± 1.77	-3.42%	0.69	0.93
Percentage Energy Loss	%	28.80 ± 5.77	26.10 ± 5.46	-9.39%	0.12	0.37
Stiffness						
Secant Modulus	kPa	314.43 ± 67.20	362.27 ± 76.79	15.21%	0.72	0.77
Viscoelastic Modulus (K1)	kPa	184.69 ± 61.88	292.72 ± 64.38	58.49%	0.61	0.09
Viscoelastic Modulus (K2)	kPa	239.31 ± 70.47	229.52 ± 68.03	-4.09%	0.22	0.92
Viscoelastic Modulus (K3)	kPa	417.33 ± 138.10	402.79 ± 120.05	-3.48%	0.50	0.91

Abreviations; K1: Initial Modulus, K2 Intermediate Modulus, K3 Final Modulus, SD: Standard Deviation, p: Paired t-Test Significance values, ICC: Intraclass Correlation Coeffiecient

Table B.2.8: Between-Day Variability for the Gait Sim Profile

Between Day - Gait		Session 1	Session 2	Variance		
Parameters	Units	Mean ± SD	Mean ± SD	Difference	p	ICC
Loading Curve Parameters						
Peak Stress	kPa	93.65 ± 22.59	91.26 ± 11.44	-2.55%	0.84	0.47
Peak Strain	(-)	0.23 ± 0.02	0.17 ± 0.04	-24.98%	0.06	0.52
Energy Dissipation						
Energy Loss	J/m^3	10.94 ± 7.31	7.67 ± 1.09	-29.87%	0.40	0.30
Percentage Energy Loss	%	42.64 ± 13.61	39.36 ± 4.27	-7.69%	0.66	0.23
Stiffness						
Secant Modulus	kPa	433.75 ± 105.58	588.73 ± 167.87	35.73%	0.06	0.84
Viscoelastic Modulus (K1)	kPa	987.76 ± 227.01	1620.25 ± 399.64	64.03%	* 0.01	0.87
Viscoelastic Modulus (K2)	kPa	299.36 ± 142.54	558.75 ± 279.02	86.65%	0.12	0.60
Viscoelastic Modulus (K3)	kPa	202.17 ± 118.96	391.75 ± 152.62	93.78%	* 0.02	0.88

Abreviations; K1: Initial Modulus, K2 Intermediate Modulus, K3 Final Modulus, SD: Standard Deviation, p: Paired t-Test Significance values, ICC: Intraclass Correlation Coeffiecient, *: Significant difference at $P<0.05$

B.2.4. Discussion

B.2.4.1. Intra-Individual Variability

Within subjects the SD and *V* was consistently low for the T-Wave condition, suggesting high within session intra-individual repeatability is achieved at low rates of compression. For the Gait-Sim condition, variation was consistently higher, suggesting the increase in compression rate results in less reliability. Although the displacement of the STRIDE platen has been shown to be consistent at high rates (Section A.6), errors in the target strain suggest that tissue compression does not follow the true platen displacement. The variation between the input (platen displacement) and the tissue compression is expected to be the result of compliance within the bracing, which is more prominent at high rates of compression. When loaded at high rates, the viscoelastic tissue resists compression and becomes rigid. In this situation the platen displacement is used to lift the foot instead of compress the tissue, resulting in a lower peak tissue strain than the target. The greatly reduced number of data points which are captured for the loading phase in the Gait-Sim condition (3-10) when compared to the much slower T-Wave condition (>50) will also restrict the accuracy of measurements due to the rapid nature of the tissue response to load. The curve-fitting techniques have been used to minimise this variation; however it remains a clear limitation of the device.

B.2.4.2. Inter-Session Variability

Within-day variability was high, with low ICC ratings for most parameters in both conditions and moderate percentage differences between sessions; however no significant differences were observed. It is likely that the inter-individual variability reduced the likelihood of detecting significant differences between sessions. When values for the within-day variability of compressibility, tissue modulus and percentage energy loss were assessed against changes observed with age, the variability was consistently lower than the greatest differences observed due to age (-21%, 57.76%, 32.82%; Values from table 2.2 in section 2.4), with the exception of the initial viscoelastic modulus for the Gait-Sim profile. This suggests difference due to age should be detectable with the present level of variability. Between-day variability was lower for most parameters when compared to the within-day variability. The ICC ratings were consistently higher, suggesting good reliability of between-day measures despite the inter-individual variance. When the values for the between day variability were assessed

against the largest observed differences with age, they were consistently lower for the T-Wave condition; however they were higher for both strain at peak stress and modulus in the Gait-Sim condition, suggesting a greater capacity for detection of change due to age with tests conducted at low loading rates. With a greater sample size, it is hypothesised that a diurnal shift would be detected in the mechanical parameters, such that within-day variability would be significantly different whilst between-day reliability would be consistently high, with non-significant variability.

B.2.5. Conclusion

Within subject reliability was found to be good at low velocities and reduced at high velocities, suggesting that caution should be taken when assessing the mechanical properties derived from high rate trials. The capacity to detect changes due to age is also increased when using low rates of compression, and it is likely that this is the result of the lower measured variability of stress and strain at low velocities (Section A.6.4). The within-day reliability was low suggesting a shift in the response of the tissue may occur throughout the repetitive daily loading. In contrast, the between-day reliability was good, suggesting that measurements taken at the same time (morning / afternoon) will be more comparable than measurements taken across a range of times. Thus it is hypothesised that diurnal variance is present within the response of the plantar soft tissue and should be considered when assessing properties derived at different times.

B.3. Study of the effects of age on the plantar soft tissue

B.3.1 Subject Grouping & Exclusion Criteria

A cohort of 38 healthy subjects was recruited from a database of interested participants at the University of Salford. The cohort was divided into two groups of mixed gender based on age; 18 – 35 years (m=11;f=10), 55 – 85 years (m=6;f=11). Recruitment required subjects to have no history of foot problems or operations to the feet and no history of systemic pathophysiologic disease. See Appendix D (Medical History /Assessment) for a full list of the diseases screened for.

B.3.2 Ethics

Ethical consent was approved by the University of Salford ethics committee (Appendix C) and a full Health and Safety Review (Appendix B) was conducted prior to commencement of testing. Each subject given a description of the test procedure (Appendix E) and was asked to provide informed consent (Appendix F).

B.3.3 Subject Characteristics

To allow for the assessment of the effects of lifestyle and health on the plantar soft tissue biometric data, footwear preference and activity levels for each subject were collected. The information was gathered using a questionnaire which was completed prior to testing (Appendix D).

B.3.3.1. Biometric Assessment

Each subject's height and weight were measured in the gait laboratory prior to testing and these values were used to calculate the subject's BMI. Shoe size was recorded and converted into European Sizing to allow for comparison. Height and shoe size remained consistent

between individuals of the same gender from different age groups. Weight and BMI were fairly consistent although showed a slight increase in the over 50's group (Table B.3.1).

Table B.3.1. Biometrics for study cohort

	18-35 Male (n=11)	18-35 Female (n=10)	50 + Male (n=6)	50+ Female (n=11)
Age	26.81 (SD 4.81)	26.4 (SD 4.62)	61.17 (SD 4.79)	61.55 (SD 4.59)
Height (m)	1.79 (SD 0.05)	1.65 (SD 0.06)	1.78 (SD 0.04)	1.61 (SD 0.08)
Weight (kg)	76.36 (SD 8.94)	61.27 (SD 7.37)	79.98 (SD 3.19)	64.97(SD 11.37)
BMI	23.80 (SD 2.26)	22.58 (SD 2.58)	25.28 (SD 1.68)	24.82 (SD 2.24)
Shoe Size (EU)	42.9 (SD 1.94)	38.67 (SD 0.98)	43.00 (SD 0.82)	38.3 (SD 2.33)

B.3.3.2. Activity Levels

Subjects were asked to record all forms of foot loading activity and the extent to which they partook in this activity in an average week. For each age group, activity participation was high: with 80 - 100% of individuals participating in some form of foot loading activity on a regular basis. However, the range of activities and level of participation were generally reduced in individuals over 50 (Figure B.3.2).

B.3.3.3. Foot Wear Preferences

Subjects were asked to select their preferred footwear or most regularly worn footwear from a range of options. A variation in preferred footwear was seen between genders and between age groups (Figure B.3.1).

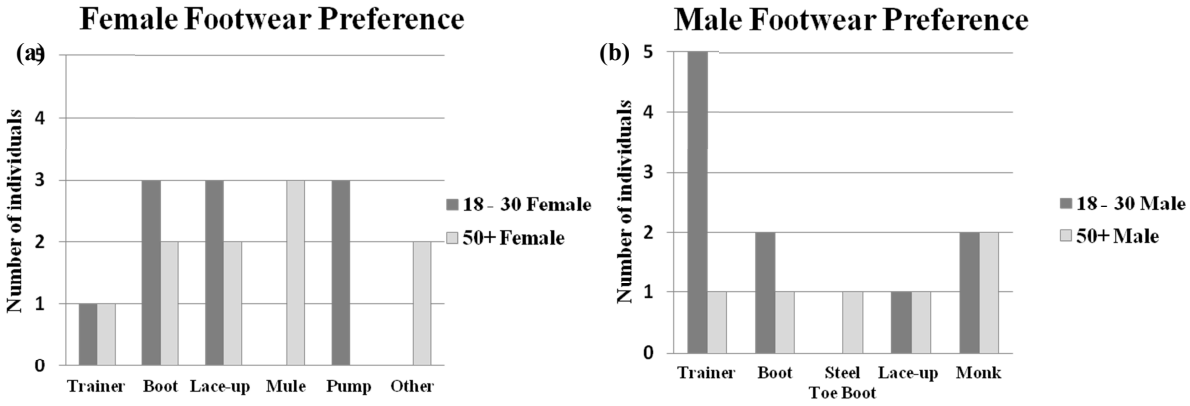

Figure B.3.1: Footwear Preference between ages, (a) Female Footwear Preference (b) Male Footwear Preference

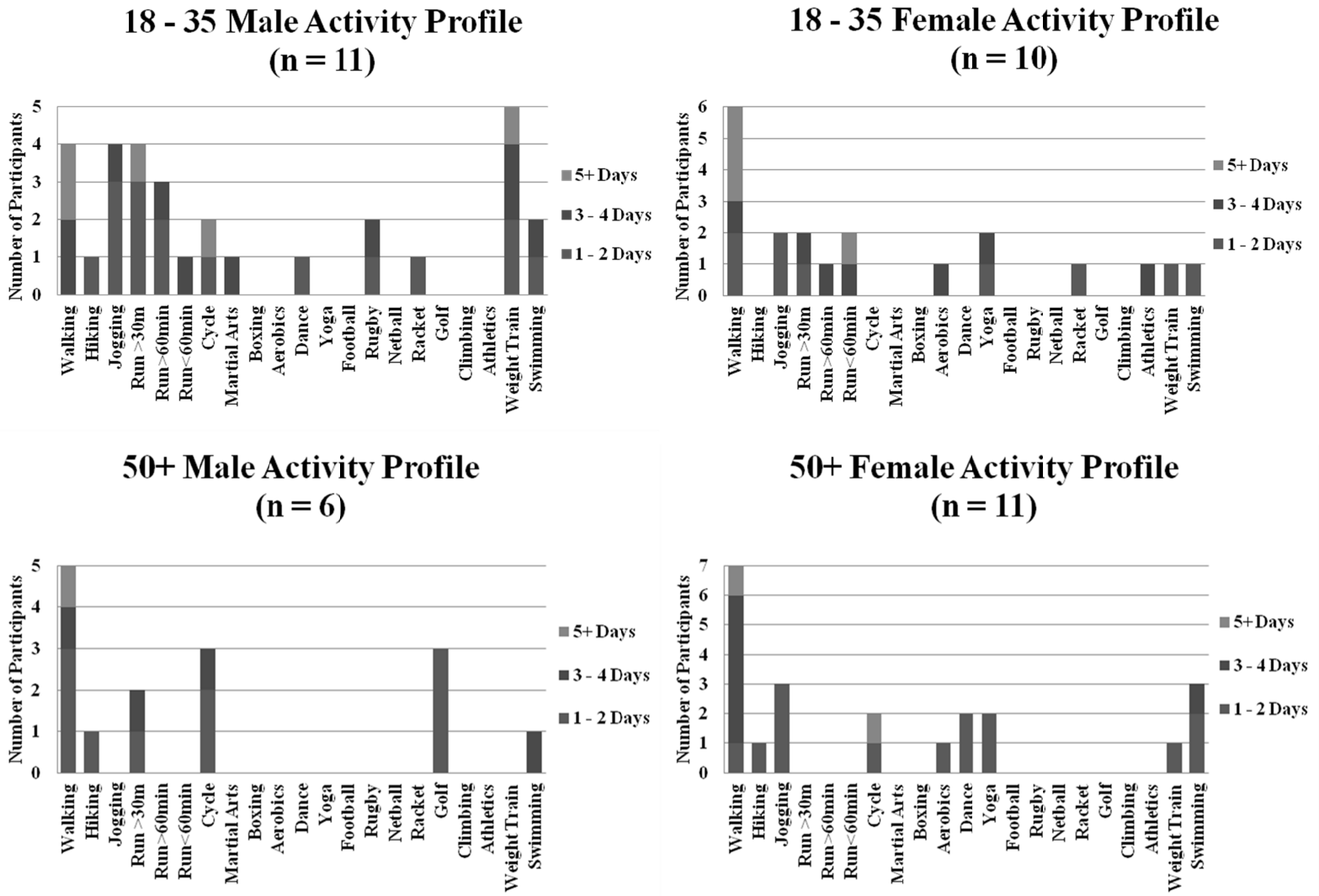

Figure B.3.2: Activity Profiles for Age and Gender Groups.

B.3.4 Test Setup

B.3.4.1. Unloaded Tissue Thickness and Subject Positioning

The region of interest identification, unloaded tissue thickness and subject positioning was conducted as per sections A.4.2.1, A.4.2.2 and A.4.2.3 to ensure a firm bracing of the subject's foot. An initial assessment of the plantar surface of the subject's right foot was then conducted to check for external damage such as cuts or scars that may affect tissue property derivation.

B.3.4.2 Tissue Compression Profiles

To characterise the mechanical response of the tissue under standardised conditions and within the tissues functional range, three test profiles were selected for each foot region: a constant low velocity profile (T-Wave), a variable low velocity profile (S-Wave) and a gait specific variable high velocity profile (Gait-Sim).

The mechanical response of the tissue to compression at a low, constant velocity was assessed using the 5mm/s T-Wave profile (For full details see Section A.4.3). Each trial of the low displacement rate profile contained 2 compressive cycles, and three trials were conducted per session, yielding 6 total compressive cycles.

The mechanical response of the tissue to compression at a variable, low velocity was assessed using the 0.5Hz S-Wave profile (For full details see Section A.4.3). Each trial of the S-Wave profile contained 5 compressive cycles, and three trials were conducted per session, yielding 15 total compressive cycles.

For the heel region, the mechanical response of the tissue to compression at a variable, high velocity was assessed using the rear foot Gait-Sim profile (For full details see Section A.4.5). This profile was derived from motion capture data for normal walking of healthy elderly individuals, based on marker velocity for the heel region. Each trial of the high displacement rate profile contained 10 compressive cycles, and three trials were conducted per session, yielding 30 total compressive cycles.

B.3.5. Mechanical Property Derivation

The loading response of the tissue has a complex rate-dependent form. On one hand it represents a viscoelastic composite with multiple and varied elastic and viscous components. However it also represents a multi layered structure with variable levels of compliance throughout. Deriving appropriate measures which fully explain this natural phenomenon is beyond the scope of this study and thus assumptions as to the tissue's nature have been made. Two routes have been followed each with independent assumptions.

Direct Characterisation of the stress strain relationship.

This route assumes that tissue is a single isotropic, homogeneous layer with a simplistic viscoelastic nature which can be characterised via curve-fitting. The derived values represent the combined elastic and viscous response and are presented as an effective viscoelastic modulus (K)

Determination of Elastic and Viscous Components of the stress-strain relationship.

This route assumes that tissue is a single isotropic, homogeneous layer with a complex viscoelastic nature which can be determined via constitutive modelling. The derived values represent the elastic and viscous components independently, and are presented as the elastic modulus (E) and the viscosity (η)

B.3.5.1. Direct Characterisation of the stress-strain relationship

Although the tissue was compressed to a target strain of 0.4, in many cases absolute peak strain varied. To assess the effect of the applied compressive profile on the compressibility of the plantar soft tissue, the absolute peak strain was recorded.

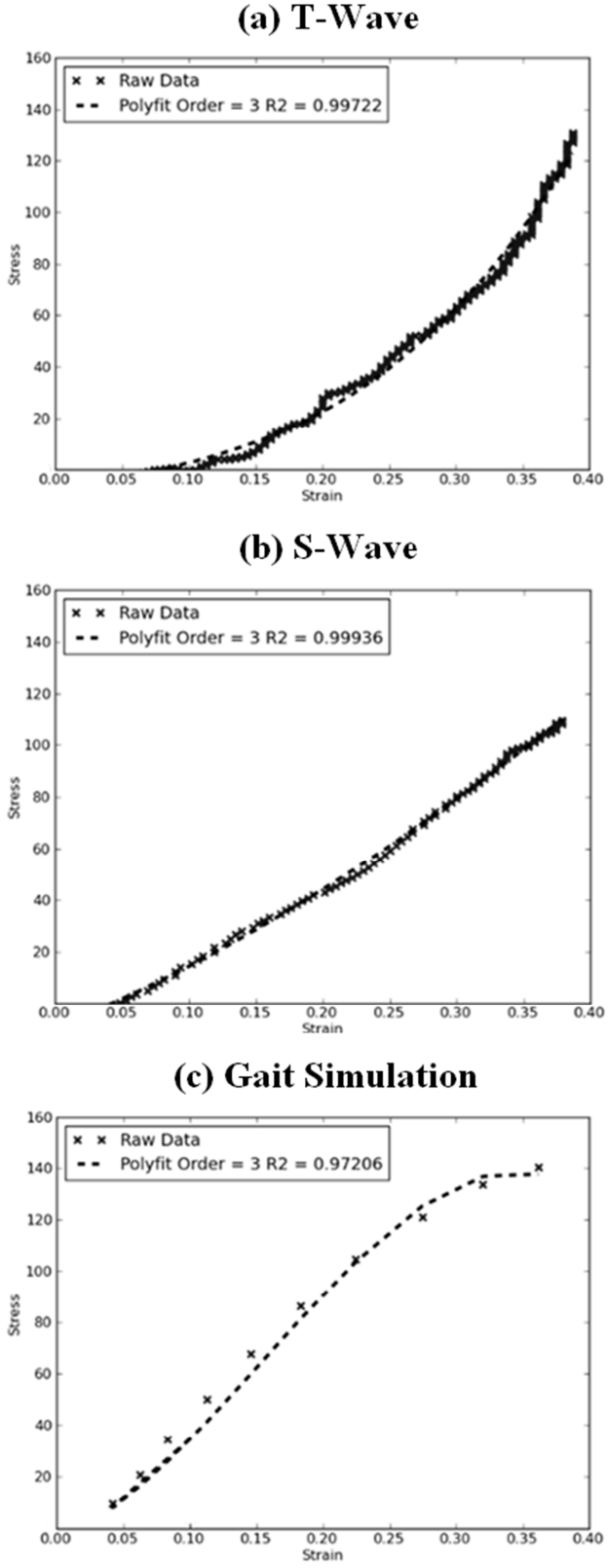

Figure B.3.3: Polynomial fit to raw Stress v Strain data.

(a) Twave, (b) Sine Wave (c) Gait Simulation

Peak stress and strain at peak stress were recorded to quantify the peak compressive response of the tissue under load. The linear stress-strain behaviour was then characterised using the secant modulus (see B.1.2.1.2). To characterise the non-linear stress-strain behaviour a 3rd order polynomial fit was selected as it was the lowest order polynomial, which consistently provided good fit to all conditions ($R^2 > 0.97$) (figure B.3.3). The curve equation to describe the non-linear stress strain relationship was:

$$\sigma = a\varepsilon^3 + b\varepsilon^2 + c\varepsilon + d \qquad \textit{(EQ B.3.1)}$$

Where σ is stress, ε is strain and a, b, c & d are polynomial curve coefficients for a 3rd order polynomial

The modulus can be calculated as the 1st derivative of the polynomial curve fit and is expressed as:

$$Modulus_{(\varepsilon)} = 3a\varepsilon^2 + 2b\varepsilon + c \qquad \textit{(EQ B.3.2)}$$

Where σ is stress, ε is strain and a, b, & c are polynomial curve coefficients for a 3rd order polynomial.

The non-linear response can then be described by calculating a viscoelastic modulus at three regions of the loading curve for each condition. The curve regions are initial, intermediate and final (Figure B.3.4); as per the methods in section B.1.2.1.3.

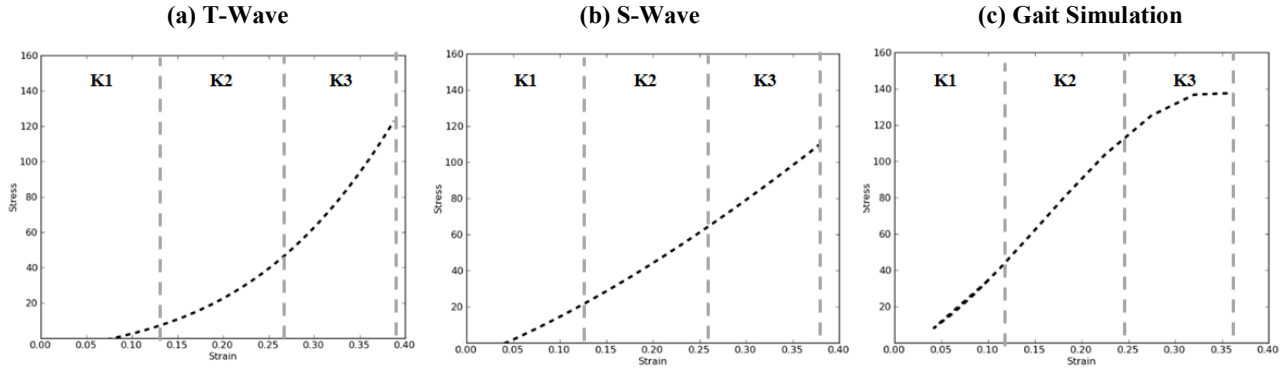

Figure B.3.4: Curve segmentation for estimation of Viscoelastic modulus (K).

(a) Twave, (b) Sine Wave, (c) Gait Simulation

B.3.5.1.5. Energy Loss and Percentage Energy Dissipation

Absolute Energy Loss and Percentage Energy Dissipation were calculated via the methods stated in in section B.1.2.1.4 using 3rd order polynomial fits to the compression and decompression segments of the stress-strain curves.

B.3.5.2 Characterisation of the Stress-Strain response via analytical models

A preliminary analysis was conducted using 1 subject's data to assess which of the previously published models provide a good fit to the data collected in this study. The models included in the initial assessment were: The Maxwell model, The Kelvin-Voigt Model, Standard Three element Viscoelastic Solids of Type A & Type B, The Non-Newtonian Kelvin-Voigt Model and The Parallel Three Element Model. A detailed explanation of these models can be found in Section B.1.

A novel Non-Newtonian, Non-Hookean Parallel Three Element Model was designed by substituting the Non-Newtonian viscous component of the Non-Newtonian Kelvin-Voigt Model into the Parallel Three Element Model to create a non-linear model that exhibits both Non-Hookean and Non-Newtonian behaviour (Figure B.3.14).

Model Equation:

Initial ($0 < \varepsilon < X_s$) $\sigma = E_2\varepsilon$ *(EQ B.3.9)*

Final ($X_s < \varepsilon < \varepsilon_{(max)}$) $\sigma = E_2\varepsilon + E_1(\varepsilon - X_s) + \eta\varepsilon\dot{\varepsilon}$ *(EQ B.3.10)*

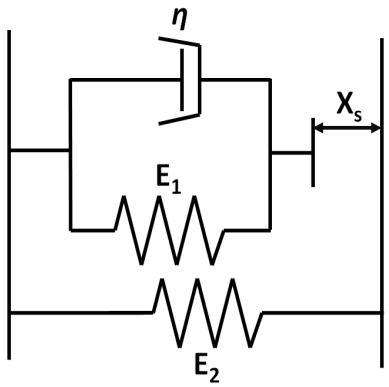

Figure B.3.5: Modified Parallel Three Element Model

B.3.5.2.1. Assessment of model fit

The Scipy package of the enthought python distribution was used to find the constant terms of the constitutive equations, for the analytical models, by least squares regression (scipy.optimize.leastsq Python2.5.4 EPD 5.1.1). Pearson's regression was used to evaluate the fit of the models to the raw data. An average of all cycle's R^2 values for each profile type was calculated to evaluate the best model fit (Table B.3.2). Fit was accepted if $R^2 > 0.8$ for all conditions. Thus the Kelvin-Voigt, Non-Newtonian, Parallel Three Element and Non-Hookean Non-Newtonian were accepted and will be used to characterise the tissue response for the full cohort.

Kelvin Voigt Model Parameters

Model Equation: $\sigma = E\varepsilon + \eta\dot{\varepsilon}$ *(EQ B.3.11)*

Where E is the elastic modulus and η is the viscosity which was derived by least squares fit.

Non-Newtonian Model Parameters

Model Equation: $\sigma = E\varepsilon + \eta\varepsilon\dot{\varepsilon}$ *(EQ B.3.12)*

Where E is the elastic modulus and η is the viscosity which was derived by least squares fit.

Parallel Three Element Model Parameters

Initial ($0 < \varepsilon < X_s$): $\sigma = E_2\varepsilon$ *(EQ B.3.13)*

Final ($X_s < \varepsilon < \varepsilon_{(max)}$): $\sigma = E_2\varepsilon + E_1(\varepsilon - X_S) + \eta\dot{\varepsilon}$ *(EQ B.3.14)*

Where E_1 & E_2 are the elastic moduli and η is the viscosity which was derived by least squares fit.

Non-Hookean Non-Newtonian Model Parameters

Initial ($0 < \varepsilon < X_s$): $\sigma = E_2\varepsilon$ *(EQ B.3.15)*

Final ($X_s < \varepsilon < \varepsilon_{(max)}$): $\sigma = E_2\varepsilon + E_1(\varepsilon - X_S) + \eta\varepsilon\dot{\varepsilon}$ *(EQ B.3.16)*

Where E_1 & E_2 are the elastic moduli and η is the viscosity which was derived by least squares fit.

Table B.3.2: All cycle average R^2 values for model fit to raw data.

	Gait Profile		SWave		Twave	
Model	Mean	SD	Mean	SD	Mean	SD
Maxwell	0.732	± 0.236	-0.381	± 0.155	0.106	± 0.174
Kelvin-Voigt	0.974	± 0.018	0.982	± 0.013	0.894	± 0.164
Viscoelastic Type A	0.093	± 0.414	0.720	± 0.520	0.405	± 0.240
Viscoelastic Type B	0.826	± 0.329	-0.004	± 0.173	0.120	± 0.186
Non-Newtonian	0.818	± 0.110	0.969	± 0.021	0.898	± 0.164
Parallel 3 Element	0.951	± 0.030	0.991	± 0.005	0.928	± 0.101
Non-Hookean Non-Newtonian	0.968	± 0.019	0.991	± 0.006	0.902	± 0.164

B.3.5.2.2. Smoothing of the Model Fit

Due to the ultrasound tracking techniques used, the raw displacement data contained noise. This noise resulted in an erratic fit of some models due to fluctuations in the strain rate. To reduce this effect but maintain the stress-strain relationship, the raw strain data were fit with a spline smoothing function (Figure B.3.15). A 4th degree univariate spline function was used which was forced to pass through 95% of the data, permitting a good reproduction of the original strain trajectory. The strain rate was then calculated based on the curve equation of the spline fit, resulting in smoothed strain and strain rate data which were used to fit the models.

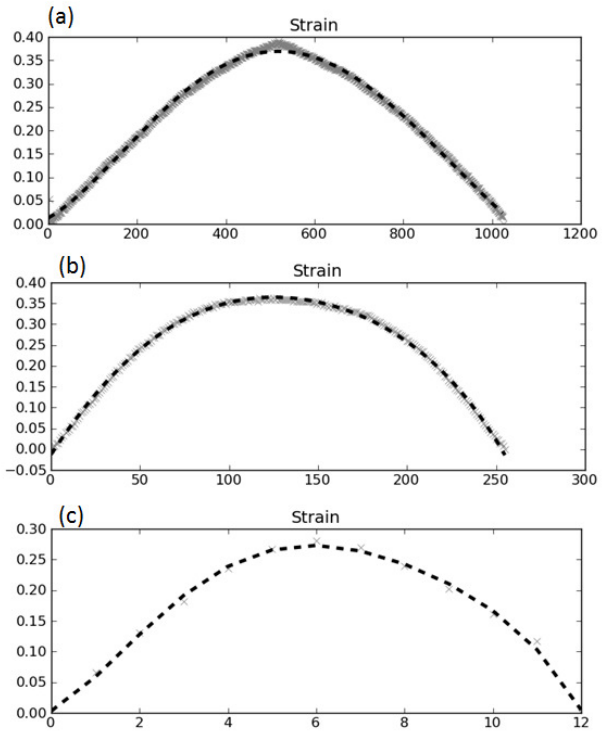

Figure B.3.6: Spline fit to strain curve. (a) Twave, (b) Swave, (c) Gait

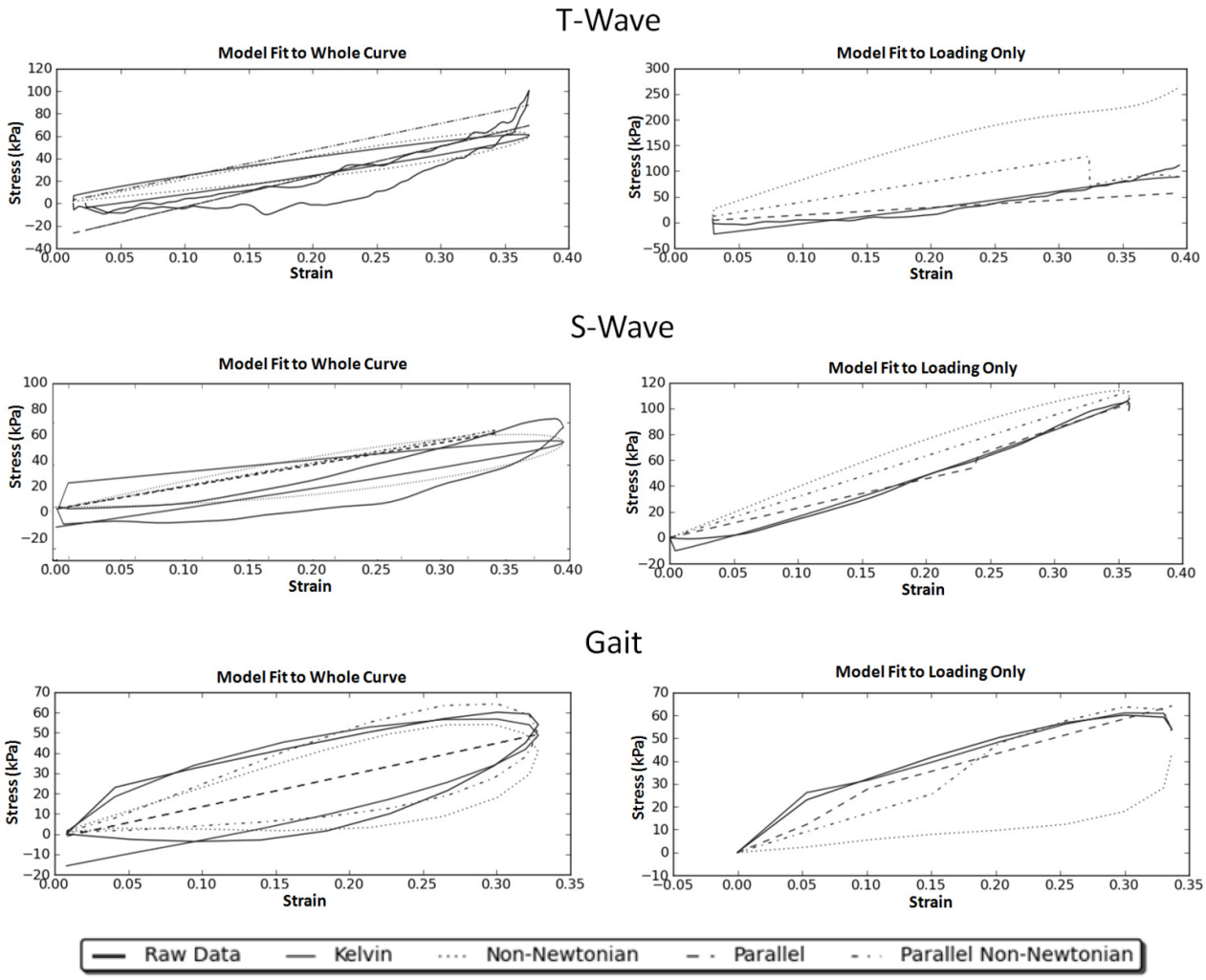

Figure B.3.7: Model fit to raw data via Least Squares fit. Left hand curves represent model fit to the whole compression cycle. Right hand curves represent model fit to the loading curve only

B.3.5.2.3. Assessment of fit to loading only and whole curve

A good Pearson's R^2 agreement was found for fits to both whole curve and loading-only; however the best fit was found to the loading curve only for all conditions (Table B.3.3). The RMS error between model fit and raw data was poor for both loading and whole curve data, suggesting that although the models are able to follow the trends of the raw (gradient and turning points) data, they do not represent the true tissue response to load (Table B.3.3). The values derived for elastic moduli and viscosity are within the range of previously reported elastic moduli and viscosity (Tables B.3.4 & B.3.5). For the purposes of this study, loading-only model fits will be used.

Table B.3.3: All cycle average R^2 values and RMS error for the loading only and whole curve model fits.

Triangle Wave	Loading only Pearsons R	Whole curve Pearsons R	Loading only RMS	Whole curve RMS
Kelvin-Voigt	0.974 ± 0.007	0.912 ± 0.004	7.719 ± 1.066	19.191 ± 0.713
Non-Newtonian	0.907 ± 0.008	0.723 ± 0.052	103.062 ± 20.836	25.464 ± 1.734
Parallel Three Element	0.963 ± 0.003	0.893 ± 0.015	12.265 ± 6.309	16.813 ± 3.034
Non Hookean Non-Newtonian	0.896 ± 0.161	0.893 ± 0.015	31.744 ± 20.183	27.790 ± 1.130
Sine Wave				
Kelvin-Voigt	0.993 ± 0.005	0.927 ± 0.020	2.998 ± 0.602	15.194 ± 5.400
Non-Newtonian	0.966 ± 0.036	0.426 ± 0.242	17.277 ± 11.759	30.927 ± 13.147
Parallel Three Element	0.987 ± 0.007	0.615 ± 0.633	8.611 ± 8.215	29.588 ± 9.177
Non Hookean Non-Newtonian	0.990 ± 0.005	0.885 ± 0.062	9.782 ± 7.689	23.129 ± 8.978
Simulated Gait				
Kelvin-Voigt	0.986 ± 0.011	0.954 ± 0.030	2.726 ± 1.622	7.118 ± 4.177
Non-Newtonian	0.502 ± 0.382	0.182 ± 0.295	26.748 ± 9.867	23.631 ± 6.255
Parallel Three Element	0.917 ± 0.073	0.764 ± 0.110	9.659 ± 7.177	15.303 ± 7.702
Non Hookean Non-Newtonian	0.936 ± 0.061	0.951 ± 0.028	7.294 ± 5.324	6.501 ± 2.465

Table B.3.4: Load Only derived modulus of Elasticity and Viscosity

Load Only Parameters	T-Wave Mean ± SD	S-Wave Mean ± SD	Gait Simulation Mean ± SD
Kelvin-Voigt			
E	258.76 ± 7.05	246.88 ± 51.33	135.33 ± 35.10
V	118.59 ± 20.74	10.57 ± 5.76	-1.01 ± 0.39
Non-Newtonian			
E	397.63 ± 35.27	255.73 ± 56.51	115.36 ± 35.10
V	-1587.95 ± 229.30	-71.49 ± 48.29	7.12 ± 2.71
Parallel 3 Element			
E(a)	215.60 ± 59.24	259.40 ± 61.28	188.33 ± 74.75
E(b)	-2.66 ± 24.74	11.95 ± 35.40	-40.84 ± 25.99
V	76.54 ± 51.75	8.68 ± 61.63	-15.38 ± 68.92
Non-Newtonian Non Hookean			
E(a)	365.49 ± 22.91	266.48 ± 59.55	129.21 ± 37.76
E(b)	29.44 ± 10.76	12.99 ± 31.31	-23.32 ± 27.98
V	-1356.42 ± 259.23	-25.73 ± 45.81	5.98 ± 2.17

Definitions: E(a) - Primary Elastic Modulus, E(b) - Secondary Elastic Modulus, V - Viscosity.

Table B.3.5: Whole Curve derived modulus of Elasticity and Viscosity

Whole Curve Parameters	T-Wave Mean ± SD	S-Wave Mean ± SD	Gait Simulation Mean ± SD
Kelvin-Voigt			
E	173.98 ± 7.56	178.56 ± 35.82	117.49 ± 21.22
V	-50.82 ± 8.19	-16.62 ± 7.48	-1.39 ± 0.50
Non-Newtonian			
E	173.94 ± 7.55	178.24 ± 35.79	113.55 ± 21.30
V	283.37 ± 42.21	130.33 ± 47.26	7.49 ± 2.11
Parallel 3 Element			
E(a)	216.96 ± 15.08	223.96 ± 94.03	167.66 ± 133.86
E(b)	-11.14 ± 20.11	39.85 ± 33.10	-6.94 ± 64.75
V	74.61 ± 32.89	10.36 ± 119.80	-7.99 ± 143.87
Non-Newtonian Non Hookean			
E(a)	245.47 ± 9.41	221.95 ± 67.50	165.56 ± 65.04
E(b)	34.80 ± 12.89	51.79 ± 71.64	-26.57 ± 40.46
V	282.74 ± 43.30	130.48 ± 47.34	7.33 ± 2.07

Definitions: E(a) - Primary Elastic Modulus, E(b) - Secondary Elastic Modulus, V - Viscosity.

B.3.6. Statistical Analysis

The combined subject data from all individuals was used to calculate average mechanical properties for each of the loading conditions. Data were excluded from the sample in some cases due to failure in tracking the tissue compression. A minimum of two trials (of multiple cycles) with complete data for stress and strain throughout were required for inclusion of a subject's data in the analysis. The total number of subjects for each condition was as follows: T- Wave = 29, S-Wave = 31, Gait-Sim = 29.

B.3.6.1. Assessment of Normality

The data for each parameter was assessed for normality using the Kolmogrov-Smirnov test in SPSS. In some cases, a positive skew was found to significantly ($p<0.05$) affect the normality of the data. To allow the use of robust multivariate parametric analysis methods, non-normal data were transformed using logarithmic transformations. Conclusions established with the parametric univariate tests (One-way Anova), were confirmed by the use of complimentary non-parametric tests (Kurskal-Wallis, Mann-Whitney), which did not require the use of data transformations.

B.3.6.2. Analysis of Data and Variance

For the assessment of the tissues response to different loading conditions (T-Wave, S-Wave, Gait-Sim) the subjects from all ages and genders were pooled. The mean, standard deviation and Coefficient of variation were calculated for each tissue characteristic and presented in both graphical and tabular form. For the assessment of difference between loading conditions, the Kurskal-Wallis test, and One-way Independent Anova test were used for each tissue characteristic. Pairwise post-hoc tests (Mann-Whitney, Bonferroni respectively), were conducted to identify the significant differences between each of the loading conditions.

For the assessment of difference between individual groups (Age, Gender), the data was assessed for each loading condition separately and also for all conditions combined. The combined data was used to produce ensemble graphs showing the overall mean difference between groups. The data for the assessment of the loading conditions separately, was presented in tables in the form of mean, standard deviation and coefficient of variation. The difference between groups was established by using Mann-Whitney tests and One-way Independent Anovas, for each characteristic, as this provided a thorough assessment of the difference between the independent subject groups. The interaction between the variance due to the loading condition and the variance due to the group (age or gender) were assessed by using a two-way Anova. The results were presented as main effects, (age, gender, rate) and interaction effects (age*rate, gender*rate).

B.3.6.3. Analysis of Correlation

To assess the relationship between the curve parameters (peak stress, strain at peak stress) and the derived mechanical properties, correlation coefficients were calculated. Correlation analysis was also conducted to assess the relationship between subject age and mechanical properties and subject gender and mechanical properties. The full correlation matrices for all parameters at each of the test conditions are presented in Appendix G.

B.4. Results

B.4.1. Differences observed between loading profiles.

B.4.1.1. Loading Curve Characteristics

The tissue's response throughout loading differed dependent on the type of applied profile (Figure B.4.1). For both the T-Wave and S-Wave profiles, the stress-strain relationship shows an upwardly convex loading curve, the unloading curve is also upwardly convex and follows a path below that of the loading curve, giving a hysteresis. The Gait-Sim profile's stress-strain relationship display an upwardly concave loading curve, while the unloading curve is upwardly convex and follows a path below that of the loading curve, giving a large hysteresis. The peak strain and strain at peak stress are similar for the T-Wave and S-Wave profiles (Table B.4.1); however, for the Gait-Sim profile a discrepancy occurred suggesting the presence of a largely viscous component during loading.

B.4.1.2. Direct Characterisation of the Stress-Strain Response

Linear

If linear modulus is assumed, a significant trend to increased secant modulus is found when the average displacement rate of the profile was increased ($p<0.05$) (Figure B.4.2.). Post-hoc Mann-Whitney tests displayed significant difference between the T-Wave and the Gait-Sim condition ($p<0.05$) (Table B.4.1).

Non-Linear

If nonlinear modulus is assumed, a more complex response is seen (Figure B.4.2.). For the T-Wave profile, the viscoelastic modulus is initially low and a trend toward increased modulus throughout loading is observed. For the S-Wave profile, the viscoelastic modulus remains at a moderate level throughout loading. For the Gait-Sim profile, the viscoelastic modulus is initially high and a trend toward decreased modulus is observed throughout loading.

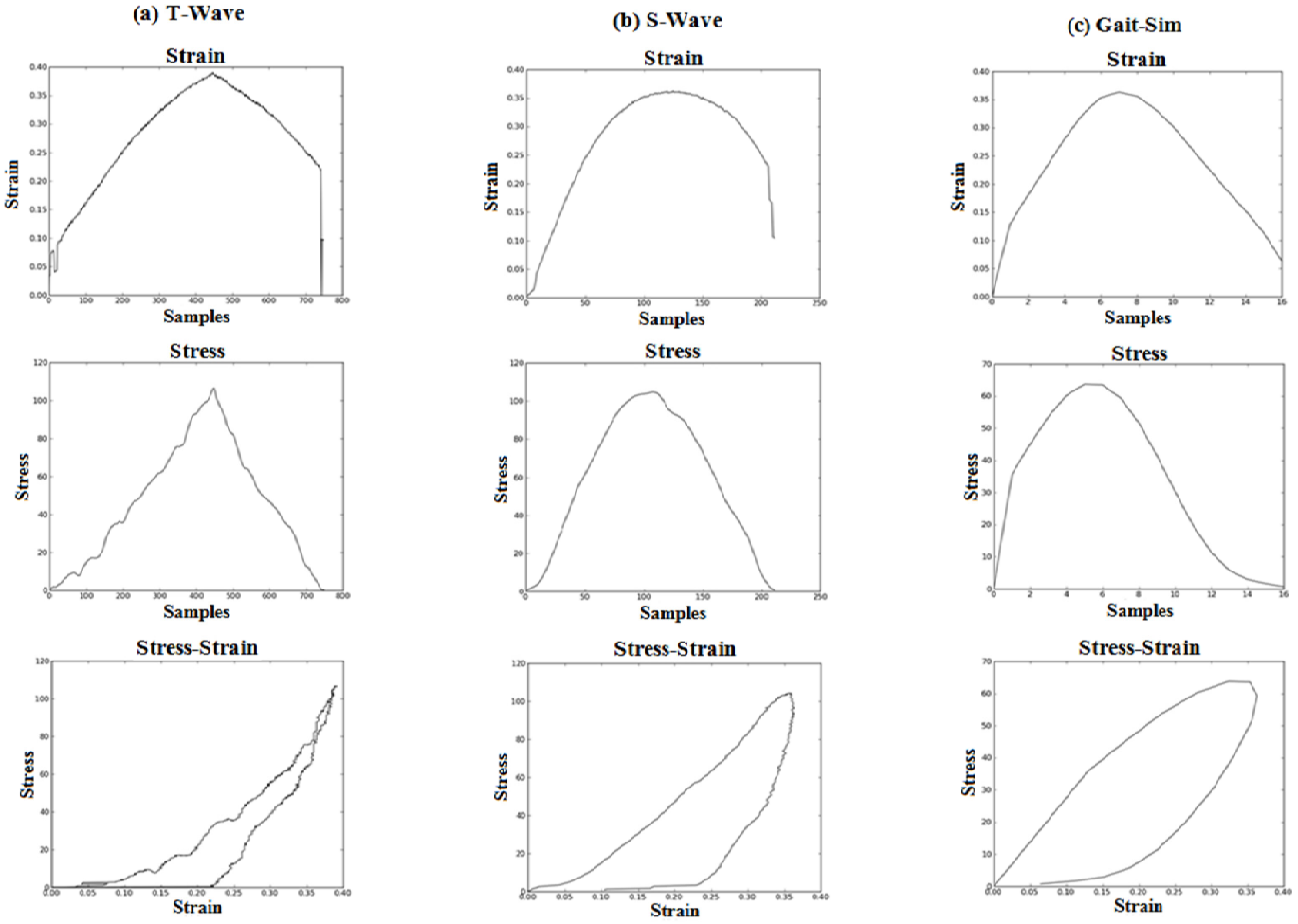

Figure B.4.1: Stress-strain relationship for the heel region. Top panels are tissue strain, Middle panels are tissue stress and bottom panels are stress-strain relationship for (a) Triangle Wave Profile, (b) Sine Wave Profile, (c) Gait Simulation Profile

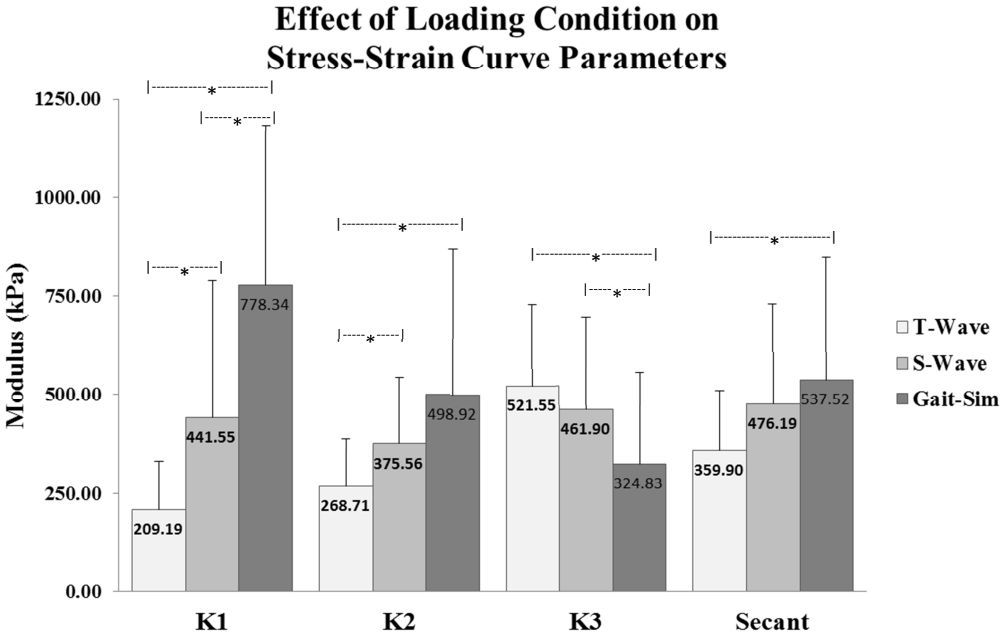

Figure B.4.2. Direct Characterisation of the Tissue Modulus for Linear and Non-Linear Response

B.4.1.3. Derivation of Elastic Moduli and Viscosity via Model Fits

The primary and secondary elastic moduli ($E_{(a)}$ & $E_{(b)}$) were found to be the most consistent for the Parallel Three Element model across all rates with no significant difference between loading conditions ($p>0.05$) (Figures B.4.3 & B.4.4 Table B.4.1), however post-hoc Mann-Whitney tests displayed significant difference in the primary elastic modulus between T-Wave and S-Wave profiles. The viscosity (V) was also found to be most consistent across all rates for the Parallel Three Element model with no significant differences ($p>0.05$) found between loading conditions (Figure B.4.5, Table B.4.1).

B.4.1.4. Direct Characterisation of Percentage Energy Dissipated and Energy Loss

The Energy loss displayed a significant increasing trend ($p<0.01$) when the average displacement rate of the loading profile was increased (Figure B.4.6, Table B.4.1). Post-hoc Bonferroni and Mann-Whitney tests displayed significant differences between the all conditions ($p<0.05$).

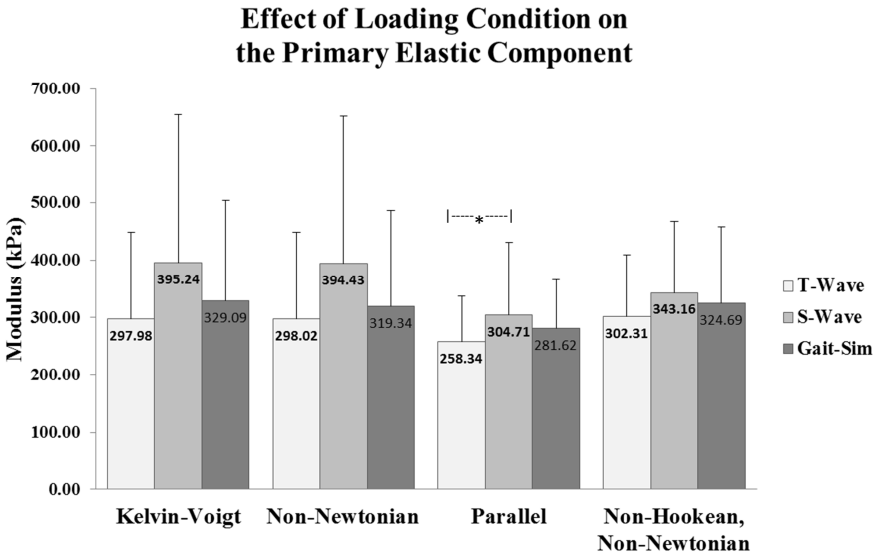

Figure B.4.3: All Subject Average Primary Elastic Modulus for each Condition

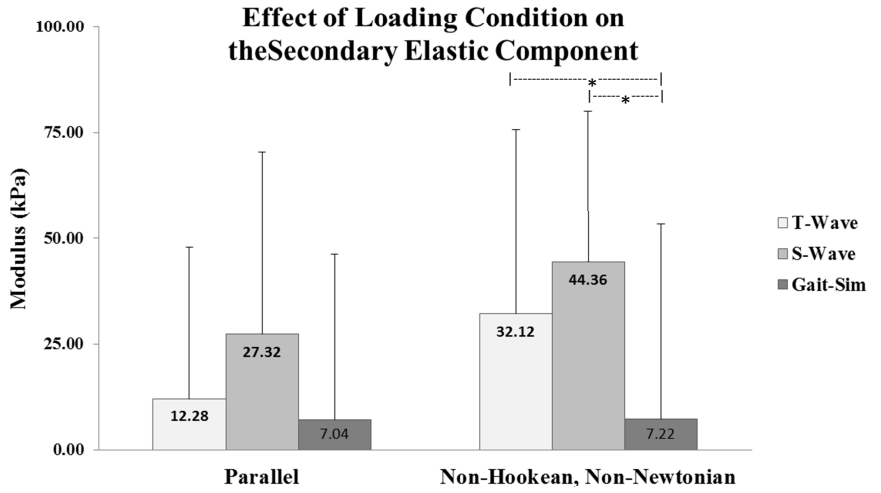

Figure B.4.4: All Subject Average Secondary Elastic Modulus for each Condition

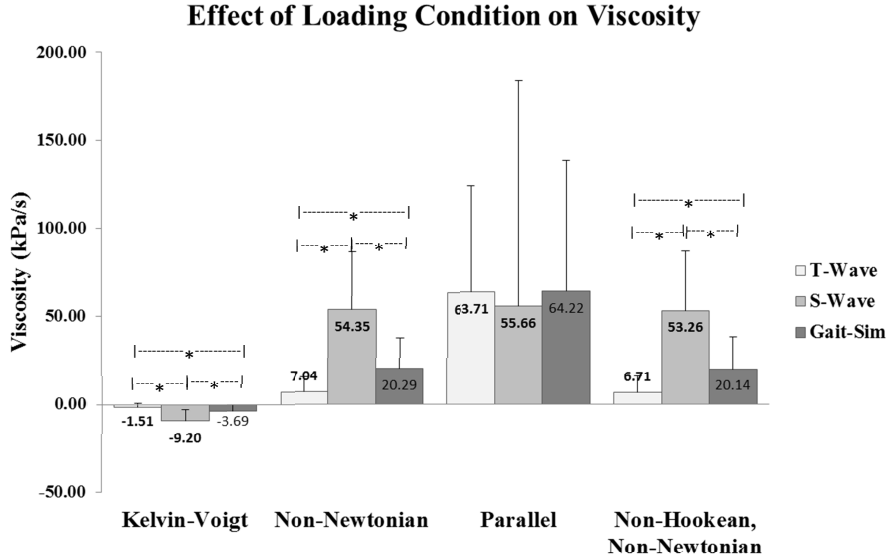

Figure B.4.5: All Subject Average Viscosity for each Condition

The Percentage Energy Dissipation showed a significant increasing trend (p<0.01) when average displacement rate was increased (Figure B.4.6, Table B.4.1). Post-hoc Bonferroni and Mann-Whitney tests displayed significant differences between the T-Wave condition and both the S-Wave condition (p<0.01) and the Gait-Sim condition (p<0.01).

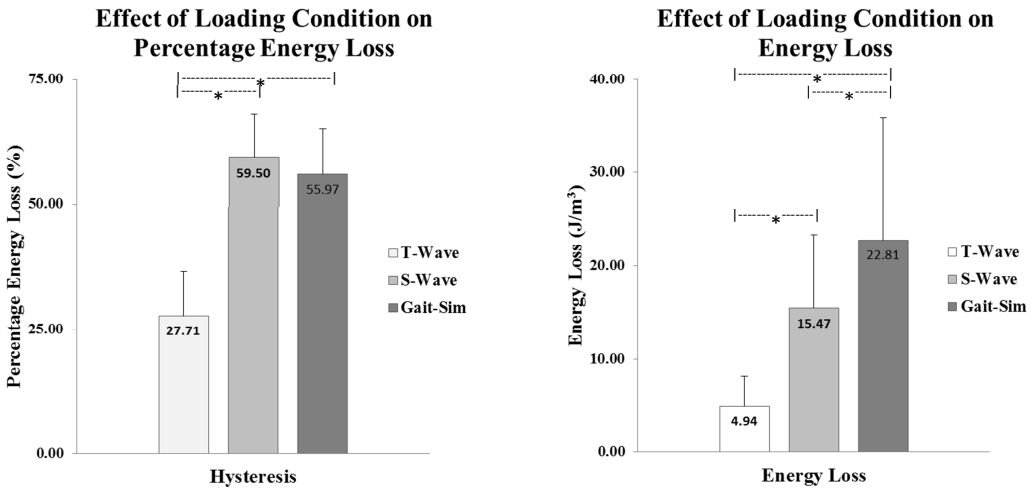

Figure B.4.6: All Subject Average Percentage Energy Dissipated & Energy Loss across all Conditions

B.4.1.5. Between Variable Correlation Analyses

Peak stress displayed a significantly high correlation (R>0.8; p<0.01) to modulus values derived from the loading curves directly (K1-3; secant modulus) and to the elastic modulus derived via the Kelvin, Non-Newtonian and Non-Newtonian Non-Hookean models for all test conditions and to the Absolute Energy Loss (R>0.8; p<0.01). These correlations suggest a high sensitivity of the analysis methods to variation in the applied loading conditions. In the Parallel Three Element model parameters moderate but significant correlations (R>0.5; p<0.01) were observed for peak stress and elastic moduli and for energy loss and viscosity, suggesting a slightly reduced sensitivity to test conditions in this model. For all conditions, a low negative correlation (R<0.5) was present between modulus measures (K1-3; secant modulus & E) and tissue compressibility, suggesting that an increase in the tissue's modulus may lead to a reduced compressive capacity.

Table B:4.1. Curve characteristics and derived mechanical properties for each test condition

Parameters	Units	T-Wave (n=29) Mean	SD	CoV	S-Wave (n=31) Mean	SD	CoV	Gait (n=29) Mean	SD	CoV	Kurskal Wallis p	Mann-Whitney T-S p	T-G p	S-G p	One-Way Anova p	F	Bonferroni T-S p	T-G p	S-G p
Curve Characteristics																			
Stress Max	kPa	127.85	± 55.27	43.23%	149.90	± 71.40	47.63%	156.72	± 88.49	56.46%	.573	.355	.367	.994	.507	.684	.981	.900	1.000
Strain at Stress Max	(-)	0.35	± 0.05	13.63%	0.32	± 0.05	16.78%	0.30	± 0.04	12.80%	* .000	* .046	.000	.095	* .000	9.783	* .053	.000	.124
Compressibility	(-)	0.36	± 0.05	13.69%	0.33	± 0.05	15.33%	0.38	± 0.04	10.21%	* .008	* .108	.109	.003	* .005	5.737	* .224	.374	.003
Energy Dissipation																			
Percentage Energy Loss	%	27.71	± 8.87	32.00%	59.50	± 8.65	14.54%	55.97	± 9.17	16.39%	* .000	* .000	.000	.164	* .000	108.613	* .000	.000	.406
Energy Loss	J/m^3	4.94	± 3.22	65.20%	15.47	± 7.88	50.96%	22.81	± 13.11	57.49%	* .000	* .000	.000	.016	* .000	27.844	* .000	.000	.008
Stress-Strain Characteristics																			
Secant	kPa	359.90	± 150.43	41.80%	476.19	± 251.93	52.91%	537.52	± 308.36	57.37%	* .039	* .060	.016	.515	* .050	3.093	ǂ .265	.053	1.000
K1	kPa	209.19	± 123.83	59.20%	441.55	± 347.49	78.70%	778.34	± 405.48	52.09%	* .000	* .001	.000	.000	* .000	23.659	* .053	.004	1.000
K2	kPa	268.71	± 117.90	43.88%	375.56	± 165.01	43.94%	498.92	± 367.45	73.65%	* .005	* .004	.006	.464	* .004	5.860	* .633	.000	.003
K3	kPa	521.55	± 205.30	39.36%	461.90	± 232.31	50.29%	324.83	± 231.16	71.16%	* .000	* .122	.000	.002	* .000	11.105	* .018	.000	.000
Kelvin																			
$E_{(a)}$	kPa	297.98	± 150.20	50.41%	395.24	± 259.28	65.60%	329.09	± 174.65	53.07%	.320	.137	.549	.371	-	-	-	-	-
V	kPa/s	-1.51	± 2.30	-151.78%	-9.20	± 6.56	-71.28%	-3.69	± 3.31	-89.83%	* .000	* .000	.000	.001	-	-	-	-	-
Non-Newtonian																			
$E_{(a)}$	kPa	298.02	± 150.21	50.40%	394.43	± 257.82	65.37%	319.34	± 167.07	52.32%	.318	.137	.658	.322	-	-	-	-	-
V	kPa/s	7.04	± 8.65	122.81%	54.35	± 32.81	60.37%	20.29	± 18.21	89.71%	* .000	* .000	.000	.000	-	-	-	-	-
Parallel 3 Element																			
$E_{(a)}$	kPa	258.34	± 78.87	30.53%	304.71	± 126.71	41.58%	281.62	± 84.37	29.96%	ǂ .088	* .024	.186	.534	.135	2.046	.139	.820	1.000
$E_{(b)}$	kPa	12.28	± 35.62	290.14%	27.32	± 43.21	158.17%	7.04	± 39.12	555.42%	.136	ǂ .120	.981	.061	ǂ .070	2.737	ǂ .270	1.000	.087
ε	(-)	-0.01	± 0.84	-16285.14%	0.08	± 0.61	749.11%	0.14	± 0.38	271.75%	.437	.467	.169	.750	.681	.386			
V	kPa/s	63.71	± 60.31	94.67%	55.66	± 128.48	230.83%	64.22	± 74.89	116.61%	.993	.853	.981	.994	.923	.080	1.000	1.000	1.000
Non-Newtonian Non-Hookean																			
$E_{(a)}$	kPa	302.31	± 106.75	35.31%	343.16	± 123.76	36.06%	324.69	± 132.87	40.92%	.433	.196	.576	.482	-	-	-	-	-
$E_{(b)}$	kPa	32.12	± 43.61	135.79%	44.36	± 35.54	80.13%	7.22	± 46.03	637.22%	* .006	* .318	.047	.001	-	-	-	-	-
ε	(-)	0.18	± 0.63	348.60%	0.05	± 0.64	1172.09%	0.09	± 0.40	461.87%	.435	.442	.155	.918	-	-	-	-	-
V	kPa/s	6.71	± 9.02	134.43%	53.26	± 34.35	64.50%	20.14	± 18.30	90.83%	* .000	* .000	.000	.000	-	-	-	-	-

Definitions: K(1,2,3) - Viscoelastic Modulus, E(a) - Primary Elastic Modulus, E(b) - Secondary Elastic Modulus, V - Viscosity.

Statistics: SD - Standard Deviation of the Mean, CoV - Coefficient of Variation of the Mean, * denotes a p-value<0.05; ǂ denotes a p-value < 0.1

B.4.2. Observed differences between age groups

B.4.2.1. Direct Characterisation of the Stress-Strain Response

There was no observed significant difference for linear and non-linear modulus when values for all rates were averaged ($p>0.05$) (Figure B.4.7). Furthermore, no significant differences were found when groups were compared for each condition separately ($p>0.05$), despite the presence of large between group differences (Table B.4.3).

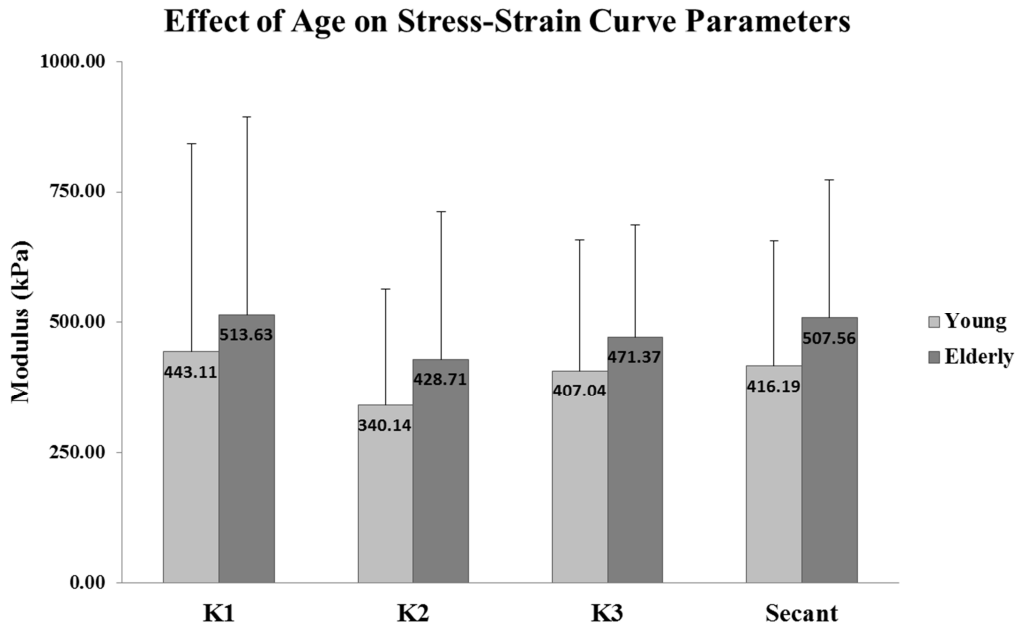

Figure B.4.7: Differences with Age for the Direct Characterisation of the Tissue Modulus for Linear and Non-Linear Response

B.4.2.2. Derivation of Elastic and Viscous Moduli via Model Fits

The primary and secondary elastic moduli ($E_{(a)}$ & $E_{(b)}$) of the models displayed an increase in the Elderly group for all models when values from all rates were combined (Figure B.4.8 & 4.9). This variance was found to be significantly different for $E_{(a)}$ in the Kelvin, Non-Newtonian and Non-Newtonian, Non-Hookean models ($p<0.05$). When conditions were assessed separately no significant differences were observed ($p>0.05$) however an increased primary elastic modulus was observed for the elderly group in all conditions.

The viscosity does not display a regular trend across the all models when assessed for the combined values from all conditions (Figure B.4.10). When conditions were assessed separately a reduced viscosity was observed in most models for the T-Wave and S-Wave conditions, this was found to be significant for the Non-Newtonian model in the T-Wave condition ($p<0.05$). For the Gait-Sim condition an increased viscosity was observed in most models. The exception to this pattern was the parallel 3 element model which displayed increased viscosity in the elderly at low rates and reduced viscosity at high rates.

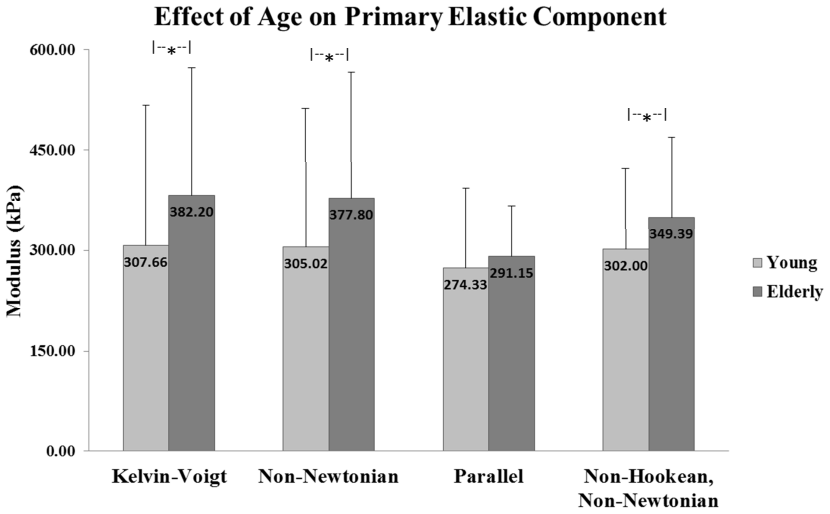

Figure B.4.8: Difference with Age for Primary Elastic Component

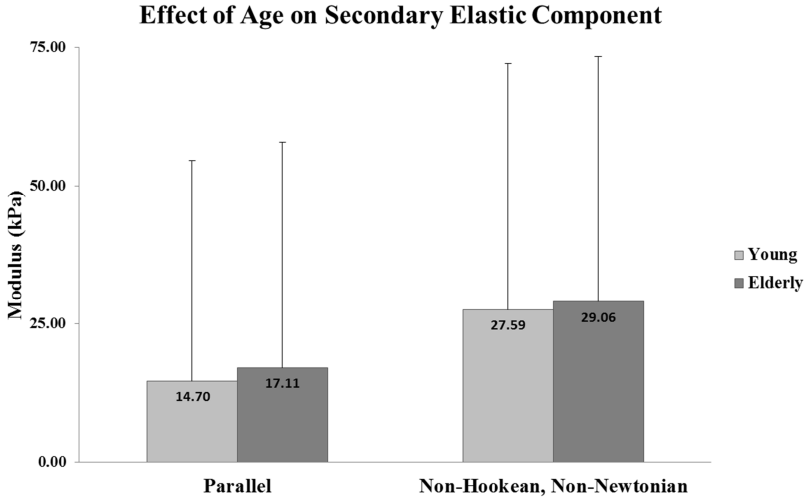

Figure B.4.9: Difference with Age for Secondary Elastic Component

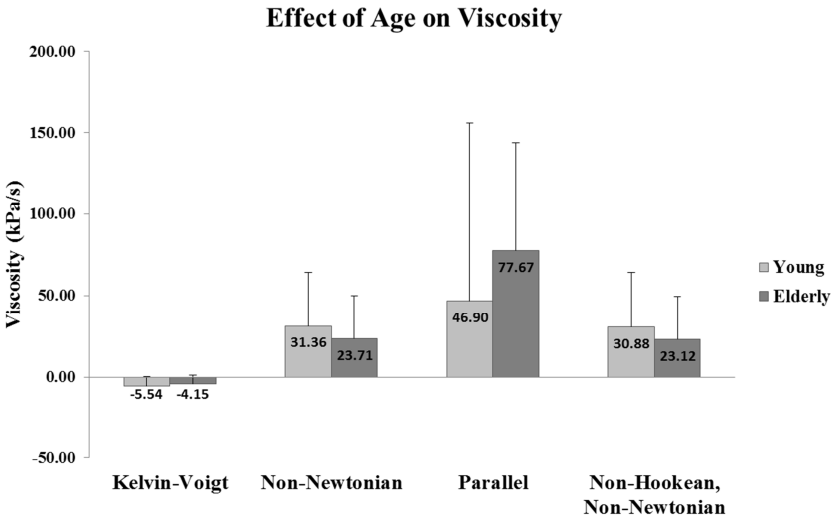

Figure B.4.10: Difference with Age for Viscosity

B.4.2.3. Direct Characterisation of Percentage Energy Dissipated and Absolute Energy Loss

The combined data for Percentage Energy Dissipated and the Absolute Energy Loss showed no significant differences with age ($p>0.05$) (Figure B.4.11). Although no significant differences were found when conditions were compared separately ($p>0.1$), large between age increases were observed for Absolute Energy Loss in the elderly group (Table B.4.3).

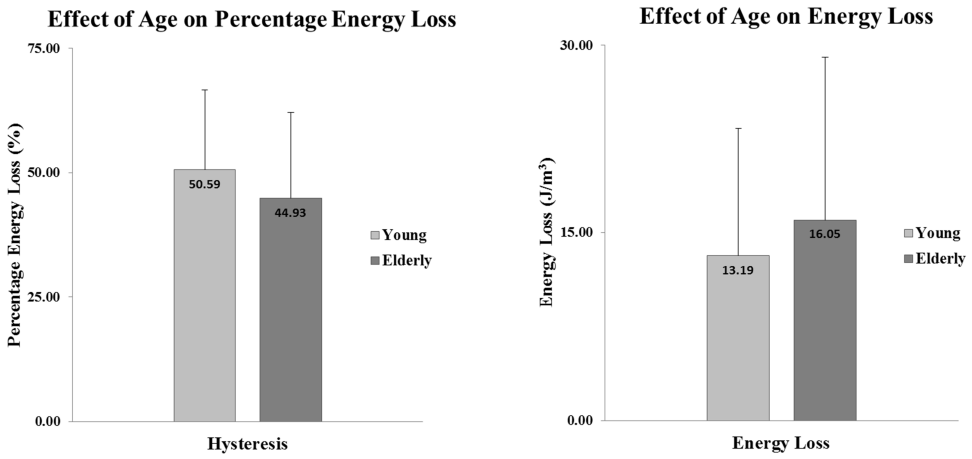

Figure B.4.11: Difference with Age for Percentage Energy Loss & Energy Loss

B.4.2.4. Multifactor Analysis

Age was found to have a main significant effect on the measured peak stress when data for all rates were combined; no other parameters displayed a significant age effect. No interactions were found between age and rate of compression in this study (Table B.4.2).

B.4.2.5. Correlations analysis of Age effects

A full matrix of correlation between age and derived mechanical properties in each test condition is presented in Appendix G. A low correlation ($R<0.4$) is observed for increased Energy loss with increased age for all conditions, and was found to be significant ($p<0.05$) for the S-Wave condition. For the Gait-Sim condition, a low but significant trend ($R<0.5$; $p<0.05$) toward increased compressibility was found with increased age.

B.4.3. Observed differences between gender groups

B.4.3.1. Direct Characterisation of the Stress-Strain Response

Slight increases were observed in the female group for linear and non-linear modulus (Secant, K1 and K2) when values for all rates were averaged (Figure B.4.12); however these results are not significantly different ($p>0.05$). Furthermore, no significant differences were found when groups were compared for each rate individually ($p>0.05$); despite between gender differences (Table B.4.4).

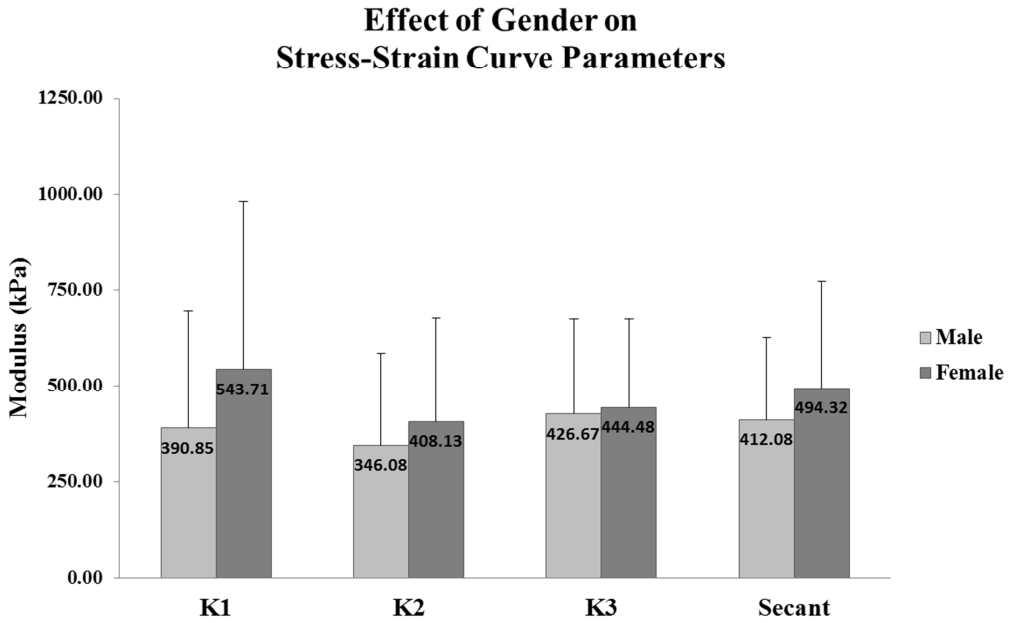

Figure B.4.12: Differences with Gender for the Direct Characterisation of the Tissue Modulus for Linear and Non-Linear Response

B.4.3.2. Derivation of Elastic Modul and Viscosity via Model Fits

The primary and secondary elastic moduli ($E_{(a)}$ & $E_{(b)}$) of the models displayed an increase in the Female group for all models when values from all rates were combined (Figure B.4.8 & 4.9). However, this variance was not found to be significant ($p>0.05$). When conditions were assessed separately no significant differences were observed ($p>0.05$).

The viscosity does not display a regular trend across the all models when assessed for the combined values from all conditions (Figure B.4.10). When conditions were assessed separately a reduced viscosity was observed in the Female group in most models for the T-Wave and S-Wave conditions, this was found to be significant for the Kelvin, Non-Newtonian and Non-Newtonian, Non-Hookean models in the S-Wave condition ($p<0.05$). For the Gait-Sim condition an increased viscosity was observed for the female group in all models however this was not found to be significant ($p>0.05$).

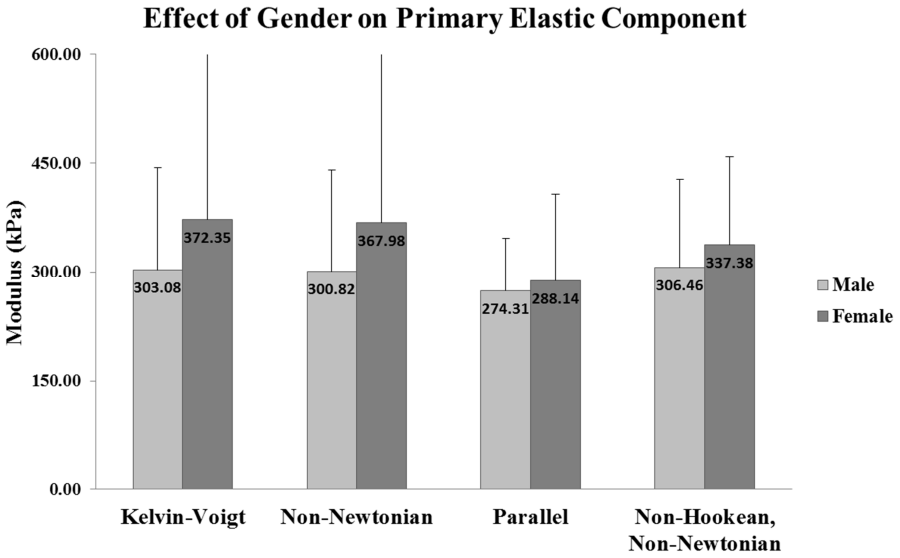

Figure B.4.13: Difference with Gender for Primary Elastic Modulus

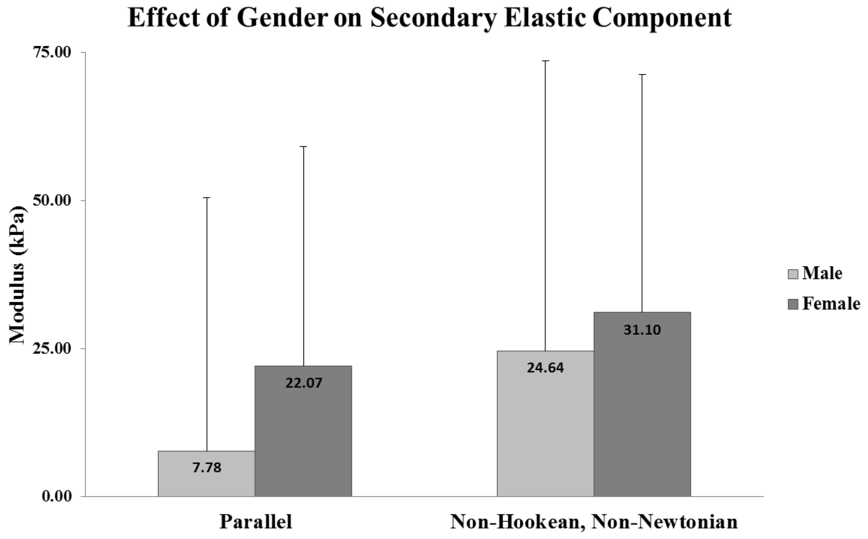

Figure B.4.14: Difference with Gender for the Secondary Elastic Modulus

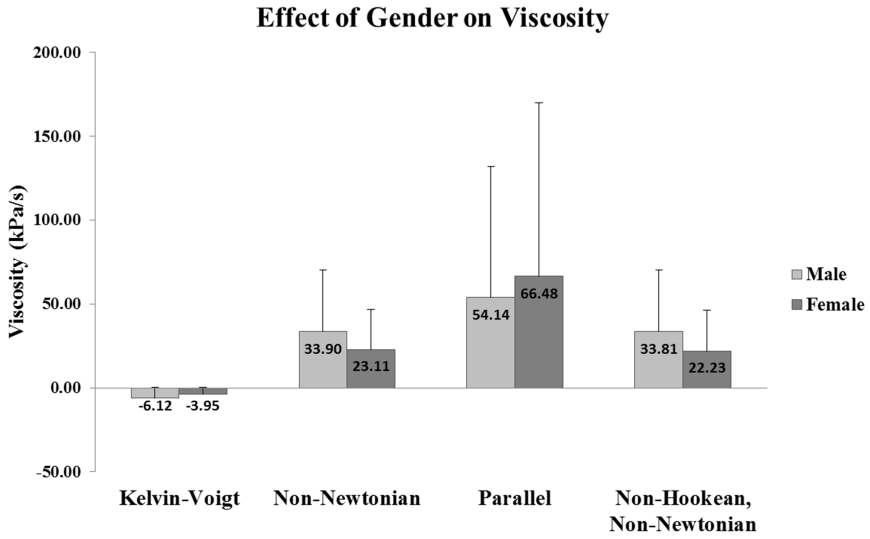

Figure B.4.15: Difference with Gender for the Viscosity

B.4.3.3. Direct Characterisation of Percentage Energy Dissipated and Absolute Energy Loss

The combined data for Percentage Energy Dissipated and the Absolute Energy Loss showed no significant differences with gender ($p>0.05$) (Figure B.4.16). The Absolute Energy Loss displayed an increase in the female group for the each condition when compared separately however this difference was not found to be significant in any case ($p>0.1$) (Table B.4.4).

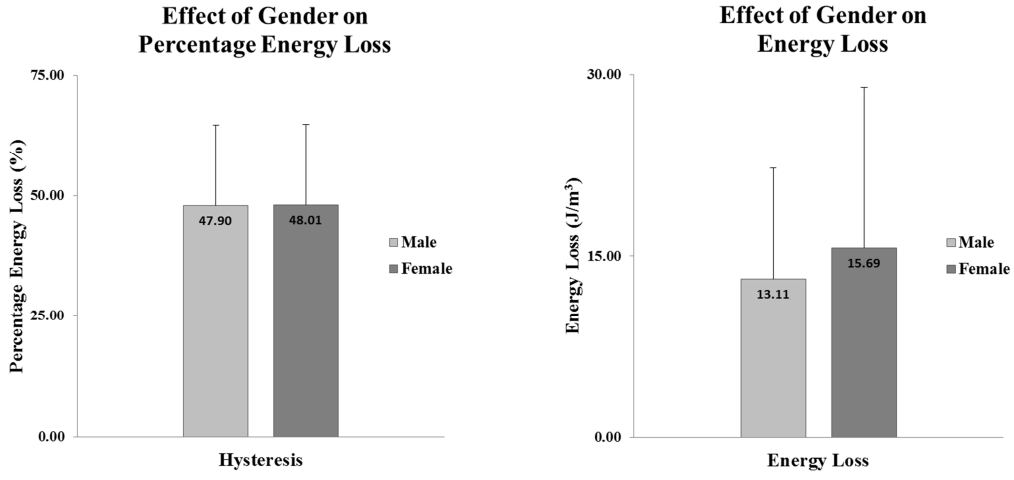

Figure B.4.16: Difference with Gender for Hysteresis & Energy Loss

B.4.3.4. Multifactor Analysis

Gender was found to have no significant ($p>0.05$) effect on the measured response of the plantar soft tissue. No interactions were found between gender and rate of compression in this study (Table B.4.2).

B.4.3.5. Correlations analysis of Gender effects

No significant correlations are present between the gender groups in this study (Appendix G); however a low positive correlation is present for viscoelastic modulus (K1) ($R<0.4$) across all conditions, suggesting a slight variation is present in the initial stress strain response between genders.

Table B.4.2: Statistical analysis of variance for pooled condition data

	Main Effects			Interaction Effects	
	Age	Rate	Gender	Age*Rate	Gender*Rate
Curve Characteristics					
Peak Stress	* .044	.656	.495	.929	.536
Strain at Peak Stress	.325	* .000	.217	.651	.268
Peak Strain	.261	* .010	.157	.615	.442
Energy Dissipation					
Hysteresis	ǂ .063	* .000	.186	.644	.809
Energy Loss	.129	* .000	.986	.894	.387
Stress-Strain Characteristics					
Secant	ǂ .085	ǂ .079	.299	.924	.832
K1	ǂ .089	* .000	ǂ .062	.779	.592
K2	.123	* .017	.261	.895	.514
K3	.184	* .000	.482	.963	.790
Parallel 3 Element					
E(a)	.590	.235	.884	.688	.957
E(b)	.749	.178	ǂ .059	.910	.599
V	.222	.906	.650	.323	.374

Definitions: K(1,2,3) - Viscoelastic Modulus, E(a) - Primary Elastic Modulus, E(b) - Secondary Elastic Modulus, V - Viscosity.
Statistics: * denotes a p-value<0.05; ǂ denotes a p-value < 0.1

Table B.4.3: Observed Age Difference for each compressive rate

T-Wave Condition

Parameter	Units	Young Mean ± SD	CoV	Elderly Mean ± SD	CoV	Difference	Mann-Whitney asymp. *p*		Anova *p*	Anova F
Curve Characteristics										
Stress Max	kPa	112.62 ± 49.19	43.68%	142.06 ± 58.44	41.14%	26.14%	.132	ǂ	.096	2.966
Strain at Stress Max	(-)	0.35 ± 0.04	12.04%	0.36 ± 0.05	15.18%	2.82%	.694		.593	.293
Compressibility	(-)	0.35 ± 0.04	12.22%	0.36 ± 0.05	15.13%	3.07%	.600		.562	.345
Energy Dissipation										
Percentage Energy Loss	%	29.71 ± 7.69	25.89%	25.97 ± 9.69	37.33%	-12.59%	.300		.273	1.252
Energy Loss	J/m^3	3.94 ± 2.08	52.86%	5.81 ± 3.82	65.69%	47.43%	.134		.128	2.471
Stress-Strain Characteristics										
Secant	kPa	328.29 ± 156.07	47.54%	389.40 ± 143.91	36.96%	18.62%	.190		.144	2.262
K1	kPa	173.54 ± 106.41	61.32%	242.45 ± 133.03	54.87%	39.71%	.106	ǂ	.082	3.256
K2	kPa	247.40 ± 116.28	47.00%	288.60 ± 119.86	41.53%	16.65%	.419		.297	1.133
K3	kPa	491.14 ± 214.20	43.61%	549.93 ± 199.76	36.32%	11.97%	.499		.277	1.233
Kelvin										
$E_{(a)}$	kPa	270.46 ± 163.56	60.47%	323.67 ± 137.17	42.38%	19.67%	.138		-	-
V	kPa/s	-2.12 ± 3.04	-143.06%	-0.94 ± 1.12	-119.18%	-55.53%	.315		-	-
Non-Newtonian										
$E_{(a)}$	kPa	270.46 ± 163.56	60.47%	323.73 ± 137.18	42.37%	19.70%	.138		-	-
V	kPa/s	10.66 ± 10.45	97.98%	3.66 ± 4.78	130.57%	-65.67%	* .036		-	-
Parallel 3 Element										
$E_{(a)}$	kPa	251.43 ± 79.80	31.74%	264.80 ± 80.22	30.29%	5.32%	.485		.657	.202
$E_{(b)}$	kPa	10.41 ± 39.21	376.73%	14.02 ± 33.22	236.90%	34.72%	.663		.790	.072
ε	(-)	-0.14 ± 1.06	-765.79%	0.12 ± 0.58	482.01%	-186.14%	.163		-	-
V	kPa/s	45.31 ± 66.24	146.19%	80.88 ± 50.46	62.39%	78.50%	.183		.114	2.669
Non-Newtonian Non-Hookean										
$E_{(a)}$	kPa	277.43 ± 101.91	36.73%	325.53 ± 109.32	33.58%	17.34%	.230		-	-
$E_{(b)}$	kPa	29.96 ± 45.57	152.10%	34.13 ± 43.20	126.59%	13.92%	.896		-	-
ε	(-)	0.02 ± 0.84	3687.69%	0.33 ± 0.30	90.67%	1338.33%	.407		-	-
V	kPa/s	10.07 ± 11.26	111.74%	3.57 ± 4.83	135.13%	-64.52%	ǂ .089		-	-

S-Wave Condition

Parameter	Units	Young Mean ± SD	CoV	Elderly Mean ± SD	CoV	Difference	Mann-Whitney asymp. *p*		Anova *p*	Anova F
Curve Characteristics										
Stress Max	kPa	137.07 ± 72.66	53.01%	167.66 ± 68.38	40.79%	22.32%	.128		.154	2.145
Strain at Stress Max	(-)	0.33 ± 0.05	16.59%	0.32 ± 0.06	17.58%	-3.05%	.659		.621	.250
Compressibility	(-)	0.34 ± 0.05	14.86%	0.33 ± 0.05	16.46%	-3.00%	.548		.595	.289
Energy Dissipation										
Percentage Energy Loss	%	61.27 ± 7.88	12.87%	56.99 ± 9.41	16.51%	-6.98%	.232		.195	1.766
Energy Loss	J/m^3	13.67 ± 7.35	53.81%	18.03 ± 8.21	45.53%	31.92%	.215		.145	2.250
Stress-Strain Characteristics										
Secant	kPa	424.44 ± 238.72	56.24%	547.85 ± 261.47	47.73%	29.07%	.161		.113	2.671
K1	kPa	383.39 ± 365.88	95.43%	517.62 ± 319.78	61.78%	35.01%	.107	ǂ	.100	2.896
K2	kPa	328.36 ± 133.68	40.71%	440.92 ± 186.50	42.30%	34.28%	ǂ .063	ǂ	.056	3.949
K3	kPa	444.94 ± 254.14	57.12%	485.38 ± 205.90	42.42%	9.09%	.246		.395	.745
Kelvin										
$E_{(a)}$	kPa	346.42 ± 273.02	78.81%	462.85 ± 232.24	50.18%	33.61%	ǂ .072		-	-
V	kPa/s	-10.33 ± 6.43	-62.24%	-7.63 ± 6.66	-87.23%	-26.14%	.317		-	-
Non-Newtonian										
$E_{(a)}$	kPa	345.47 ± 271.00	78.44%	462.23 ± 231.43	50.07%	33.80%	ǂ .072		-	-
V	kPa/s	60.06 ± 36.05	60.03%	46.44 ± 27.07	58.29%	-22.67%	.378		-	-
Parallel 3 Element										
$E_{(a)}$	kPa	304.67 ± 161.30	52.94%	304.77 ± 57.27	18.79%	0.03%	.230		.998	.000
$E_{(b)}$	kPa	24.23 ± 42.11	173.82%	31.60 ± 46.06	145.76%	30.44%	.447		.647	.214
ε	(-)	0.22 ± 0.59	274.47%	-0.09 ± 0.61	-643.96%	-143.79%	.258		-	-
V	kPa/s	31.36 ± 155.95	497.33%	89.32 ± 68.59	76.80%	184.84%	ǂ .085		.221	1.565
Non-Newtonian Non-Hookean										
$E_{(a)}$	kPa	317.00 ± 125.01	39.43%	379.38 ± 117.06	30.85%	19.68%	ǂ .093		-	-
$E_{(b)}$	kPa	42.95 ± 36.94	85.99%	46.30 ± 34.91	75.39%	7.79%	.603		-	-
ε	(-)	0.16 ± 0.73	449.36%	-0.10 ± 0.46	-482.08%	-158.88%	.118		-	-
V	kPa/s	59.36 ± 37.40	63.00%	44.82 ± 28.91	64.51%	-24.50%	.307		-	-

Gait-Sim Condition

Parameter	Units	Young Mean ± SD	CoV	Elderly Mean ± SD	CoV	Difference	Mann-Whitney asymp. *p*		Anova *p*	Anova F
Curve Characteristics										
Stress Max	kPa	138.76 ± 80.73	58.18%	178.83 ± 95.73	53.53%	28.88%	.236		.196	1.755
Strain at Stress Max	(-)	0.29 ± 0.04	12.28%	0.30 ± 0.04	13.28%	5.31%	.368		.286	1.186
Compressibility	(-)	0.37 ± 0.04	10.05%	0.38 ± 0.04	10.25%	4.57%	.254		.247	1.401
Energy Dissipation										
Percentage Energy Loss	%	56.21 ± 10.66	18.97%	55.68 ± 7.35	13.21%	-0.95%	.725		.879	.024
Energy Loss	J/m^3	20.19 ± 11.10	54.96%	26.04 ± 15.06	57.86%	28.97%	.313		.239	1.449
Stress-Strain Characteristics										
Secant	kPa	483.81 ± 283.90	58.68%	603.62 ± 335.47	55.58%	24.76%	.357		.273	1.250
K1	kPa	742.44 ± 415.57	55.97%	822.54 ± 404.87	49.22%	10.79%	.511		.491	.489
K2	kPa	434.53 ± 327.63	75.40%	578.15 ± 410.54	71.01%	33.05%	.254		.303	1.101
K3	kPa	290.82 ± 245.15	84.30%	366.69 ± 214.74	58.56%	26.09%	.136		.194	1.771
Kelvin										
$E_{(a)}$	kPa	296.59 ± 161.43	54.43%	369.08 ± 188.29	51.02%	24.44%	.324		-	-
V	kPa/s	-3.13 ± 2.54	-81.17%	-4.38 ± 4.08	-93.12%	39.97%	.483		-	-
Non-Newtonian										
$E_{(a)}$	kPa	289.74 ± 159.21	54.95%	355.77 ± 175.61	49.36%	22.79%	.273		-	-
V	kPa/s	17.19 ± 14.77	85.93%	24.12 ± 21.72	90.08%	40.32%	.293		-	-
Parallel 3 Element										
$E_{(a)}$	kPa	260.25 ± 85.81	32.97%	307.92 ± 77.77	25.26%	18.32%	ǂ .051		.133	2.405
$E_{(b)}$	kPa	7.73 ± 38.13	493.20%	6.20 ± 41.87	675.42%	-19.81%	.965		.919	.011
ε	(-)	0.19 ± 0.43	222.88%	0.08 ± 0.33	415.46%	-58.90%	.569		-	-
V	kPa/s	65.77 ± 72.10	109.63%	62.32 ± 81.13	130.17%	-5.24%	.965		.905	.015
Non-Newtonian Non-Hookean										
$E_{(a)}$	kPa	306.63 ± 134.30	43.80%	346.92 ± 132.97	38.33%	13.14%	.392		-	-
$E_{(b)}$	kPa	8.23 ± 46.58	565.98%	5.98 ± 47.21	788.83%	-27.29%	.965		-	-
ε	(-)	0.15 ± 0.47	305.59%	0.01 ± 0.30	5667.81%	-96.57%	.392		-	-
V	kPa/s	17.04 ± 14.71	86.35%	23.96 ± 21.95	91.61%	40.62%	.283		-	-

Definitions: K(1,2,3) - Viscoelastic Modulus, E(a) - Primary Elastic Modulus, E(b) - Secondary Elastic Modulus, V - Viscosity.
Statistics: SD - Standard Deviation of the Mean, CoV - Coefficient of Variation of the Mean, * denotes a p-value<0.05; ǂ denotes a p-value < 0.1

Table B.4.4: Observed Gender difference for each compressive rate

T-Wave Condition

Parameter	Units	Male Mean ± SD	CoV	Female Mean ± SD	CoV	Difference	Mann-Whitney asymp. *p*	Anova *p*	Anova F
Curve Characteristics									
Stress Max	kPa	120.90 ± 40.51	33.50%	132.75 ± 64.47	48.57%	9.80%	.773	.767	.090
Strain at Stress Max	(-)	0.36 ± 0.05	14.20%	0.34 ± 0.04	13.11%	-5.27%	.156	.298	1.125
Compressibility	(-)	0.37 ± 0.05	14.17%	0.35 ± 0.05	13.38%	-4.63%	.268	.366	.845
Energy Dissipation									
Percentage Energy Loss	%	26.27 ± 7.49	28.51%	28.78 ± 9.87	34.30%	9.57%	.486	.468	.542
Energy Loss	J/m^3	4.65 ± 2.21	47.61%	5.17 ± 3.87	74.96%	11.09%	.889	.919	.011
Stress-Strain Characteristics									
Secant	kPa	330.33 ± 117.25	35.49%	380.76 ± 170.39	44.75%	15.27%	.376	.498	.471
K1	kPa	180.43 ± 99.65	55.23%	229.48 ± 137.66	59.99%	27.19%	.452	.302	1.108
K2	kPa	252.33 ± 94.57	37.48%	280.27 ± 133.54	47.65%	11.07%	.740	.734	.118
K3	kPa	493.83 ± 162.16	32.84%	541.12 ± 233.88	43.22%	9.57%	.894	.629	.239
Kelvin									
$E_{(a)}$	kPa	278.08 ± 124.72	44.85%	312.03 ± 168.16	53.89%	12.21%	.642	-	-
V	kPa/s	-1.58 ± 2.31	-146.08%	-1.46 ± 2.36	-160.90%	-7.38%	.626	-	-
Non-Newtonian									
$E_{(a)}$	kPa	278.08 ± 124.72	44.85%	312.09 ± 168.18	53.89%	12.23%	.642	-	-
V	kPa/s	7.95 ± 7.43	93.57%	6.40 ± 9.58	149.66%	-19.45%	.250	-	-
Parallel 3 Element									
$E_{(a)}$	kPa	260.08 ± 79.03	30.39%	257.12 ± 81.17	31.57%	-1.14%	.842	.857	.033
$E_{(b)}$	kPa	8.80 ± 39.11	444.64%	14.73 ± 33.96	230.49%	67.51%	.565	.667	.190
ε	(-)	0.05 ± 1.09	2253.89%	-0.04 ± 0.65	-1509.46%	-188.83%	.965	.779	.080
V	kPa/s	46.97 ± 59.70	127.10%	75.53 ± 59.64	78.97%	60.81%	.308	.215	1.612
Non-Newtonian Non-Hookean									
$E_{(a)}$	kPa	285.17 ± 86.99	30.50%	314.41 ± 119.85	38.12%	10.26%	.611	-	-
$E_{(b)}$	kPa	30.88 ± 45.36	146.91%	32.99 ± 43.72	132.53%	6.84%	.894	-	-
ε	(-)	0.23 ± 0.65	281.49%	0.14 ± 0.63	435.55%	-36.88%	.859	-	-
V	kPa/s	7.86 ± 7.71	98.19%	5.90 ± 9.99	169.29%	-24.86%	.250	-	-

S-Wave Condition

Parameter	Units	Male Mean ± SD	CoV	Female Mean ± SD	CoV	Difference	Mann-Whitney asymp. *p*	Anova *p*	Anova F
Curve Characteristics									
Stress Max	kPa	140.83 ± 60.31	42.83%	158.39 ± 81.49	51.45%	12.47%	.441	.790	.072
Strain at Stress Max	(-)	0.33 ± 0.05	15.15%	0.31 ± 0.06	18.06%	-7.20%	.192	.220	1.569
Compressibility	(-)	0.35 ± 0.05	13.66%	0.32 ± 0.05	16.57%	-6.99%	.143	.193	1.775
Energy Dissipation									
Percentage Energy Loss	%	58.98 ± 8.14	13.81%	60.05 ± 9.45	15.73%	1.82%	.570	.745	.108
Energy Loss	J/m^3	15.08 ± 6.58	43.64%	15.89 ± 9.32	58.66%	5.33%	1.000	.763	.093
Stress-Strain Characteristics									
Secant	kPa	421.67 ± 165.44	39.23%	527.31 ± 309.25	58.65%	25.05%	.635	.504	.457
K1	kPa	330.93 ± 183.88	55.56%	552.17 ± 435.99	78.96%	66.85%	.178 ǂ	.081	3.279
K2	kPa	345.47 ± 131.85	38.17%	403.78 ± 190.98	47.30%	16.88%	.323	.497	.473
K3	kPa	460.47 ± 252.02	54.73%	463.25 ± 220.57	47.61%	0.60%	.693	.927	.008
Kelvin									
$E_{(a)}$	kPa	327.47 ± 127.69	38.99%	458.78 ± 332.16	72.40%	40.10%	.580	-	-
V	kPa/s	-12.40 ± 6.14	-49.47%	-6.20 ± 5.57	-89.87%	-49.98%	* .007	-	-
Non-Newtonian									
$E_{(a)}$	kPa	327.13 ± 127.65	39.02%	457.53 ± 330.09	72.15%	39.86%	.580	-	-
V	kPa/s	68.13 ± 34.95	51.30%	41.43 ± 25.39	61.28%	-39.19%	* .033	-	-
Parallel 3 Element									
$E_{(a)}$	kPa	286.13 ± 51.86	18.12%	322.13 ± 170.09	52.80%	12.58%	.921	.933	.007
$E_{(b)}$	kPa	14.73 ± 46.62	316.44%	39.11 ± 37.39	95.60%	165.48%	ǂ .097	.118	2.596
ε	(-)	0.19 ± 0.60	311.44%	-0.03 ± 0.62	-2060.38%	-115.58%	.481	.325	1.002
V	kPa/s	67.78 ± 88.65	130.79%	44.30 ± 159.36	359.74%	-34.64%	.813	.619	.252
Non-Newtonian Non-Hookean									
$E_{(a)}$	kPa	327.67 ± 124.98	38.14%	357.69 ± 124.85	34.90%	9.16%	.304	-	-
$E_{(b)}$	kPa	40.52 ± 37.63	92.86%	47.95 ± 34.30	71.54%	18.32%	.323	-	-
ε	(-)	0.19 ± 0.50	261.86%	-0.07 ± 0.74	-1027.26%	-138.08%	.304	-	-
V	kPa/s	67.99 ± 35.54	52.28%	39.46 ± 27.59	69.92%	-41.97%	* .031	-	-

Gait-Sim Condition

Parameter	Units	Male Mean ± SD	CoV	Female Mean ± SD	CoV	Difference	Mann-Whitney asymp. *p*	Anova *p*	Anova F
Curve Characteristics									
Stress Max	kPa	138.77 ± 89.92	64.80%	169.40 ± 87.93	51.91%	22.08%	.199	.253	1.362
Strain at Stress Max	(-)	0.29 ± 0.03	10.57%	0.30 ± 0.04	14.12%	4.21%	.478	.404	.719
Compressibility	(-)	0.37 ± 0.04	9.62%	0.38 ± 0.04	10.83%	1.70%	.808	.670	.186
Energy Dissipation									
Percentage Energy Loss	%	55.67 ± 9.86	17.71%	56.19 ± 8.96	15.95%	0.94%	1.000	.883	.022
Energy Loss	J/m^3	19.10 ± 10.33	54.11%	25.43 ± 14.49	56.97%	33.18%	.184	.222	1.561
Stress-Strain Characteristics									
Secant	kPa	481.83 ± 309.30	64.19%	576.82 ± 310.90	53.90%	19.71%	.268	.347	.917
K1	kPa	676.17 ± 352.13	52.08%	850.47 ± 434.87	51.13%	25.78%	.250	.262	1.315
K2	kPa	440.58 ± 380.89	86.45%	540.09 ± 363.58	67.32%	22.59%	.184	.290	1.166
K3	kPa	317.25 ± 285.93	90.13%	330.18 ± 192.95	58.44%	4.08%	.232	.454	.578
Kelvin									
$E_{(a)}$	kPa	297.58 ± 173.83	58.41%	351.32 ± 177.01	50.38%	18.06%	.413	-	-
V	kPa/s	-2.82 ± 2.53	-89.75%	-4.30 ± 3.72	-86.51%	52.42%	.215	-	-
Non-Newtonian									
$E_{(a)}$	kPa	290.67 ± 172.33	59.29%	339.58 ± 165.47	48.73%	16.83%	.376	-	-
V	kPa/s	17.07 ± 15.93	93.34%	22.57 ± 19.80	87.74%	32.20%	.268	-	-
Parallel 3 Element									
$E_{(a)}$	kPa	273.75 ± 88.57	32.35%	287.18 ± 83.57	29.10%	4.90%	.658	.652	.208
$E_{(b)}$	kPa	-1.92 ± 42.70	-2222.78%	13.37 ± 36.37	271.97%	-796.17%	.268	.308	1.078
ε	(-)	0.10 ± 0.40	399.77%	0.17 ± 0.39	225.05%	73.86%	.565	.624	.246
V	kPa/s	44.27 ± 83.95	189.66%	78.31 ± 66.78	85.28%	76.91%	.250	.235	1.479
Non-Newtonian Non-Hookean									
$E_{(a)}$	kPa	301.25 ± 147.59	48.99%	341.24 ± 123.36	36.15%	13.27%	.298	-	-
$E_{(b)}$	kPa	-1.47 ± 57.59	-3926.38%	13.36 ± 36.49	273.15%	-1010.77%	.452	-	-
ε	(-)	0.04 ± 0.36	823.73%	0.12 ± 0.43	371.10%	165.67%	.773	-	-
V	kPa/s	17.04 ± 15.89	93.25%	22.33 ± 20.00	89.55%	31.04%	.288	-	-

Definitions: K(1,2,3) - Viscoelastic Modulus, E(a) - Primary Elastic Modulus, E(b) - Secondary Elastic Modulus, V - Viscosity.
Statistics: SD - Standard Deviation of the Mean, CoV - Coefficient of Variation of the Mean, * denotes a p-value<0.05; ǂ denotes a p-value < 0.1

B.5. Discussion & Conclusions

B.5.1 Introduction

The plantar soft tissue mechanical properties have been effectively characterised to assess variance within the tissue, due to the applied loading rate and between populations, due to the effects of age and gender. Large inter-subject variation has been observed within the mechanical properties derived directly from the loading curves. This highlights the sensitivity of these measures to the applied peak stress and strain. However the variation was consistent across the range of loading rates. This suggests an inherent inter-subject variation may occur for the plantar soft tissue.

B.5.2 Measured Tissue Properties

B.5.2.1. Tissue Compressibility

Although a target of 40% tissue compression was used in this study, in many cases the tissue became incompressible at thicknesses lower than this target (33-38%). Due to the low RMS error observed for tissue strain at both low and high displacement rates in this study (Section A.6.4), the under-compression of the tissue observed here is expected to be the result of external factors such as compliance within the bracing. The reported range of tissue compressibility in the literature is large (12% - 60%) and varies greatly with the test methods used (Figure B.5.1). For in-vivo methods, manual indentation studies have displayed a range of 12-50% (Erdemir *et al.* 2006, Zheng *et al.* 2012a), bulk compression studies have shown a range of 35-38% (Tong 2003, Uzel *et al.* 2006), whilst in-gait studies have displayed a range of 35%-60% compressibility (De Clercq 1994, Gefen *et al.* 2001). The target strain of 0.4 was selected as it sat within this range of previous methods and could be achieved easily when the initial assessment of the foot was conducted. The main difference between the initial assessment and the compression testing was the platen size. For the initial assessment, the

probe was used and permitted indentation with a surface area of 5cmx1cm, whereas in the compression tests the STRIDE platen was used and permitted only bulk compression of the tissue. Thus it is expected that the use of a bulk compression method in this study restricts the total tissue compression that can be achieved. Therefore, to prevent over-compression of the tissue, a compression target of 35% should be used for bulk compression studies of this nature.

B.5.2.2. Measures of Tissue Modulus

B.5.2.2.1. Secant Modulus

The secant modulus is highly dependent on both peak stress and the strain at peak stress. In this study the measurements for stress and strain have displayed low standard deviations for the region of peak compression (Section A.6.4) and the derived values have been shown to be consistent when tested within subjects (Section B.2.3.1). However, valid comparisons can only be made between subjects when the applied peak stress and strains are within similar ranges. As noted previously, the compressibility of tissues when tested with indentation methods is generally larger. These methods also tend to apply low loads due to manual load application. As a result, the secant modulus values derived from manual indentation methods are generally low (Figure B.5.1): 104.33kPa – 221kPa, (Hsu, Wang, *et al.* 1998, Hsu *et al.* 2009). In-gait methods use bulk compression of the tissue and body weight loads; thus peak stress and peak strain are within a similar range to those observed in this study (Figure B.5.1). Wearing (2009) reports a secant modulus of 580kPa during normal walking, this value is within one standard deviation of both the Gait-Sim (538kPa) and S-Wave (476kPa) values recorded in this study. This suggests that the basic loading conditions of gait (peak stress & peak strain) can be achieved using an imposed compression with only displacement and velocity control.

B.5.2.2.2. Effective Viscoelastic Modulus

The plantar soft tissue has been shown to exhibit a non-linear response to load for a range of test methods (Rome 1998). It is generally reported that the tissue exhibits an initial low gradient region over which large strain can be achieved with minimal force application. Following this, a period of increasing gradient occurs as the tissue nears incompressibility (De

Clercq 1994, Gefen *et al.* 2001, Klaesner 2002, Tong 2003, Zheng *et al.* 2012b). This study has displayed three distinct patterns of loading. At low displacement rates (T-Wave), the expected response is observed with an initial low gradient/high compliance followed by an increasing trend. For the low rate profile, the stress and strain measurements showed low standard deviations throughout loading (Section A.6), and the viscoelastic modulus were consistent when tested within individuals (Section B.2.3.1). At medium displacement rates (S-Wave), an initially moderate gradient is seen, followed by a reduced gradient/levelling-off and finally an increasing trend to peak compression. This medium rate response has also previously been observed for pendulum and in-gait studies and has been linked to the increased percentage energy loss and energy loss recorded by these methods (Alcántara 2002, Wearing *et al.* 2009). For the high rate profile, the stress and strain measurements showed initially high standard deviations, suggesting a low validity of the initial response; however throughout the remainder of the loading curve the variation was consistently low (Section A.6). The viscoelastic modulus displayed large variations within subjects, suggesting a low reliability of these direct curve measures (Section B.2.3.1). The observed curve for the high rate condition has an initially high gradient, which is followed by a gradually reducing gradient to peak load. This high rate response has not been previously reported and may be caused by the increased level of constraint used on the foot in this study compared to the previous high rate techniques such as in-gait and pendulum methods. The fixing of the foot and lower leg in this study focuses compression on a single region; a more dynamic foot may permit transfer of load to be distributed throughout the whole tissue more uniformly, reducing the demand borne by the tissue.

B.5.2.2.3. Model Parameters

The most robust model assessed in this study was the Parallel Three Element model which gave an initial elastic response in the range 7 – 27kPa, a primary elastic modulus in the range 258-304kPa (Figure B.5.1), and a viscosity in the range 55-64kPa. Although this model did display a trend to increased modulus values with increased displacement velocity, the difference was found to be significant only for the primary elastic modulus between the T-Wave and S-Wave conditions ($p<0.05$ assessed by mann-whitney), and thus can be said to be the most stable across the range of test methods. The Parallel Three Element model has previously only been applied to the plantar soft tissue by an indenter system with

force/displacement measurements and no normalisation to tissue stress or strain (Klaesner 2002); thus no direct comparisons can be made to this study. Other studies which utilised modelling have reported a range of moduli, A study which used the Quasi-Linear Viscoelastic Theory was conducted in vitro (Ledoux 2007), and reported high values for the elastic modulus when tested at moderate to fast rates of compression (Figure B.5.1). However, for all tests conducted in Ledoux's study the stress did not begin to increase until a strain of approximately 0.2; thus no initial viscous response was noted at any velocity (peak approx. 0.6m/s). The lack of a viscous response suggests that the sectioning techniques, using cylindrically cut core samples, may have disrupted the ordered arrangement of chambers and resulted in an altered response to compression. Gefen (2001) reports an elastic modulus of 175kPa and a viscosity of 22kPa from in gait studies using the Non-Newtonian model (Figure B.5.1). In this study, the Non-Newtonian model was less stable than the Parallel Three Element model, but under gait-like conditions both the non-newtonian and the parallel models gave similar results to Gefen's paper with elastic moduli of 324 and319kPa respectively and a viscosity of 20 and 64kPa/s respectively. The discrepancy between this study and the values reported by Gefen may be due to a combination of the reduced compression rate used in Gefen's study and the high inter-subject variance observed in this study in conjunction with the low subject numbers (n=2) in Gefen's study.

B.5.2.3. Percentage Energy Loss and Energy Loss

The values for energy loss and percentage energy loss displayed moderate within subject variance at both low and high displacement rates (Section B.2.3.1), suggesting a high sensitivity to the loading conditions. The values of percentage energy loss observed in this study when tested at low displacement rates (27.71%) matched well to previous low displacement rate studies in-vivo, which ranged from 20.7% to 35.3% (Hsu, Wang, *et al.* 1998, Wang *et al.* 1999, T.-C. Hsu, C.-L. Wang, Y.-W. Shau, F.-T. Tang, K.-L. Li, *et al.* 2000a) (Figure B.5.1), and also to tests conducted at low displacement rates in-vitro which ranged from 28.6% - 40% (Bennett and Ker 1990, Ker 1996, Ledoux 2007) (Figure B.5.1). The results of experiments which tested the plantar soft tissue at higher rates of compression varied greatly between studies both within and between different experimental techniques. In-vitro studies have previously reported both low (27%) and high percentage energy loss values (65%; 63.3%) when tested using materials testing machines at high frequencies (Bennett and

Ker 1990, Ledoux 2007, Pai and Ledoux 2010). Pendulum studies suggested generally high percentage energy loss values (Figure B.5.1); however values among studies ranged from 51% to 90%, dependent on test rates, the contact area of the pendulum and the bracing of the subject (Frederick 1984, Cavanagh 1999, Pain 2001). The previous in-Gait studies have also reported large differences and contrasting values, with Wearing (2009) stating a percentage energy loss of 69% while Gefen (2001) reported only 17.8% during walking however much different impact velocities were reported in these studies (Figure B.5.1). In many cases, this range of values has been attributed to the 'lower leg effect', in which the inclusion of compression/energy dissipation within other structures of the lower leg adds to the measured energy loss; therefore an inflated result is observed (Aerts *et al.* 1995, Pain 2001). It is likely that this is the case in pendulum studies where the motion of the pendulum mass is used to define tissue compression and any movement of the leg is therefore incorporated into the result. However, for techniques which measure the true tissue strain (CT, X-Ray, Ultrasound), as used by Gefen, Wearing and this study, the compression within the other lower leg tissues is not included, and thus these methods represent the tissue-specific response to load. The results of this study at medium rates (59.50%) and high displacement rates (55.97%) are similar to Wearing's in-gait results; however they show a large difference from Gefen's data. The discrepancy between this study and Gefen's results may be related to the reduced walking speed and reduced peak stress used in Gefen's study, which is likely to reduce the demand placed onto the tissue.

Values for the energy loss (J/m^3) are not detailed in the literature with the percentage energy loss more commonly used as it provides a normalised value, which is easier for comparison between studies with different test methodologies. It is however useful to provide context for the percentage energy loss values and give an indication of the true capacity for energy loss within the tissue. When comparing values recorded at low displacement rates to those at medium and high displacement rates, both increased percentage energy loss and increased absolute energy loss are observed. This suggests the tissue behaves as a typical viscoelastic material, providing a greater capacity for energy loss at higher rates of compression (Ennos 2011). However, when comparing the values from the medium rate condition to those of the high rate condition, a small reduction in percentage energy loss is present, while an increased absolute energy loss occurs. Although the tissue maintains its ability to dissipate a greater absolute amount of energy at higher displacement rates, the efficacy of this function has reached a plateau. It is possible that this reduced performance at high rates compared to

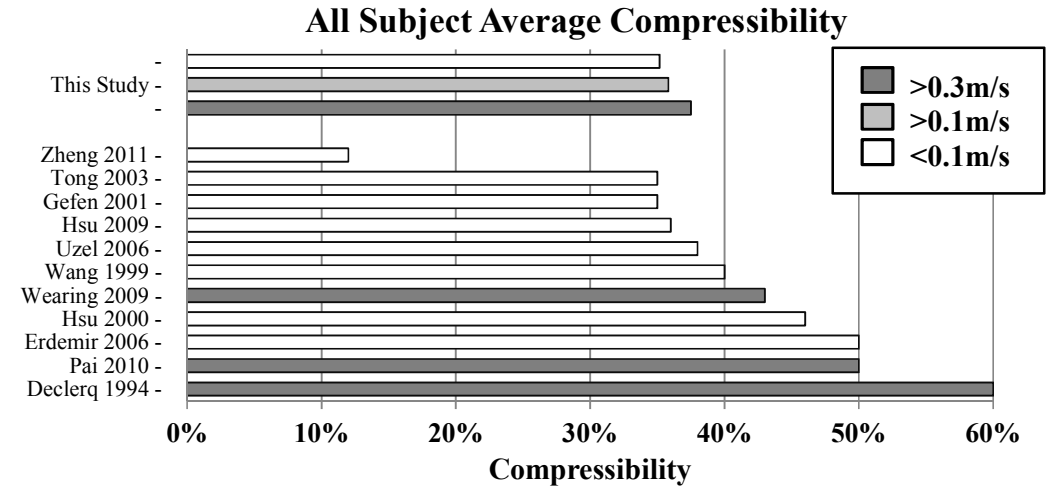

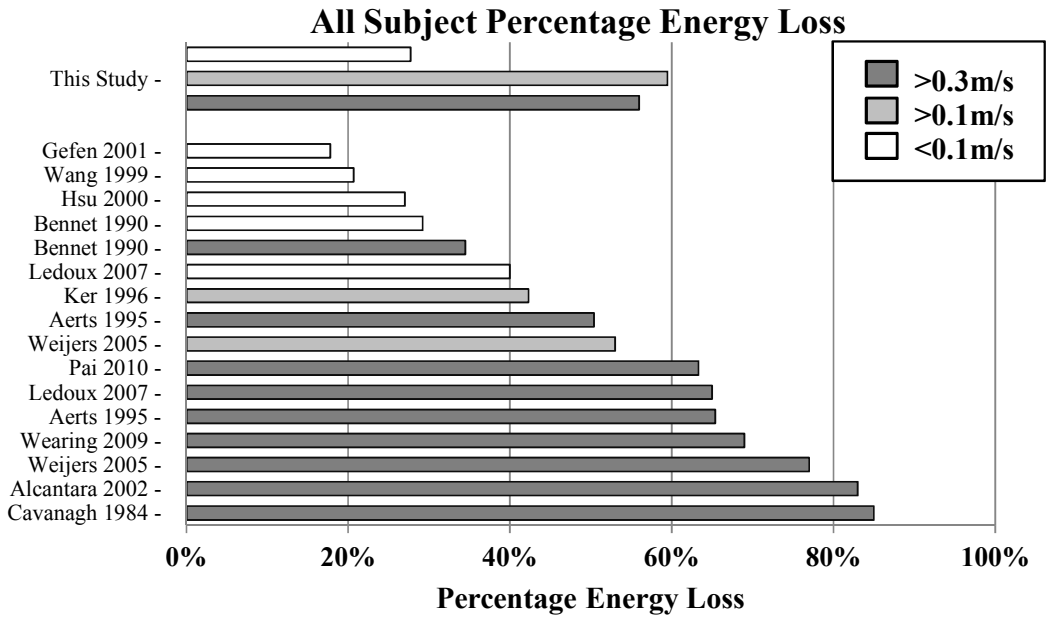

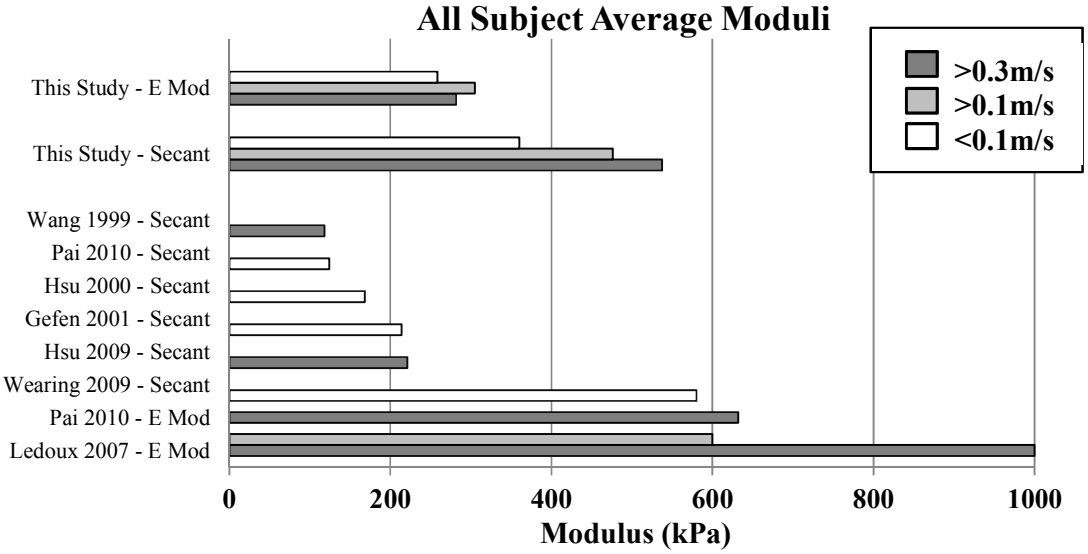

Figure B.5.1 Comparative Results Graphs for Energy Loss, Compressibility and Modulus Values

moderate rates is due to the period of rest between tissue compressions (Aerts *et al.* 1995, Ker 1996). With a rest time of 1s in the S-Wave condition and only 0.5s between compressions for the Gait simulation condition, full relaxation of the tissue may not occur during the gait simulation tests, resulting in a reduced capacity on subsequent cycles, and thus leading to a perceived loss of functionality (Aerts *et al.* 1995, Ker 1996). Although the gait simulation condition is based on a typical cycle time for normal walking, it is possible that over a prolonged period of walking an individual may adjust their gait-cycle time to permit more effective tissue recovery between compressions.

B.5.3 Differences with Rate of Compression

Many of the stress-strain characteristics derived in this study were significantly affected by changes to the applied displacement rate and loading type. Thus it is possible to accept the hypothesis that the rate of compression will affect the response of the plantar soft tissue when tested in-vivo using controlled bulk compression. The literature has shown significant rate effects on modulus (secant & elastic) and percentage energy loss across a range of loading conditions (Hsu 2005, Weijers 2005, Ledoux 2007); in all previous cases an increased modulus and percentage energy loss was observed with increased rate. This rate-dependent response suggests that the viscous component of the tissue plays a significant role in managing the stress-strain interaction during loading. For this study, the displacement control and feedback mechanisms of the actuator within STRIDE mean that the tissue was compressed as per the input profile (within limits discussed in Section A.6). In this situation, when the tissue is strained at high rates, the viscous response will act to increase the stress required to achieve the input profile, by resisting/dampening the compression (Ennos 2011). This was seen to result in a significantly greater curve gradient initially ($p<0.05$) and a trend toward increased peak stress ($p>0.05$) compared to an equivalent tissue strain conducted at low rates, where less viscous resistance is imposed. The work done by the viscous component to resist the tissue compression is converted into heat via frictional mechanisms which occur within the tissue: bond breaking, shearing and fluid flow (Frost 1971). The result of this is a net loss in the energy returned during unloading of the tissue, which is observed as a

significantly increased energy loss and percentage energy loss (p<0.05) for a viscoelastic soft tissue (Ennos 2011). The low percentage energy loss observed for the T-Wave condition suggests a low involvement of the viscous component, and thus a greater dependence on the elastic component of the tissue at low displacement rates. For this study, the percentage energy loss observed at high rates of compression is lower than that generally reported in the literature for equivalent rates (Figure B.5.1). In this study, the similarity between S-Wave and Gait-sim conditions suggests an upper limit to the capacity of the viscous component, to dampen the compression, has been reached. This upper limit may in part be explained by the much shorter time to peak load for the Gait-Sim condition (0.1s) compared to the S-Wave condition (0.5s). However the generally reduced capacity compared to previous high rate studies may be linked to the previous studies inability to isolate specific tissues. In pendulum studies where whole foot/leg motion is measured, and not the specific heel pad tissue compression, the percentage energy loss reported is a composite of multiple dampening components (Pain, 2001) which will act to enhance the capacity to dissipate energy. In gait this inclusion of auxiliary tissues for the dampening of forces at high rates of compression is likely to reduce the risk of damage within individual tissues. The interaction between the rate of compression and the involvement of the elastic or viscous components places emphasis on the need to characterise the response of the plantar soft tissue across a range of loading rates, and suggests that care should be taken when inferring the effect of differences measured outside of the functionally relevant range.

B.5.4 Differences with Age

The results of this study suggest that, subject age does not affect the mechanical properties of the plantar soft tissue and thus the previously stated hypothesis is unlikely to be true. However large between group differences were observed in this study, and align with previous studies, linking the known structural changes, which occur with age to changes in mechanical properties, when measured at low rates of compression (Hsu 2002, Kwan *et al.* 2010). Throughout aging, the regular structure becomes disrupted as glycation causes the formation of cross links and collagen bundles (Brash *et al.* 1999). The cross-links act to resist

the normal expansion of the macrochambers under compression, causing the pressure within the chambers to increase which in turn acts to restrict tissue compression. This increased pressure will also result in stress concentrations at the cross links, making them susceptible to damage and breakdown, and eventually leading to the formation of micro-tears within the tissue (Kwan *et al.* 2010). These changes are focused on the elastic components of the tissue (septal walls) and thus the properties related to this component are expected to be effected the most. In this study increases were found in the modulus values (Secant, Effective Viscoelastic and Elastic Modulus) for the elderly group, suggesting some structural changes may have occurred to affect the elastic component. However based on the assessment of variance with rate the response of the tissue at high rates is expected to be governed by the viscous component. Thus the previously noted structural changes to the elastic components will have less influence on the tissues response during compression at rates equivalent to normal gait. The percentage energy loss was not found to differ with age in this study for any of the rates of compression used. The high rate results also reflect a previous pendulum based study which assessed the effect of age (Alcántara 2002) in which no difference was observed. This suggests that the viscous response maintains its normal rate dependent nature in the elderly group, i.e. a greater viscous response is observed at higher rates of compression. However the absolute energy loss was shown to display a large, yet non-significant (p>0.05), increase in the elderly group (+30-50%) across all rates of compression, suggesting that the level of viscous activity occurring has increased. As increased energy dissipation is related to the function of the viscous component (Vincent 1992), it is expected that the proposed structural changes due to glycation may have also affected the viscous components (adipose tissue), and thus the normal viscous mechanisms. However, structural studies do not currently exist to confirm this potential change in the plantar fatty pad composition with age. The subjects in this study were all healthy individuals within a controlled BMI range; the average age in the elderly group was 61. In previous studies, which, assessed age variance the elderly groups were generally older (group average 65-70), and BMI was not as tightly controlled (Hsu, Wang, C., *et al.* 1998, Alcántara 2002). These differences may explain the less extreme effect of age observed in this study.

B.5.5 Differences with Gender

The results of this study suggest that, subject gender does not affect the mechanical properties of the plantar soft tissue and thus the previous hypothesis is unlikely to be true. The effect of gender has not been considered in many studies within the literature, and thus it is difficult to compare this outcome. However some previous studies have stated a physical difference in the tissue between gender groups based on body build and hormonal variance (Jorgensen and Bojsen-Moller 1989, Rome 1998, Alcántara 2002). Alćantara (2002), who did assess the effect of gender on the mechanical response of the tissue, at high rates of compression, showed a significantly reduced percentage energy loss and final viscoelastic modulus in the female group. This would suggest that the female tissue is generally less viscoelastic and that the hydrostatic response is reduced compared to the male tissue, however neither the magnitude nor the direction of change was found to be similar in this study. No significant differences were established between gender groups in this study, however large differences in the initial viscoelastic modulus and the viscosity parameters (±15%), suggest a potential variance in the initial viscous response of the tissue. Due to the high between subject variability within this study it has been difficult to isolate the true root of the difference between genders. For a greater understanding of this difference, a larger pool of subjects should be used with a focus on the viscous and elastic components.

B.5.6 Interaction of Rate and Subject Group

In this study no interactions were observed between subject groups (age or gender) and rate of compression used during tests. Thus we can accept the original null hypothesis. This suggests that the rate dependent nature of the tissue is maintained across all subject groups despite the potential structural changes to the plantar soft tissue.

B.5.7 Limitations and Future Work

Limitations exist within aspects of the device setup and operation for the current protocol. Increases in temperature within the plantar soft tissue have been shown to affect the measured percentage energy loss as a result of changes to the liquid state of the viscous component (Bennett and Ker 1990). Although temperature was not controlled in this study, all testing was conducted in the same lab environment, which had a regular room temperature of 23^{o}C. It is possible that the temperature of the foot may have fluctuated due to the heat production in the viscous response of the tissue, the constant blood flow (which provides a source of heat) and the brace system which may act to insulate the foot and permit the tissues temperature to increase during the dynamic tests. Future examinations of the soft tissue properties should aim to monitor and control the variation of the tissue temperature throughout testing.

The target strain was not achieved during the dynamic tests due to a lower dynamic compressibility than static compressibility. As a result, all subjects were assessed to their peak compression; however a standard peak strain was not applied for all subjects. Error in peak strain has been shown to have a significant effect on peak stress and thus curve-based parameters (Pai and Ledoux 2010). Further testing should aim to achieve a constant peak strain during dynamic testing.

The initial tissue response could not always be measured due to a large presence of noise within the ultrasound images. As a result, the feature of interest could not always be identified from the instant of contact with the tissue, and thus no data for the initial compression were present in some cases. This issue had a greater effect at high rates of compression where initial tissue strain was rapid. The inclusion of a water bag or ultrasound spacer has been used at low rates of compression to reduce this effect, by providing a constant image of the region both before and after tissue compression (Hsu 2007). Future testing of the plantar soft tissue with ultrasound should aim to capture the full response within the tissue.

Limitations are also present within the analysis methods used to derive the plantar soft tissue properties. For this study a single layer approach has been taken, assuming that the skin, microchambers and macrochambers respond as a single homogenous layer. Previous in-vivo studies have shown that this assumption is not valid (Hsu 2007), with the microchamber layer acting as a stiff supporting layer to the highly compressible macrochamber layer. Challenges

within the ultrasound feature tracking prevented this level of detail within the current study. However, it is expected that the inclusion of a multilayered approach to the examination of the heel pad properties would provide a clearer understanding of the functional responses within the tissue.

The testing in this study was restricted to the response of the tissue along the vertical axis for the single point of the calcaneal apex. This provides a simplified representation of a tissue which is both dynamic in shape (bulging, shearing) and in function (gait roll over). Within the current dataset, it may be possible to examine the response of the tissue at points medial or lateral to the apex and also medial and lateral motion (bulging) of the tissue via speckle tracking. However this level of detailed processing was beyond the scope of this study.

The temporal resolution of the ultrasound system (201Hz) had some limitations when the tissue was tested at high rates of compression. The low number of data points provided to characterise the tissue's response to loading at high displacement rates (5-10) created potentially ambiguous regions in which the true response could not be measured. Future examination of the tissue at high rates of compression requires a system with a minimum capture rate of 1000Hz, which would provide approximately 50 data points to describe the loading response.

B.5.8 Conclusions

The variance in mechanical properties, observed with the rate of compression, suggests there is an interaction of two mechanisms, which govern the response of the plantar soft tissue.

Mechanism A is governed by the elastic components of the tissue structure; the collagen and elastin fibres in the chamber walls. An initially low effective viscoelastic modulus is present as the chambers are compressed and the fibres are stretched. When the compliance within the fibres is exhausted, tension within the chamber walls will increase as the internal pressure of the chamber increases, resulting in a hydrostatic response, and a high final viscoelastic modulus.

Mechanism B is governed by the viscous component of the tissue; the adipose held within the chambers. This component has a highly rate-dependent response; at low rates of compression it is passive permitting Mechanism A to control the tissue response, however at high rates it is dominant and controls the tissue's response. When high rates of compression are applied, the viscous component works to resist compression by converting energy into heat and dampening the high compressive forces. When the fibres of the chamber walls have reached their tensile capacity, the hydrostatic response observed in Mechanism A becomes dominant, preventing over-compression of the tissue.

No significant differences were observed with age in this cohort, however large between groups differences align with previous changes due to aging. The changes observed suggest that both the elastic and viscous components of the tissue may have been affected by the negative cumulative effects of glycation. No significant differences were observed for the mechanical properties between gender groups however a slight variance was observed for the initial compressive response.

This complex interaction of elastic and viscous components is the key to understanding the function of the plantar soft tissue. Future work should aim to understand the true nature of the structures which underpin these mechanisms, and test the limits for which these mechanisms are effective.

Overall Conclusions

The work within this PhD details both the development and evaluation of a novel device and the implementation of that device to characterise the mechanical response of the plantar soft tissue.

The development component of this study brought together techniques from previous studies to produce a highly adaptable mechanism for the characterisation of the plantar soft tissue. A bespoke device was designed which permitted bulk compression of the plantar soft tissue, at a variety of compression rates, in combination with region-specific load and tissue thickness measurement. Loading profiles were developed to permit the testing to be conducted for the full compressive range of the plantar soft tissue. Limitations existed within some aspects of the design; however the device was shown to be capable of highly repeatable device motion and provided a good between cycle reliability of measured tissue stress and strain.

The implementation component of this study acted both as a proof of principle for the developed device and to highlight the rate-dependent nature of the plantar soft tissue. A large between-subject variance was present for the derived mechanical properties in this study, which could be a result of limitations within the device operation. Changes to the applied loading rate were found to have a significant effect on many of the derived mechanical properties, and it is suggested that a range of loading rates should be used when testing the plantar soft tissue. Within the cohort tested for this study, despite large between groups differences, no significant differences were found due to age or gender effects. It is expected that an increased subject number and increased upper age limit would allow clearer conclusions to be drawn.

Original Contributions

The novel work within this PhD can be summarised as:

- The development of a bespoke device to characterise the plantar soft tissue, for a wide and adaptable range of loading routines.
- The development of a Gait Simulation profile to assess the response of the plantar soft tissue to cyclic loading akin to normal walking.
- A comprehensive data set, detailing the response of the plantar soft tissue to a range of loading routines and the differences observed between age and population groups, derived by both direct curve characterisation and mechanical modelling approaches.

Future Work

The future work will aim to address the limitations highlighted in the discussion and conclusion sections of part A and B of the thesis. In addition to this, further possible studies are of two main forms, those which aim to provide a more detailed exploration of the tissue's response and those which aim to apply the novel techniques developed in this work to a wider range of subject populations and tissue types.

To expand on the assessment of the current dataset, a more detailed assessment of the plantar soft tissue structure can conducted by adapting the ultrasound tracking algorithm to identify and track the individual tissue layers throughout compression. To achieve this effectively, a new set of templates would be required which can detect the less clear boundaries present within the soft tissue (Figure A.5.6 in Section A.5.3). Previous studies which have assessed the multi-layered structure have shown clear differences between the mechanical properties of the Macrochamber and Microchamber layers at the heel, suggesting that each layer exhibits a functionally specific role during normal gait (C.-C. Hsu, W.-C. Tsai, C.-L. Wang, S.-H. Pao, Y.-W. Shau, *et al.* 2007). The tissue layers have also been shown to display specific

differences between populations (Healthy/Diabetes, Hsu, 2009), therefore it is likely that any age or gender differences observed for the whole tissue in this study will become clearer when assessed for individual layers.

Further investigation of the elastic and viscous constituents of the plantar soft tissue will also enhance the understanding of the current dataset and the validity of conclusions drawn from it. Although the parallel three element model used in this study was shown to perform well across all rates, the RMS error reported between the model data and the raw dataset was high. A wider assessment of appropriate viscoelastic models or the development and adaptation of the current models will allow a more effective characterisation of the plantar soft tissue response. Once an effective model has been established, the level of control required within the testing device can be reduced; permitting the plantar soft tissue properties to be derived using simple and quick tests which are more suitable for use in a clinical setting (Klaesner 2002).

To enhance the validity of the gait simulation generated by STRIDE, the use of shear and compression together should be introduced. This would aim to replicate the natural anterior-posterior or medio-lateral dynamics of the foot in synchronisation with the vertical tissue compression. This could be achieved by actuating the subject brace system, such that the foot is moved during tissue compression. Effective shear measurement has previously been shown in-vivo using a shaker plate; an increased shear modulus was reported for the tissue under the calcaneal apex compared to a control site at the lateral border of the heel, suggesting a variable shear response within the tissue (Weaver *et al.* 2006).

The inclusion of an assessment of the effects of age on the tissue properties across a wider range of plantar soft tissue regions (MTHs, Hallux), would provide a greater understanding of how the full functional response of the tissue is affected in the elderly. Considering the vastly different roles of the rearfoot (impact) and the forefoot (pushoff) during normal walking, it is expected that a systemic change in tissue structure due to age may have a varied impact on the response of these tissues to the different dynamics of loading. To study this effect, it is necessary to develop and validate at forefoot simulation profile and implement a protocol for the forefoot which assesses the tissue across the full functional range. Forefoot dynamics were assessed when the specification of the device was conducted to ensure the device would be capable of implementing a forefoot gait simulation profile.

Biological tissue has been shown to exhibit an adaptive nature, with a moderate level of stress required to maintain the normal functional structure and increased or decreased stress resulting in hypertrophy or atrophy of the tissue's structure (Mueller and Maluf 2002). Previous studies have shown this potential for tissue adaptation, with runners (rear-foot loading) displaying a reduced stiffness compared to cyclists (forefoot loading) when measured at low rates of compression (Challis 2008). Additionally, previous in-vivo studies have shown sedentary lifestyles, and the associated increased BMI, to have a significant effect on the measured tissue response when tested at high rates of compression, with reduced stiffness and increased percentage energy dissipation in subjects who were obese (Alcántara 2002). This suggests potential changes have occurred that affect the viscous component of the plantar soft tissue. To gain a greater understanding of the effect of lifestyle and the extent to which adaption can occur within the plantar soft tissue, a much wider sample which incorporates both a broad range of BMI and of activity levels must be studied using the protocol presented in this thesis. A longitudinal study of novice runners throughout a period of training may also provide insights as to the nature of this potential adaptive response and the impact of tissue change on function and performance.

Diabetes has been shown to cause a large disruption to the normal structure of the plantar soft tissue (Brash *et al.* 1999, Wang *et al.* 2011) and has been shown to result in a significant increase in the stiffness of the tissue at both the heel and forefoot (Hsu 2002, Pai and Ledoux 2010). If pathological populations such as diabetes are tested across the full range of loading conditions, using the protocol established in this study, a pathology specific base line may be established which could be used as an assessment tool or to infer the functionally relevant effects of a pathology when measures are taken at slow rates using clinical devices.

The ability to effectively characterise the plantar soft tissue will benefit both clinical practice and the assessment of athletic performance, with implications on the development of novel interventions tailored to optimise the function of the plantar soft tissue.

Appendix A

Detailed Specifications for Developed Device

Actuator

Use – Provide motion of the platen

Performance (with 3:1 Mechanical Advantage)

Operational Range – displacement 90mm, velocity 2m/s, acceleration 50m/s^2

Loadings – continuous of 400N, peak of 500N

Manufacture

Made in/Buyout – Buy Out

Materials – Metal, Non-Corrosive

Production Time – 6month lead time

Handling

Size – Low vertical profile >0.5m

Installation – Fixable to base plate

Controller

Use – Provide displacement and velocity control over device motion

Performance

Operational Range – Mains single phase supply

Loadings – 13A, 240V

Manufacture

Made in/Buyout – Buy Out

Materials – Metal, Non-Corrosive

Production Time – 6month lead time

Handling

Size – low vertical profile >0.5m

Installation – Fixable to base plate, mounting close to actuator.

Coupling

Use – Provide a mechanical advantage for motion and remove direct loading of actuator

Performance

Operational Range – Vertical Travel: 30mm, Horizontal Travel: 90mm

Loadings – Continuous of 2000N, peak of 3000N

Manufacture

Made in/Buyout – Machine Out, Assemble/Adapt in house

Materials – Hard Metal, Non-Corrosive

Production Time – 3month lead time, 1month assembly and adaptation

Handling

Size –low vertical profile <0.5m

Installation – assembly in workshop

Platen

Use – Provide Bulk compression of tissue in a single plane and permit housing of the tissue measurement and load measurement components

Performance

Loadings – Continuous of 2000N, peak of 3000N

Manufacture

Made in/Buyout – Machine out, Assemble/Adapt in house

Materials – Hard Metal, Non-Corrosive

Production Time – 3month lead time, 1 month assembly and adaptation

Handling

Size – low vertical profile <0.5m

Installation – assembly in workshop

Tissue Measurement Device

Use – Provide accurate measurement of tissue thickness in a single plane

Performance

Operational Range – >30mm depth

Loadings – less than 100N

Manufacture

Made in/Buyout – Buy Out

Materials – Non-Corrosive, Plastic

Production Time – Pre-existing or 1month max

Handling

Size – Probe <0.2m vertical profile

Installation – Clamped within Platen using Bracket

Load Measurement Device

Use – Provide accurate measurement of tissue load during compression

Performance

Operational Range – 0 – 3000N

Loadings – Continuous of 2000N, peak of 3000N

Manufacture

Made in/Buyout – Buy Out

Materials – Metal, Non-Corrosive

Production Time – 1 month lead time

Handling

Size – very small vertical profile, <0.1m

Installation – fixable within platen

Subject Positioning and Bracing

Use – Provide a means to fix the subjects foot to allow repeated loading of a tissue site

Performance

Loadings – Continuous of 2000N, peak of 3000N

Manufacture

Made in/Buyout – Make in

Materials – Hard Wood

Production Time – 1 month production time, 2weeks adaptation

Handling

Size – low vertical profile <0.3m, floor space < 0.5m x 0.5m

Installation – Assembly in workshop

Device Housing

Use – Provide an enclosure to conceal moving elements and protect the subject

Performance

Loadings – Continuous of 2000N, peak of 3000N

Manufacture

Made in/Buyout – Machine out, assemble in house

Materials – Hard Wood

Production Time – 1month lead time, 2 weeks assembly

Handling

Size – subject platform height: 0.5m, floor space 1.5mx1.5m, total height <2m

Installation – Assembly in workshop

Appendix B

Health & Safety Procedures for Device

Policy #:	Title:	Effective Date:
	Operation of Soft Tissue Response Imaging Device (STRIDE)	Dec 2011

TITLE:

Operation of Soft Tissue Response Imaging Device (STRIDE)

PURPOSE:

To ensure safe operation of the STRIDE

PROCEDURE:

General Procedure

- Subjects will be given information regarding the operation of the device and complete an informed consent prior to beginning testing
- Subject is to complete a health questionnaire before testing
    - Should subject answer negatively to any question on the health questionnaire then the subject will not be tested
- Ensure subject has no allergies to ultrasound gel
- Operators must be familiar with HPL8 – good lab practice guidelines
    - Including knowledge of emergency procedures and the raising of alarm (Maxwell Security 53333)
- Subjects will be informed of the emergency and evacuation procedures for the lab prior to testing
- Subjects will be informed of test procedure
    - How the device will operate
    - The position of and use of emergency stops (electrical cut offs)
- Maintain a clear walk way/platform permitting unobstructed bracing of the subject prior to testing
- Check test surface, to ensure no scratches or visible marks are present
- Clean surface after each use, to prevent cross contamination.
    - Clean all contact surfaces
    - Remove all ultrasound gel
- Switch off power to device when adjusting the mechanism
- Test device can move through full operational range without obstruction
- Ensure ultrasound probe cable is untwisted, free from obstruction and of sufficient length to allow movement of the device through the full operational range
- Prior to seating subject ensure;
    - Top plate is locked on
    - Outer housing is in place
    - Device is in neutral position (top plate flush with level of outer housing)
- When bracing foot ensure;
    - Knee is at 90^0 or greater extension
    - Bracing does not constrict subjects foot

- The Operator must be capable of viewing both the image/data collection and the subject/limb motion during testing.
- Minimise the risk of trips and falls by ensuring all cables and trailing wires are taped to the floor or strung up in the roof
    - Cables within the housing must be tied and directed away from the moving parts of the mechanism
- Check electrical emergency cut-off switches (subject and operator controlled cut off) are operating and capable of stopping device during motion.
- Check safety limiters and cut offs prior to testing
    - Displacement limits (mechanical range of device).
    - Velocity limits (imposed via actuator controller).

Actuator Operation

- Run device through full cycle with no subject in bracing to test operational range
- Ensure E-stop Circuit is active and E-sense input is set to disable axis.
- Programme subject specific cut offs into device control mechanism
    - Velocity Maximum
    - Load maximum

RESPONSIBLE DEPARTMENTS:

Directorate of Sport, Exercise & Physiotherapy, School of Health Sciences

PEOPLE AFFECTED:

Researchers from IHSCR, students, staff, visitors

Appendix C

Ethical Approval for Subject Testing

Academic Audit and Governance Committee

Research Ethics Panel
(REP)

THE UNIVERSITY OF SALFORD

MEMORANDUM

To	Daniel Parker
cc:	Professor Chris Nester, Ms Sue Braid
From	Jayne Hunter, Contracts Administrator
Date	26th September 2011

Subject: **Approval of your Project by REP**

Project Title: **The effects of aging on the biomechanical properties of the plantar soft tissue (bottom of the foot)**

REP Reference: **REP10/092**

Following your responses to the Panel's queries, based on the information you provided, I can confirm that they have no objections on ethical grounds to your project on condition that the Health and Safety information which is still outstanding is provided for the Panel at your earliest opportunity.

If there are any changes to the project and/or its methodology, please inform the Panel as soon as possible.

Regards,

Jayne Hunter
Contracts Administrator

For enquiries please contact
Jayne Hunter
Contracts Administrator
Contracts Office
Enterprise Division
Faraday House
Telephone: 0161 295 3530 Facsimile: 0161 295 5494
E-mail: j.hunter@salford.ac.uk

Appendix D

Subject Questionnaire

University of Salford MANCHESTER

Centre Health Science Research
Brian Blatchford Building
Frederick Rd
University of Salford
Salford
M6 6PU

December 2011

General Health & Foot Health Questionnaire

Today's Date	**Time**	**Participant Number**

Personal Details

Male ☐	Female ☐	D.O.B.	Age

Height	Weight	BMI

White British	☐	White Irish	☐	Any other White background	☐	Mixed White & Black Caribbean	☐
Mixed White & Black African	☐	Mixed White & Asian	☐	Any other mixed background	☐	Indian	☐
Pakistani	☐	Bangladeshi	☐	Any other Asian background	☐	Black Caribbean	☐
Black African	☐	Any other Black background	☐	Chinese	☐	Any other ethnic group / Not Stated	☐

Occupation details …….	Alcohol Consumption: Weekly Units ……	Smoker: Number per day ……
Standing ☐ Sitting ☐ Moving ☐	Daily ☐ Weekly ☐ Monthly ☐ Rarely ☐ Never ☐	Ex-Smoker ☐ Never ☐
No. of Years in Above Occupation …….	Typical Length of Work Day: ……	

Medical History/Assessment

Allergies	Operations on foot ……	Scar tissue on plantar surface (Op./Trauma) ……
	Yes ☐ No ☐	Yes ☐ No ☐

Do you suffer from or have you ever suffered from	
Cardiovascular Disorders	
High/Low Blood Pressure	
Cold, fever in last 2 weeks	
Loss of consciousness	

Loss of balance due to dizziness	
Respiratory disorders, asthma, bronchitis	
Diabetes	
Epilepsy/Seizures	
Are you currently receiving advice from a medical advisor i.e. GP or Physiotherapist **not** to participate in physical activity because of back pain or any musculoskeletal (muscle, joint or bone) problems	

Any Other Medical Conditions (Past & Present) please include as much information as possible.	Use of Orthotics: Yes ☐ No ☐ ……..

Perception of every-day comfort

Generally OK	Sometimes uncomfortable	Uncomfortable
☐	☐	☐

Medication

Normal Arch	R	L	Pes Planus	R	L	Pes Cavus	R	L	Prom. Met. Head	R	L	Hallux Valgus	R	L

Shoe size: ……. Leg Length Difference: …….cm	Right Left
Current Foot Pathology (include any deformation and current pain)	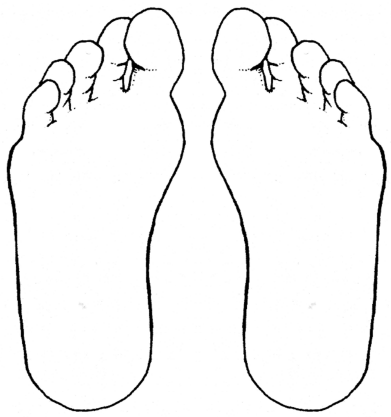
Past Foot Pathology or Treatment	

Physical Activity

Transport Walk	Vehicle owner	Bicycle	Public transport	Do you walk a dog daily	Yes	No
☐	☐	☐	☐	☐		☐

Do you take part in any Activity	Weekly participation 1-2	3-4	5-6	7+
Walking (Exercise)				
Hiking				

Activity	Weekly participation 1-2	3-4	5-6	7+
Football				
Rugby				

Jogging						Netball / Basketball / Volleyball				
Running >30minutes						Racket sport				
Running 31-60 minutes						Golf				
Running 61+ minutes						Climbing				
Cycling						Athletics				
Martial arts (Bare foot)						Weight Training				
Martial Arts / Boxing						Swimming				
Aerobics						Other				
Dance / Ballet										
Yoga / Pilates / Tai Chi										
Length of time involved in above activity (in months/years)										

Footwear

Footwear worn for work N/A			
Trainer		Mule	
Boot		Sandal	
Steel-toe-cap boot		Ballet pump	
Clog		Ugg (Similar)	
Lace-up		High heels (>xxcm)	
Monk / Male Slip on		Other	
Moccasin			

Footwear worn out-side work			
Trainer		Mule	
Boot		Sandal	
Slippers		Ballet pump	
Clog		Ugg (Similar)	
Lace-up		High heels (>xxcm)	
Monk / Male Slip on		Other	
Moccasin			

Sporting Footwear ☐ N/A High Heel Wearers ☐ N/A Other Footwear Notes ☐

Footwear worn during physical activity Professionally fitted sports shoe…… Specialist sports shoe…… General sports shoe…… Converse-type shoes……	If high heel wearer: average wear time: ……..hr/day ……day/wk Typical shoe forefoot shape/fit: Tight ☐ Comfortable ☐ Loose ☐ Shape ……..	

Appendix E

Participant Information Sheet

University of Salford MANCHESTER

Centre for Health Sciences Research
Brian Blatchford Building
Frederick Rd
University of Salford
Salford
M6 6PU

Participant Information Sheet (Healthy Volunteer)

Plantar Tissue Imaging

You are being invited to take part in a research study. Before you decide it is important for you to understand why the research is being done and what it will involve. Please take time to read the following information carefully. Talk to others about the study if you wish.

Our device will look at the fatty pads under the foot and measure their properties, for example is the pad softer at the heel than at the ball of your foot. To do this we will use ultrasound, to produce images of the fatty pad. Our ultrasound works the same way as those used to scan babies and you will be able to see images of the fatty pads. This will allow us to understand how the fatty pads work when you walk over them.

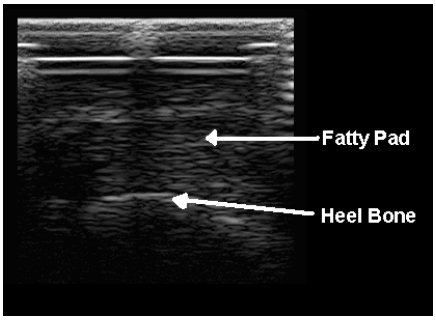

Fig 1. Ultrasound image of heel fatty pad

Do you have to take part?

No. It is up to you to decide whether or not to take part. If you do, you will be given this information sheet to keep and be asked to sign a consent form, but you are free to withdraw at any time without giving a reason.

What will be involved and what is the device being tested?

Our device will be used to compress the tissue on the bottom of the foot. You will be seated and your foot will be placed in a shoe, which is attached to the device. Your foot will then be positioned using straps; this will stop your foot moving too much during testing. The device will push against the bottom of your foot which will flatten the fatty pad in the same way you flatten the fatty pad when you walk over it. During this three measurements will be taken. We will look at the load applied to the bottom of the foot by the device, the movement of the device and the fatty pads thickness will be measured using ultrasound. Several test types will be used to allow us to see how the fatty pad works in different situations for example multiple compressions will show us how it works in walking. A steady load will show us how it works when you stand on it for a long time. The fatty

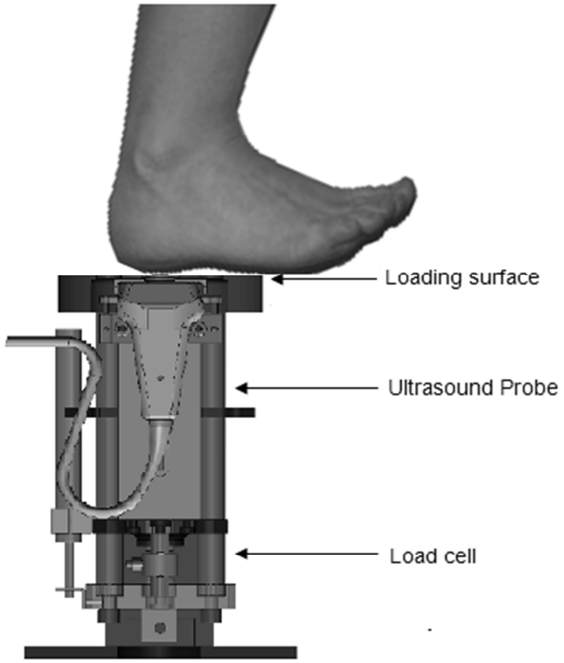

pads response to speed will also be tested, so trials will be run at slower than and faster than normal walking speeds. The test should take about 90 minutes in total.

What are the side effects and other possible disadvantages and risks of taking part?

In preparation for this study we have tested the device with healthy volunteers in the Gait Laboratory at Salford University. We know that it is accurate and easy to use in this setting and now want to test on a larger group of healthy volunteers. The testing is low risk, as you will be seated throughout and it involves loading the fatty pad on the bottom of the foot in a similar way to how you would normally load it during walking, but using a machine. It is considered that no increased risks, discomforts or distresses are likely to result from the data collection above those associated with normal walking. A contact name and number will be provided to you for use if you have any queries about any part of your participation in the analysis and you are free to ask questions at any time.

What are the possible benefits of taking part?

You will not benefit directly from taking part in this research but, if successful, the research will inform the design of footwear and orthotic devices to aid those who have problems with the fatty pad on the sole of the foot.

Contact Details:

If you have any questions or would like more information, please do not hesitate to contact:

Mr D Parker (PhD student)
Brian Blatchford Building,
Frederick Rd Campus
University of Salford,
Salford, M6 6PU
Tel: 0161 295 0459 Email: d.parker@edu.salford.ac.uk

Will my taking part in this study be kept confidential?

The information obtained in this study will be collected and stored in accordance with the Data Protection Act 1998. Any information obtained in connection with this study will be treated as privileged and confidential. All information will be anonymised so that you cannot be identified, except by a single paper form which will be stored securely in a lockable filing cabinet at Salford University. The research team, their colleagues, the sponsors and people who need to audit the conduct of our research will have access to the identifiable forms. All computer records and the data will be coded so individuals can not be identified. The data will be analysed to complete the study as outlined above. We will also keep the data for at least five years and may use it in future studies to improve our understanding of the plantar tissue. For example, we may wish to combine the data from this study with that of future studies to enable us to use more powerful analysis techniques. Ethical approval will not normally be sought for these studies.

Involvement of the General Practitioner/Family doctor (GP)

Your GP will not be informed that you have taken part in the study, as it will not affect your health care, well-being or lifestyle.

What will happen to the results of the research study?

The results of this study will be published in scientific and clinical journals and conferences. They will also be used for feedback and development of footwear products. We also make regular reports to the SSL group who funded this study and have an interest in the progress of the study. None of the people who have taken part in the study will be identifiable from any of the results

Appendix F

Informed Consent Form

Centre for Health Sciences Research
Brian Blatchford Building
Frederick Rd
University of Salford
Salford
M6 6PU

Consent Form for a Study of Healthy Volunteers

Plantar Tissue Imaging

Name of Researcher: **Please initial or tick the box**

1. I confirm that I have read and understand the information sheet dated Dec 2011 for the above study and have had the opportunity to ask questions. ☐

2. I confirm that I have completed a health questionnaire ☐

3. I understand that my participation is voluntary and that I am free to withdraw at any time, without giving any reason, without my medical care or legal rights being affected. ☐

4. I agree to take part in the above study. ☐

Name of Participant	Date	Signature
Name of Person taking consent (if different from researcher)	Date	Signature
Researcher	Date	Signature

Appendix G

Correlation Matrices

Table Ap.G.1. Pearson's Correlation Coefficients for the T-Wave Condition

T-Wave																													
Pearsons Correlation		K(1)	K(2)	K(3)	Secant	Hysteresis	Energy Loss	Strain(σmax)	Stress(σmax)	Compressibility	Velocity	Kelvin			Non-Newtonian			Parallel 3 Element					Non-Newtonian Non-Hookean					
												E	V		E	V	$E_{(\infty)}$	$E_{(0)}$	ε	V	$E_{(0)}$	$E_{(\infty)}$	ε	V
K(1)		1	.661**	.742**	.869**	-.015	.680**	-.182	.807**	-.158	.206	.868**	-.271		.887**	.288	.423**	.356	.009	.431**	.782**	.299	-.302**	.275
K(2)		.661**	1	.823**	.887**	.029	.619**	.008	.830**	.017	.139	.783**	-.427**		.780**	.400	.593**	.722**	.214**	.445	.923**	.759**	.051	.401**
K(3)		.742**	.823**	1	.900**	.251**	.737**	.076**	.877**	.092**	.110**	.739**	-.370**		.736**	.360**	.624**	.583**	.243**	.407**	.906**	.650**	.045**	.355**
Secant		.869**	.887**	.900**	1	.089**	.774**	-.037**	.948**	-.021**	.170**	.923**	-.407**		.921**	.416**	.581**	.547**	.064**	.448**	.910**	.601**	-.197**	.414**
Hysteresis		-.015	.029	.251**	.089**	1	.446**	.340**	.194**	.372**	-.183**	-.080**	-.276**		-.081**	.201**	.159**	.056**	-.221**	.012**	.102**	.217**	.219**	.197**
Energy Loss		.680**	.619**	.737**	.774**	.446**	1	.420**	.909**	.437**	.214**	.659**	-.620**		.656**	.576**	.508**	.363**	.028**	.315**	.740**	.374**	.112**	.578**
Strain(σmax)		-.182**	.008	.076**	-.037**	.340**	.420**	1	.250**	.996**	-.014**	-.166**	-.125**		-.168**	.000**	.160**	.113**	-.031**	-.114**	.059**	.078**	.497**	.005**
Stress(σmax)		.807**	.830**	.877**	.948**	.194**	.909**	.250**	1	.265**	.215**	.849**	-.445**		.846**	.417**	.593**	.541**	.041**	.408**	.894**	.573**	-.066**	.418**
Compressibility		-.158**	.017	.092**	-.021**	.372**	.437**	.996**	.265**	1	-.005**	-.155**	-.130**		-.156**	.006**	.169**	.116**	-.041**	-.113**	.067**	.082**	.482**	.012**
Velocity		.206**	.139**	.110**	.170**	-.183**	.214**	-.014**	.215**	-.005**	1	.270**	-.110**		.271**	.098**	-.153**	.111**	.086**	.332**	.228**	-.112**	.078**	.110**
Kelvin																													
E		.868**	.783**	.739**	.923**	-.080**	.659**	-.166**	.849**	-.155**	.270**	1	-.277**		1.000**	.297**	.273**	.424**	-.013**	.649**	.824**	.422**	-.295**	.293**
V		-.271**	-.427**	-.370**	-.407**	-.276**	-.620**	-.125**	-.445**	-.130**	-.110**	-.277**	1		-.275**	-.988**	-.314**	-.207**	-.178**	-.176**	-.385**	-.377**	-.083**	-.957**
Non-Newtonian																													
E		.867**	.780**	.736**	.921**	-.081**	.656**	-.168**	.846**	-.156**	.271**	1.000**	-.275**		1	.296**	.288**	.420**	-.014**	.652**	.822**	.419**	-.295**	.292**
V		.288**	.400**	.360**	.416**	.201**	.576**	.000**	.417**	.006**	.098**	.297**	-.968**		.296**	1	.294**	.106**	.186**	.158**	.343**	.306**	-.002**	.998**
Parallel 3 Element																													
$E_{(\infty)}$		.423**	.593**	.624**	.581**	.159**	.508**	.160**	.593**	.169**	-.153**	.273**	-.314**		.288**	.294**	1	.582**	.154**	-.382**	.567**	.620**	.020**	.303**
$E_{(0)}$		.356**	.722**	.583**	.547**	.056**	.363**	.113**	.541**	.116**	.111**	.424**	-.207**		.420**	.106**	.582**	1	.434**	.147**	.729**	.767**	.355**	.097**
ε		.009**	.214**	.243**	.064**	-.221**	.028**	-.031**	.041**	-.041**	.086**	-.013**	-.178**		-.014**	.186**	.154**	.434**	1	.095**	.284**	.221**	.537**	.178**
V		.431**	.445**	.407**	.448**	.012**	.315**	-.114**	.408**	-.113**	.332**	.649**	-.176**		.652**	.158**	-.382**	.147**	.095**	1	.518**	.179**	.012**	.142**
Non-Newtonian Non-Hookean																													
$E_{(\infty)}$		.782**	.923**	.906**	.910**	.102**	.740**	.059**	.894**	.067**	.228**	.824**	-.385**		.822**	.343**	.567**	.729**	.284**	.518**	1	.646**	.103**	.338**
$E_{(0)}$		.299**	.759**	.650**	.601**	.217**	.374**	.078**	.573**	.082**	-.112**	.422**	-.377**		.419**	.306**	.620**	.767**	.221**	.179**	.646**	1	.106**	.286**
ε		-.302**	.051	.045**	-.197**	.219**	.112**	.497**	-.066**	.482**	.078**	-.295**	-.083**		-.295**	-.002**	.020**	.355**	.537**	.012**	.103**	.106**	1	.000**
V		.275**	.401**	.355**	.414**	.197**	.578**	.005**	.418**	.012**	.110**	.293**	-.957**		.292**	.998**	.303**	.097**	.178**	.142**	.338**	.296**	.000**	1

**. Correlation is significant at the 0.01 level (2-tailed).

*. Correlation is significant at the 0.05 level (2-tailed).

Table Ap.G.2. Pearson's Correlation Coefficients for the S-Wave Condition

S-Wave											Kelvin		Non-Newtonian		Parallel 3 Element				Non-Newtonian Non-Hookean			
Pearsons Correlation	K(1)	K(2)	K(3)	Secant	Hysteresis	Energy Loss	Strain(σmax)	Stress(max)	Compressibility	Velocity	E	V	E	V	$E_{(a)}$	$E_{(b)}$	ε	V	$E_{(a)}$	$E_{(b)}$	ε	V
K(1)	1	.645**	.307	.921**	.124	.750**	-.422*	.749**	-.373*	-.401*	.967**	-.488**	.967**	.398*	.171	.158	-.642**	.664**	.543**	.494**	-.658**	.357*
K(2)	.645**	1	.822**	.845**	.152	.826**	.011	.883**	.024	-.112	.721**	-.668**	.716**	.600**	.413*	.598**	-.142	.825**	.915**	.670**	-.037	.577**
K(3)	.307	.822**	1	.636**	.122	.770**	.314	.821**	.319	.086	.428*	-.695**	.422*	.637**	.645**	.653**	.177	.538**	.828**	.655**	.287	.630**
Secant	.921**	.845**	.636**	1	.091	.846**	-.240	.933**	-.199	-.307	.954**	-.700**	.951**	.611**	.375*	.393*	-.427*	.733**	.754**	.642**	-.416*	.576**
Hysteresis	.124	.152	.122	.091	1	.462*	.255	.141	.282	.265	-.020	-.294	-.021	.293	.163	.197	.147	.083	.182	.122	.321	.302
Energy Loss	.750**	.826**	.770**	.846**	.462*	1	.185	.893**	.219	.060	.785**	-.908**	.784**	.857**	.660**	.438*	.093	.773**	.821**	.518**	.049	.859**
Strain(σmax)	-.422*	.011	.314	-.240	.255	.185	1	.088	.995**	.370*	-.319	.000	-.319	-.134	.123	.469*	.227	-.208	.075	.058	.572**	-.121
Stress(max)	.749**	.883**	.821**	.933**	.141	.893**	.088	1	.123	-.133	.839**	-.740**	.836**	.613**	.507**	.585**	-.269	.693**	.849**	.691**	-.166	.587**
Compressibility	-.373*	.024	.319	-.199	.282	.219	.995**	.123	1	.359*	-.278	-.026	-.277	-.114	.118	.480*	.201	-.204	.079	.072	.530**	-.104
Velocity	-.401*	-.112	.086	-.307	.265	.060	.370*	-.133	.359*	1	-.383*	.062	-.384*	-.053	.313	.251	.466**	-.262	.008	.088	.509**	-.029
Kelvin																						
E	.967**	.721**	.428*	.954**	-.020	.785**	-.319	.839**	-.278	-.383*	1	-.495**	1.000**	.381*	.211	.301	-.607**	.699**	.629**	.524**	-.538**	.342
V	-.488**	-.668**	-.695**	-.700**	-.294	-.908**	.000	-.740**	-.026	.062	-.495**	1	-.490**	-.934**	-.612**	-.332	-.038	-.411*	-.636**	-.436*	-.008	-.926**
Non-Newtonian																						
E	.967**	.716**	.422*	.951**	-.021	.784**	-.319	.836**	-.277	-.384*	1.000**	-.490**	1	.375*	.206	.300	-.612**	.695**	.623**	.523**	-.540**	.335
V	.398*	.600**	.637**	.611**	.293	.857**	-.134	.613**	-.114	-.053	.381*	-.934**	.375*	1	.594**	.154	.157	.332	.537**	.271	-.037	.998**
Parallel 3 Element																						
$E_{(a)}$	.171	.413*	.645**	.375*	.163	.660**	.123	.507**	.118	.313	.211	-.612**	.206	.594**	1	.310	.299	.126	.599**	.324	.250	.607**
$E_{(b)}$	.158	.598**	.653**	.393*	.197	.438*	.469**	.585**	.480**	.251	.301	-.332	.300	.154	.310	1	.021	.287	.611**	.660**	.455*	.139
ε	-.642**	-.142	.177	-.427*	.147	.093	.227	-.269	.201	.466**	-.607**	-.038	-.612**	.157	.299	.021	1	-.272	-.047	-.094	.607**	.194
V	.664**	.825**	.538**	.733**	.083	.773**	-.208	.693**	-.204	-.262	.699**	-.411*	.695**	.332	.126	.287	-.272	1	.806**	.493**	-.211	.314
Non-Newtonian Non-Hookean																						
$E_{(a)}$	.543**	.915**	.828**	.754**	.182	.821**	.075	.849**	.079	.008	.629**	-.636**	.623**	.537**	.599**	.611**	-.047	.806**	1	.546**	.092	.528**
$E_{(b)}$	.494**	.670**	.655**	.642**	.122	.518**	.058	.691**	.072	.088	.524**	-.436*	.523**	.271	.324	.660**	-.094	.493**	.546**	1	.173	.245
ε	-.658**	-.037	.287	-.416*	.321	.049	.572**	-.166	.530**	.509**	-.538**	-.008	-.540**	-.037	.250	.455*	.607**	-.211	.092	.173	1	-.012
V	.357*	.577**	.630**	.576**	.302	.859**	-.121	.587**	-.104	-.029	.342	-.926**	.335	.998**	.607**	.139	.194	.314	.528**	.245	-.012	1

**. Correlation is significant at the 0.01 level (2-tailed).

*. Correlation is significant at the 0.05 level (2-tailed).

Table Ap.G.3. Pearson's Correlation Coefficients for the Gait Sim Condition

Gait Simulation											Kelvin		Non-Newtonian		Parallel 3 Element				Non-Newtonian Non-Hookean			
Pearsons Correlation	K(1)	K(2)	K(3)	Secant	Hysteresis	Energy Loss	Strain(σmax)	Stress(max)	Compressibility	Velocity	E	V	E	V	$E_{(a)}$	$E_{(b)}$	ε	V	$E_{(a)}$	$E_{(b)}$	ε	V
K(1)	1	.786**	.465**	.837**	.004	.440*	-.574**	.598**	-.468**	-.045	.926**	-.160	.923**	.185	.631**	.387*	-.690**	.890**	.900**	.221	-.554**	.189
K(2)	.786**	1	.765**	.969**	.011	.414*	-.554**	.667**	-.487**	-.006	.890**	-.417*	.889**	.452**	.748**	.446*	-.648**	.818**	.879**	.374*	-.470**	.455**
K(3)	.465**	.765**	1	.824**	-.111	.059	-.664**	.220	-.661**	-.278	.507**	-.129	.506**	.175	.594**	.223	-.512**	.350*	.492**	.147	-.217	.178
Secant	.837**	.969**	.824**	1	-.071	.359*	-.669**	.614**	-.596**	-.107	.897**	-.332	.897**	.372*	.734**	.420*	-.699**	.798**	.878**	.277	-.463**	.376*
Hysteresis	.004	.011	-.111	-.071	1	.528**	.403*	.212	.388*	.241	-.126	-.236	-.131	.167	.129	.428*	.295	-.067	-.017	.449**	.022	.159
Energy Loss	.440*	.414*	.059	.359*	.528**	1	.325	.897**	.297	.289	.544**	-.789**	.543**	.724**	.580**	.518**	.086	.593**	.595**	.599**	-.182	.721**
Strain(σmax)	-.574**	-.554**	-.664**	-.669**	.403*	.325	1	.021	.939**	.342*	-.528**	-.251	-.525**	.175	-.257	-.069	.640**	-.449**	-.478**	.223	.278	.168
Stress(max)	.598**	.667**	.220	.614**	.212	.897**	.021	1	.033	.234	.771**	-.842**	.775**	.831**	.714**	.555**	-.235	.730**	.806**	.561**	-.351*	.831**
Compressibility	-.468**	-.487**	-.661**	-.596**	.388*	.297	.939**	.033	1	.380*	-.443**	-.162	-.442**	.079	-.333	-.055	.476**	-.341*	-.417**	.145	.188	.074
Velocity	-.045	-.006	-.278	-.107	.241	.289	.342*	.234	.380*	1	.017	-.275	.016	.257	.051	-.141	.238	.092	.021	.125	.039	.254
Kelvin																						
E	.926**	.890**	.507**	.897**	-.126	.544**	-.528**	.771**	-.443**	.017	1	-.416*	1.000**	.455**	.701**	.419*	-.679**	.953**	.979**	.283	-.558**	.459**
V	-.160	-.417*	-.129	-.332	-.236	-.789**	-.251	-.842**	-.162	-.275	-.416*	1	-.423*	-.987**	-.565**	-.434*	-.031	-.324	-.465**	-.502**	.162	-.986**
Non-Newtonian																						
E	.923**	.889**	.506**	.897**	-.131	.543**	-.525**	.775**	-.442**	.016	1.000**	-.423*	1	.462**	.703**	.418*	-.679**	.952**	.979**	.282	-.558**	.467**
V	.185	.452**	.175	.372*	.167	.724**	.175	.831**	.079	.257	.455**	-.987**	.462**	1	.597**	.396*	-.017	.353*	.506**	.446**	-.185	1.000**
Parallel 3 Element																						
$E_{(a)}$	.631**	.748**	.594**	.734**	.129	.580**	-.257	.714**	-.333	.051	.701**	-.565**	.703**	.597**	1	.323	-.250	.554**	.748**	.512**	-.314	.597**
$E_{(b)}$	.387*	.446**	.223	.420*	.428*	.518**	-.069	.555**	-.055	-.141	.419*	-.434*	.418*	.396*	.323	1	-.060	.450**	.482**	.728**	.054	.391*
ε	-.690**	-.648**	-.512**	-.699**	.295	.086	.640**	-.235	.476**	.238	-.679**	-.031	-.679**	-.017	-.250	-.060	1	-.604**	-.586**	.211	.761**	-.026
V	.890**	.818**	.350*	.798**	-.067	.593**	-.449**	.730**	-.341*	.092	.953**	-.324	.952**	.353*	.554**	.450**	-.604**	1	.945**	.309	-.502**	.355*
Non-Newtonian Non-Hookean																						
$E_{(a)}$	.900**	.879**	.492**	.878**	-.017	.595**	-.478**	.806**	-.417*	.021	.979**	-.465**	.979**	.506**	.748**	.482**	-.586**	.945**	1	.324	-.481**	.509**
$E_{(b)}$	.221	.374*	.147	.277	.449**	.599**	.223	.561**	.145	.125	.283	-.502**	.282	.446**	.512**	.728**	.211	.309	.324	1	.051	.438**
ε	-.554**	-.470**	-.217	-.463**	.022	-.182	.278	-.351*	.188	.039	-.558**	.162	-.558**	-.185	-.314	.054	.761**	-.502**	-.481**	.051	1	-.192
V	.189	.455**	.178	.376*	.159	.721**	.168	.831**	.074	.254	.459**	-.986**	.467**	1.000**	.597**	.391*	-.026	.355*	.509**	.438**	-.192	1

**. Correlation is significant at the 0.01 level (2-tailed).

*. Correlation is significant at the 0.05 level (2-tailed).

Table Ap.G.4. Pearson's Correlation Coefficients of Subject Parameters for the T-Wave Condition

T-Wave											Kelvin		Non-Newtonian		Parallel 3 Element				Non-Newtonian Non-Hookean			
	K(1)	K(2)	K(3)	Secant	Hysteresis	Energy Loss	Strain(σmax)	Stress(max)	Compressibility	Velocity	E	V	E	V	$E_{(a)}$	$E_{(b)}$	ε	V	$E_{(a)}$	$E_{(b)}$	ε	V
Abs_Age	.241	.096	.109	.148	-.168	.322	.151	.233	.156	.066	.117	-.059	.117	.104	.218	.041	.165	-.039	.199	-.047	.167	.122
Gender	.199	.119	.115	.168	.143	.081	-.200	.107	-.174	-.044	.113	.204	.113	-.160	.228	.129	.017	-.107	.116	.138	.070	-.146
BMI	.222	.312	.166	.176	-.458*	.047	-.084	.145	-.100	.393*	.183	-.079	.184	.056	.106	.213	.083	.197	.288	.164	.213	.058
Height	.027	.251	.123	.161	-.133	.053	.056	.148	.038	.095	.188	-.341	.187	.262	-.070	.168	-.066	.277	.171	.177	-.177	.242
Weight	.145	.385*	.198	.227	-.347	.072	.004	.201	-.021	.297	.251	-.311	.251	.229	.011	.272	-.002	.335	.311	.245	.014	.214

Table Ap.G.5. Pearson's Correlation Coefficients of Subject Parameters for the S-Wave Condition

S-Wave											Kelvin		Non-Newtonian		Parallel 3 Element				Non-Newtonian Non-Hookean			
	K(1)	K(2)	K(3)	Secant	Hysteresis	Energy Loss	Strain(σmax)	Stress(max)	Compressibility	Velocity	E	V	E	V	$E_{(a)}$	$E_{(b)}$	ε	V	$E_{(a)}$	$E_{(b)}$	ε	V
Abs_Age	.177	.345	.143	.246	-.069	.378*	-.008	.239	-.004	-.291	.186	-.323	.182	.339	.021	-.054	-.005	.273	.243	-.158	-.229	.337
Gender	.326	.136	-.031	.194	-.039	.000	-.275	.085	-.288	-.486**	.241	-.075	.242	.075	-.132	-.030	-.256	.154	.040	.031	-.265	.061
BMI	-.244	.058	.027	-.149	-.027	.004	.149	-.080	.138	.481**	-.200	-.063	-.201	.115	.054	.153	.231	-.106	.043	-.164	.129	.131
Height	-.179	-.111	.043	-.054	-.012	.051	.079	.012	.086	.548**	-.073	.009	-.074	-.022	.214	.101	.134	-.103	-.008	.223	.184	-.013
Weight	-.265	-.030	.051	-.122	-.033	.037	.132	-.036	.130	.691**	-.167	-.027	-.169	.046	.176	.168	.238	-.114	.031	.075	.213	.062

Table Ap.G.6. Pearson's Correlation Coefficients of Subject Parameters for the Gait Sim Condition

Gait											Kelvin		Non-Newtonian		Parallel 3 Element				Non-Newtonian Non-Hookean			
	K(1)	K(2)	K(3)	Secant	Hysteresis	Energy Loss	Strain(σmax)	Stress(max)	Compressibility	Velocity	E	V	E	V	$E_{(a)}$	$E_{(b)}$	ε	V	$E_{(a)}$	$E_{(b)}$	ε	V
Abs_Age	-.153	-.116	-.160	-.135	.087	.322	.413*	.200	.419*	.065	-.071	-.322	-.068	.267	.035	-.115	.124	-.109	-.085	.054	-.039	.267
Gender	.115	.080	-.072	.069	.140	.282	.152	.208	.155	.152	.099	-.161	.098	.096	.056	.162	.084	.158	.092	.274	.044	.094
BMI	-.172	-.142	-.155	-.175	-.087	-.055	.079	.002	-.110	-.320	-.083	-.208	-.078	.212	-.017	-.017	.112	-.102	-.054	-.012	-.001	.213
Height	.194	.223	.264	.244	-.147	-.167	-.410*	.007	-.426*	-.129	.208	.015	.210	.043	.220	.038	-.308	.109	.195	-.067	-.188	.046
Weight	.033	.078	.105	.073	-.162	-.156	-.258	.007	-.392*	-.277	.101	-.124	.106	.171	.151	.010	-.155	.016	.108	-.058	-.136	.173

List of References

Aerts, P., Ker, R.F., De Clercq, D., and Ilsley, D.W., 1996. The effects of isolation on the mechanics of the human heel pad. *Journal of Anatomy*, 188 (2), 417–423.

Aerts, P., Ker, R.F., De Clercq, D., Ilsley, D.W., and Alexander, R.M., 1995. The mechanical properties of the human heel pad: A paradox resolved. *Journal of Biomechanics*, 28 (11), 1299–1308.

Alcántara, E., Forner, A., Ferrús, E., García, A.-C., and Ramiro, J., 2002. Influence of age, gender, and obesity on the mechanical properties of the heel pad under walking impact conditions. *Journal of Applied Biomechanics*, 18 (4), 345–356.

Alexander, R.M., Bennett, M.B., and Ker, R.F., 1986a. Mechanical properties and function of the paw pads of some animals. *J Zool*, 209, 405–419.

Asakawa, D.S., Nayak, K.S., Blemker, S.S., Delp, S.L., Pauly, J.M., Nishimura, D.G., and Gold, G.E., 2003. Real-time imaging of skeletal muscle velocity. *Journal of Magnetic Resonance Imaging*, 18 (6), 734–739.

Bennett, M.B. and Ker, R.F., 1990. The mechanical properties of the human subcalcaneal fat pad in compression. *Journal of Anatomy*, 171, 131–138.

Bland, D.R., 1960. *The theory of linear viscoelasticity*. London: Pergamon Press.

Blechschmidt, E., 1982. The structure of the calcaneal padding. *Foot and Ankle*, 2 (5), 260–283.

Brash, P.D., Foster, J., Vennart, W., Anthony, P., and Tooke, J.E., 1999. Magnetic resonance imaging techniques demonstrate soft tissue damage in the diabetic foot. *Diabetic Medicine*, 16 (1), 55–61.

Buschmann, W.R., Hudgins, L.C., Kummer, F., Desai, P., and Jahss, M.H., 1993. Fatty acid composition of normal and atrophied heel fat pad. *Foot & ankle*, 14 (7), 389.

Buschmann, W.R., Jahss, M.H., Kummer, F., Desai, P., Gee, R.O., and Ricci, J.L., 1995. Histology and histomorphometric analysis of the normal and atrophic heel fat pad. *Foot & Ankle International / American Orthopaedic Foot and Ankle Society [and] Swiss Foot and Ankle Society*, 16 (5), 254–258.

Cavanagh, P.R., 1999. Plantar soft tissue thickness during ground contact in walking. *Journal of Biomechanics*, 32 (6), 623–628.

Challis, J.H., Murdoch, C., and Winter, S.L., 2008. Mechanical properties of the human heel pad: A comparison between populations. *Journal of Applied Biomechanics*, 24 (4), 377–381.

Chao, C.Y.L., Zheng, Y.-P., Huang, Y.-P., and Cheing, G.L.Y., 2010. Biomechanical properties of the forefoot plantar soft tissue as measured by an optical coherence tomography-based air-jet indentation system and tissue ultrasound palpation system. *Clinical Biomechanics*, 25 (6), 594–600.

Chen, W.-M., Phyau-Wui Shim, V., Park, S.-B., and Lee, T., 2011. An instrumented tissue tester for measuring soft tissue property under the metatarsal heads in relation to metatarsophalangeal joint angle. *Journal of biomechanics*, 44 (9), 1801–1804.

Chen, W.-P., Tang, F.-T., and Ju, C.-W., 2001. Stress distribution of the foot during mid-stance to push-off in barefoot gait: A 3-D finite element analysis. *Clinical Biomechanics*, 16 (7), 614–620.

Ciacci, S., Di Michele, R., and Merni, F., 2010. Kinematic analysis of the braking and propulsion phases during the support time in sprint running. *Gait & Posture*, 31 (2), 209–212.

De Clercq, D., 1994. The mechanical characteristics of the human heel pad during foot strike in running: An in vivo cineradiographic study. *Journal of Biomechanics*, 27 (10), 1213–1222.

De Cock, A., De Clercq, D., Willems, T., and Witvrouw, E., 2005. Temporal characteristics of foot roll-over during barefoot jogging: reference data for young adults. *Gait & posture*, 21 (4), 432–439.

Ennos, R., 2011. *Solid Biomechanics*. Princeton University Press.

Erdemir, A. a, Viveiros , M.L., Ulbrecht, J.S., and Cavanagh, P.R., 2006. An inverse finite-element model of heel-pad indentation. *Journal of Biomechanics*, 39 (7), 1279–1286.

Frederick, E.C., 1984. *Sport Shoes and Playing Surfaces: Biomechanical Properties*. Human Kinetics Pub.

Frost, H., 1971. *Introduction to Biomechanics*. Charles C Thomas Pub Ltd.

Gefen, A., Megido-Ravid, M., and Itzchak, Y., 2001. In vivo biomechanical behavior of the human heel pad during the stance phase of gait. *Journal of Biomechanics*, 34 (12), 1661–1665.

Giddings, V.L., Beaupré, G.S., Whalen, R.T., and Carter, D.R., 2000. Calcaneal loading during walking and running. *Medicine and Science in Sports and Exercise*, 32 (3), 627–634.

Han, L., Noble, J.A., and Burcher, M., 2003. A novel ultrasound indentation system for measuring biomechanical properties of in vivo soft tissue. *Ultrasound in Medicine & Biology*, 29 (6), 813–823.

Harris, G.F., Acharya, K.R., and Bachschmidt, R.A., 1996. Investigation of spectral content from discrete plantar areas during adult gait: an expansion of rehabilitation technology. *IEEE Transactions on Rehabilitation Engineering*, 4 (4), 360 –374.

Hennig, E.M. and Sterzing, T., 2009. Sensitivity Mapping of The Human Foot: Thresholds at 30 Skin Locations. *Foot & Ankle International*, 30 (10), 986–991.

Hsu, C.-C., Tsai, W.-C., Chen, C.P.-C., Shau, Y.-W., Wang, C.-L., Chen, M.J.-L., and Chang, K.-J., 2005. Effects of aging on the plantar soft tissue properties under the metatarsal heads at different impact velocities. *Ultrasound in Medicine and Biology*, 31 (10), 1423–1429.

Hsu, C.-C., Tsai, W.-C., Hsiao, T.-Y., Tseng, F.-Y., Shau, Y.-W., Wang, C.-L., and Lin, S.-C., 2009. Diabetic effects on microchambers and macrochambers tissue properties in human heel pads. *Clinical Biomechanics*, 24 (8), 682–686.

Hsu, C.-C., Tsai, W.-C., Shau, Y.-W., Lee, K.-L., and Hu, C.-F., 2007. Altered energy dissipation ratio of the plantar soft tissues under the metatarsal heads in patients with type 2 diabetes mellitus: A pilot study. *Clinical Biomechanics*, 22 (1), 67–73.

Hsu, C.-C., Tsai, W.-C., Wang, C.-L., Pao, S.-H., Shau, Y.-W., and Chuan, Y.-S., 2007. Microchambers and macrochambers in heel pads: Are they functionally different? *Journal of Applied Physiology*, 102 (6), 2227–2231.

Hsu, T.-C., Lee, Y.-S., and Shau, Y.-W., 2002. Biomechanics of the heel pad for type 2 diabetic patients. *Clinical Biomechanics*, 17 (4), 291–296.

Hsu, T.-C., Wang, C.-L., Shau, Y.-W., Tang, F.-T., Li, K.-L., and Chen, C.-Y., 2000b. Altered heel-pad mechanical properties in patients with Type 2 diabetes mellitus. *Diabetic Medicine*, 17 (12), 854–859.

Hsu, T.C., Wang, C.L., Tsai, W.C., Kuo, J.K., and Tang, F.T., 1998. Comparison of the mechanical properties of the heel pad between young and elderly adults. *Archives of physical medicine and rehabilitation*, 79 (9), 1101–1104.

Jahss, M.H., Kummer, F., and Michelson, J.D., 1992. Investigations into the fat pads of the sole of the foot: Heel pressure studies. *Foot and Ankle*, 13 (5), 227–232.

Jorgensen, U., 1985. Achillodynia and loss of heel pad shock absorbency. *American Journal of Sports Medicine*, 13 (2), 128–132.
Jorgensen, U. and Bojsen-Moller, F., 1989. Shock absorbency of factors in the shoe/heel interaction. With special focus on role on the heel pad. *Foot and Ankle*, 9 (6), 294–299.
Ker, R.F., 1996. The time-dependent mechanical properties of the human heel pad in the context of locomotion. *Journal of Experimental Biology*, 199 (7), 1501–1508.
Klaesner, J.W., Hastings, M.K., Zou, D., Lewis, C., and Mueller, M.J., 2002. Plantar tissue stiffness in patients with diabetes mellitus and peripheral neuropathy. *Archives of Physical Medicine and Rehabilitation*, 83 (12), 1796–1801.
Klaesner, J.W.., Commean, P.K., Hastings, M.K., Zou, D., and Mueller, M.J.., 2001. Accuracy and reliability testing of a portable soft tissue indentor. *IEEE Transactions on Neural Systems and Rehabilitation Engineering*, 9 (2), 232–240.
Kwan, R.L.-C., Zheng, Y.-P., and Cheing, G.L.-Y., 2010. The effect of aging on the biomechanical properties of plantar soft tissues. *Clinical Biomechanics*, 25 (6), 601–605.
Ledoux, W.R. and Blevins, J.J., 2007. The compressive material properties of the plantar soft tissue. *Journal of Biomechanics*, 40 (13), 2975–2981.
Lockett, F.J., 1972. *Nonlinear viscoelastic solids*. London: Academic Press.
Masoro, E.J. and Austad, S.N., eds., 2006. *Handbooks of Aging: Handbook of the Biology of Aging, Sixth Edition*. 6th ed. Academic Press.
Miller-Young, J.E., Duncan, N.A., and Baroud, G., 2002. Material properties of the human calcaneal fat pad in compression: experiment and theory. *Journal of biomechanics*, 35 (12), 1523–1531.
Mueller, M.J. and Maluf, K.S., 2002. Tissue adaptation to physical stress: a proposed 'Physical Stress Theory' to guide physical therapist practice, education, and research. *Physical Therapy*, 82 (4), 383.
Noe, D.A., Voto, S.J., Hoffmann, M.S., Askew, M.J., and Gradisar, I.A., 1993. Role of the calcaneal heel pad and polymeric shock absorbers in attenuation of heel strike impact. *Journal of biomedical engineering*, 15 (1), 23–26.
Nordin, M. and Frankel, V.H., 2001. *Basic Biomechanics of the Musculoskeletal System*. 3rd Revised edition. Lippincott Williams and Wilkins.
Pai, S. and Ledoux, W.R., 2010. The compressive mechanical properties of diabetic and non-diabetic plantar soft tissue. *Journal of Biomechanics*, 43 (9), 1754–1760.
Pain, M.T. and Challis, J.H., 2001. The role of the heel pad and shank soft tissue during impacts: a further resolution of a paradox. *Journal of Biomechanics*, 34 (3), 327–333.
Paul, R.G. and Bailey, A.J., 1996. Glycation of collagen: the basis of its central role in the late complications of ageing and diabetes. *The international journal of biochemistry & cell biology*, 28 (12), 1297–1310.
Petre, M., Erdemir, A., and Cavanagh, P.R., 2008. An MRI-compatible foot-loading device for assessment of internal tissue deformation. *Journal of Biomechanics*, 41 (2), 470–474.
Prichasuk, S., 1994. The heel pad in plantar heel pain. *Journal of Bone & Joint Surgery, British Volume*, 76-B (1), 140–142.
Richards, J., 2008b. *Biomechanics in Clinic and Research*. 1st Edition. Lippincott Williams & Wilkins.
Rome, K., 1998. Mechanical properties of the heel pad: Current theory and review of the literature. *Foot*, 8 (4), 179–185.
Rome, K., Campbell, R., Flint, A., and Haslock, I., 1998. Reliability of weight-bearing heel pad thickness measurements by ultrasound. *Clinical Biomechanics*, 13 (4-5), 374–375.

Rome, K. and Webb, P., 2000. Development of a clinical instrument to measure heel pad indentation. *Clinical Biomechanics*, 15 (4), 298–300.
Rome, K., Webb, P., Unsworth, A., and Haslock, I., 2001. Heel pad stiffness in runners with plantar heel pain. *Clinical Biomechanics*, 16 (10), 901–905.
Salathe Jr., E.P., Arangio, G.A., and Salathe, E.P., 1990. The foot as a shock absorber. *Journal of Biomechanics*, 23 (7), 655–659.
Shrout, P.E. and Fleiss, J.L., 1979. Intraclass correlations: Uses in assessing rater reliability. *Psychological Bulletin*, 86 (2), 420–428.
Snell, R.S., 2004. *Clinical Anatomy: An Illustrated Review With Questions and Explanations*. Lippincott Williams & Wilkins.
Sopher, R., Nixon, J., McGinnis, E., and Gefen, A., 2011b. The influence of foot posture, support stiffness, heel pad loading and tissue mechanical properties on biomechanical factors associated with a risk of heel ulceration. *Journal of the Mechanical Behavior of Biomedical Materials*, 4 (4), 572–582.
Spears, I.R., Miller-Young, J.E., Sharma, J., Ker, R.F., and Smith, F.W., 2007. The potential influence of the heel counter on internal stress during static standing: A combined finite element and positional MRI investigation. *Journal of Biomechanics*, 40 (12), 2774–2780.
Spears, I.R., Miller-Young, J.E., Waters, M., and Rome, K., 2005. The effect of loading conditions on stress in the barefooted heel pad. *Medicine and Science in Sports and Exercise*, 37 (6), 1030–1036.
Suetens, P., 2002. *Fundamentals of Medical Imaging*. Cambridge University Press.
Titianova, E.B., Mateev, P.S., and Tarkka, I.M., 2004. Footprint analysis of gait using a pressure sensor system. *Journal of Electromyography and Kinesiology*, 14 (2), 275–281.
Tong, J., Lim, C.S., and Goh, O.L., 2003. Technique to study the biomechanical properties of the human calcaneal heel pad. *Foot*, 13 (2), 83–91.
Trew, M. and Everett, T., 2001. *Human Movement: An Introductory Text*. Elsevier Health Sciences.
Uzel, M., Cetinus, E., Bilgic, E., Ekerbicer, H., and Karaoguz, A., 2006. Comparison of ultrasonography and radiography in assessment of the heel pad compressibility index of patients with plantar heel pain syndrome. Measurement of the fat pad in plantar heel pain syndrome. *Joint Bone Spine*, 73 (2), 196–199.
Vincent, J.F.., 1990. *Structural biomaterials*. Princeton Univ Pr.
Vincent, J.F.., 1992. *Biomechanics–materials: a practical approach*. Oxford University Press, USA.
Vogel, S., 1994. *Life in Moving Fluids: The Physical Biology of Flow*. Princeton University Press.
Wang, C.-L., Shau, Y.-W., Hsu, T.-C., Chen, H.-C., and Chien, S.-H., 1999. Mechanical properties of heel pads reconstructed with flaps. *Journal of Bone and Joint Surgery - Series B*, 81 (2), 207–211.
Wang, Y., Abumi, K., and Ledoux, W., 2011. Histomorphological evaluation of diabetic and non-diabetic plantar soft tissue. *Foot and Ankle International*, 32 (8), 802–810.
Wearing, S.C., Smeathers,, J.E., Yates, B., Urry, S.R., and Dubois, P., 2009. Bulk compressive properties of the heel fat pad during walking: A pilot investigation in plantar heel pain. *Clinical Biomechanics*, 24 (4), 397–402.
Weaver, J.B., Miller, T.B., Perrinez, P.R., Doyley, M.M., Wang, H., Cheung, Y.Y., Wrobel, J.S., Comi, R.J., Kennedy, F.E., and Paulsen, K.D., 2006. MR elastographic methods for the evaluation of plantar fat pads: Preliminary comparison of the shear modulus for

shearing deformation and compressive deformation in normal subjects. *In*: *Progress in Biomedical Optics and Imaging - Proceedings of SPIE*. 6143 I.

Weijers, R., Kessels, A., and Kemerink, G., 2005. The damping properties of the venous plexus of the heel region of the foot during simulated heelstrike. *Journal of Biomechanics*, 38 (12), 2423–2430.

Winter, D.A., 1987. *The biomechanics and motor control of human gait*. University of Waterloo Press.

Zheng, Y.P., Choi, Y.K.C., Wong, K., and Mak, A.F.T., 1999. Indentation Assessment of Plantar Foot Tissues in Diabetic Patients. *In*: *Annual International Conference of the IEEE Engineering in Medicine and Biology*. 634.

Zheng, Y.P., Huang, Y.P., Zhu, Y.P., Wong, M., He, J.F., and Huang, Z.M., 2012. Development of a foot scanner for assessing the mechanical properties of plantar soft tissues under different bodyweight loading in standing. *Medical Engineering & Physics*, 34 (4), 506–511.

Zheng, Y.P., Mak, A.F.., and Lue, B., 1999. Objective assessment of limb tissue elasticity: development of a manual indentation procedure. *Journal of rehabilitation research and development*, 36 (2), 71–85.

Zheng, Y.P.., Choi, Y.K.C., Wong, K., Chan, S., and Mak, A.F.T., 2000. Biomechanical assessment of plantar foot tissue in diabetic patients using an ultrasound indentation system. *Ultrasound in Medicine and Biology*, 26 (3), 451–456.